Reconfigurable Integrated Control for Urban Vehicles with Different Types of Control Actuation

by

Mansour Ataei

A thesis
presented to the University of Waterloo
in fulfillment of the
thesis requirement for the degree of
Doctor of Philosophy
in
Mechanical and Mechatronics Engineering

Waterloo, Ontario, Canada, 2017

Examining committee membership:

The following served on the Examining Committee for this thesis. The decision of the Examining Committee is by majority vote.

Supervisors:	**Prof. Amir Khajepour**	Professor	Mechanical and Mechatronics Department
	Prof. Soo Jeon	Associate Professor	Mechanical and Mechatronics Department
External Examiner:	**Prof. Fengjun Yan**	Associate Professor	McMaster University Department of Mechanical Engineering
Internal-external:	**Prof. Nasser Lashgarian Azad**	Associate Professor	System Design Engineering
Internal:	**Prof. William Melek**	Professor	Mechanical and Mechatronics Department
Internal:	**Prof. Ehsan Toyserkani**	Professor	Mechanical and Mechatronics Department

AUTHOR'S DECLARATION

I hereby declare that I am the sole author of this thesis. This is a true copy of the thesis, including any required final revisions, as accepted by my examiners.

I understand that my thesis may be made electronically available to the public.

Abstract

Urban vehicles are designed to deal with traffic problems, air pollution, energy consumption, and parking limitations in large cities. They are smaller and narrower than conventional vehicles, and thus more susceptible to rollover and stability issues. This thesis explores the unique dynamic behavior of narrow urban vehicles and different control actuation for vehicle stability to develop new reconfigurable and integrated control strategies for safe and reliable operations of urban vehicles.

A novel reconfigurable vehicle model is introduced for the analysis and design of any urban vehicle configuration and also its stability control with any actuation arrangement. The proposed vehicle model provides modeling of four-wheeled (4W) vehicles and three-wheeled (3W) vehicles in Tadpole and Delta configurations in one set of equations. The vehicle model is also reconfigurable in the sense that different configurations of control actuation can be accommodated for controller design. To develop the reconfigurable vehicle model, two reconfiguration matrices are introduced; the corner and actuator reconfiguration matrices that are responsible for wheel and actuator configurations, respectively. Simulation results show that the proposed model properly matches the high-fidelity CarSim models for 3W and 4W vehicles.

Rollover stability is particularly important for narrow urban vehicles. This thesis investigates the rollover stability of three-wheeled vehicles including the effects of road angles and road bumps. A new rollover index (RI) is introduced, which works for various road conditions including tripped and un-tripped rollovers on flat and sloped roads. The proposed RI is expressed in terms of measurable vehicle parameters and state variables. In addition to the effects of the lateral acceleration and roll angle, the proposed RI accounts for the effects of the longitudinal acceleration and the pitch angle, as well as the effects of road angles. Lateral and vertical road inputs are also considered since they can represent the effects of curbs, soft soil, and road bumps as the main causes of tripped rollovers. Sensitivity analysis is provided to evaluate and compare the effects of different vehicle parameters and

state variables on rollover stability of 3W vehicles. A high-fidelity CarSim model for a 3W vehicle has been used for simulation and evaluation of the proposed RI accuracy.

As a potentially useful mechanism for urban vehicles, wheel cambering is also investigated in this study to improve both lateral and rollover stability of narrow vehicles. A suspension system with active camber has an additional degree of freedom for changing the camber angle through which vehicle handling and stability can be improved. Conventionally, camber has been known for its ability to increase lateral forces. In this thesis, the benefits of cambering for rollover stability of narrow vehicles are also investigated and compared with a vehicle tilt mechanism. The simulation results indicate that active camber systems can improve vehicle lateral stability and rollover behavior. Furthermore, by utilizing more friction forces near the limits, the active camber system provides more improvement in maneuverability and lateral stability than the active front steering does.

The proposed reconfigurable vehicle model leads us to the development of a general integrated reconfigurable control structure. The reconfigurable integrated controller can be used to meet different stability objectives of 4W and 3W vehicles with flexible combinations of control actuation. Employing the reconfigurable vehicle model, the proposed unified controller renders reconfigurability and can be easily adapted to Tadpole and Delta configurations of 3W as well as 4W vehicles without reformulating the problem. Different types and combinations of actuators can be selected for the control design including or combination of differential braking, torque vectoring, active front steering, active rear steering, and active camber system. The proposed structure provides integrated control of the main stability objectives including handling improvement, lateral stability, traction/braking control, and rollover prevention. The Model Predictive Control (MPC) approach is used to develop the reconfigurable controller. The performance of the introduced controller has been evaluated through CarSim simulations for different vehicles and control actuation configurations.

Acknowledgements

Foremost, I would like to express my sincere appreciation to my supervisors, Prof. Amir Khajepour and Prof. Soo Jeon, for their constant guidance, support and encouragement, without which this work would not have been possible.

Besides my supervisors, I am grateful to my committee members, Prof. Fengjun Yan, Prof. Nasser Lashgarian Azad, Prof. William Melek, and Prof. Ehsan Toyserkani, for their valuable and insightful comments on my thesis.

My sincere thanks also goes to my friends, Ehsan Asadi, Amir Soltani, Saeid Khosravani, Asal Nahidi, Iman Fadakar, Ehsan Hashemi, Chen Tang, and also Prof. Avesta Goodarzi, for their support and assistance during my studies at the University of Waterloo.

Finally, I would like to express my deepest gratitude to my parents for their love, patience, and sacrifices to support me in my whole life. I am also extremely grateful to my family members and my friends all around the world who encouraged and supported me emotionally to achieve the goal.

Dedication

Dedicated to my parents for their endless love, support, and encouragement

Table of Contents

List of Figures

List of Tables

Chapter 1
Introduction

1.1 Motivation

Urban vehicles can alleviate traffic congestion, parking problems, energy consumption, and pollution in large cities because of their smaller sizes, higher maneuverability, and lower fuel consumptions. Traffic congestion is a serious problem in big cities all over the world (Figure 1-1). It is estimated that more than 5 billion hours are spent annually waiting on freeways [1]. Traffic congestion also results in wasting more fuel and causes more air pollution. Development of new roads and highways is very expensive and requires substantial time and resources. Hence, efficient utilization of the existing roads would be more practical and desirable in dealing with this problem[1], [2]. Air pollution is another significant problem that the inhabitants of big cities have been facing, especially in urban centers with high population density. A significant portion of this pollution comes from vehicle emissions. Reportedly, internal combustion engines in U.S account for 95% of city CO emissions, 32% of NO_x emissions, and 25% of volatile organic compound emissions [3]. Today's vehicles are significant contributors to emission of greenhouse gases, and thus they not only pose risks to human health but also disturb agricultural and ecological systems [4]. The vehicle emissions also create smog and impact the appearance of cities.

Figure 1-1: Traffic congestion and air pollution in a populated city [5]

Another important problem is the excessive consumption of non-renewable energy resources [4]. Fuel shortage in future could be an important economic problem, so the development of efficient and

low consumption vehicles is in high demand [2]. Furthermore, the lack of parking spaces is a big concern for populated cities especially in urban centers. In fact, solving the congestion problem is of little use if the urban centers are densely occupied and there is no sufficient space for other vehicles to arrive and park [6].

In addition, reports show that passenger cars are underutilized; for example, the average number of passengers per vehicle in U.S is 1.58 [2] resulting in unnecessary weight and fuel consumption compared to their average passenger loads [2] [6]. Typically, modern passenger vehicles are designed for driving on city roads and highways. Thus, they are designed to provide more power and speed than what is needed for urban areas. Hence, it is reasonable to design vehicles just for city driving. Furthermore, it is observed that a large part of personal vehicles are used with a small annual mileage (less than 10000 km/year) [7]. For instance, the daily usage of cars in Europe is shown in Figure 1-2 [7].

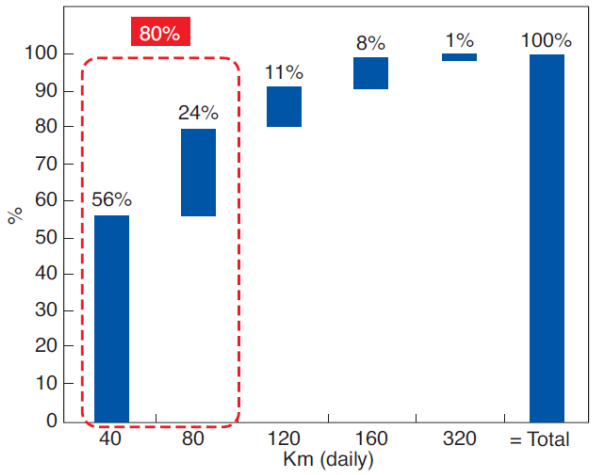

Figure 1-2: Daily usage of cars in Europe [7]

Design of urban vehicles could be inspired by the design of cars, motorcycles, bikes, or it may be something new. They are usually designed for a maximum of two passengers, and their maximum speed is usually lower than that of conventional cars. Being smaller and narrower than the present cars, this new generation of vehicles would be more practical and useful for dealing with traffic congestion and parking problems in big cities [8]. These vehicles can potentially increase parking and road capacities [6]. Since they are smaller and lighter than conventional cars, they are more fuel efficient. In addition, they have lower aerodynamic drag because of smaller front areas, which will also contribute to the reduction in fuel consumption and emission [9]. The urban vehicles should

provide an acceptable level of comfort and safety similar to the average existing passenger cars. In addition, they need to be aesthetically pleasing to be accepted as an alternative for conventional cars. To provide comfort and safety, it is essential that passengers are fully enclosed in a tight structure that can protect them against potential impact situations [9]. Two concept urban vehicles are shown in Figure 1-3 [10].

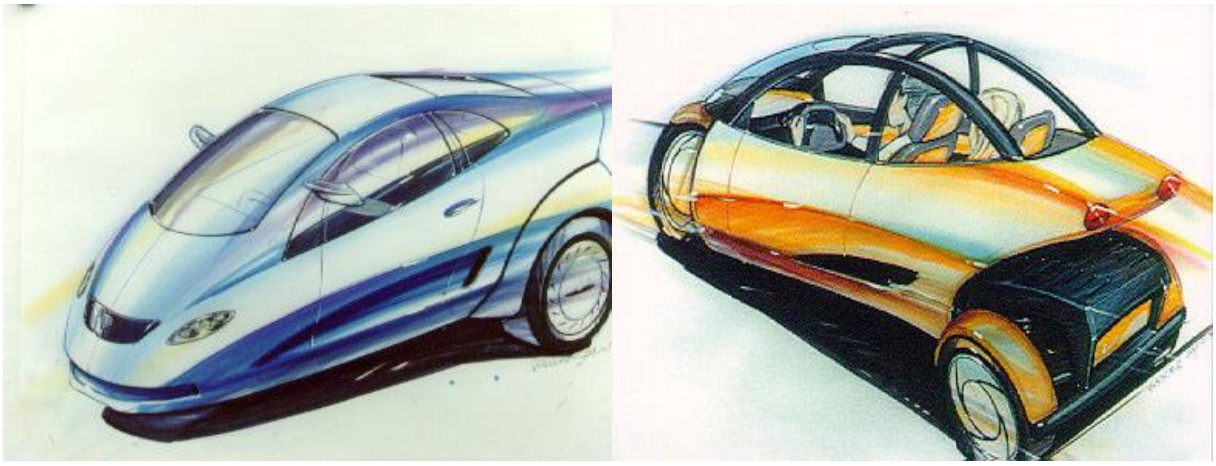

Figure 1-3 : Two Concept Urban Vehicles [10]

Although there are many advantages for the development of urban vehicles, there have been many challenges in their designs [6] [9] [8]. One of main issues is the rollover stability, which results from the difficulty in the compensation of overturning moment when vehicles are made small and narrow [6] [9] [8]. In fact, there exists a theoretical limit in the minimum width of a vehicle that can ensure safety in standard maneuvers without using active safety systems [6]. An important characteristic of standard vehicles is that their lateral slip threshold is less than their rollover threshold. Since rollover is more dangerous and fatal than slipping [11], this characteristic acts as a passive safety factor [6] [12]. In contrast, the narrow or tall vehicles reach their rollover limit before reaching lateral slip (skidding) [6]. In fact, conventional cars have a passive fail-safe system that can prevent rollover, but there is no similar mechanism for narrow or tall vehicles [6]. Since this problem cannot be solved without active safety systems, development of vehicles with narrow track width have not been a practical alternative for conventional cars so far.

In addition to rollover stability, lateral stability is also an important concern for all class of vehicles including urban vehicles. Recent advances in automotive technology have resulted in more precise measurements and/or estimations in real-time. As a result, more advanced controllers have been employed to improve vehicle safety and performance. Active lateral stability systems are developed

to prevent vehicles from spinning and drifting, thereby increasing vehicle safety. Lateral stability systems deal with handling and maneuverability, lateral slip, and longitudinal slip in traction and braking. These systems are intended to assist the driver under harsh conditions such as slippery roads or aggressive maneuvers to safely control and stabilize the vehicle. To develop new urban vehicles and specifically the ones with three-wheeled (3W) configurations, the stability and driver assistant systems should be designed considering their unique dynamics behavior and characteristics.

1.2 Thesis Objectives

The main objective of this study is to develop a general integrated reconfigurable control structure to handle different stability and safety problems of urban vehicles with any configuration. Handling improvement, lateral stability, rollover prevention, slip control in traction and braking, and longitudinal control are the control objectives that are considered for the design of the general integrated controller. The controller is also intended to be reconfigurable to be easily adjusted for different configurations of three- and four-wheeled vehicles. In addition, the reconfigurable control structure is desired to readily be adjusted for different types and combinations of actuators including differential braking, torque vectoring (TV), active front steering (AFS), active rear steering (ARS), and active camber system. This study also investigates tripped and un-tripped rollover stability of 3W vehicles on flat and sloped roads and introduces a new rollover index (RI) to detect rollovers in various situations. The concept of wheel cambering is also investigated, and the effectiveness of active camber systems for lateral stability improvement and rollover prevention of vehicles is explored with emphasis on urban vehicles application.

1.3 Thesis outline

The rest of this thesis includes literature review, reconfigurable vehicle modeling, rollover stability of three-wheeled vehicles, active camber system, integrated reconfigurable control design, and future work. Literature review is provided in Chapter 2 which begins with reviewing the studies about the urban vehicles. Three-wheeled vehicles, tilting mechanism, and some industrial urban vehicles are discussed in this chapter. Then, the methods for lateral stability control and rollover mitigation are explained. Finally, camber mechanism and the related work are discussed. Chapter 3 presents the development of the reconfigurable vehicle model for different configurations of urban vehicles. Chapter 4 focuses on rollover stability of three-wheeled vehicles in tripped and un-tripped conditions. In Chapter 5, active camber system is presented. At first, the potential capability of cambering is

discussed, and then the effects of cambering on lateral stability and rollover prevention of three- and four-wheeled vehicles are investigated. Chapter 6 presents the integrated reconfigurable controller. Control objectives and actuators' constraints are defined and considered in the development of an MPC controller for the general reconfigurable model. Simulation results for different vehicles are provided in this chapter to evaluate the controller performance. Finally, Chapter 7 provides conclusions and discusses future work for dynamics modeling, controller design, and implementation of the control system on actual vehicles.

Chapter 2: Literature Review

This chapter first goes over the previous studies for the design and development of urban vehicles. Then, active vehicle stability systems are reviewed. Finally, the literature on active camber system is discussed.

2.1 Urban Vehicles

Small and narrow vehicles have mainly been developed to address the concerns of conventional vehicles. Such vehicles are referred to as *urban vehicles* in this study.

2.1.1 Three-wheeled vehicles

Three-wheeled vehicles have been suggested for the design of urban vehicles [13]. Two different configurations are considered in development of three-wheeled vehicles. The first configuration, called the Delta configuration, has one wheel in the front and two wheels in the rear. The second configuration, called Tadpole configuration, has two wheels in the front and one in the rear (Figure 2-1) [12].

Delta configuration is the most common configuration that has been commercially available for many years. Easy fabrication is the main advantage of this type of three-wheeled vehicles. The most critical disadvantage of this configuration is the rollover stability problem. Design of Tadpole configuration has been more popular in recent years. The main advantage of this configuration is that it is more stable in rollover than the Delta configuration during braking in turn. Besides, the vehicle's track in the front makes it more stable in cornering and braking [14].

Dynamic stability of three-wheeled vehicles have been investigated in reference [14]. Both Delta-shape and Tadpole-shape are considered and the results are also compared with standard four-wheeled vehicles. For each vehicle, lateral stability and rollover stability are studied. Different situations including lateral acceleration, braking, and longitudinal accelerating are considered in rollover study. Based on this work, the governing equations for lateral stability of both three-wheeled cases are similar to that of four-wheeled vehicles. However, CG location must be different for them to obtain a similar level of lateral stability. In fact, to ensure an understeer behavior for a Tadpole-shape vehicle the CG location must be in the front third of the vehicle, for the Delta-shape it should be in the front two thirds, and for the four-wheeled vehicle it should be in the front half of the vehicle. For

rollover stability, the equations for the three-wheeled vehicles are developed, which showed that the three-wheeled vehicles cannot provide rollover stability similar to the four-wheeled vehicles.

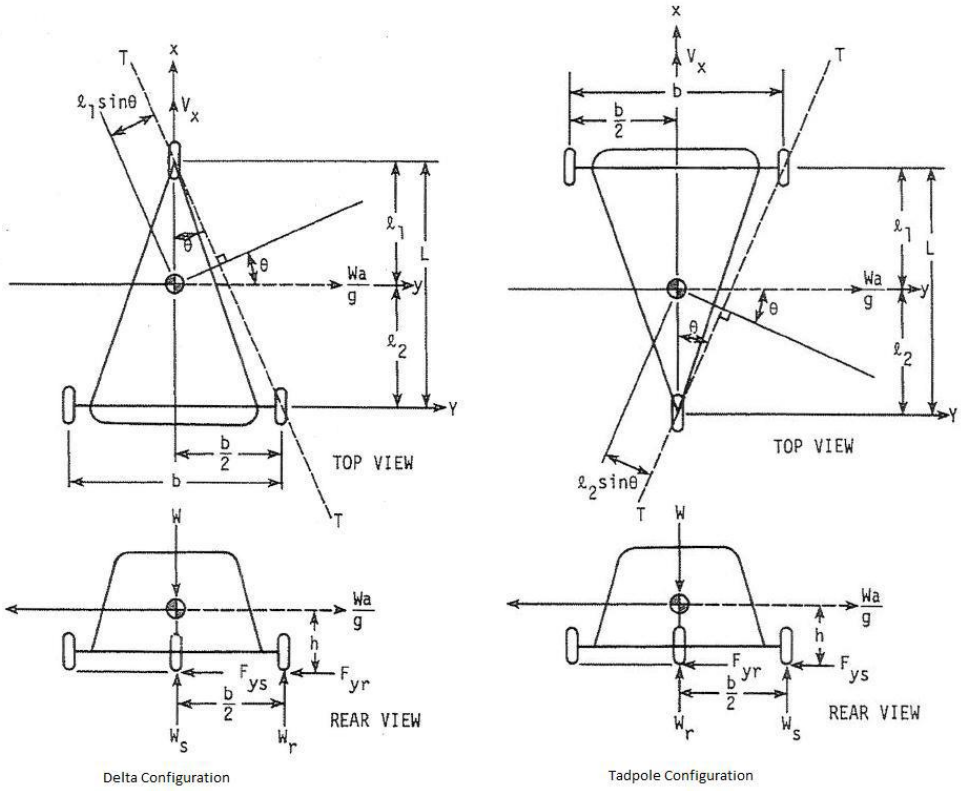

Figure 2-1: Delta (left) and Tadpole (right) configurations [12]

2.1.2 Tilt mechanism

As mentioned in the previous section, the most important problem of narrow vehicles is the rollover stability. One proposed solution is that narrow vehicles are made to lean inward to prevent rollover in cornering. This is known as a tilting mechanism [15]. This method is essentially the same as how two wheeled vehicles (i.e. motorcycles) drive around corners. One of the difficulties of this mechanism even for two wheeled vehicles is that driving of leaning vehicles requires specific skills. Without sufficient skill and experience, it can be dangerous especially in emergency situations [16]. Since urban vehicles are supposed to have an enclosed passenger cabin to provide comfort and safety, they are heavier than a normal two wheeled vehicle and the balance control is more difficult for the driver [17]. Consequently, automatic tilting systems have been developed for narrow urban vehicles. The tilt control system determines the desired tilt angle and activates appropriate tracking controllers

to provide safe and comfort driving while keeping the vehicle in balance [17]. There are two different types of tilt control systems [1] [16] [17]:

1. Direct Tilt Control (DTC) in which an actuator such as a hydraulic actuator is used to directly control the tilt motion.
2. Steering Tilt Control (STC) in which the steering is used to achieve the required tilt angle.

Having an actuator to directly apply tilting torque allows the controller to provide any desired angle for the vehicle. There are two important technical issues that the DTC systems need to handle. The first issue is how to determine the desired tilt angle for the vehicle in different situations. The second issue is the need for a suitable strategy to decrease the required torque that the actuator should apply. Using this method may cause a delay in the vehicle response and create vehicle oscillations. Therefore, complicated control systems are usually required to accommodate different driving conditions [17]. In the STC method, the lateral force between the road and the wheels keeps the vehicle in balance, which is essentially what motorcycles do. In fact, the driver controls the leaning angle by properly steering the front wheels and thus is called "Steering Tilt Control". Steering input by the driver creates a tilting motion that finally approaches a balanced leaning angle. When STC is performed by the driver, it needs significant skill and experiences [16] [17]. One drawback of this method is that it does not work at low speeds. Another drawback is that the balancing is difficult in slippery road because of lack of tire friction force and may cause an unsafe maneuver [17]. One possible option to overcome limitations of each method is to integrate them into a single control system [17]. Specifically, DTC can be used for low speeds while STC is used for high speeds [16]. However, it is a challenge to design such a combined system while having low complexity, high reliability, and low cost [17].

Since the introduction of tilt mechanisms for small narrow vehicles, dynamics of tilting motion has become an integral part of the vehicle dynamics for three-wheeled vehicles. Regarding tilt mechanisms, many researches have been reported in the past decades. Karnopp and Frag originated the idea that narrow vehicles could lean into the turn to prevent rollover similar to the motorcycles [8] [15]. They also discussed the optimum desired lean angle and worked on modeling and tilt control of narrow tilting vehicles describing both DTC and STC systems. A hybrid system that combines both DTC and STC systems was proposed by Snell. In this strategy, the tilting started with STC and then switched to DTC to hold the desired angle [9] [8]. A four-wheeled narrow tilting vehicle is also fabricated at the National Chiao Tung University in Taiwan [2] [18]. This diamond shape vehicle is

equipped with a double loop PID controller for control of both tilt angle and its rate. Also, a three-wheeled tilting vehicle was designed with a tilting mechanism on the vehicle's body at the University of Bath. The controller of this vehicle worked based on the DTC concept [9]. Notable studies have been carried out at the University of Minnesota since 2002 where several papers for modeling and control of tilting three-wheeled vehicles have been published [1] [16] [19] [20] [21] [22]. They also proposed several strategies for tilt control such as an RHC (Receding Horizon Control) based on LQR design criterion combined with a PD controller [20]. They designed and constructed a tilting three-wheeled prototype and implemented different control methods to verify the simulation results (Figure 2-2) [22].

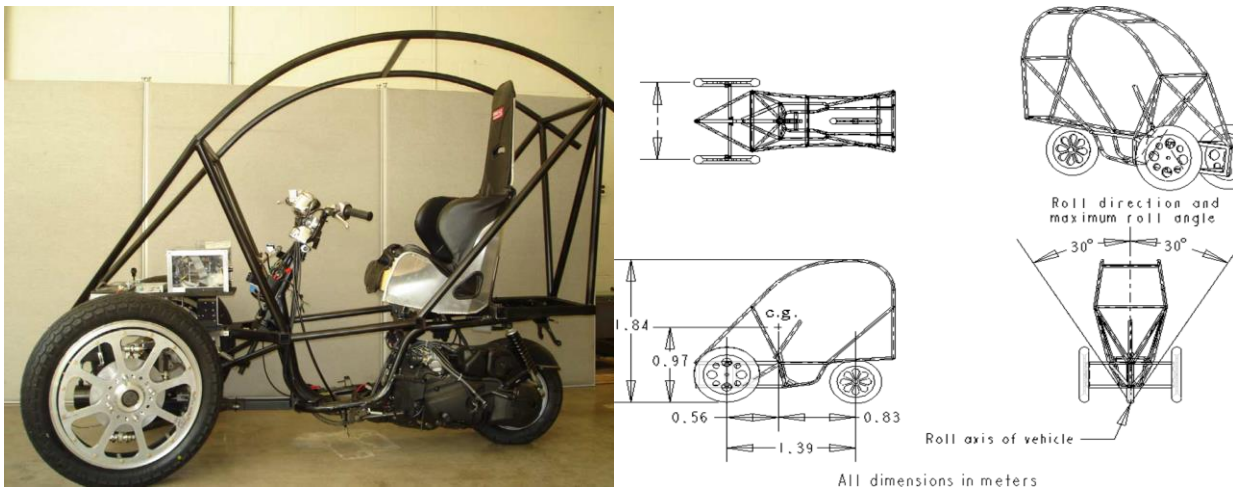

Figure 2-2: Tilting three-wheeled vehicle designed at University of Minnesota [22]

2.1.3 Industrial urban vehicles

In the 1950s, a two wheeled vehicle equipped with a gyroscopic stabilization system called Gyron was proposed by Ford Motor Company [6] (Figure 2-3a) and built later. The unique aspect of this design was to use a gyroscope to stabilize the leaning vehicle in cornering. It could tolerate cornering at lateral accelerations up to 1.0g's [6] [8].

Also, in 1960s a tilting vehicle was fabricated at MIT based on a motorcycle design. It was proposed as a small narrow commuter vehicle for reducing parking problems in big cities. The vehicle was equipped with an "active roll mode suspension" to provide tilting motion with a roll center at the ground level for decoupling vertical and roll motions of the suspension system. One major disadvantage of this vehicle was that the control system was not fast enough to handle transient

responses because of the low bandwidth of the sensors and actuators and added complexity of the non-electronic sensors besides poor conceptual design [6].

Another famous design was the "Lean Machine" proposed by General Motors in 1970s (Figure 2-3b). This three-wheeled delta-shape tilting vehicle worked similar to a motorcycle in cornering controlled by the driver. It had a non-tilting rear pod and a tilting front body. Tilting mechanism was not working automatically and was controlled by the driver through foot pedals, so the driver needed to learn how to control the tilting motion. This characteristic was the main drawback of this vehicle [6] [8]. The major advantages of these vehicles were efficient aerodynamic shapes, low energy consumption, and decreased parking space [6].

(a) (b)

Figure 2-3: a) Gyron [23]**, and b) Lean Machine** [24]

(a) (b)

Figure 2-4: Mercedes Benz F-300 Life-Jet: a) rear view [25]**, b) front view** [26]

A three-wheeled vehicle has also been developed by Mercedes-Benz called F-300 Life-Jet [22] (Figure 2-4). This vehicle employs a hydraulic actuator to realize an active tilt control system. However, its track width is approximately 1.56m which is similar to an average sedan and cannot provide the advantages of narrow vehicles.

Carver is another interesting three-wheeled vehicle which has been commercially available in Europe [22] [27] (Figure 2-5a). This vehicle, proposed by Brink Dynamics, has one wheel in front and two in rear (Delta-shape). This vehicle is the first commercial leaning vehicle and is equipped with non-tilting rear wheels and a tilting body. The front wheel applies steering and the rear wheels drive the vehicle.

Smera is a four-wheeled two-seater tilting vehicle developed by Lumeneo [8] [28] (Figure 2-5b). The vehicle's length and width are 2500 mm and 820 mm, respectively, and it can have maximum of 25 degree of tilting. This electric vehicle is regulated as a car in Europe and has a maximum speed of 80 mph (128.7 km/h) with a range of 90 mile (145 kilometers) for a single charge. Lumeneo Neoma was the production version of this vehicle that was commercially available in May 2013 but the company filed for bankruptcy in November 2013.

(a) (b)

Figure 2-5: a) Carver [29]**, and b) Lumeneo Smera** [30]

A narrow tilting concept is also proposed by Nissan at 2009 called Land Glider [8] [31] (Figure 2-6). This four-wheeled vehicle can have 17 degrees of tilting for cornering. This electric car is also equipped with a wireless charging system.

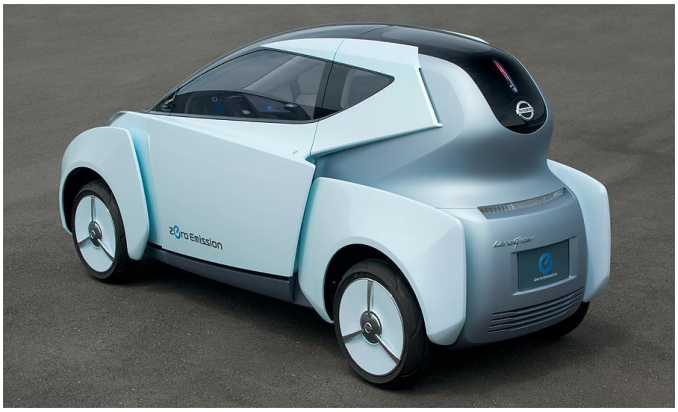

Figure 2-6: Land Glider designed by Nissan [32]

One of recent developments in the field of urban vehicles is the Toyota i-Road [33] (Figure 2-7). This vehicle is often considered as a Personal Mobility Vehicle. This Tadpole-shape three-wheeled vehicle is a two-seater all-electric vehicle designed for short distance urban areas and can travel for about 30 miles (48 km) on a single charge. This vehicle also is equipped with an active tilting system that can automatically balance the vehicle. This completely narrow vehicle has a track width of 85 cm.

(a) (b)

Figure 2-7: Toyota i-Road [34]

2.2 Vehicle Stability Control

In order to improve vehicles' performance and safety and enhance their stability, handling, and comfort, active control systems are widely designed and implemented since the late 1970s. Generally, these systems are called vehicle dynamics control (VDC) systems and can be classified as follows [35][36][37]:

1. Vertical control systems such as active suspension systems (ASS), semi-active suspension systems, and active body control (ABC). They are developed for improvement in vehicle's ride comfort and to some extent for vehicle's handling.
2. Longitudinal control systems that are related to braking and traction including anti-lock brake systems (ABS), traction control systems (TCS), and electronic stability program (ESP).
3. Lateral control systems that control yaw and lateral motions and are developed for improvement of lateral stability and handling of vehicles. Electric power steering system (ESP), active front steering (AFS), active four-wheel steering (4WS), differential braking, and differential traction are some examples of this category.
4. Rollover prevention systems that prevent the vehicles from rolling over in harsh situations. Roll motion also affects handling and safety of the vehicles, so active roll control is also considered for improvement of planar motion. Active suspension systems and active anti-roll bar are two examples of these control systems.

Parts of vehicle dynamics control systems are related to vehicle stability and are called active stability (or safety) systems. These systems are developed to prevent vehicles from spinning, drifting, and rolling over thus increasing vehicle safety [38]. The most important objectives of active stability systems are to provide handling improvement, lateral stability, slip control in traction and braking, and rollover prevention. For normal conditions, active stability systems can compensate for the loss of performance and handling mainly caused by the nonlinearity and saturations of the lateral and longitudinal tire forces. The more important purpose is to assist the driver under harsh conditions such as slippery road or aggressive maneuvers to safely control and stabilize the vehicle. The role of the controller in handling improvement is to provide handling behavior close to the linear vehicle characteristics which is familiar to the driver [39] [40]. Lateral stability control systems are generally designed to prevent skidding and spinning out and to improve vehicle yaw response and lateral motion. The objective of the lateral stability control is to keep the vehicle within the stable handling region in such situations as slippery roads or aggressive maneuvers [39]. For the vehicle's

longitudinal control, the main objective has been the regulation of the longitudinal slip to optimize the braking and traction forces while keeping enough lateral forces for lateral stability [41]. However, longitudinal velocity tracking has also been considered in some studies [41]–[44]. Active rollover prevention systems are introduced to avoid rollover as a serious safety problem. A common approach for rollover prevention is to set up a rollover index (RI) and to restrict the vehicle maneuvers in a safe region through the control of the planar motion [45] [46] [47] [48].

Recent advances in automotive technology have resulted in more precise measurements and/or estimations in real-time. As a result, more advanced controllers have been employed to improve vehicle safety and performance [40]. In particular, the Model Predictive Control (MPC) is widely used in recent years in vehicle stability [49][50][51] and rollover control [52][53].

2.2.1 Lateral stability control

Several approaches are introduced and implemented for the vehicles to obtain the stability and safety objectives. The most important ones are anti-lock brake systems (ABS) [41], [54]–[56], traction control systems (TCS) [57]–[60], differential braking [61], [62] [63], [64], Torque Vectoring (TV) [65]–[68], and active steering (AS) [40], [69]–[73]. Early studies have been focused on tire slip control to improve longitudinal and lateral stability in braking and traction. ABS prevents the wheels from being locked during braking and TCS prevents the wheels from large slips during acceleration. Both of these systems not only increase the longitudinal performance of the vehicle, but also improve lateral stability and handling of the vehicle by control of lateral forces [71]. Differential braking systems and Torque vectoring are later proposed in order to improve handling and lateral stability of the vehicles. Using different brake and traction forces on left and right sides of the vehicle, these systems provide a yaw moment on the vehicle body for yaw motion control and stabilization of the vehicle. Active steering systems are also developed for improvement of handling and stability of vehicles. Active front steering, active rear steering and four-wheel steering systems are different active steering systems that are studied and implemented [74]–[76].

As mentioned, lateral stability systems have been developed by applying yaw moments on the vehicle. Regarding different approaches for providing yaw moment, lateral stability control systems are categorized into two distinct groups [35]:

- *Direct Yaw Control (DYC):* Yaw moment can be applied to the vehicle by an unequal distribution of longitudinal forces on left and right wheels. This method is called DYC and

can be performed from differential braking and differential traction. The most practical method for development of DYC systems is differential braking that can be implemented by modifying ABS systems.

- *Indirect Yaw Control (IDYC):* Steering creates side slip angles and causes change in the lateral force on tires. These changes affect yaw motion of the vehicle. This method of yaw controlling that is carried out from vehicle steering is known as indirect yaw control systems.

In addition to braking, traction, and steering systems, active camber systems are also lately suggested for handling improvement and lateral stability of the vehicle. The suspension systems with the capability of changing the camber angle are developed based on the idea of employing the cambering lateral forces [77][78]. The increased overall lateral force can be used to improve handling and stability of the vehicle. Combinations of actuators have been adopted as well to improve the stability and to handle different control objectives. Nowadays, the advances in vehicle technology provide the opportunities to control different objectives simultaneously through multiple actuators [39]. However, when different control objectives are pursued independently, their control actions may have conflicts and the overall performance of the vehicle may be degraded [79]. To overcome these problems, integrated vehicle dynamics control has been proposed. They improve vehicle behavior through the integration of deferent control objectives and different actuators [36] [79]. One of the most notable examples of integrated stability system in the literature is the integration of active steering and differential braking for handling improvement and lateral stability [39], [50], [64], [80]–[82]. In fact, each of them has better performance for specific regions of handling, so the optimized performance can be achieved by proper combination of them. Integration of torque vectoring and active steering is another example that have been investigated in the literature [63], [83].

2.2.2 Rollover prevention

Vehicle rollover is a serious safety problem for all classes of light vehicles. Rollover accidents contribute to large portion of dangerous and fatal accidents [84]. In the United States, rollover accidents are the second most dangerous form of accident after head-on collisions [11]. Based on a report from National Highway Traffic Safety Administration (NHTSA) in the United States, among about 11 million crashes in 2002 for passenger cars, SUVs, pickups, and vanes, 2.6% were involved in rollover; however, the percentage of fatal crashes caused by rollover accidents was about 21.1% [45]. This statistic shows that although a small portion of all accidents involve rollover, they

constitute to a disproportionately large portion of fatal ones. Considering these facts, many researchers have been studying the methods for improving rollover stability.

Rollover prevention of a vehicle usually includes two steps. A proper detection of a rollover risk is the first step, and the development of an appropriate rollover mitigation strategy is the second step. Undoubtedly, accurate knowledge about the rollover risk of a vehicle is essential in developing a practical rollover prevention system. Several different rollover indices have been proposed in the literature. In [47], the authors investigated some of the widely-used Rollover Indices (RIs) and compared them under different rollover situations. Initially, RIs were defined based on static or steady-state rollover models such as the well-known Static Stability Factor (SSF) [85][86][87]. Various dynamic RIs including vehicle states are also suggested to provide more accurate rollover indication for dynamic situations. The lateral acceleration [88], [89], roll angle [90], [91][92], and roll rate [52], [93] have been used as simple dynamic indicators of the rollover risk. A linear combination of the lateral acceleration, roll angle, and roll rate has also been suggested [84]. By far, the most realistic RI is the lateral load transfer ratio (LTR), which is widely considered for dynamic situations. Since the vertical tire forces cannot be measured easily [94] [95], different representations of the LTR are suggested in terms of measurable vehicle parameters and states. The different representations are suggested based on the vehicle's body parameters [94], [96], [97], suspension parameters [23][24][99], or tire deflection [100]–[102].

Once an appropriate RI is chosen, the next step is to develop a rollover prevention controller to avoid the rollover. The existing rollover prevention methods can be categorized into two types [45]:

1. The methods that directly influence the roll motion and rollover behavior such as active suspensions, active anti-roll bars, and active stabilizers.
2. The methods that indirectly affect the roll motion by control of the planar motion such as differential braking systems and active steering methods.

In the approach of using active suspension for rollover prevention, lateral load transfer is controlled to directly affect the rollover [103] [104]. The rollover stability improved through this approach is limited. Also, the drawback of this approach is that it can influence the lateral stability of the vehicle and cause an over-steer characteristic [103].

The most common approach for indirect control of rollover is based on reduction of the lateral acceleration by decreasing the yaw rate. This approach is implemented through differential braking and active front steering [105] [106]. The limitation of this approach is the loss of maneuverability,

which may cause another accident [45] [103]. Some studies have been conducted to solve this problem for having both rollover prevention and good lateral stability [45] [103] [107] [52].

Generally, for un-tripped rollovers on flat roads, the lateral acceleration is the most dominant factor to cause rollover. Therefore, the most common approach for rollover mitigation is to lower the lateral acceleration which can be achieved by decreasing the yaw rate or the longitudinal speed of the vehicle. Yaw rate reduction can be obtained through lateral stability control with the existing methods such as differential braking, active steering, and torque vectoring [46][99][105][106]. A limitation of this approach is the loss of maneuverability [45][103]. Some studies have been conducted to solve this problem providing both rollover prevention and good lateral stability [45][103][107][52].

Uneven roads and terrains also play crucial roles in rollover. The RIs that consider sloped roads and terrain properties have also been studied in the literature [85][108][109][110][111]. In particular, for some special types of vehicles such as All-Terrain Vehicles (ATVs) or military vehicles, the effects of terrain configuration is critical [110]. More attention has been paid to the impact of banked roads, since it directly affects rollover risk. Road disturbances such as curbs and road bumps may also contribute to rollover even on flat roads. Considering these factors, rollovers are sometimes categorized into two main types: un-tripped rollover and tripped rollover [112]. Un-tripped rollovers refer to rollovers caused by fast maneuvering on smooth roads. On the other hand, the tripped rollovers happen because of sudden impacts that may apply lateral or vertical forces to the vehicle, e.g., digging into soft soil, or hitting road objects such as curbs, guardrails, or bumps. The RIs, introduced in the literature, are mainly for un-tripped rollovers, as discussed so far, and have limitations in detecting tripped rollovers. An RI is introduced by references [95] for both un-tripped and tripped rollovers. Tripped rollovers of three-wheeled vehicles are also investigated by reference [113]. Energy based methods can also be used for tripped rollover to a certain extent, especially when absolute rollover is considered [112].

The rollover stability is a more crucial problem when vehicles are made small and narrow [6] [9] [8]. In fact, there exists a theoretical limit in the minimum width of a vehicle that can ensure safety in standard maneuvers without using active safety systems [6]. To formulate the rollover problem, it is useful to make the distinction between narrow vehicles and conventional vehicles more precisely. The important parameter for defining narrow or tall vehicles is the aspect ratio: the proportion of the center of gravity height to the track width (H/T). To have a better idea on the range of the aspect ratio for existing vehicles, 38 passenger cars have been investigated in [6]. The aspect ratio for passenger

cars ranges from 0.34 to 0.40. Narrow or tall vehicles are defined as the vehicles with considerably greater aspect ratio than these values such as 0.6 [6]. An important characteristic of standard vehicles is that their lateral slip threshold is less than their rollover threshold. Since rollover is more dangerous and fatal than slipping [11], this characteristic acts as a passive safety factor [6] [12]. In contrast, the narrow or tall vehicles reach their rollover limit before reaching lateral slip (skidding) [6] which is a fundamental difference between narrow vehicles and standard conventional vehicles. In fact, conventional cars have a passive fail-safe system that can prevent rollover, but there is no similar mechanism for narrow or tall vehicles [6]. Since this problem cannot be solved without active safety systems, development of vehicles with narrow track width have not been a practical alternative for conventional cars so far.

Rollover stability of the 3W vehicles has also been investigated in the literature. The main difference from the rollover of 4W vehicles is that, for the 3W vehicles, the axis which the vehicle rolls about is not at the center of the vehicle. The vehicle rolls about the line joining the single wheel to one of the wheels on the two-wheeled axle, aptly named, the tipping axis [9]. Rollover stability of both Delta-shape and Tadpole-shape is studied in reference [14], which is one of the primary studies about 3W vehicles, and the results are also compared to standard 4W vehicles. In order to explore the rollover stability of 3W vehicles, the moments about the tipping axis are calculated. The overturning moment, mainly caused by lateral and longitudinal accelerations, must be less than the holding gravitational moment during different vehicle maneuvers to ensure rollover stability of the vehicle. Three different maneuvers are explored in that study including steady state turning, acceleration in a turn, and braking in a turn. For each maneuver, a different inequality is derived in terms of vehicle parameters and states. These inequalities represent the necessary constraints on the maximum lateral and longitudinal accelerations to prevent rollover. However, no explicit function is provided for the maximum value of the lateral acceleration that the vehicle can tolerate when the vehicle maneuver includes longitudinal acceleration. In addition, a separate equation should be used for each maneuver. Some important effects have not been considered either such as the roll and pitch effects and the effects of road grade and bank angle. In fact, using the approach from [14] to determine rollover stability limit (calculation of moments about the tipping axis) results in a complicated geometry that makes it hard to incorporate more complexities of the vehicle, such as roll and pitch angles and road bank and grade effects. When comparing 3W vehicles to the rollover stability of 4W vehicles, the aforementioned study has shown that the 3W vehicles cannot provide similar rollover stability. Later studies also have used similar approaches to investigate rollover stability by calculating the maximum

moment about the tipping axis that is tolerable by the vehicle [114], [115]. Explicit equations for the maximum lateral acceleration that also include the effects of longitudinal acceleration and roll angle are provided for both 3W configurations [116].

2.2.3 Integrated Vehicle Dynamics Control

Despite the advantages of vehicle dynamics control systems, when they work independently in a vehicle, some problems may arise. First, as the number of control systems and their capabilities increases, additional sensors, actuators, and other equipment are required. As a result, the design of software and hardware would be more complicated. Second, since the vehicle dynamics are inherently coupled, when the control systems work independently their control actions may have conflicts. Sometimes, the overall performance of the vehicle may be worse than each independent subsystem or even worse than a vehicle without any control system [79]. For instance, ABS and ESP both work based on control of slip ratio. The former, wants to keep the wheel slip ratio around peak friction coefficient for good braking, while the latter wants to improve vehicle stability and, regarding this objective, may determine different slip ratios for the wheels [79].

To overcome these problems, an approach called integrated vehicle dynamics control has been proposed that improves vehicle behavior in handling, comfort, safety, and other performance criteria through coordination of all vehicle control systems [36] (Figure 2-8).

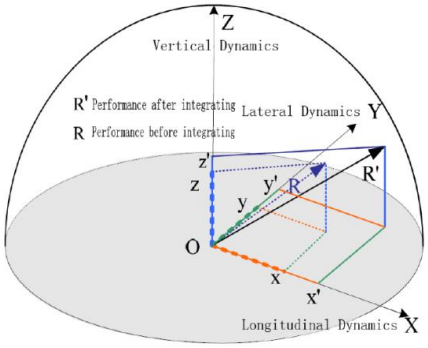

Figure 2-8: improvement of performance via integrated control [36]

The integrated vehicle dynamics control is intended to have two important advantages [79]:

1. Prevent conflicts of control objectives and actions of subsystems.
2. Achieve capacities of all subsystems by coordinating them.

Usually, IVDS is developed to systematically coordinate control objectives of several subsystems considering both software and hardware [79].

2.2.4 Reconfigurable Vehicle Dynamics Control

Design of a reconfigurable controller can be considered for both off-line and real-time situations. The off-line reconfigurable control design provides the users with the freedom to choose every configuration of actuators based of needs and working conditions by activating or deactivating any of them. In fact, having a general and reconfigurable controller, it is not required to reformulate the problem for adding or subtracting any actuator, and the reconfigurable controller can be easily adjusted to the new configuration. Reconfigurable control design also provides another important advantage when it is used for the real-time controllers. Real-time reconfigurable controllers have a significant capability to deal with failures in actuators. Since they are updating at every time-step, they can adjust with the new situation of failing of any actuator by redistribution of control efforts on the remaining actuators.

As a new approach for vehicle stability enhancement, especially for over-actuated vehicles, Control Allocation (CA) approach has been introduced into the ground vehicles, recently [117]. The control allocation approach matches the actual moment and forces of the vehicle to the desired ones while providing an optimal set of actuator commands and considering the constraints. This approach is generally useful when the number of actuators is more than the control objectives and different configurations of actuators are possible for obtaining the same results. In addition to the important achievement of optimally distributing the control efforts, an essential feature of control allocation approach is that of on-line reconfiguration ability. In fact, if any actuator fails during the mission, this approach can redistribute the control efforts among the other actuators to compensate for failure of that actuator [118]. A control allocation algorithm is used to design a reconfigurable control system for dealing with braking actuator failures in a vehicle equipped with brake-by-wire and steer-by-wire systems in reference [119]. Also, a coordinated reconfigurable vehicle dynamics control is provided by reference [117] in which an innovative control allocation scheme is introduced for distributing the generalized forces/moment to the slip and slip angle of each tire.

Another useful approach for an on-line reconfigurable control design is using an MPC controller which solves a constraint optimization at each step-time. Such a real-time controller appropriately matches the purpose of having a reconfigurable controller and in dealing with actuator failures. A reconfigurable flight controller by using MPC as an optimization-based control method is reported in reference [120].

2.3 Camber mechanism

Camber is the tilt of the wheels relative to the vertical surface as viewed from front or rear (Figure 2-9). A tire that tilts outward at the top is defined to have a positive camber angle and a tire with inward tilt at the top is defined to have a negative one as shown in Figure 2-9. Camber angle results in a lateral force on the wheel known as camber thrust or camber force [121]. For the conventional suspension systems, small predetermined amount of positive or negative camber angles are applied when they are designed to improve handling and steering of the vehicle; these small camber angles are not variable. In addition to these designed camber angles, the vehicle body's roll in cornering and the jounce and rebound can also result in camber change. This kind of cambering is not desirable and can degrade the handling properties.

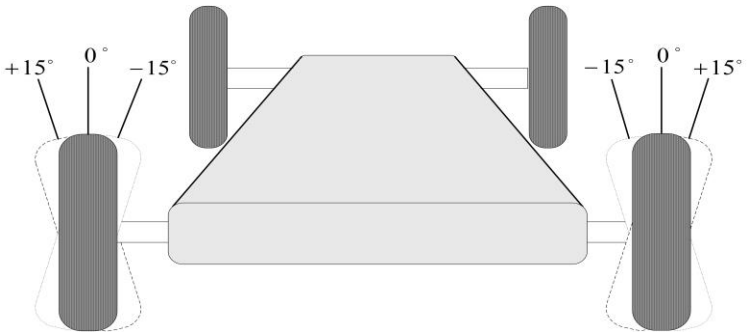

Figure 2-9: wheel's cambering

Recently, the suspension systems with the capability of purposefully changing the camber angle are developed based on the idea of employing the cambering lateral force. The new suspension systems have additional degree of freedom for changing the camber angle in order to improve handling and stability of the vehicle. There are a few studies that have considered camber mechanism and camber control in vehicles. As an interesting research project, an active camber system is developed at Stanford University with the goal of increasing vehicle maneuverability [77]. Based on this study, cambering can increase tire lateral force up to 30% thereby considerably enhancing turning capacity of the vehicles and making them more maneuverable. The first part of this study is about tires suitable for camber change. In fact, conventional tires are not appropriate for large camber angles, so the vehicles need to have specialized tires to achieve advantages of cambering. At the second part, an active camber suspension system is developed. A prototype has also been constructed to validate the performance of the suspension system and different tires.

In another study, a variable geometry suspension system is designed to recognize camber change for improvement of vehicle stability [122]. This suspension system is controlled with a robust control system that automatically changes the camber angles of the rear wheels. The control system is responsible for enhanced vehicle performance in various situations considering roll stability and geometry limits. Also, an electronic camber suspension mechanism is proposed that can decrease the undesirable camber angle in conventional vehicles [123]. It is shown that reducing unwanted camber angle improves the vehicle stability including yaw rate and lateral acceleration. This suspension system is designed by improvement in double wishbone type suspension and a control system is established using the bicycle model for the vehicle. In fact, for non-controlled vehicle the unwanted camber angle contributes to increasing yaw rate and side slip angle resulting in vehicle instability. In contrast, for the controlled vehicle, reduction in camber angle helps the vehicle to have better cornering performance and to improve lateral stability. As another research, a system is introduced to modify roll steer characteristics of the vehicle by controlling rear wheel camber [124]. This modification results in stability factor increase for about 11%. The main advantage of this system is that it can be implemented using a simple mechanism. It is demonstrated that this improvement can be applied to various vehicles. Another important active camber system is designed for Mercedes F400 Carving Concept which is developed in 2002 [77] [125] (Figure 2-10). The purpose of this design is to show the capability of this new technology for increasing lateral force and utilization of potential friction capacity. A special suspension system with special tires is designed for this vehicle that can provide a cambering angle of 20 degrees for outer wheels in a turn. It is shown that this mechanism can increase the peak lateral force by 28%.

Figure 2-10: Mercedes Benz F400 [77]

Chapter 3: Reconfigurable Vehicle Model

This chapter introduces a general reconfigurable vehicle model for analysis, design, and stability control of four- and three-wheeled vehicles with different types of control actuation including differential braking, torque vectoring, active steering, and active camber. The proposed vehicle model provides modeling of four-wheeled vehicles and Tadpole and Delta configurations of three-wheeled vehicles in one set of equations. The vehicle model is also reconfigurable in the sense that different configurations of control actuation can be accommodated for control design of various vehicles without reformulating the problem. To develop the reconfigurable vehicle model, a matrix approach is introduced for vehicle modeling. Two reconfiguration matrices are defined called the corner reconfiguration matrix and the actuator reconfiguration matrix that are responsible for wheel and actuator configurations of the vehicle, respectively. Simulation results for four-wheeled and three-wheeled vehicles are provided using high-fidelity CarSim models.

3.1 Reconfigurable Vehicle Model

The reconfigurable vehicle model can be derived in three steps. At first, the relation between local tire forces at each corner and the corresponding total corner forces are derived using the introduced actuator reconfiguration matrix. Then, the relation between corner forces and the total CG forces and moment are provided including the introduced corner reconfiguration matrix. As the third step, the equations for vehicle's body dynamics are provided assuming forces and moment on CG as the inputs. Combining the three sets of equations together with the reconfiguration matrices, the reconfigurable full vehicle model from tire local forces to the vehicle states can be achieved. The procedure is explained in detail as follows.

3.1.1 Corner forces

In general, the vehicle is assumed to be equipped with three different actuators on each wheel including torque/brake, steering, and camber control. As shown in Figure 3-1, local forces are expressed in the axes attached to the tire and include the longitudinal force from torque/brake and the lateral force from steering and camber. Each local force includes a term from the driver command and a correction term applied by the controller. The resultant of all local forces on each wheel is a set of total longitudinal and lateral forces on the corner called corner forces for the corresponding wheel.

The local driver and controller forces and the associated corner forces for a single wheel are shown in Figure 3-1.

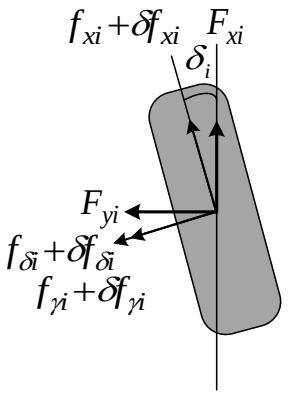

Figure 3-1: Local and corner forces on a wheel

The relation between local tire forces and corner forces for wheel number i can be described as:

$$F_{xi} = (f_{xi} + t_{xi}\delta f_{xi})\cos\delta_i - (f_{\delta i} + t_{\delta i}\delta f_{\delta i})\sin\delta_i - (f_{\gamma i} + t_{\gamma i}\delta f_{\gamma i})\sin\delta_i \quad (3\text{-}1)$$

$$F_{yi} = (f_{xi} + t_{xi}\delta f_{xi})\sin\delta_i + (f_{\delta i} + t_{\delta i}\delta f_{\delta i})\cos\delta_i + (f_{\gamma i} + t_{\gamma i}\delta f_{\gamma i})\cos\delta_i \quad (3\text{-}2)$$

where f_{xi}, $f_{\delta i}$, and $f_{\gamma i}$ denote the local longitudinal, steering, and camber forces for wheel number i, respectively. δf_{xi}, $\delta f_{\delta i}$, and $\delta f_{\gamma i}$ show the corrections on the corresponding local forces applied by the controller. F_{xi} and F_{yi} are the longitudinal and lateral corner forces, and δ_i is the steering angle. The parameters t_{xi}, $t_{\delta i}$, and $t_{\gamma i}$ are binary values defined with respect to the longitudinal force, steering force and camber force, respectively. These parameters can take either 1 (the corresponding actuator is available) or 0 (the actuator is not available). The equations can be written in matrix forms to facilitate reconfigurable vehicle model formulation. The local forces can be written in a vector as:

$$f_i = [f_{xi}, f_{\delta i}, f_{\gamma i}]^T \quad (3\text{-}3)$$

Similarly, the correction inputs applied by the controller can be written as:

$$\delta f_i = [\delta f_{xi}, \delta f_{\delta i}, \delta f_{\gamma i}]^T \quad (3\text{-}4)$$

The corner force vector for the i^{th} wheel F_{ci}, is also shown as:

$$F_{ci} = [F_{xi}, F_{yi}]^T \quad (3\text{-}5)$$

Then, the local actuator reconfiguration matrix for wheel number i can be defined as a diagonal matrix with t_{xi}, $t_{\delta i}$, and $t_{\gamma i}$ as:

$$T_{wi} = \begin{bmatrix} t_{xi} & 0 & 0 \\ 0 & t_{\delta i} & 0 \\ 0 & 0 & t_{\gamma i} \end{bmatrix} \tag{3-6}$$

Finally, the mapping matrix L_{wi} can be defined which relates the local tire forces with the corner forces as:

$$L_{wi} = \begin{bmatrix} \cos\delta_i & -\sin\delta_i & -\sin\delta_i \\ \sin\delta_i & \cos\delta_i & \cos\delta_i \end{bmatrix} \tag{3-7}$$

Then, the relation between the corner forces and the local forces including the local actuator reconfiguration matrix for wheel number i in matrix form can be written as:

$$F_{ci} = L_{wi}(f_i + T_{wi}\delta f_i) \tag{3-8}$$

The equations for all four wheels can be combined in one set of equations in a matrix form. More specifically, vectors including all wheels are defined as:

$$f = \begin{bmatrix} {f_1}^T & {f_2}^T & {f_3}^T & {f_4}^T \end{bmatrix}^T \tag{3-9}$$

$$\delta f = \begin{bmatrix} {\delta f_1}^T & {\delta f_2}^T & {\delta f_3}^T & {\delta f_4}^T \end{bmatrix}^T \tag{3-10}$$

$$F_c = \begin{bmatrix} {F_{c1}}^T & {F_{c2}}^T & {F_{c3}}^T & {F_{c4}}^T \end{bmatrix}^T \tag{3-11}$$

where f, δf, and F_c are vectors including local forces, corrections, and corner forces for all wheels. Wheel number 1 to 4 show the front-left, front-right, rear-left, and rear-right wheels, respectively. The local actuator reconfiguration matrices for all wheels can also be combined into one matrix called actuator reconfiguration matrix as:

$$T_w = \text{blockdiag}(T_{w1}, T_{w2}, T_{w3}, T_{w4}) \tag{3-12}$$

The obtained actuator reconfiguration matrix is:

$$T_w = \begin{bmatrix} \begin{bmatrix} t_{x1} & 0 & 0 \\ 0 & t_{\delta 1} & 0 \\ 0 & 0 & t_{\gamma 1} \end{bmatrix} & 0\ 0\ 0\ 0\ 0\ 0\ 0\ 0\ 0 \\ 0\ 0\ 0 & \begin{bmatrix} t_{x2} & 0 & 0 \\ 0 & t_{\delta 2} & 0 \\ 0 & 0 & t_{\gamma 2} \end{bmatrix} & 0\ 0\ 0\ 0\ 0\ 0 \\ 0\ 0\ 0\ 0\ 0\ 0 & \begin{bmatrix} t_{x3} & 0 & 0 \\ 0 & t_{\delta 3} & 0 \\ 0 & 0 & t_{\gamma 3} \end{bmatrix} & 0\ 0\ 0 \\ 0\ 0\ 0\ 0\ 0\ 0\ 0\ 0\ 0 & \begin{bmatrix} t_{x4} & 0 & 0 \\ 0 & t_{\delta 4} & 0 \\ 0 & 0 & t_{\gamma 4} \end{bmatrix} \end{bmatrix} \tag{3-13}$$

The mapping matrices for all wheels can be combined as:

$$L_w = \text{blockdiag}(L_{w1}, L_{w2}, L_{w3}, L_{w4}) \tag{3-14}$$

where L_w is the mapping matrix for all wheels. Then, the final equation for the relation between local and corner forces of all wheels including the actuator reconfiguration matrix is obtained in a matrix form as:

$$F_c = L_w(f + T_w \delta f) \tag{3-15}$$

where $T_w \delta f$ is the effective actuator vector. This term provides the possibility to determine different configurations of actuators for the control design. To illustrate how the actuator reconfiguration matrix works, examples are provided for the cases that are not equipped with full actuators on all wheels. Specifically, let us consider a vehicle equipped with front active steering and rear torque vectoring. The actuator reconfiguration matrix T_w for this case is:

$$T_w = \begin{bmatrix} 0 & 0 & 0 & 0 & 0 & 0 & 0 & 0 & 0 & 0 & 0 & 0 \\ 0 & 1 & 0 & 0 & 0 & 0 & 0 & 0 & 0 & 0 & 0 & 0 \\ 0 & 0 & 0 & 0 & 0 & 0 & 0 & 0 & 0 & 0 & 0 & 0 \\ 0 & 0 & 0 & 0 & 0 & 0 & 0 & 0 & 0 & 0 & 0 & 0 \\ 0 & 0 & 0 & 0 & 1 & 0 & 0 & 0 & 0 & 0 & 0 & 0 \\ 0 & 0 & 0 & 0 & 0 & 0 & 0 & 0 & 0 & 0 & 0 & 0 \\ 0 & 0 & 0 & 0 & 0 & 0 & 1 & 0 & 0 & 0 & 0 & 0 \\ 0 & 0 & 0 & 0 & 0 & 0 & 0 & 0 & 0 & 0 & 0 & 0 \\ 0 & 0 & 0 & 0 & 0 & 0 & 0 & 0 & 0 & 0 & 0 & 0 \\ 0 & 0 & 0 & 0 & 0 & 0 & 0 & 0 & 0 & 1 & 0 & 0 \\ 0 & 0 & 0 & 0 & 0 & 0 & 0 & 0 & 0 & 0 & 0 & 0 \\ 0 & 0 & 0 & 0 & 0 & 0 & 0 & 0 & 0 & 0 & 0 & 0 \end{bmatrix} \tag{3-16}$$

and the effective actuator vector can be obtained as:

$$\begin{bmatrix} 0 \\ \delta f_{\delta 1} \\ 0 \\ 0 \\ \delta f_{\delta 2} \\ 0 \\ \delta f_{x3} \\ 0 \\ 0 \\ \delta f_{x4} \\ 0 \\ 0 \end{bmatrix} = \begin{bmatrix} 0 & 0 & 0 & 0 & 0 & 0 & 0 & 0 & 0 & 0 & 0 & 0 \\ 0 & 1 & 0 & 0 & 0 & 0 & 0 & 0 & 0 & 0 & 0 & 0 \\ 0 & 0 & 0 & 0 & 0 & 0 & 0 & 0 & 0 & 0 & 0 & 0 \\ 0 & 0 & 0 & 0 & 0 & 0 & 0 & 0 & 0 & 0 & 0 & 0 \\ 0 & 0 & 0 & 0 & 1 & 0 & 0 & 0 & 0 & 0 & 0 & 0 \\ 0 & 0 & 0 & 0 & 0 & 0 & 0 & 0 & 0 & 0 & 0 & 0 \\ 0 & 0 & 0 & 0 & 0 & 0 & 1 & 0 & 0 & 0 & 0 & 0 \\ 0 & 0 & 0 & 0 & 0 & 0 & 0 & 0 & 0 & 0 & 0 & 0 \\ 0 & 0 & 0 & 0 & 0 & 0 & 0 & 0 & 0 & 0 & 0 & 0 \\ 0 & 0 & 0 & 0 & 0 & 0 & 0 & 0 & 0 & 1 & 0 & 0 \\ 0 & 0 & 0 & 0 & 0 & 0 & 0 & 0 & 0 & 0 & 0 & 0 \\ 0 & 0 & 0 & 0 & 0 & 0 & 0 & 0 & 0 & 0 & 0 & 0 \end{bmatrix} \begin{bmatrix} \delta f_{x1} \\ \delta f_{\delta 1} \\ \delta f_{\gamma 1} \\ \delta f_{x2} \\ \delta f_{\delta 2} \\ \delta f_{\gamma 2} \\ \delta f_{x3} \\ \delta f_{\delta 3} \\ \delta f_{\gamma 3} \\ \delta f_{x4} \\ \delta f_{\delta 4} \\ \delta f_{\gamma 4} \end{bmatrix} \tag{3-17}$$

As can be seen, the effective actuator vector includes the corrections only on front steering and rear torque/brake inputs. Thus, the controller designed based on this model only provides control actions for these available actuators.

3.1.2 CG forces

As the next step for reconfigurable vehicle modeling, the relation between corner forces and CG forces/moment are derived for both 4W and 3W vehicles. Figure 3-2 illustrates the relation between corner forces and the CG forces/moment.

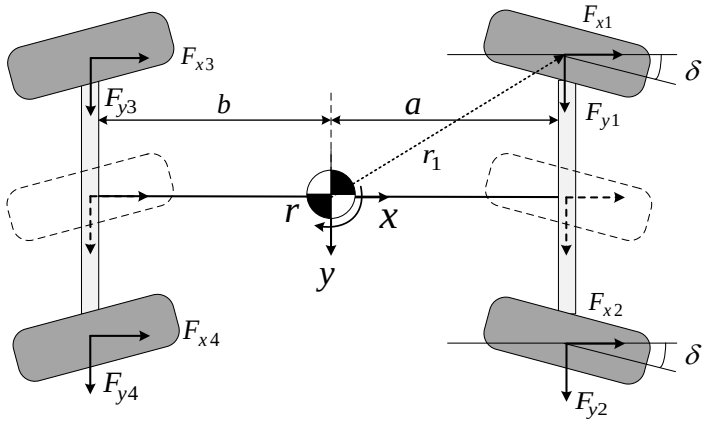

Figure 3-2: Relation between corner forces and CG forces and moment

The total longitudinal force F_X, total lateral force F_Y, and total yaw moment M_Z on CG of the vehicle can be written in terms of corner forces as:

$$F_X = \sum_{i=1}^{4} t_{cxi} F_{xi} \tag{3-18}$$

$$F_Y = \sum_{i=1}^{4} t_{cyi} F_{yi} \tag{3-19}$$

$$M_Z = \sum_{i=1}^{4} r_i \times (t_{ci}{}^T . F_{ci}) \tag{3-20}$$

where t_{cxi} and t_{cyi} are binary parameters (0 or 1) that indicate the presence of the corresponding wheel. t_{ci} is a vector including t_{cxi} and t_{cyi} as $t_{ci} = \left[t_{cxi} \;\; t_{cyi}\right]^T$. r_i is the displacement vector from the CG of the vehicle to the contact point of the tire. If the corner forces for the i^{th} wheel are not available, there is no wheel on that corner and for that wheel $t_{ci} = [0,\ 0]^T$. Then, the model can represent a 3W vehicle. The moment on the CG can be expanded as:

$$\begin{aligned} M_Z = \sum_{i=1,3} \left(\frac{T_i}{2} + R_w \sin\gamma_i\right) t_{cxi} F_{xi} - \sum_{i=2,4} \left(\frac{T_i}{2} + R_w \sin\gamma_i\right) t_{cxi} F_{xi} + a \sum_{i=1,2} t_{cyi} F_{yi} \\ - b \sum_{i=3,4} t_{cyi} F_{yi} \end{aligned} \tag{3-21}$$

T_i is the vehicle track on front or rear associated with the wheel number i. Specifically, the front track for the Delta configuration and the rear track for the Tadpole configuration are zero for the 3W vehicles. R_w is the effective wheel radius, and γ_i is the camber angle for the i^{th} wheel. Eqs. (3-18)-(3-20) can be rewritten in matrix form. Denoting the force vector on CG by F, it can be written as:

$$F = [F_X \;\; F_Y \;\; M_Z]^T \tag{3-22}$$

Then, the corner reconfiguration matrix denoted as T_c, can be defined as:

$$T_c = \begin{bmatrix} t_{cx1} & 0 & 0 & 0 & 0 & 0 & 0 & 0 \\ 0 & t_{cy1} & 0 & 0 & 0 & 0 & 0 & 0 \\ 0 & 0 & t_{cx2} & 0 & 0 & 0 & 0 & 0 \\ 0 & 0 & 0 & t_{cy2} & 0 & 0 & 0 & 0 \\ 0 & 0 & 0 & 0 & t_{cx3} & 0 & 0 & 0 \\ 0 & 0 & 0 & 0 & 0 & t_{cy3} & 0 & 0 \\ 0 & 0 & 0 & 0 & 0 & 0 & t_{cx4} & 0 \\ 0 & 0 & 0 & 0 & 0 & 0 & 0 & t_{cy4} \end{bmatrix} \tag{3-23}$$

and the mapping matrix from corner forces to CG forces is denoted by L_c as:

$$L_c = \begin{bmatrix} 1 & 0 & 1 & 0 & 1 & 0 & 1 & 0 \\ 0 & 1 & 0 & 1 & 0 & 1 & 0 & 1 \\ -T_f/2 - R_w \sin\gamma_1 & a & T_f/2 + R_w \sin\gamma_2 & a & -T_r/2 - R_w \sin\gamma_3 & -b & T_r/2 + R_w \sin\gamma_4 & -b \end{bmatrix} \quad (3\text{-}24)$$

where T_f and T_r denote the vehicle's track for front and rear wheels of the vehicle. Then, the force equation that reflects the relation between corner forces and CG forces and moment is expressed as:

$$F = L_c T_c F_c \quad (3\text{-}25)$$

where $T_c F_c$ is the effective corner forces and moment transferred to the CG. If the vehicle is a 4W vehicle, T_c is an identity matrix. An example is provided to explain the reconfigurable vehicle model for 3W vehicles. For a Delta-configuration 3W vehicle, the second wheel can be removed from the equations by adjusting the effective corner force as:

$$\begin{bmatrix} F_{x1} \\ F_{y1} \\ 0 \\ 0 \\ F_{x3} \\ F_{y3} \\ F_{x4} \\ F_{y4} \end{bmatrix} = \begin{bmatrix} 1 & 0 & 0 & 0 & 0 & 0 & 0 & 0 \\ 0 & 1 & 0 & 0 & 0 & 0 & 0 & 0 \\ 0 & 0 & 0 & 0 & 0 & 0 & 0 & 0 \\ 0 & 0 & 0 & 0 & 0 & 0 & 0 & 0 \\ 0 & 0 & 0 & 0 & 1 & 0 & 0 & 0 \\ 0 & 0 & 0 & 0 & 0 & 1 & 0 & 0 \\ 0 & 0 & 0 & 0 & 0 & 0 & 1 & 0 \\ 0 & 0 & 0 & 0 & 0 & 0 & 0 & 1 \end{bmatrix} \begin{bmatrix} F_{x1} \\ F_{y1} \\ F_{x2} \\ F_{y2} \\ F_{x3} \\ F_{y3} \\ F_{x4} \\ F_{y4} \end{bmatrix} \quad (3\text{-}26)$$

As can be seen, the second wheel is removed from the effective corner forces, so it represents a Delta 3W vehicle.

3.1.3 Vehicle body dynamics

The next step for the development of the reconfigurable vehicle model is to derive the equations of vehicle body dynamics with respect to forces and moment on CG. In this study, four degrees of freedom are considered for the vehicle including the longitudinal motion, the lateral motion, the yaw motion, and the roll motion. Figure 3-3 demonstrates the roll motion of the vehicle.

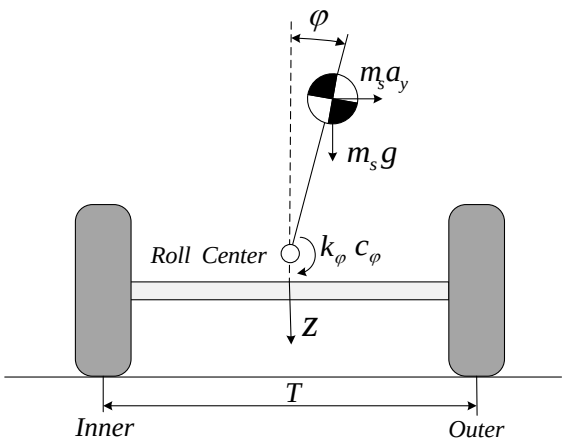

Figure 3-3: Roll motion of the sprung mass

The vehicle body equations have been developed and widely used in the literature [126]. Let u, v, r, and φ denote the longitudinal velocity, the lateral velocity, the yaw rate, and the roll angle, respectively. The equations are:

$$m(\dot{u} - vr) = F_X \tag{3-27}$$

$$m(\dot{v} + ur) + m_s h_s \ddot{\varphi} = F_Y \tag{3-28}$$

$$I_{zz}\dot{r} = M_z \tag{3-29}$$

$$I_{xx}\ddot{\varphi} + m_s h_s(\dot{v} + ur) + c_\varphi \dot{\varphi} + (k_\varphi - m_s g h_s)\varphi = 0 \tag{3-30}$$

where m and m_s are the vehicle's total mass and the sprung mass, respectively. h_s is the distance of the CG of the sprung mass from the roll center. I_{xx}, I_{yy}, and I_{zz} are the roll, pitch, and yaw moments of inertia, respectively. g is the gravitational acceleration. k_φ and c_φ represent the effective torsional stiffness and torsional damping in the roll direction, respectively. Then, choosing the vehicle states as

$$X_b = [u \;\; v \;\; r \;\; \varphi \;\; \dot{\varphi}]^T \tag{3-31}$$

the nonlinear vehicle equations on CG, in matrix form, can be expressed as:

$$h(X_b, \dot{X}_b) = B_{F1}F \tag{3-32}$$

where

$$h(X_b, \dot{X}_b) = \begin{bmatrix} \dot{u} - vr \\ \dot{v} + ur + \dfrac{m_s h_s \ddot{\varphi}}{m} \\ \dot{r} \\ I_{xx}\ddot{\varphi} + m_s h_s(\dot{v} + ur) + c_\varphi \dot{\varphi} + (k_\varphi - m_s g h_s)\varphi \end{bmatrix} \tag{3-33}$$

and

$$B_{F1} = \begin{bmatrix} 1/m & 0 & 0 \\ 0 & 1/m & 0 \\ 0 & 0 & 1/I_{zz} \\ 0 & 0 & 0 \end{bmatrix} \tag{3-34}$$

3.1.4 Reconfigurable full vehicle model

Combining the three layers of vehicle modeling, Eqs. (3-15), (3-25), and (3-32), the final reconfigurable vehicle model including the actuator reconfiguration matrix and the corner reconfiguration matrix can be obtained as:

$$h(X_b, \dot{X}_b) = B_{F1} L_c T_c L_w (f + T_w \delta f) \tag{3-35}$$

This is nonlinear system of vehicle equations not only because of the term $h(X_b, \dot{X}_b)$ but also because of the nonlinearities in tire forces f and δf. The longitudinal and lateral local tire forces, in general, can be written as:

$$f_{xi} = f_{xi}(\alpha_i, S_i, F_{zi}, \gamma_i) \tag{3-36}$$

$$f_{\delta i} = f_{\delta i}(\alpha_i, S_i, F_{zi}, \gamma_i) \tag{3-37}$$

$$f_{\gamma i} = f_{\gamma i}(\alpha_i, S_i, F_{zi}, \gamma_i) \tag{3-38}$$

where α_i, S_i, F_{zi}, and γ_i represent the side slip angle, the slip ratio, the normal force, and the camber angle for wheel number i ($i = 1\ to\ 4$), respectively.

3.2 Linearized reconfigurable vehicle model

In this section, the vehicle body dynamics and tire forces are linearized to provide a general reconfigurable linear state-space form of vehicle model. Some common assumptions in vehicle dynamics control are made to simplify the vehicle model suitable for control design as follows.

3.2.1 Linearized tire forces

The longitudinal forces of tires can be approximated proportional to the torques (denoted by Q_i) of the wheels for small slip ratio as:

$$f_{xi} = \frac{Q_i}{R_w} \tag{3-39}$$

For the lateral tire forces, an affine tire model is used on each corner of the vehicle. The lateral forces are linearized at the operation points of side slip and camber angles by holding the zeroth and first-order terms of the Taylor expansion [40]. Let $\bar{f}_{yi}$, $\tilde{c}_{\alpha_i}$, and $\tilde{c}_{\gamma_i}$ represent the lateral tire force, the cornering coefficient, and the camber coefficient at the side slip and camber angles of the operating point for tire i.Then, the affine tire model can be expressed as:

$$f_{yi} = \bar{f}_{yi} + \tilde{c}_{\alpha_i}(\alpha_i - \bar{\alpha}_i) + \tilde{c}_{\gamma_i}(\gamma_i - \bar{\gamma}_i) \quad for\ i = 1\ to\ 4 \tag{3-40}$$

where α_i and γ_i represent the side slip and camber angles as the variables of the affine tire equation. The terms of the lateral forces for steering and camber can be separated as:

$$f_{\delta i} = \bar{f}_{yi} + \tilde{c}_{\alpha_i}(\alpha_i - \bar{\alpha}_i) \tag{3-41}$$

$$f_{\gamma i} = \tilde{c}_{\gamma_i}(\gamma_i - \bar{\gamma}_i) \tag{3-42}$$

Note that the positive and negative camber angles are defined differently from those in conventional suspension systems. Here, the camber angle is calculated using the coordinate system, and thus having similar values of camber angles means that the wheels are parallel. The side slip angle for tire i can be written as:

$$\alpha_i = \delta_i - \frac{v + a_i r}{u} \tag{3-43}$$

$$a_i = \begin{cases} a & i = 1,2 \\ -b & i = 3,4 \end{cases} \tag{3-44}$$

where a and b are the horizontal distances of the CG to the front and rear tires. Then, the linearized tire forces for tire number i, in matrix from, can be written as:

$$f_i = B_{1i}X_b + B_{2i}W_i + D_{1i} \tag{3-45}$$

where

$$B_{1i} = \begin{bmatrix} 0 & 0 & 0 & 0 & 0 \\ 0 & -\frac{c_{\alpha i}}{u} & -\frac{a_i c_{\alpha i}}{u} & 0 & 0 \\ 0 & 0 & 0 & 0 & 0 \end{bmatrix}, \quad \mathrm{B_{2i}} = \begin{bmatrix} \frac{1}{R_w} & 0 & 0 \\ 0 & c_{\alpha i} & 0 \\ 0 & 0 & c_{\gamma i} \end{bmatrix},$$

$$D_{1i} = \begin{bmatrix} 0 \\ \bar{f}_{yi} - \tilde{c}_{\alpha_i}\bar{\alpha}_i \\ \tilde{c}_{\gamma_i}\bar{\gamma}_i \end{bmatrix}$$

and W_i is the driver's command on wheel number i as:

$$W_i = [Q_i, \delta_i, \gamma_i]^T \tag{3-46}$$

It should be mentioned that the tire forces in Eq.(3-45) include three terms: the first term depends on vehicle states, the second term is the driver's commands, and the last term is a constant vector. Combining the linearized tire forces for all wheels in one set of equations gives

$$f = B_1 X_b + B_2 W + D_1 \tag{3-47}$$

where

$$B_1 = [{B_{11}}^T \ {B_{12}}^T \ {B_{13}}^T \ {B_{14}}^T]^T \tag{3-48}$$

$$B_2 = \mathrm{blockdiag}(B_{21}, B_{22}, B_{23}, B_{24}) \tag{3-49}$$

$$D_1 = [{D_{11}}^T \ {D_{12}}^T \ {D_{13}}^T \ {D_{14}}^T]^T \tag{3-50}$$

$$W = [{W_1}^T \ {W_2}^T \ {W_3}^T \ {W_4}^T]^T \tag{3-51}$$

Using the linearized tire model, the controller input is defined as:

$$\begin{bmatrix} \delta f_{xi} \\ \delta f_{\delta i} \\ \delta f_{\gamma i} \end{bmatrix} = \begin{bmatrix} \frac{1}{R_w} & 0 & 0 \\ 0 & c_{\alpha i} & 0 \\ 0 & 0 & c_{\gamma i} \end{bmatrix} \begin{bmatrix} \Delta Q_i \\ \Delta \delta_i \\ \Delta \gamma_i \end{bmatrix} \tag{3-52}$$

This equation can be written as:

$$\delta f_i = B_{2i} U_i \tag{3-53}$$

where

$$U_i = [\Delta Q_i, \Delta \delta_i, \Delta \gamma_i]^T \tag{3-54}$$

Then, for all wheels, the equation for the control inputs is:

$$\delta f = B_2 U \tag{3-55}$$

where

$$U = [{U_1}^T \ {U_2}^T \ {U_3}^T \ {U_4}^T]^T \tag{3-56}$$

Therefore, the nonlinear terms of tire forces can be replaced by a linear set of equations as:

$$f + T_w \delta f \approx B_1 X_b + B_2 W + D_1 + T_w B_2 U \tag{3-57}$$

3.2.2 Linearized vehicle body dynamics

The other source of nonlinearity is the vehicle body equations. However, linear vehicle body equations are used commonly in vehicle dynamics studies. An important step to obtain a linear vehicle model is to separate the longitudinal dynamic equation from the equations for the lateral, yaw, and roll dynamics. Ignoring the effects of the lateral motion on longitudinal dynamics and adding other important effects, a revised linear model is used for the longitudinal dynamics as:

$$m\dot{u} = F_X - F_{rr} - F_a - F_g \tag{3-58}$$

where F_{rr}, F_a, and F_g are the rolling resistance force, the aerodynamic force, and the gravity force (due to the road grade), respectively [44]. Separating longitudinal dynamics from the equations for the lateral, yaw, and roll motions, the longitudinal speed is assumed as a vehicle parameter in these equations to avoid nonlinearity. Then, Eqs. (3-28), (3-29), and (3-30) can be considered as a linear integrated set of equations for lateral, yaw, and roll motions. These three equations can be rearranged to have explicit equations for $\dot{v}$, $\dot{r}$, and $\ddot{\varphi}$. Then, the linearized vehicle's body equations, in matrix form, can be written as:

$$\dot{X}_b = A_F X_b + B_F F + D_F \tag{3-59}$$

where

$$A_F = \begin{bmatrix} 0 & 0 & 0 & 0 & 0 \\ 0 & 0 & -u & \dfrac{m_s h_s (k_\varphi - m_s g h_s)}{(-{m_s}^2 {h_s}^2 + m I_{xx})} & \dfrac{m_s h_s c_\varphi}{(-{m_s}^2 {h_s}^2 + m I_{xx})} \\ 0 & 0 & 0 & 0 & 0 \\ 0 & 0 & 0 & 0 & 1 \\ 0 & 0 & 0 & \dfrac{-m(k_\varphi - m_s g h_s)}{(-{m_s}^2 {h_s}^2 + m I_{xx})} & \dfrac{-m c_\varphi}{(-{m_s}^2 {h_s}^2 + m I_{xx})} \end{bmatrix} \tag{3-60}$$

$$B_F = \begin{bmatrix} 0 & & \\ \frac{1}{m} & \frac{I_{xx}}{\left(-{m_s}^2{h_s}^2 + mI_{xx}\right)} & 0 \\ 0 & & 0 \\ 0 & 0 & \frac{1}{I_{zz}} \\ 0 & & 0 \\ 0 & \frac{m_s h_s}{\left(-{m_s}^2{h_s}^2 + mI_{xx}\right)} & 0 \end{bmatrix} \tag{3-61}$$

$$D_F = \begin{bmatrix} \frac{1}{m}\left(-F_{rr} - F_a - F_g\right) \\ 0 \\ 0 \\ 0 \\ 0 \end{bmatrix} \tag{3-62}$$

3.2.3 Reconfigurable state-space equation

Using the linear equations for tire forces and vehicle body dynamics and combining Eqs. (3-15), (3-25), and (3-57), then substituting into (3-59) results in:

$$\dot{X}_b = A_F X_b + B_F L_c T_c L_w (B_1 X_b + B_2 W + D_1 + T_w B_2 U) + D_F \tag{3-63}$$

Rearranging the elements in Eq. (3-63) and writing in standard state-space form, the linearized reconfigurable state-space vehicle model is achieved as:

$$\dot{X}_b = A_b X_b + E_b W + B_b U + D_b \tag{3-64}$$

$$X_b = [u \;\; v \;\; r \;\; \varphi \;\; \dot{\varphi}]^T \tag{3-65}$$

$$W = [Q_1 \;\; \delta_1 \;\; \gamma_1 \;\; Q_2 \;\; \delta_2 \;\; \gamma_2 \;\; Q_3 \;\; \delta_3 \;\; \gamma_3 \;\; Q_4 \;\; \delta_4 \;\; \gamma_4]^T \tag{3-66}$$

$$U = [\Delta Q_1 \;\; \Delta\delta_1 \;\; \Delta\gamma_1 \;\; \Delta Q_2 \;\; \Delta\delta_2 \;\; \Delta\gamma_2 \;\; \Delta Q_3 \;\; \Delta\delta_3 \;\; \Delta\gamma_3 \;\; \Delta Q_4 \;\; \Delta\delta_4 \;\; \Delta\gamma_4]^T \tag{3-67}$$

where

$$A_b = A_F + B_F L_c T_c L_w B_1 \tag{3-68}$$

$$E_b = B_F L_c T_c L_w B_2 \tag{3-69}$$

$$B_b = B_F L_c T_c L_w T_w B_2 \tag{3-70}$$

$$D_b = B_F L_c T_c L_w D_1 + D_F \tag{3-71}$$

It should be noted that the matrices of the reconfigurable state-space vehicle model are expressed in terms of the introduced actuator reconfiguration matrix and corner reconfiguration matrix.

3.3 Reconfigurable vehicle model including wheel dynamics

To provide a more general control model, the wheel dynamics can also be added to the system's equations for slip control. This section explains how the wheel dynamic can be added to the reconfigurable vehicle model.

3.3.1 Wheel dynamics

The dynamics equation for rotation of wheel number i can be written as:

$$I_w\dot{\omega}_i = Q_i + \Delta Q_i - R_w\bar{f}_{xi} \tag{3-72}$$

where I_w is the rotational moment of inertia and ω_i is the rotational speed. $\bar{f}_{xi}$ is the measured or estimated longitudinal force. Slip ratio (S_i) is defined as:

$$S_i = \frac{R_w\omega_i - u}{\max(u, R_w\omega_i)} \tag{3-73}$$

Denoting $X_w = [\omega_1 \;\; \omega_2 \;\; \omega_3 \;\; \omega_4]^T$, the state-space equation for the wheel dynamics can be written as:

$$\dot{X}_w = A_w X_w + E_w W + B_w U + D_w \tag{3-74}$$

$$X_w = [\omega_1 \;\; \omega_2 \;\; \omega_3 \;\; \omega_4]^T \tag{3-75}$$

where A_w, E_w, B_w, and D_w are system matrices for the wheel dynamics. It should be noted that Eq. (3-74) is deliberately written with respect to W and U which also show up in Eq. (3-64). This formulation is useful for combining the vehicle dynamic equations with wheel equations as provided in the next subsection.

3.3.2 General reconfigurable state-space equation

The linearized vehicle dynamics equations and the wheel dynamics equations can be combined to provide a general reconfigurable vehicle model in state-space form. The new state vector is defined as:

$$X = [X_b^T \;\; X_w^T]^T = [u \;\; v \;\; r \;\; \varphi \;\; \dot{\varphi} \;\; \omega_1 \;\; \omega_2 \;\; \omega_3 \;\; \omega_4]^T \tag{3-76}$$

Then, the final equations for the general reconfigurable vehicle model in standard state-space form can be achieved as:

$$\dot{X} = AX + EW + BU + D \tag{3-77}$$

where

$$A = \text{blockdiag}(A_b, A_w) \tag{3-78}$$

$$E = [E_b^T \;\; E_w^T]^T \tag{3-79}$$

$$B = [B_b^T \;\; B_w^T]^T \tag{3-80}$$

$$D = [D_b^T \;\; D_w^T]^T \tag{3-81}$$

3.4 Simulation results

The performance of the proposed reconfigurable vehicle model Eq. (3-77) is evaluated through simulations of the Delta and Tadpole configurations of 3W vehicles as well as a conventional 4W vehicle. The results are then compared with high-fidelity CarSim simulations. CarSim provides comprehensive and efficient simulation for the performance of vehicles which can be used for vehicle dynamics analysis and active controllers' development. CarSim is a well-known and widely used software with the real-world validation of about twenty years by automotive researchers [127]. The multibody systems such as rigid bodies, fluids, tires, and other dynamic parts are modeled by ordinary differential equations (ODEs). There are 15 mechanical degrees of freedom with over 110 ordinary differential equations for the multibody mechanical system of a four-wheeled vehicle. To fully express the state of a vehicle, about 200 state variables are defined including the ODE variables and others. Several tire models are included in CarSim. Table-based tire models are used for the simulated vehicles in this study. The tables includes nonlinear lateral and longitudinal forces and aligning and overturning moments as functions of slip, load, and camber. The relations between lateral and longitudinal forces are also considered using the combined slip theory based on Pacejka and Sharp studies [127].

The vehicle parameters for the three cases are shown in Table 3-1.

Table 3-1: Vehicles' Parameters

Parameters	*Definition*	*Delta-3W*	*Tadpole-3W*	*SUV*	*Unit*
m	Vehicle mass	867	867	1860	kg
m_s	Sprung mass	747	747	1590	kg
m_u	un-sprung mass	120	120	270	kg
T	Vehicle track	1.05	1.05	1.575	m
H	CG height	0.5026	0.5026	0.72	m
l	Wheelbase	2.025	2.025	2.95	m
a	Horizontal distance from CG to front tires	1.350	0.675	1.18	m
b	Horizontal distance from CG to rear tires	0.675	1.350	1.77	m
I_{xx}	Roll Inertia	288.4	288.4	894.4	kg/m^2
I_{zz}	Yaw Inertia	1242.4	1111	2687.1	kg/m^2
h_s	CG to roll center distance	0.44	0.40	0.57	m
h_u	Un-sprung mass CG height	0.2	0.2	0.2	m
h_R	Roll center to ground distance	0.0625	0.1025	0.15	m
k_φ	Effective torsional stiffness	28429	32923	189506	N/rad
c_φ	Effective torsional damping	1604	1604	6364	$N.s/rad$
R_w	Effective wheel radius	0.268	0.268	0.393	m
I_w	Wheel rotational inertia	0.6	0.6	1.1	kg/m^2

The reconfigurable vehicle model can be simply used for a specific vehicle by including the corresponding vehicle parameters and adjusting the reconfiguration matrices. The performance of the vehicle model is evaluated for modeling of the integrated lateral, longitudinal, yaw, and roll motions of vehicles. Three specific cases are considered in the simulation. In the first case, the proposed model is used to simulate the dynamic behavior of a Delta-configuration of 3W vehicles. This vehicle is assumed to be rear-wheel drive with front steering. In the second case, a Tadpole-configuration of 3W vehicles is considered. The assumed Tadpole case is three-wheel drive and three-wheel steering. As the next case, the proposed model is used to simulate a SUV, four-wheel drive with front steering, as a conventional 4W vehicle. The longitudinal dynamics in accelerating and braking is also considered in this case, and the performance of the proposed model is examined through an integrated maneuver including lateral, longitudinal, yaw, and roll motions. It should be mentioned that the introduced vehicle model needs the inputs on the wheels to provide the vehicle dynamic responses. Thus, whether the vehicle is conventional or electric vehicle, as long as the applied torque, steering,

and camber angle on the wheels are known, the vehicle model can be used to simulate vehicle dynamics.

3.4.1 Vehicle model for a Delta 3W vehicle

Figure 3-4 shows a 3W vehicle in Delta configuration with rear-wheel drive and front steering.

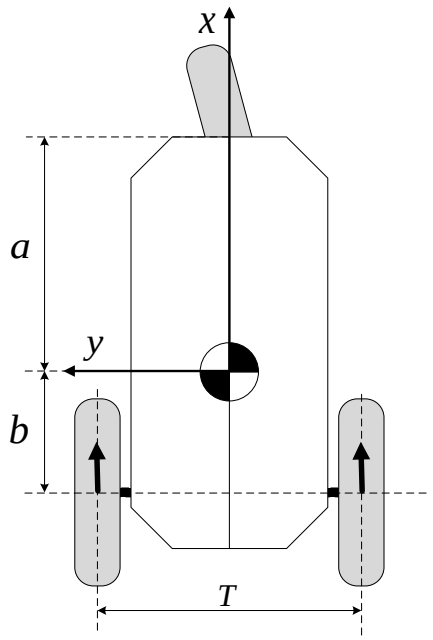

Figure 3-4: A Delta-configuration 3W vehicle with rear-wheel drive and front steering

The corner reconfiguration matrix and the actuator reconfiguration matrix for this case are:

$$T_c = \begin{bmatrix} 1 & 0 & 0 & 0 & 0 & 0 & 0 & 0 \\ 0 & 1 & 0 & 0 & 0 & 0 & 0 & 0 \\ 0 & 0 & 0 & 0 & 0 & 0 & 0 & 0 \\ 0 & 0 & 0 & 0 & 0 & 0 & 0 & 0 \\ 0 & 0 & 0 & 0 & 1 & 0 & 0 & 0 \\ 0 & 0 & 0 & 0 & 0 & 1 & 0 & 0 \\ 0 & 0 & 0 & 0 & 0 & 0 & 1 & 0 \\ 0 & 0 & 0 & 0 & 0 & 0 & 0 & 1 \end{bmatrix} \qquad T_w = \begin{bmatrix} 0 & 0 & 0 & 0 & 0 & 0 & 0 & 0 & 0 & 0 & 0 & 0 \\ 0 & 1 & 0 & 0 & 0 & 0 & 0 & 0 & 0 & 0 & 0 & 0 \\ 0 & 0 & 0 & 0 & 0 & 0 & 0 & 0 & 0 & 0 & 0 & 0 \\ 0 & 0 & 0 & 0 & 0 & 0 & 0 & 0 & 0 & 0 & 0 & 0 \\ 0 & 0 & 0 & 0 & 0 & 0 & 0 & 0 & 0 & 0 & 0 & 0 \\ 0 & 0 & 0 & 0 & 0 & 0 & 0 & 0 & 0 & 0 & 0 & 0 \\ 0 & 0 & 0 & 0 & 0 & 0 & 1 & 0 & 0 & 0 & 0 & 0 \\ 0 & 0 & 0 & 0 & 0 & 0 & 0 & 0 & 0 & 0 & 0 & 0 \\ 0 & 0 & 0 & 0 & 0 & 0 & 0 & 0 & 0 & 0 & 0 & 0 \\ 0 & 0 & 0 & 0 & 0 & 0 & 0 & 0 & 0 & 1 & 0 & 0 \\ 0 & 0 & 0 & 0 & 0 & 0 & 0 & 0 & 0 & 0 & 0 & 0 \\ 0 & 0 & 0 & 0 & 0 & 0 & 0 & 0 & 0 & 0 & 0 & 0 \end{bmatrix}$$

A maneuver is considered with simultaneous steering and acceleration. The simulation starts with the vehicle moving at a constant speed of $20km/h$. Then, from $t = 6s$ to $t = 10s$, the vehicle is

accelerated by a constant torque with magnitude of $150\ N.m$. A $\frac{1}{8}$ Hz sinusoidal steering input with 50 degrees of magnitude is applied to the vehicle from $t = 4s$ to $t = 20s$. Figure 3-5 shows the applied steering and torques on front and rear wheels.

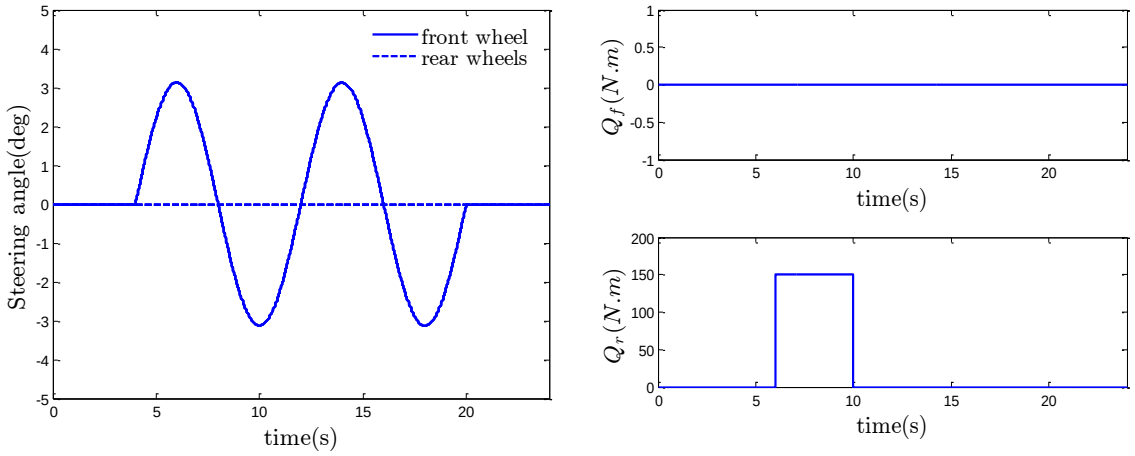

Figure 3-5: The applied steering and torques on Delta 3W vehicle

The five state variables of the vehicle including the yaw rate, lateral velocity, roll angel, roll rate, and longitudinal speed obtained from the model and CarSim are shown in Figure 3-6. The lateral acceleration from CarSim model is also shown to have some idea about the harshness of the maneuver. The results show that the proposed model properly reflects the fundamental characteristics of the vehicle with excellent agreement with the high-fidelity CarSim model for a Delta 3W vehicle.

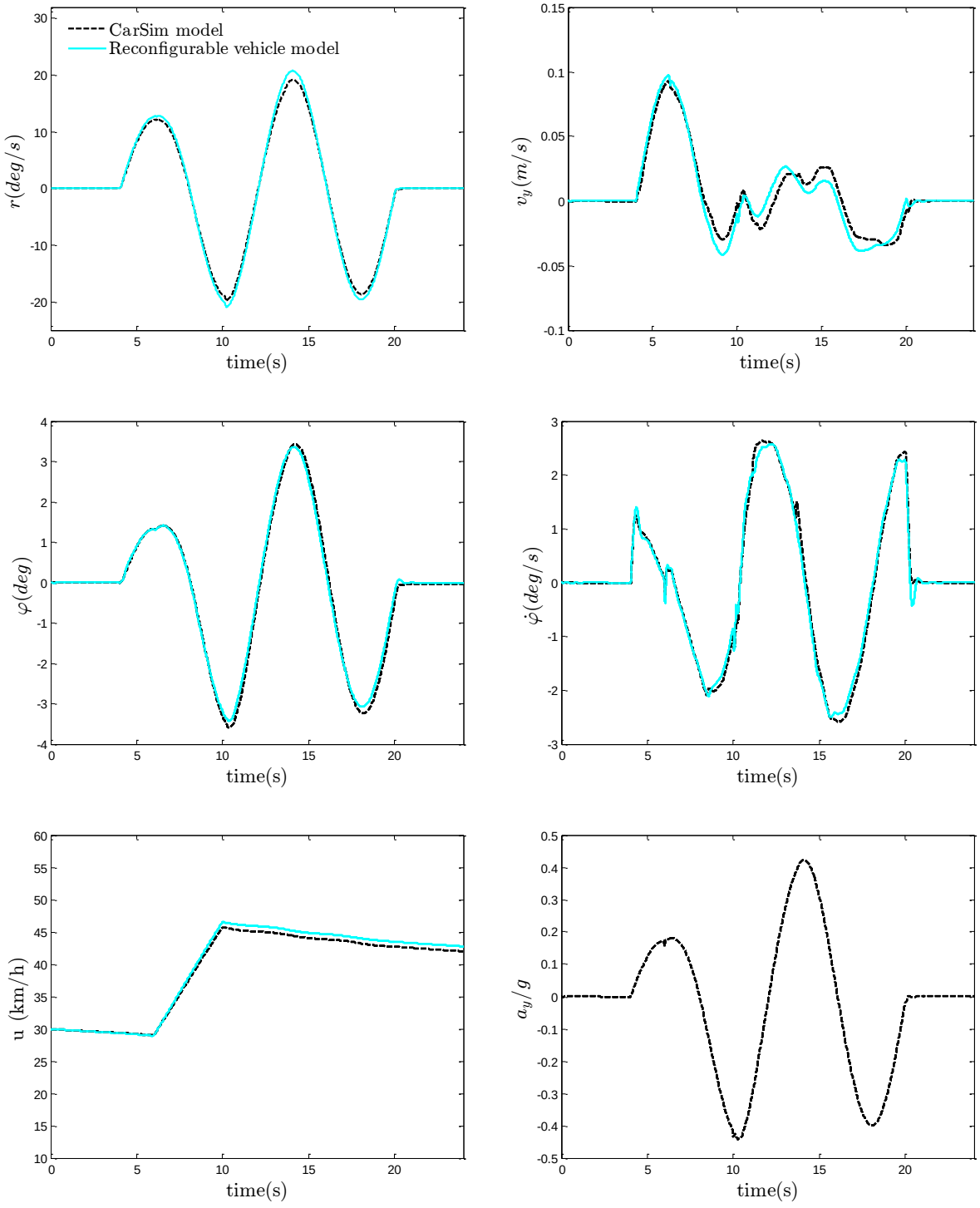

Figure 3-6: Comparison of the reconfigurable model and CarSim model for a Delta 3W vehicle

3.4.2 Vehicle model for a Tadpole 3W vehicle

For the next simulation, the reconfigurable vehicle model is evaluated for a Tadpole 3W vehicle. This vehicle is three-wheel drive with steering on all three wheels as shown in Figure 3-7.

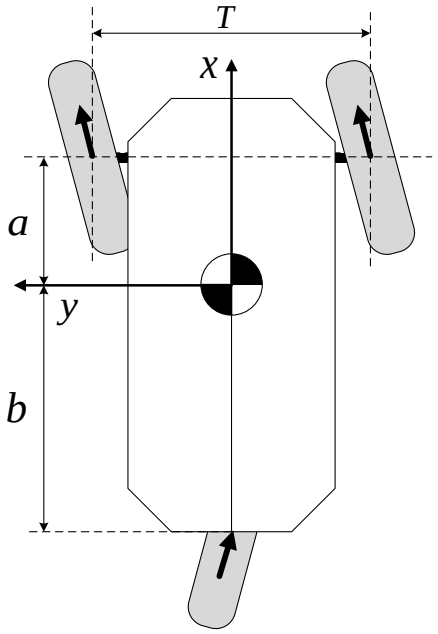

Figure 3-7: A Tadpole-configuration 3W vehicle with three-wheel drive and three-wheel steering

The corner reconfiguration matrix and the actuator reconfiguration matrix for this case are:

$$T_c = \begin{bmatrix} 1 & 0 & 0 & 0 & 0 & 0 & 0 & 0 \\ 0 & 1 & 0 & 0 & 0 & 0 & 0 & 0 \\ 0 & 0 & 1 & 0 & 0 & 0 & 0 & 0 \\ 0 & 0 & 0 & 1 & 0 & 0 & 0 & 0 \\ 0 & 0 & 0 & 0 & 1 & 0 & 0 & 0 \\ 0 & 0 & 0 & 0 & 0 & 1 & 0 & 0 \\ 0 & 0 & 0 & 0 & 0 & 0 & 0 & 0 \\ 0 & 0 & 0 & 0 & 0 & 0 & 0 & 0 \end{bmatrix} \qquad T_w = \begin{bmatrix} 1 & 0 & 0 & 0 & 0 & 0 & 0 & 0 & 0 & 0 & 0 & 0 \\ 0 & 1 & 0 & 0 & 0 & 0 & 0 & 0 & 0 & 0 & 0 & 0 \\ 0 & 0 & 0 & 0 & 0 & 0 & 0 & 0 & 0 & 0 & 0 & 0 \\ 0 & 0 & 0 & 1 & 0 & 0 & 0 & 0 & 0 & 0 & 0 & 0 \\ 0 & 0 & 0 & 0 & 1 & 0 & 0 & 0 & 0 & 0 & 0 & 0 \\ 0 & 0 & 0 & 0 & 0 & 0 & 0 & 0 & 0 & 0 & 0 & 0 \\ 0 & 0 & 0 & 0 & 0 & 0 & 1 & 0 & 0 & 0 & 0 & 0 \\ 0 & 0 & 0 & 0 & 0 & 0 & 0 & 1 & 0 & 0 & 0 & 0 \\ 0 & 0 & 0 & 0 & 0 & 0 & 0 & 0 & 0 & 0 & 0 & 0 \\ 0 & 0 & 0 & 0 & 0 & 0 & 0 & 0 & 0 & 0 & 0 & 0 \\ 0 & 0 & 0 & 0 & 0 & 0 & 0 & 0 & 0 & 0 & 0 & 0 \\ 0 & 0 & 0 & 0 & 0 & 0 & 0 & 0 & 0 & 0 & 0 & 0 \end{bmatrix}$$

The driving torque is assumed to be distributed equally on the three wheels. The rear wheel steering is assumed to be 30% of the front steering in opposite direction. The rear steering helps the vehicle to increase its maneuverability. The vehicle speed is assumed to be constant at 40 km/h. Only

a small torque (5 N.m) is applied to each wheel to compensate for rolling resistance and to keep the vehicle at a constant speed. The steering input is a sinusoidal signal with 45 degrees amplitude (steering angle) and $\frac{1}{8}$ Hz of frequency. The applied steering of front and rear wheels are shown in Figure 3-8.

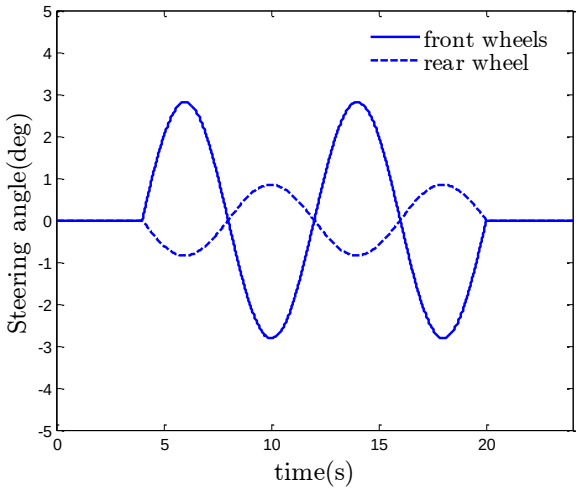

Figure 3-8: Applied steering on front and rear wheels for the Tadpole 3W vehicle

Figure 3-9 shows the dynamic responses of the vehicle from the proposed reconfigurable model and those from the CarSim model. The simulation results show that the proposed model correctly represents the dynamic characteristics of the Tadpole 3W vehicle.

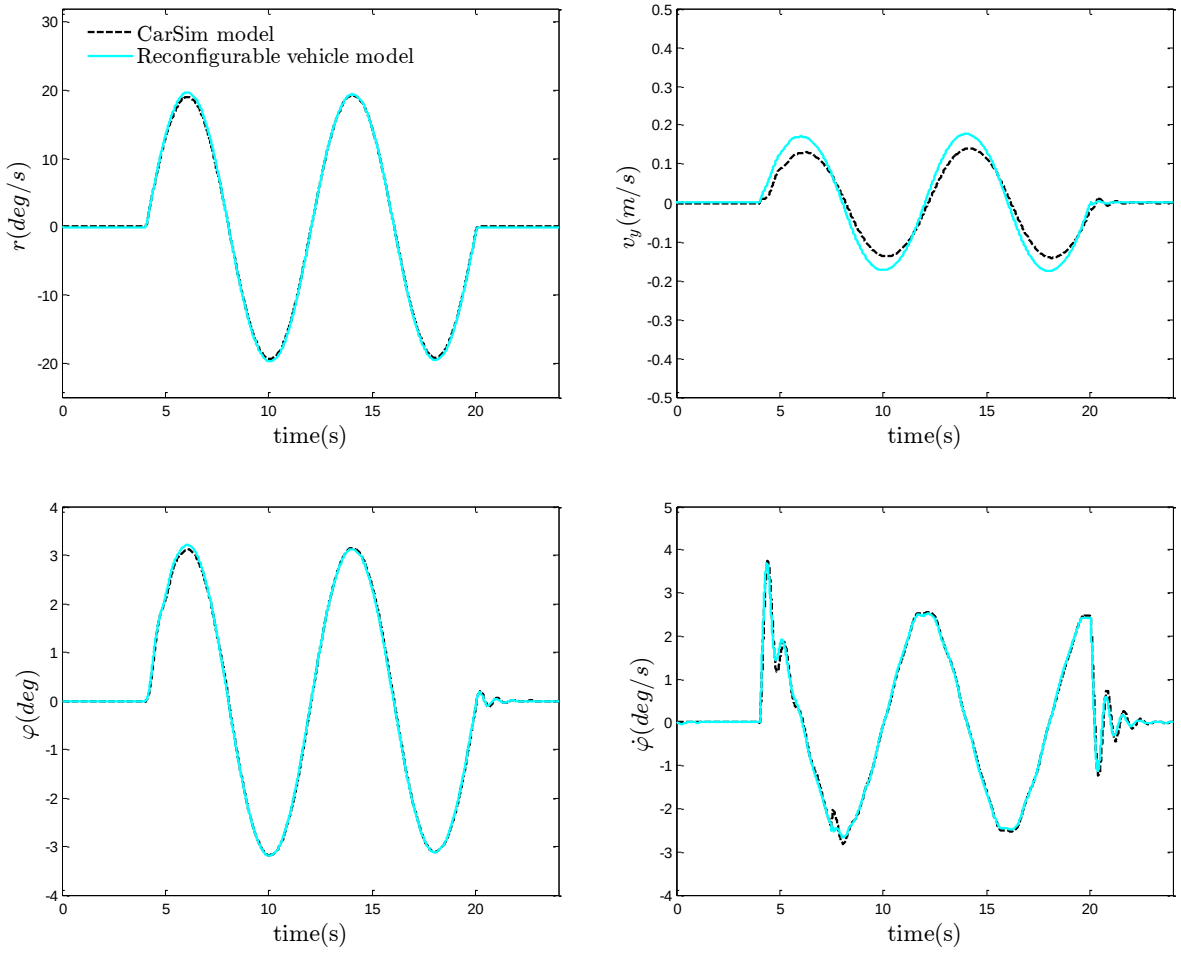

Figure 3-9: Comparison of the reconfigurable model and CarSim model for a Tadpole 3W vehicle

3.4.3 Vehicle model for a SUV

The performance of the proposed vehicle model is also investigated for a SUV as a conventional 4W vehicle. The vehicle is four-wheel drive with front steering as shown in Figure 3-10.

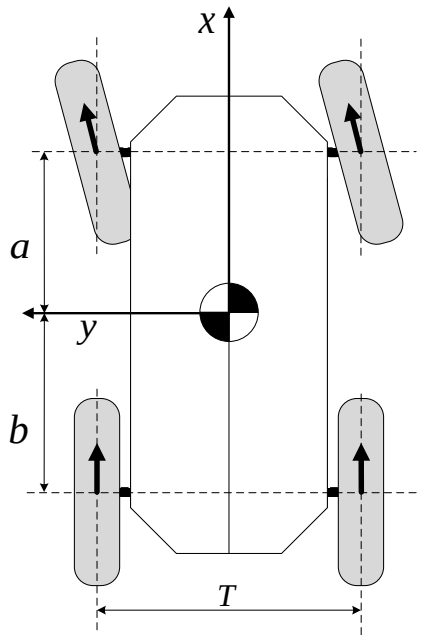

Figure 3-10: A 4W vehicle with four-wheel drive and front steering

The corner reconfiguration matrix and the actuator reconfiguration matrix for this case are:

$$T_c = \begin{bmatrix} 1 & 0 & 0 & 0 & 0 & 0 & 0 & 0 \\ 0 & 1 & 0 & 0 & 0 & 0 & 0 & 0 \\ 0 & 0 & 1 & 0 & 0 & 0 & 0 & 0 \\ 0 & 0 & 0 & 1 & 0 & 0 & 0 & 0 \\ 0 & 0 & 0 & 0 & 1 & 0 & 0 & 0 \\ 0 & 0 & 0 & 0 & 0 & 1 & 0 & 0 \\ 0 & 0 & 0 & 0 & 0 & 0 & 1 & 0 \\ 0 & 0 & 0 & 0 & 0 & 0 & 0 & 1 \end{bmatrix} \qquad T_w = \begin{bmatrix} 1 & 0 & 0 & 0 & 0 & 0 & 0 & 0 & 0 & 0 & 0 & 0 \\ 0 & 1 & 0 & 0 & 0 & 0 & 0 & 0 & 0 & 0 & 0 & 0 \\ 0 & 0 & 0 & 0 & 0 & 0 & 0 & 0 & 0 & 0 & 0 & 0 \\ 0 & 0 & 0 & 1 & 0 & 0 & 0 & 0 & 0 & 0 & 0 & 0 \\ 0 & 0 & 0 & 0 & 1 & 0 & 0 & 0 & 0 & 0 & 0 & 0 \\ 0 & 0 & 0 & 0 & 0 & 0 & 0 & 0 & 0 & 0 & 0 & 0 \\ 0 & 0 & 0 & 0 & 0 & 0 & 1 & 0 & 0 & 0 & 0 & 0 \\ 0 & 0 & 0 & 0 & 0 & 0 & 0 & 0 & 0 & 0 & 0 & 0 \\ 0 & 0 & 0 & 0 & 0 & 0 & 0 & 0 & 0 & 0 & 0 & 0 \\ 0 & 0 & 0 & 0 & 0 & 0 & 0 & 0 & 0 & 1 & 0 & 0 \\ 0 & 0 & 0 & 0 & 0 & 0 & 0 & 0 & 0 & 0 & 0 & 0 \\ 0 & 0 & 0 & 0 & 0 & 0 & 0 & 0 & 0 & 0 & 0 & 0 \end{bmatrix}$$

The longitudinal dynamics are also considered for the SUV including accelerating and braking. The initial vehicle speed is 40 km/h. During the accelerating, constant torques are applied to the wheels to increase the speed, and then the braking is applied to the vehicle to decrease the vehicle speed. The applied torques for accelerating and braking are shown in Figure 3-11. A constant torque of $400\ N.m$ is applied to each wheel from $t = 2s$ to $t = 12s$ during accelerating. On the other hand, $-210\ N.m$ is applied to the front wheels and $-90\ N.m$ to rear wheels from $t = 15s$ to $t = 20s$ for braking. A sinusoidal steering input with $50\ degrees$ of amplitude and $\frac{1}{4}$ Hz of frequency is applied to the

vehicle during accelerating and braking. Note that the driving scenario can be considered as an integrated maneuver, which involve different vehicle state variables simultaneously.

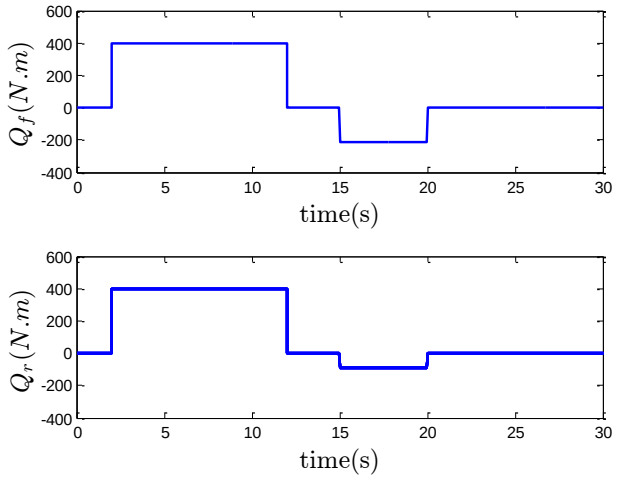

Figure 3-11: Comparison of the new reconfigurable model and CarSim model for a 4W vehicle

Figure 3-12 shows the state variables including the longitudinal speeds for the proposed and CarSim models. The results show that the proposed vehicle model can also appropriately reflect the important characteristics of vehicle dynamics for 4W vehicles. Simulation results confirm the generality of the proposed vehicle model which can be used for 4W and both configurations of 3W vehicles. Also the results show that the proposed model properly reflects the key characteristics of the vehicle dynamic behavior in lateral, longitudinal, yaw, and roll motions which are important for vehicle stability studies and for the development of active vehicle stability systems. It should be noted that the main contribution of this study is the approach used to provide the reconfigurable vehicle model. Thus, the simplified vehicle model has been compared with the high-fidelity one mainly for the purpose of illustration. The proposed strategy can easily be extended to more complex models. In fact, many different simplified vehicle models are proposed in the literature with different assumptions and complexities to customize the model for specific applications while the proposed reconfigurable vehicle model can be easily modified to reflect those requirements as well.

It should also be mentioned that the simulation part focuses on reconfigurability of the model to reflect 3W and 4W vehicle behavior. The advantages of the vehicle model for reconfigurable control design to include or exclude different actuators and to provide fault-tolerant control design is not covered in this study and is left for the future works.

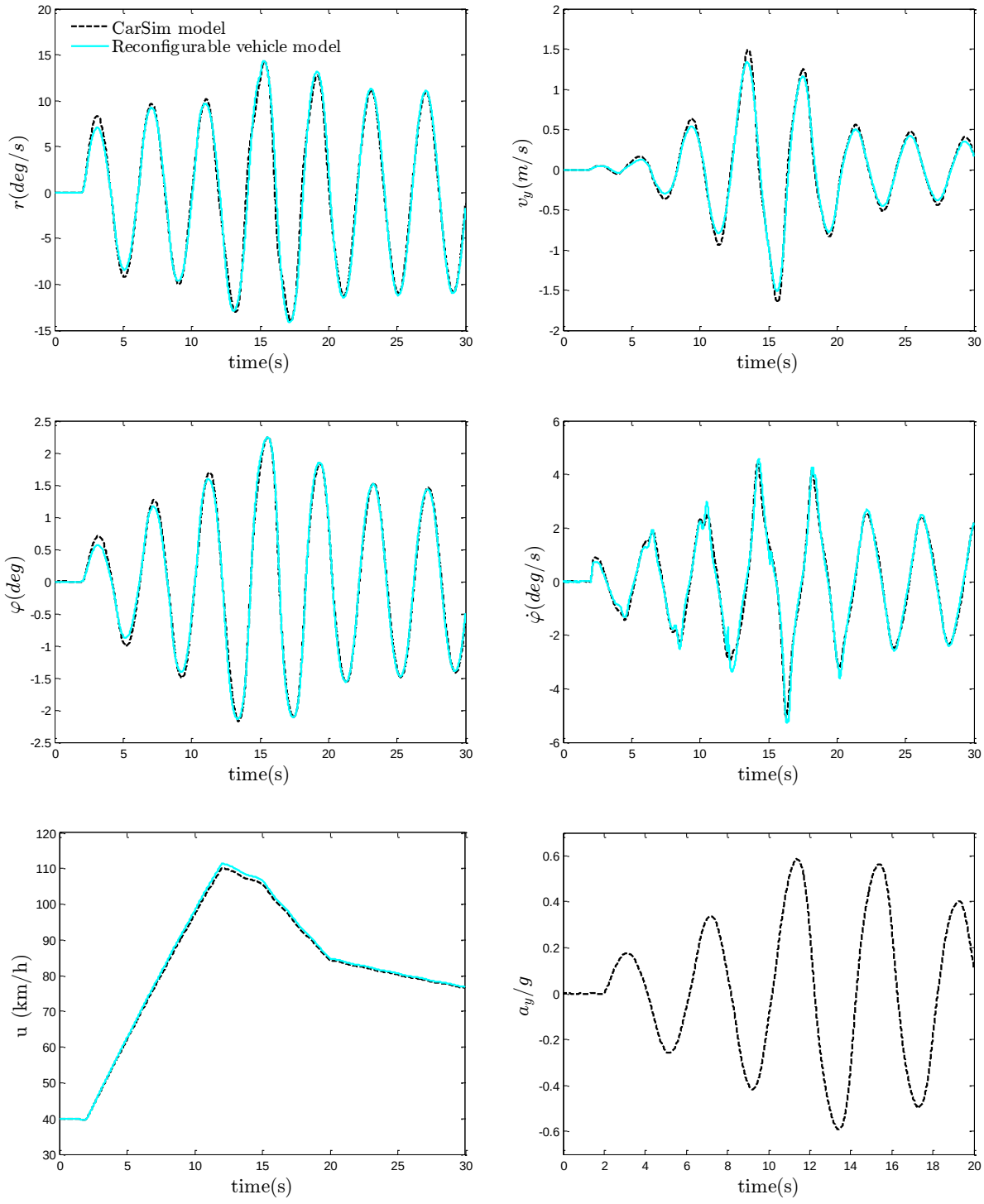

Figure 3-12: Comparison of the new reconfigurable model and CarSim model for a 4W vehicle including longitudinal dynamics

3.5 Applications of the reconfigurable vehicle model

The proposed reconfigurable vehicle model can be used for vehicle stability study and for modeling of the dynamic behavior of different 4W and 3W vehicles. It can also be used for control design of a wide range of vehicles with different stability objectives and different actuation systems. The proposed vehicle model will be particularly useful for fault-tolerant control design because any sudden change in actuator configuration can easily be accommodated in real-time. In this section, key benefits of the proposed reconfigurable vehicle model and some of its main applications are discussed.

- *Unified model for four-wheeled and three-wheeled vehicles*

The proposed vehicle model combines modeling of 4W vehicles and both Delta and Tadpole configurations of 3W vehicles in one set of equations. The proposed model can be used for modeling of dynamics behavior, for stability analysis, and for stability control of these vehicles.

- *Off-line reconfigurable control design for different actuator configurations*

The reconfigurable model is a general model regarding different available actuators in active vehicle stability systems. It includes differential braking, torque vectoring, active steering, and active camber for stability control. More importantly, it provides the freedom to easily add or remove any of these actuators. In fact, vehicles are rarely equipped with all of these actuators, so it is important to have a model to adjust with the available actuators on the vehicles. The reconfigurable vehicle model can be easily adjusted for a wide range of vehicles equipped with different actuators.

- *Interchanging between actuators*

For the vehicles that are equipped with redundant actuators, the proposed model provides the capability to switch easily from any actuator to other actuators based on the needs and the conditions. In fact, the performance of actuators like differential braking and active steering are not similar at different situations, and each of them may be more effective for specific conditions (e.g. energy efficiency or driving performance). Therefore, the proposed vehicle model can be useful for online management of vehicle actuators.

- *Real-time fault-tolerant controller*

The reconfigurable vehicle model is also applicable for the design and development of real-time fault-tolerant controllers in active vehicle stability systems. The proposed model can be easily

adjusted when there is a failure in any of the actuators, and the controller can be redesigned instantly by redistributing the control efforts to the remaining actuators.

- *General integrated control design for active stability*

The proposed vehicle model is also useful for the design of general integrated controllers. Namely, the proposed model can be useful for the design of vehicle controllers that are required to meet multiple control objectives such as handling improvement, lateral stability, rollover prevention, slip control, and longitudinal control. In addition, the model takes the interaction of the objectives into account and can be used for integrated model-based control design.

3.6 Conclusion

A general integrated reconfigurable vehicle model was introduced in this chapter that can be used for stability studies and control design of 4W vehicles and both configurations of 3W vehicles. The vehicle model can also be used for active stability control of a wide variety of vehicles with different stability objectives and different actuator configurations. The key idea is to introduce two reconfiguration matrices, one for the actuators and the other for the corner modules. The configuration of the available actuators and the number of wheels for the vehicle can be defined by adjusting the diagonal elements of these matrices. The available actuators for the vehicle are differential braking, torque vectoring, active steering, and active camber on all wheels. The state-space form of the vehicle model including the introduced matrices was also provided that could be easily used for the control design. The vehicle model includes the state variables that are commonly used for important stability objectives. Thus, it can be used to design integrated controllers for handling improvement, lateral stability, rollover prevention, longitudinal control, and slip control. Simulation results showed that the general reconfigurable vehicle model can be effectively used for different 4W and 3W vehicles. The proposed reconfigurable vehicle model is used for the development of an integrated reconfigurable controller which will be presented in next chapters.

Chapter 4: Rollover Stability of Three-Wheeled Vehicles

This chapter investigates the rollover stability of three-wheeled vehicles including the effects of road configurations. Tripped and un-tripped rollovers on flat and sloped roads are studied and a new rollover index (RI) is introduced. To explore the unique dynamic behavior of three-wheeled vehicles, the rollover stability is investigated based on the lateral load transfer ratio, and the proposed RI is expressed in terms of measurable vehicle parameters and state variables. The effects of the lateral acceleration, roll angle, longitudinal acceleration, and the pitch angle are taken into account as well as the effects of banked and graded roads. Lateral and vertical road inputs are also considered since they can represent the effects of curbs, soft soil, and road bumps as the main causes of tripped rollovers. Sensitivity analysis is provided in order to evaluate and compare the effects of different vehicle parameters and state variables on rollover stability of 3W vehicles.

4.1 Vehicle Rollover Modeling

A rollover is defined as a situation where one of the left or right wheels of a 3W vehicle lifts off the ground (front wheels for the Tadpole and rear wheels for the Delta). In other words, rollover threshold is reached when the vertical force of one of the left or right wheels reaches zero. Thus, the lateral load transfer ratio (LTR), which represents the relative vertical force on tires between left and right sides of the vehicle, is used as the most realistic indication of rollover. More specifically, the LTR is written as:

$$LTR = \frac{F_{zr} - F_{zl}}{F_{zr} + F_{zl}} \tag{4-1}$$

where F_{zr} and F_{zl} are the right and left vertical tire forces of the vehicle. Rollover happens when F_{zr} or F_{zl} reaches zero or equivalently, LTR reaches -1 or 1, respectively. Since, the vertical tire forces cannot be easily measured [95], the LTR is commonly represented in terms of other measurable parameters and states. Moreover, representation of the LTR in terms of vehicle states will be useful for the design of model-based rollover mitigation controllers.

In order to include the effects of road configuration on rollover behavior of 3W vehicles, a six-degree of freedom (6-DOF) model is used including roll, pitch, and vertical motions of the sprung and un-sprung masses. Figure 4-1 shows the vehicle's roll and pitch motions on a sloped uneven road.

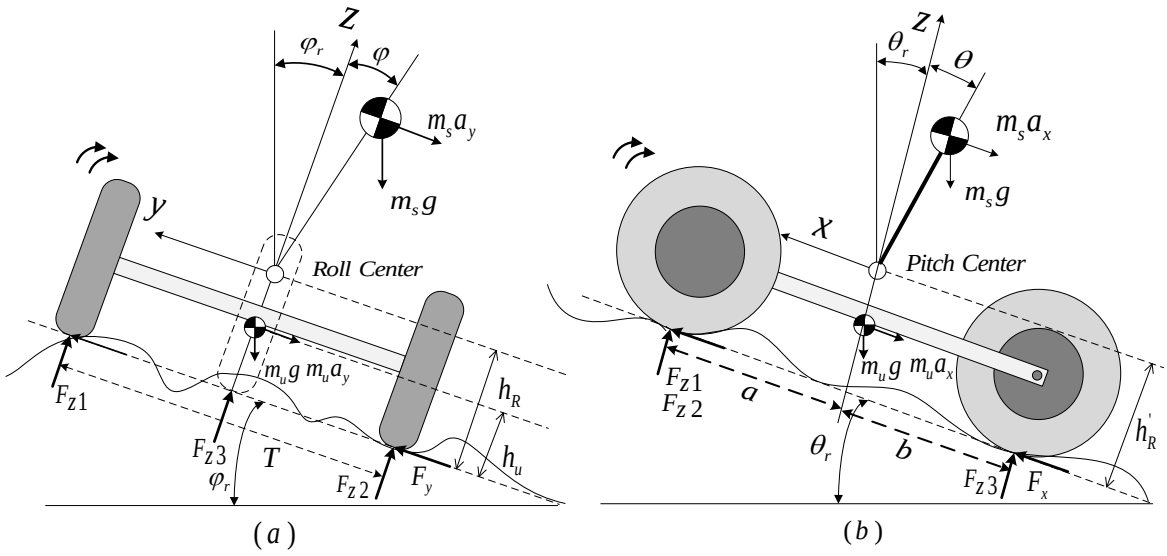

Figure 4-1: 6-DOF rollover model on a sloped uneven road: (a) roll motion, (b) pitch motion

The derivation of the equations is explained in detail for the Tadpole configuration, and the same approach can be used for the Delta configuration. The three vertical forces of the three wheels can be calculated using the following equations for the sprung and un-sprung masses:

$$\sum F_z = m\ddot{z} \tag{4-2}$$

$$\sum M_x = I_{xx}\ddot{\varphi} \tag{4-3}$$

$$\sum M_y = I_{yy}\ddot{\theta} \tag{4-4}$$

where F_z, M_x, and M_y are the vertical force and the moments around x and y axes, respectively. m, I_{xx}, and I_{yy} denote the mass and the moment of inertia around x and y axes. z, φ and θ are the vertical position and the roll and pitch angles. For simplicity, the wheels are numbered by the subscript. Specifically, for the Tadpole configuration, F_{z1}, F_{z2}, and F_{z3} denote the normal forces of the front left wheel, the front right wheel, and the rear wheel, respectively. Moreover, s and u are used by the subscript for the sprung and un-sprung masses, respectively.

If F_{zs} shows the total vertical force between sprung and un-sprung masses, then the equation for the vertical motion of the sprung mass is:

$$F_{zs} - m_s g \cos\varphi_r \cos\theta_r = m_s \ddot{z}_s \tag{4-5}$$

where φ_r and θ_r represent the bank and grade angles. The balance of the vertical forces for the un-sprung mass gives:

$$F_{z1} + F_{z2} + F_{z3} - m_u g \cos\varphi_r \cos\theta_r - F_{zs} = m_u \ddot{z}_u \tag{4-6}$$

Then, using $m = m_u + m_s$ and substituting F_{zs} from Eq. (4-5) into Eq. (4-6) leads to:

$$F_{z1} + F_{z2} + F_{z3} = mg \cos\varphi_r \cos\theta_r + m_u \ddot{z}_u + m_s \ddot{z}_s \tag{4-7}$$

Taking the moment around the x-axis at the roll center for the sprung mass gives:

$$-c_\varphi \dot{\varphi} - k_\varphi \varphi + m_s a_y h_s \cos\varphi + m_s g h_s \sin(\varphi + \varphi_r) = \left(I_{xx\_s} + m_s h_s^2\right)\ddot{\varphi} \tag{4-8}$$

where a_y is the lateral acceleration, h_s denotes the distance of the Center of Gravity (CG) of the sprung mass from the roll center. For the rest of this study, φ and θ are used as the roll and pitch angles of the sprung mass relative to the body coordinate frame. k_φ and c_φ represent the effective torsional stiffness and torsional damping in the roll direction. It should be mentioned that the roll and pitch angles are assumed to be small. Thus, the vertical acceleration of the sprung mass is assumed to be along the joining line of the roll (pitch) center to the sprung mass's CG. Then, the effects of vertical motion is ignored in roll and pitch motions. Also, the moment balance in the x direction for the un-sprung mass around its CG yields:

$$F_{z1}\frac{T}{2} - F_{z2}\frac{T}{2} + c_\varphi \dot{\varphi} + k_\varphi \varphi + F_y h_u + m_s(h_R - h_u)a_y + m_s g(h_R - h_u)\sin\varphi_r = I_{xx\_u}\ddot{\varphi}_u \tag{4-9}$$

where T denotes the vehicle track, F_y is the summation of all wheels' lateral forces, and h_R and h_u denote the roll center height and the height of the un-sprung mass' CG, respectively. The vertical and lateral forces include the effects of external road inputs, so the overall lateral force is a summation of both friction and tripped lateral forces ($F_y = F_{y\_friction} + F_{y\_tripped}$) and can be expressed as:

$$F_y = (m_s + m_u)a_y + (m_s + m_u)g \sin\varphi_r \tag{4-10}$$

Assuming a small roll angle results in $\sin(\varphi + \varphi_r) \cong \varphi \cos\varphi_r + \sin\varphi_r$. Then, combining Eqs. (4-8), (9), and (10) along with the assumption of small roll angle leads to:

$$\begin{aligned} F_{z1} - F_{z2} = \frac{2}{T}\Big((-m_s h_s - m_s h_R - m_u h_u)a_y + (-m_s h_s - m_s h_R - m_u h_u)g\sin\varphi_r \\ - m_s g h_s \varphi \cos\varphi_r + \left(I_{xx\_s} + m_s h_R^2\right)\ddot{\varphi} + I_{xx\_u}\ddot{\varphi}_u\Big) \end{aligned} \tag{4-11}$$

If H denotes the whole vehicle CG height, it can be achieved from the following equation:

$$H = \frac{m_u h_u + m_s(h_s + h_R)}{m_u + m_s} \tag{4-12}$$

Then, using $m = m_u + m_s$, the term of $(m_s h_s + m_s h_R + m_u h_u)$ is replaced by mH, and Eq. (4-11) is rewritten as:

$$F_{z1} - F_{z2} = \frac{2}{T}\left(-mHa_y - mgH\sin\varphi_r - m_s g h_s \varphi\cos\varphi_r + \left(I_{xx\_s} + m_s h_s^2\right)\ddot{\varphi} + I_{xx\_u}\ddot{\varphi}_u\right) \tag{4-13}$$

Taking the moment around y-axis at the pitch center for the sprung mass gives:

$$-c_\theta\dot{\theta} - k_\theta\theta - m_s a_x h_s'\cos\theta + m_s g h_s'\sin(\theta + \theta_r) = \left(I_{yy\_s} + m_s {h_s'}^2\right)\ddot{\theta} \tag{4-14}$$

where a_x is the longitudinal acceleration, h_s' denotes the distance of the CG of the sprung mass from the pitch center. k_θ and c_θ represent the effective torsional stiffness and torsional damping in the pitch direction. The moment balance in the y direction for the un-sprung mass around its CG also yields:

$$\begin{aligned}-(F_{z1} + F_{z2})a + F_{z3}b + c_\theta\dot{\theta} + k_\theta\theta - F_x h_u - m_s(h_R' - h_u)a_x - m_s g(h_R' - h_u)\sin\theta_r \\ = I_{yy\_u}\ddot{\theta}_u\end{aligned} \tag{4-15}$$

where a and b are the horizontal distances of the CG to the front and rear tires, respectively. F_x is the summation of all wheels' longitudinal forces and h_R' denotes the pitch center height. The overall longitudinal force can also be a summation of both friction and tripped longitudinal forces ($F_x = F_{x\_friction} + F_{x\_tripped}$) and can be shown as $F_x = (m_s + m_u)a_x + (m_s + m_u)g\sin\theta_r$. Assuming a small pitch angle results in $\sin(\theta + \theta_r) \cong \theta\cos\theta_r + \sin\theta_r$. Then, using $m_s h_s + m_s h_R + m_u h_u = mH$ and combining Eqs. (4-14) and (4-15) leads to:

$$\begin{aligned}(F_{z1} + F_{z2})a - F_{z3}b \\ = -mHa_x + mHg\sin\theta_r + m_s g h_s'\theta\cos\theta_r - \left(I_{yy} + m_s {h_s'}^2\right)\ddot{\theta} - I_{yy\_u}\ddot{\theta}_u\end{aligned} \tag{4-16}$$

Then, when solving the three equations of (4-7), (4-13) and (4-16), simultaneously, the three vertical forces for the Tadpole configuration can be calculated as:

$$\begin{aligned}F_{z1} = \frac{F_{zT}}{2}\frac{b}{l} + \frac{1}{2l}\left(-mHa_x + mHg\sin\theta_r + m_s g h_s'\theta\cos\theta_r - \left(I_{yy\_s} + m_s {h_s'}^2\right)\ddot{\theta} - I_{yy\_u}\ddot{\theta}_u\right) \\ + \frac{1}{T}\left(-mHa_y - mHg\sin\varphi_r - m_s g h_s\varphi\cos\varphi_r + \left(I_{xx\_s} + m_s h_s^2\right)\ddot{\varphi} + I_{xx\_u}\ddot{\varphi}_u\right)\end{aligned} \tag{4-17}$$

$$F_{z2} = \frac{F_{zT}}{2}\frac{b}{l} + \frac{1}{2l}\left(-mHa_x + mHg\sin\theta_r + m_s g h_s'\theta\cos\theta_r - \left(I_{yy\_s} + m_s h_s'^2\right)\ddot{\theta} - I_{yy\_u}\ddot{\theta}_u\right) - \frac{1}{T}\left(-mHa_y - mHg\sin\varphi_r - m_s g h_s\varphi\cos\varphi_r + \left(I_{xx\_s} + m_s h_s^2\right)\ddot{\varphi} + I_{xx\_u}\ddot{\varphi}_u\right) \quad (4\text{-}18)$$

$$F_{z3} = F_{zT}\frac{a}{l} - \frac{1}{l}\left(-mHa_x + mHg\sin\theta_r + m_s g h_s'\theta\cos\theta_r - \left(I_{yy\_s} + m_s h_s'^2\right)\ddot{\theta} - I_{yy\_u}\ddot{\theta}_u\right) \quad (4\text{-}19)$$

where $F_{zT} = mg\cos\varphi_r\cos\theta_r + m_u\ddot{z}_u + m_s\ddot{z}_s$ and l is the vehicle wheelbase. Substituting Eqs. (4-17) and (4-18) in Eq. (4-1), the RI for the Tadpole configuration is obtained as:

$$RI = \frac{2}{T}\frac{mHa_y + mHg\sin\varphi_r + m_s g h_s\varphi\cos\varphi_r - \left(I_{xx\_s} + m_s h_s^2\right)\ddot{\varphi} - I_{xx\_u}\ddot{\varphi}_u}{\left(mg\cos\varphi_r\cos\theta_r + m_u\ddot{z}_u + m_s\ddot{z}_s\right)\frac{b}{l} - ma_x\left(\frac{H}{l}\right) + m\left(\frac{H}{l}\right)g\sin\theta_r + m_s g\left(\frac{h_s'}{l}\right)\theta\cos\theta_r - \frac{1}{l}\left(I_{yy\_s} + m_s h_s'^2\right)\ddot{\theta} - \frac{1}{l}I_{yy\_u}\ddot{\theta}_u} \quad (4\text{-}20)$$

A similar approach is used to derive the vertical tire forces for the Delta configuration of the three-wheeled vehicles, and the three vertical forces are:

$$F_{z1} = F_{zT}\frac{b}{l} + \frac{1}{l}\left(-mHa_x + mHg\sin\theta_r + m_s g h_s'\theta\cos\theta_r - \left(I_{yy\_s} + m_s h_s'^2\right)\ddot{\theta} - I_{yy\_u}\ddot{\theta}_u\right) \quad (4\text{-}21)$$

$$F_{z2} = \frac{F_{zT}}{2}\frac{a}{l} - \frac{1}{2l}\left(-mHa_x + mHg\sin\theta_r + m_s g h_s'\theta\cos\theta_r - \left(I_{yy\_s} + m_s h_s'^2\right)\ddot{\theta} - I_{yy_u}\ddot{\theta}_u\right) + \frac{1}{T}\left(-mHa_y - mHg\sin\varphi_r - m_s g h_s\varphi\cos\varphi_r + \left(I_{xx\_s} + m_s h_s^2\right)\ddot{\varphi} + I_{xx\_u}\ddot{\varphi}_u\right) \quad (4\text{-}22)$$

$$F_{z3} = \frac{F_{zT}}{2}\frac{a}{l} - \frac{1}{2l}\left(-mHa_x + mHg\sin\theta_r + m_s g h_s'\theta\cos\theta_r - \left(I_{yy\_s} + m_s h_s'^2\right)\ddot{\theta} - I_{yy_u}\ddot{\theta}_u\right) - \frac{1}{T}\left(-mHa_y - mHg\sin\varphi_r - m_s g h_s\varphi\cos\varphi_r + \left(I_{xx\_s} + m_s h_s^2\right)\ddot{\varphi} + I_{xx\_u}\ddot{\varphi}_u\right) \quad (4\text{-}23)$$

Then, the RI for the Delta configuration is:

$$RI = \frac{2}{T}\frac{mHa_y + mHg\sin\varphi_r + m_s g h_s\varphi\cos\varphi_r - \left(I_{xx\_s} + m_s h_s^2\right)\ddot{\varphi} - I_{xx\_u}\ddot{\varphi}_u}{\left(mg\cos\varphi_r\cos\theta_r + m_u\ddot{z}_u + m_s\ddot{z}_s\right)\frac{a}{l} + ma_x\left(\frac{H}{l}\right) - m\left(\frac{H}{l}\right)g\sin\theta_r - m_s g\left(\frac{h_s'}{l}\right)\theta\cos\theta_r + \frac{1}{l}\left(I_{yy\_s} + m_s h_s'^2\right)\ddot{\theta} + \frac{1}{l}I_{yy\_u}\ddot{\theta}_u} \quad (4\text{-}24)$$

4.2 Tripped rollover measurement

As mentioned, since the RI involves the term of lateral acceleration, the effects of any lateral forces such as friction and tripped lateral forces are included. Therefore, the effects of road conditions such as slippery roads are also taken into account. To measure the tripped rollovers of 3W vehicles,

caused by vertical road disturbances, the proposed RI includes un-sprung mass' accelerations and the sprung mass' vertical accelerations.

RIs are desired as terms of measurable parameters and state variables, but some of the variables in the derived RI such as $\ddot{\theta}_u$ and $\ddot{\varphi}_u$ are not easy to measure. The effects of longitudinal dynamics on rollover are considerably less than the effects of lateral dynamics; moreover, the effects of the un-sprung mass is considerably less than the effects of the sprung mass, so the effect of the un-sprung mass pitch acceleration $\left(\frac{1}{l} I_{yy\_u} \ddot{\theta}_u\right)$ is assumed to be negligible. To measure the un-sprung mass' roll acceleration ($\ddot{\varphi}_u$) an approach that can be used is to place two accelerometers on the right and left sides of the un-sprung mass. Then, $\ddot{\varphi}_u$ can be calculated as:

$$\ddot{\varphi}_u = \frac{(\ddot{z}_{ul} - \ddot{z}_{ur})}{l_u} \tag{4-25}$$

where $\ddot{z}_{ul}$ and $\ddot{z}_{ur}$ denote the left and right un-sprung mass' vertical accelerations (for the Tadpole $\ddot{z}_{ul} = \ddot{z}_1$ and $\ddot{z}_{ur} = \ddot{z}_2$), and l_u shows the distance between those two accelerometers. Also, the un-sprung mass is not a single solid mass and the front and rear suspensions are not connected (for the independent suspension the left and right suspensions are also not connected). Thus, instead of using $m_u \ddot{z}_u \frac{b}{l}$ in Eq. (4-20), the effect of the suspension of the two-wheeled axle is used as $m_{ut} \ddot{z}_{ut}$ where m_{ut} is the mass of the un-sprung mass at the two-wheeled axle. $\ddot{z}_{ut}$ is the associated vertical acceleration that can be calculated as $\ddot{z}_{ut} = \frac{(\ddot{z}_{ul} + \ddot{z}_{ur})}{2}$. It should also be noted that although the effects of the un-sprung mass' pitch acceleration is neglected, it can be measured using a similar approach to that of the un-sprung mass' roll acceleration, if needed. Reference [95] suggested to measure $\ddot{\varphi}$ also by placing two accelerometers at the right and left sides of the sprung mass with the same horizontal and vertical distances from the roll center. Then, if the horizontal distance is $\frac{l_s}{2}$, the value of $\ddot{\varphi}$ can be measured as:

$$\ddot{\varphi} = \frac{\ddot{z}_{sl} - \ddot{z}_{sr}}{l_s} \tag{4-26}$$

where $\ddot{z}_{sl}$ and $\ddot{z}_{sr}$ are the left and the right accelerometer measurements, respectively.

The proposed RI can also be revised for independent suspensions. In fact, the un-sprung mass can be assumed as two masses with one in the right and the other in the left side of the vehicle with the distance of $\frac{l_u}{2}$ to the roll center. Then, the rotational inertia effects of the left and right un-sprung

masses can be calculated as $m_{u2}\frac{l_u}{2}\ddot{z}_{ul}$ and $-m_{u2}\frac{l_u}{2}\ddot{z}_{ur}$, respectively ($m_{u2}=\frac{m_{ut}}{2}$). Then, the term of $I_{xx\_u}\ddot{\varphi}_u$ can be replaced by $\frac{l_u}{2}m_{u2}(\ddot{z}_{ul}-\ddot{z}_{ur})$. Therefore, the RI for the independent suspensions is suggested as

$$RI_T=\frac{2}{T}\frac{mHa_y+mHg\sin\varphi_r+m_sgh_s\varphi\cos\varphi_r-\left(I_{xx\_s}+m_sh_s^2\right)\ddot{\varphi}-\frac{l_u}{2}m_{u2}(\ddot{z}_{ul}-\ddot{z}_{ur})}{(mg\cos\varphi_r\cos\theta_r+m_s\ddot{z}_s)\frac{b}{l}+m_{u2}(\ddot{z}_{ul}+\ddot{z}_{ur})-ma_x\left(\frac{H}{l}\right)+m\left(\frac{H}{l}\right)g\sin\theta_r+m_sg\left(\frac{h_s'}{l}\right)\theta\cos\theta_r-\frac{1}{l}\left(I_{yy\_s}+m_sh_s'^2\right)\ddot{\theta}} \quad (4\text{-}27)$$

$$RI_D=\frac{2}{T}\frac{mHa_y+mHg\sin\varphi_r+m_sgh_s\varphi\cos\varphi_r-\left(I_{xx\_s}+m_sh_s^2\right)\ddot{\varphi}-\frac{l_u}{2}m_{u2}(\ddot{z}_{ul}-\ddot{z}_{ur})}{(mg\cos\varphi_r\cos\theta_r+m_s\ddot{z}_s)\frac{a}{l}+m_{u2}(\ddot{z}_{ul}+\ddot{z}_{ur})+ma_x\left(\frac{H}{l}\right)-m\left(\frac{H}{l}\right)g\sin\theta_r-m_sg\left(\frac{h_s'}{l}\right)\theta\cos\theta_r+\frac{1}{l}\left(I_{yy\_s}+m_sh_s'^2\right)\ddot{\theta}} \quad (4\text{-}28)$$

for Tadpole and Delta configurations, respectively. Even for the solid axle suspensions, using $I_{xx\_u}\ddot{\varphi}_u=\frac{l_u}{2}m_{u2}(\ddot{z}_{ul}-\ddot{z}_{ur})$ can be a good approximation to simplify the measurement, thus Eqs. (4-27) and (4-28) are suggested to be used for both the solid axle and the independent suspensions.

It should also be noted that the RI involves several parameters and state variables that have measurement or real-time estimation. The values of lateral and vertical accelerations (a_y, $\ddot{z}_{ur}$, $\ddot{z}_{ul}$, $\ddot{z}_s$) are supposed to be measured by accelerometers. $\ddot{\varphi}$ can be measured using Eq. (4-26) [95].

Estimations of the vehicle's roll angle and bank and grade angles are also proposed in the literature [95][128][129]–[131]. About the vehicle's parameters, the values for the CG distances to the roll center (h_s) and the pitch center (h_s') may have measurement difficulties. However, since the main effects in rollover come from the accelerations, the inaccuracy in measuring these parameters will not pose a problem, and an approximate estimation can be helpful. For simplification, it can be assumed that the pitch center coincides with the roll center, and the vehicle's sprung mass rotates in the pitch direction around the roll center.

The introduced RI can be used not only for the real-time detection of rollover threats in 3W vehicles, but it can also be used for off-line evaluation of the rollover stability of 3W vehicles as well as design of 3W vehicle. In fact, the effects of several important parameters in rollover such as vehicle track, CG height, CG horizontal location, and other parameters can be evaluated using this RI.

4.3 Un-tripped rollover of 3W vehicles

The introduced RIs for rollovers of the Tadpole and Delta 3W configurations include the effects of longitudinal acceleration, so they are useful for accelerating and braking situations as well as steady-state turning. These RIs also include roll and pitch angles, so they consider the effects of the

suspension. The effects of the road's bank and grade angles are also included. To understand the effects of different parameters on the rollover stability of 3W vehicles and to be able to compare the proposed RI with the existing RIs, some specific rollover conditions are discussed here. As a specific case, for a constant speed un-tripped rollover on a flat road, the RIs can be simplified as:

$$RI_T = \frac{2}{T\frac{b}{l}}\left(\frac{mHa_y + m_s g h_s \sin\varphi - \left(I_{xx\_s} + m_s h_s^2\right)\ddot{\varphi}}{mg}\right) \tag{4-29}$$

$$RI_D = \frac{2}{T\frac{a}{l}}\left(\frac{mHa_y + m_s g h_s \sin\varphi - \left(I_{xx\_s} + m_s h_s^2\right)\ddot{\varphi}}{mg}\right) \tag{4-30}$$

Comparing these equations to the RI for 4W vehicles [47] shows that the T for 4W vehicles becomes $\frac{b}{l}T$ and $\frac{a}{l}T$ for the Tadpole and Delta configurations of 3W vehicles, respectively. These results confirm the previously suggested modification for converting the RIs of 4W vehicles to 3W vehicles. It has been suggested [9][14] to multiply the effect of track by the ratio of the location of CG to the wheelbase of the vehicle. The previous studies reach this conclusion by using the approach of taking a moment around the tipping axis, and in this study, a similar conclusion is achieved by using the LTR for the rollover study.

As a more general case, it is assumed that the vehicle has maneuvers on a flat surface while including braking and accelerating. The equations for the Tadpole and Delta configurations are shown in Eqs. (4-31) and (4-32), respectively.

$$RI_T = \frac{2}{T}\frac{mHa_y + m_s g h_s \varphi - \left(I_{xx\_s} + m_s h_s^2\right)\ddot{\varphi}}{mg\frac{b}{l} - ma_x\left(\frac{H}{l}\right) + m_s g\left(\frac{h_s'}{l}\right)\theta - \frac{1}{l}\left(I_{yy\_s} + m_s h_s'^2\right)\ddot{\theta}} \tag{4-31}$$

$$RI_D = \frac{2}{T}\frac{mHa_y + m_s g h_s \varphi - \left(I_{xx\_s} + m_s h_s^2\right)\ddot{\varphi}}{mg\frac{a}{l} + ma_x\left(\frac{H}{l}\right) - m_s g\left(\frac{h_s'}{l}\right)\theta + \frac{1}{l}\left(I_{yy\_s} + m_s h_s'^2\right)\ddot{\theta}} \tag{4-32}$$

These equations show that the effects of longitudinal dynamics i.e. longitudinal acceleration, pitch angle, and pitch acceleration are opposite for the Tadpole and Delta configurations, as expected. In fact, for the Tadpole, accelerating the vehicle and the corresponding negative pitch angle increases the rollover risk while braking and a positive pitch angle reduce rollover threat. Conversely, for the Delta, accelerating and the corresponding negative pitch angle decrease the rollover threat while braking and a positive pitch angle increase rollover risk. It should be mentioned that since braking is

typically more aggressive than accelerating action, and the longitudinal acceleration during braking is greater than that in gaining speed, the rollover stability of the Tadpole configuration has been reported [12] [14] to be better than that of the Delta. The derived equations in this study confirm this conclusion.

As such, when considering the rollover on sloped roads, it can be revealed that the effects of grade angles on a rollover are opposite for Tadpole and Delta configurations, similar to the effects of longitudinal dynamics. The effects of banked angles are the same for both configurations, similar to the effects of lateral dynamics. Also, comparing the RIs for flat roads (Eqs. (4-31) and (4-32)) to the general forms (Eqs. (4-27) and (4-28)), it can be seen that the sloped road effects lie in the terms related to mg. In fact, for the banked and graded road, the summation of vertical tire forces will change to $mg\cos\varphi_r\cos\theta_r$. The bank and grade angles also contribute to the lateral and longitudinal load transfer, respectively.

4.4 Simulation results

A high-fidelity CarSim model is used to conduct simulations for the investigation of the rollover stability of three-wheeled vehicles as well as the evaluation of the introduced RI. Since the available 3W vehicle in CarSim is a Delta configuration, the results of the simulations are limited to the Delta configuration. Different rollover conditions are considered including flat and sloped roads as well as un-tripped and tripped rollovers. The proposed RI for Delta configuration (Eq. (4-28)) is compared to two other suggested RIs in the literature. Reference [116] suggested an equation for the maximum lateral acceleration of the Delta configuration as:

$$a_{y\_max} = \frac{\frac{T}{2}\frac{a}{l} + h_s \sin\varphi}{H - h_s(1-\cos\varphi)} g + \frac{T}{2l} a_x \tag{4-33}$$

To be able to compare the maximum lateral acceleration with the introduced RI in this study, the normalized lateral acceleration is defined as $RI = \frac{a_y}{a_{y\_max}}$. This RI is denoted as Rollover Index_1 in this study. As mentioned, the other suggested strategy in the literature is to modify the RI of four-wheeled vehicles by using $\frac{a}{l}T$ instead of T. The general RI suggested by reference [47] is assumed as the RI for four-wheeled vehicles. The modified RI is denoted as Rollover Index_2 in this study. The three RIs are compared to the lateral load transfer ratio (Eq. (4-1)), which, unlike in real world conditions, can be directly measured in CarSim.

4.4.1 Un-tripped rollovers on flat roads

At first, un-tripped rollovers on flat roads are investigated through two well-known maneuvers: the double lane change (DLC) and the fishhook maneuver. A DLC maneuver has been conducted at speed of 80 km/h on a dry road as shown in Figure 4-2. Figure 4-3 shows a fishhook maneuvers at speed of 35 km/h. These figures show that the proposed RI can appropriately detect the un-tripped rollover threats for the vehicles on the flat roads, and the RI indication is very close to the value of the LTR. The Rollover Index_1 underestimates the rollover threat while Rollover Index_2, similar to the proposed RI, properly indicates the rollover risk. Comparing the introduced RI with Rollover Index_2 also confirms that the previously mentioned modification on 4W vehicles' RI (using $\frac{a}{l}T$ instead of T) works well for un-tripped rollovers of 3W vehicles on flat roads.

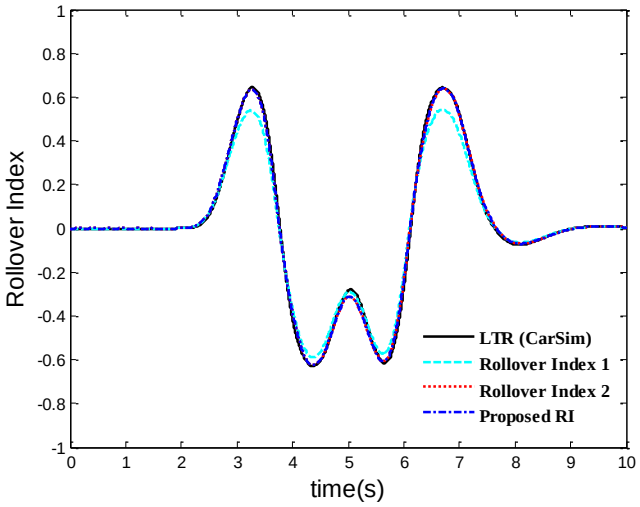

Figure 4-2: DLC maneuver at speed of 80 km/h

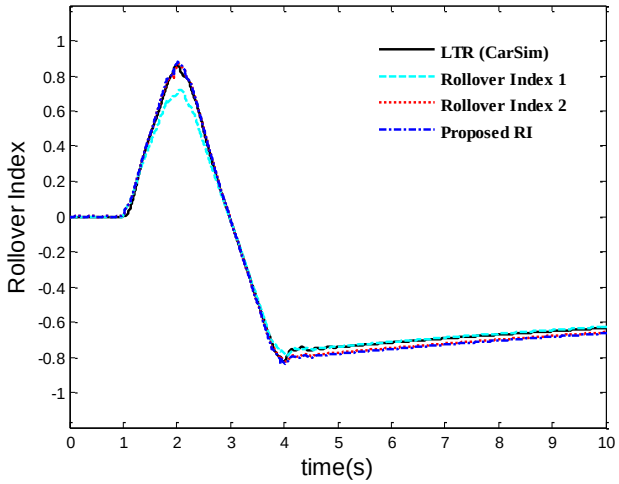

Figure 4-3: Fishhook maneuver at speed of 35 km/h

4.4.2 Rollovers on sloped roads

Un-tripped rollovers on sloped roads are investigated by including banked and graded roads. A DLC maneuver with a speed of 60 km/h on a banked road is shown in Figure 4-4. The bank angle is $\varphi_r = 16.7\ degrees$. As shown, the differences between the proposed RI and the LTR are small, so the proposed RI can also detect rollover risk on banked roads. Rollover Index_1 fails to indicate rollover risk while Rollover Index_2 also properly reflects the effects of banked road on rollover risk of 3W vehicles.

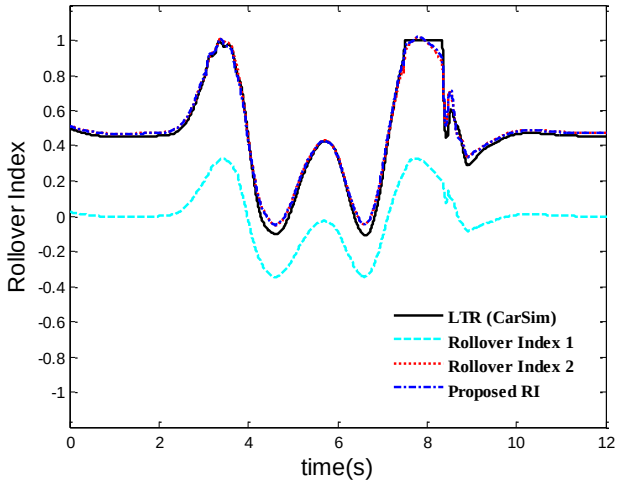

Figure 4-4: DLC on a banked road

In order to evaluate the rollover stability of the 3W vehicle and the proposed RI's performance on a graded road, DLC maneuvers are also conducted on roads with downhill and uphill grade angles. The speeds are $u = 50\ km/h$ and $u = 40\ km/h$ and the downhill and uphill grade angles are 34 and 31 $degrees$, respectively. Figure 4-5 and Figure 4-6 show the effectiveness of the proposed RI in detecting the rollover risk on graded roads. On the other hand, the previously proposed RIs in the literature cannot properly indicate rollover danger in these situations.

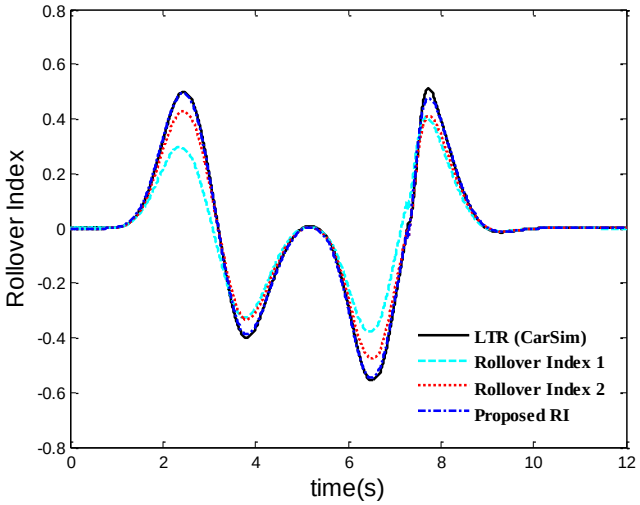

Figure 4-5: DLC on a downhill graded road

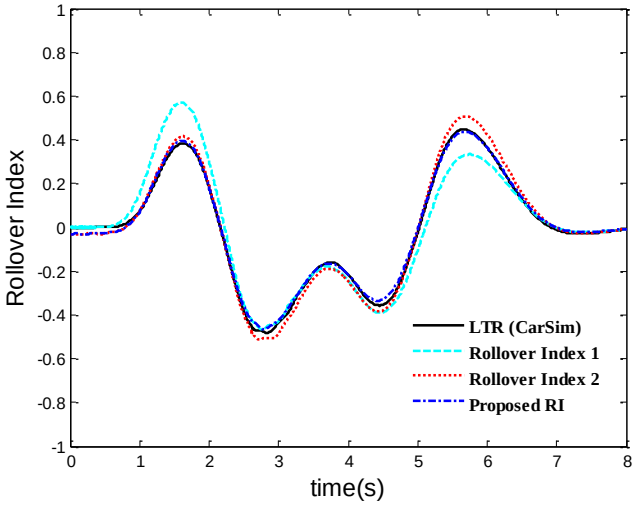

Figure 4-6: DLC on an uphill graded road

4.4.3 Rollovers on accelerating and braking

As mentioned before, accelerating and braking are effective in rollover stability of 3W vehicles. To investigate the effects of accelerating, a DLC maneuver is conducted including a longitudinal acceleration of $a_x = 0.3g$, and the results are shown in Figure 4-7. It can be seen that the proposed RI indicates the effect of longitudinal acceleration while the other RIs fail to detect that. Braking in a turn is also conducted to evaluate the proposed RI as shown in Figure 4-8. The longitudinal acceleration is about $a_x = -0.5g$. This aggressive maneuver, that includes wheel lift off, properly indicates the efficacy of the proposed RI in detection of rollover danger compared to the other RIs. It also should be mentioned that the differences between the proposed RI and Rollover Index_2 represent the effects of longitudinal acceleration on the rollover of the Delta configuration since Rollover Index_2 includes the effects of other terms except the longitudinal acceleration's effects.

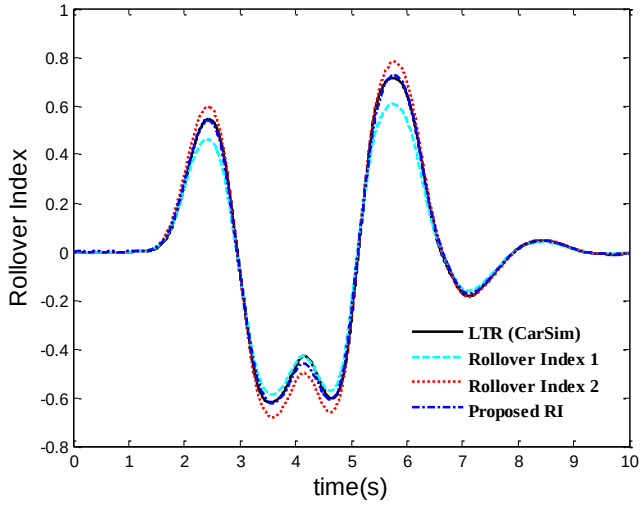

Figure 4-7: A DLC with longitudinal acceleration of $a_x = 0.3g$

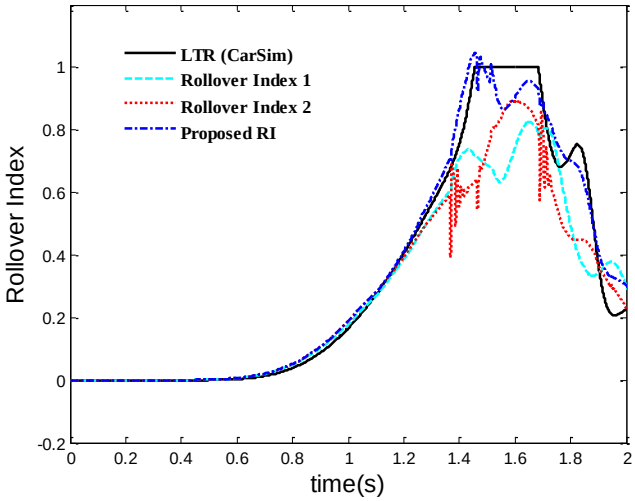

Figure 4-8: Braking in a turn with $a_x = -0.5g$

4.4.4 Tripped rollovers

The tripped rollover detection is examined through two maneuvers. The first maneuver includes a fast entrance to a banked road from a flat road where the vehicle's wheel on one side lifts off the ground. The second maneuver is moving on an uneven road. These maneuvers excite the vehicle's vertical motion since non-constant vertical forces are applied on the vehicle. The road configuration and the simulation results for the first tripped maneuver are shown in Figure 4-9. The road contour starts from a flat surface; then, the road bank gradually increases. After $15m$, the vehicle reaches a road with a constant bank angle of $\varphi_r = 16.7\ degrees$. As can be seen, at about $t = 1.3s$, the wheel lifts off the ground. This plot shows that the proposed RI properly detects the time of wheel lift off. After that time, the rollover has already occurred and the indication is not useful. After the wheel comes down and is in contact with the ground, the RI indication is again close to the LTR. On the other hand, Rollover Index_1 completely fails to detect tripped rollovers. Rollover Index_2, which is the modified RI from 4W vehicles including tripped rollover, cannot properly shows the tripped rollover threat of 3W vehicles.

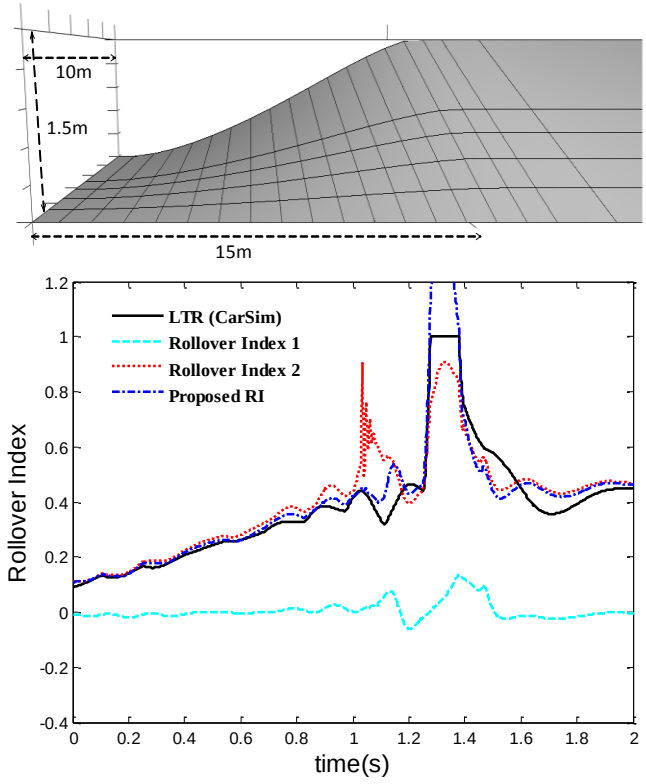

Figure 4-9: Tripped rollovers: entrance to a banked road

An uneven road is also considered to excite the vehicle's vertical motions. This configuration includes a smooth entrance to a short banked road and then a sharp exit from that with speed of 30 km/h as shown in Figure 4-10. The RI's performance is also shown in this figure. Again, it can be seen that the RI can properly detect the rollover risk before the wheel lifts off the ground while the other RIs fail to detect that.

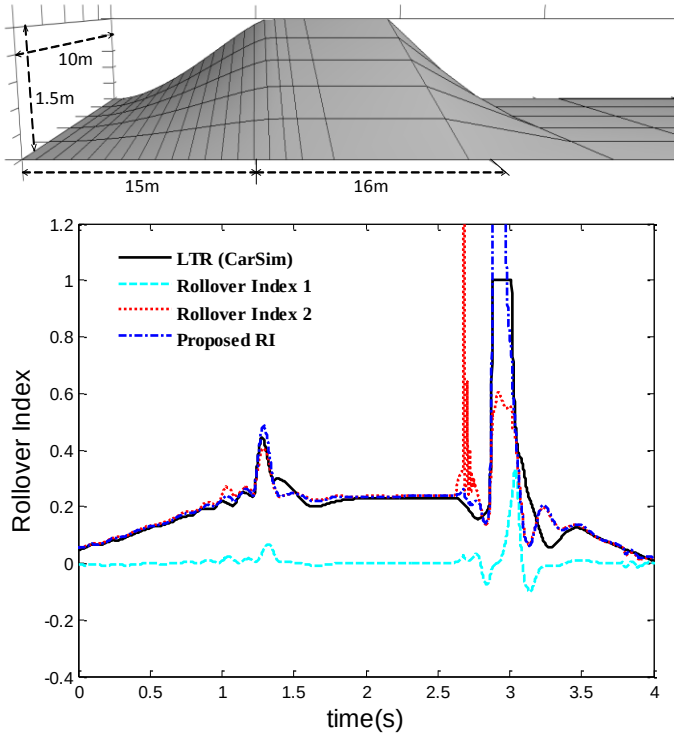

Figure 4-10: Tripped rollovers: an uneven road

4.5 Sensitivity analysis

In this subsection, sensitivity analysis is presented to understand quantitatively how the RI is affected by the parameter variations and the measurement errors. The equation for the RI includes the terms of vehicle parameters and state variables. Therefore, sensitivity coefficient for each variable can be calculated using the partial derivative of the RI as [132]:

$$\phi_i = \frac{\partial RI}{\partial X_i}\left(\frac{X_i}{RI}\right) \tag{4-34}$$

where X_i is the ith variable and ϕ_i is the sensitivity coefficient corresponding to X_i. The term $\frac{X_i}{RI}$ is used to normalize the sensitivity coefficient and thus to make it dimensionless. For the specific case used for the simulations in this study, the sensitivity coefficients are calculated assuming specific values of the state variables as shown in Table 1. These state variables represent the situation where the RI is close to 1; thus, the vehicle is at the threshold of rollover. The corresponding sensitivity coefficients are then computed by Eq. (4-34) and are shown in the right-hand side of Table 4-1.

Table 4-1: Sensitivity coefficients

Variable (X_i)	Value	Sensitivity Coefficient (ϕ_i)
Vehicle Parameters		
a	$1.35\ m$	-1.20
H	$0.503\ m$	1.19
l	$2.025\ m$	1
T	$1.05\ m$	-1
m	$867\ kg$	0.14
m_s	$747\ kg$	0.12
m_{u2}	$40\ kg$	-0.11
h_s	$0.35\ m$	0.10
l_u	$1\ m$	-0.09
h_s'	$0.4\ m$	0.02
I_{xx_s}	$288.4\ kg/m^2$	-0.007
I_{yy_s}	$1111\ kg/m^2$	-0.005
State Variables		
a_y	$0.4g$	0.77
φ_r	$7°$	0.25
θ_r	$10°$	0.13
$\ddot{z}_s$	$-0.1g$	0.12
φ	$5°$	0.10
a_x	$-0.2g$	0.10
$\ddot{z}_{ul}$	$5\ m/s^2$	-0.09
θ	$3°$	0.02
$\ddot{\varphi}$	$3\ °/s^2$	-0.009
$\ddot{\theta}$	$2\ °/s^2$	-0.005
$\ddot{z}_{ur}$	$-5\ m/s^2$	0.003

The sensitivity coefficients are sorted in descending order to compare the importance of each variable in rollover stability of the 3W vehicle. As shown in the table, the more important vehicle parameters in rollover of Delta configuration 3W vehicles are a, H, l, T. In other words, the vehicle track (T), the CG height (H), and the ratio of the horizontal distance of the CG from the single wheel to the wheel base ($\frac{a}{l}$ for Delta and $\frac{b}{l}$ for Tadpole) are more dominant than others for rollover. This also confirms the effectiveness of the static stability factor ($SSF = \frac{2Hl}{Ta}$) which has been widely used for rollover stability. An important point about a 3W vehicle is that the vehicle's mass may

considerably change by changing vehicle load and passengers' mass. The sensitivity analysis shows that the change of vehicle's mass is not a dominant factor in rollover as according to its sensitivity coefficient which is around 0.14. Thus, it can be expected that the mass variation does not result in significant inaccuracy in rollover detection. The sensitivity analysis also shows that the RI is not highly dependent on h_s, h_s', and l_u which are difficult to accurately measure, so approximate values of them may be used. Regarding the state variables to be measured or estimated in real-time, the most important factor is the lateral acceleration. Its large sensitivity coefficient shows that the lateral acceleration measurement should be accurate enough to have reliable rollover detection. The next important variable is the road bank angle which has considerable effects on rollover risk. The RI is not highly sensitive to the other state variables according to the sensitivity analysis.

4.6 Conclusion

In this chapter, the rollover stability of 3W vehicles was studied and a new rollover index was introduced to detect different rollover situations. The rollover stability of both configurations of 3W vehicles, Delta configuration and Tadpole configuration, was investigated and compared. Since the normal tire force is not easy to directly measure, the proposed RI is in the terms of measurable parameters and state variables of the vehicle. This study considers not only the effects of lateral acceleration and roll angle, but also the effects of longitudinal acceleration and pitch angle on the un-tripped rollover of 3W vehicles. In addition, the effects of road configuration are also taken into account by including road bank and grade effects. Tripped rollovers are also considered including the effects of lateral and vertical road disturbances to represent bumps, curbs, and soft soil effects. In order to evaluate its performance, the proposed RI is compared to the LTR measured in CarSim. The simulation results showed that the RI's indication was very close to the LTR as the unmeasurable rollover indication. The proposed RI was also compared with two existing RIs to show its effectiveness in situations that the other RIs fail to detect rollover threat. The proposed RI is useful not only for the detection of real-time rollover threat but also can be used for the design of 3W vehicles and the design of rollover mitigation systems. In fact, it properly reflects the effects of different vehicle parameters and state variables on the rollover of 3W vehicles.

The proposed RI will be used for the development of the general integrated controller in the following chapters. In this study, only the un-tripped rollovers are considered, and tripped rollover control is left for future work.

Chapter 5: Active Camber System

In this chapter, the concept of wheel cambering is investigated as a new technology for improving stability of vehicles. In this study, in addition to the idea of increasing lateral force and improving lateral stability, the capability of cambering in rollover stability of narrow vehicles is also investigated and compared with a tilt mechanism.

5.1 Camber Angle and Vehicle Parameters

A camber angle changes some characteristics of a vehicle, and consequently its dynamic behavior. Specifically, camber affects tire lateral forces, vehicle track, and vehicle's CG height.

5.1.1 Camber and lateral forces

Turning ability is an important characteristic of vehicles and an essential factor that shows their maneuverability [77]. For conventional cars, turning ability comes from tire lateral forces which arise from side slip angles. Applying a steering angle on a vehicle results in the side slip angle and, consequently, lateral forces on both front and rear wheels. The limitation of turning ability comes from limitation of tire lateral forces. The maximum capacity of tire lateral forces is limited by friction force between the tire and road. The tire contact patch during cambering is completely different from that of side slip angle. Accordingly, the available friction force is utilized in a different way. Thus, camber can increase the maximum lateral forces for vehicles. It is shown that camber has the potential of increasing the lateral forces by up to 30% [77].

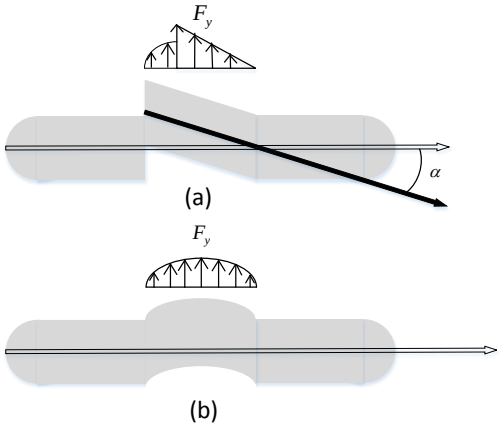

Figure 5-1: Tire contact patch for lateral force creation in side slip and camber

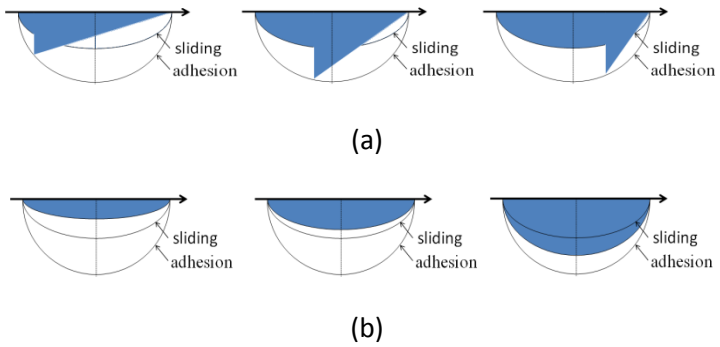

Figure 5-2: Friction utilization in side slip (a) and camber (b) lateral forces

Figure 5-1 shows a simple 1D tire brush model for side slip angle and camber [77]. The deformation in tire contact patch, caused by side slip angle, is demonstrated in Figure 5-1a. As can be seen, this lateral deformation causes a triangular force distribution that summation of these restoring forces will be the lateral tire force from side slip angle. On the other hand, the contact patch deformation in cambering is completely different and the brush has an arc shape as shown in Figure 5-1b. This arc shape contact patch contributes in increasing the utilized friction capacity. As a result, higher friction capacities will be available by switching from side slip to camber for lateral force generation. The utilization of friction from side slip angle and camber angle are also shown in Figure 5-2 [77].

5.1.2 Tire model with camber

To study the camber effects on lateral stability, the tire model should appropriately take into account the cambering lateral forces. In this regard, the Magic tire formula for motorcycles [133] is used which represents the generated lateral forces for different side slip and camber angles. The Magic tire formula for lateral forces in pure side-slip and camber is [133]:

$$F_{yo} = D_y \sin\Big(C_y \arctan\Big(B_y\alpha - E_y\big(B_y\alpha - \arctan\big(B_y\alpha\big)\big)\Big) + C_\gamma \arctan\Big(B_\gamma\gamma - E_\gamma\big(B_\gamma\gamma - \arctan\big(B_\gamma\gamma\big)\big)\Big)\Big) \tag{5-1}$$

where

$$D_y = \mu_y F_z$$

$$C_y = p_{Cy1}$$

$$\mu_y = \frac{p_{Dy1}\, exp\big(p_{Dy2} df_z\big)}{1 + p_{Dy3}\gamma^2}$$

$$E_y = p_{Ey1} + p_{Ey2}\gamma^2 + p_{Ey4}\gamma sgn(\alpha)$$

$$B_y = \frac{K_{y\alpha}}{C_y D_y}$$

$$K_{y\alpha} = \frac{K_{y\alpha o}}{1 + p_{Ky5}\gamma^2}$$

$$K_{y\alpha o} = p_{Ky1} F_{zo} \sin\left(p_{Ky2} arcta\, n\left(\frac{F_z}{(p_{Ky3} + p_{Ky4}\gamma^2)F_{zo}}\right)\right)$$

$$C_\gamma = p_{Cy2}$$

$$E_\gamma = p_{Ey5}$$

$$B_\gamma = \frac{K_{y\gamma}}{C_\gamma D_\gamma}$$

$$K_{y\gamma} = (p_{Ky6} + p_{Ky7} df_z) F_z$$

α and γ represent side-slip and camber angles. F_z and F_{zo} represent normal load and nominal normal load, respectively; df_z is also defined as $df_z = \frac{F_z - F_{zo}}{F_{zo}}$. p_{Cy1}, p_{Dy1}, p_{Dy2}, p_{Dy3}, p_{Ey1}, p_{Ey2}, p_{Ey4}, p_{Ky1}, p_{Ky2}, p_{Ky3}, p_{Ky4}, p_{Ky5}, p_{Cy2}, p_{Ky6}, p_{Ky7}, p_{Ey5} are tire parameters.

The lateral forces for different side slip and camber angles (with normal force of $3000N$) are plotted for a $180/55\,ZR17$ motorcycle tire in Figure 5-3 [133]. The parameters' values are shown in Appendix A.

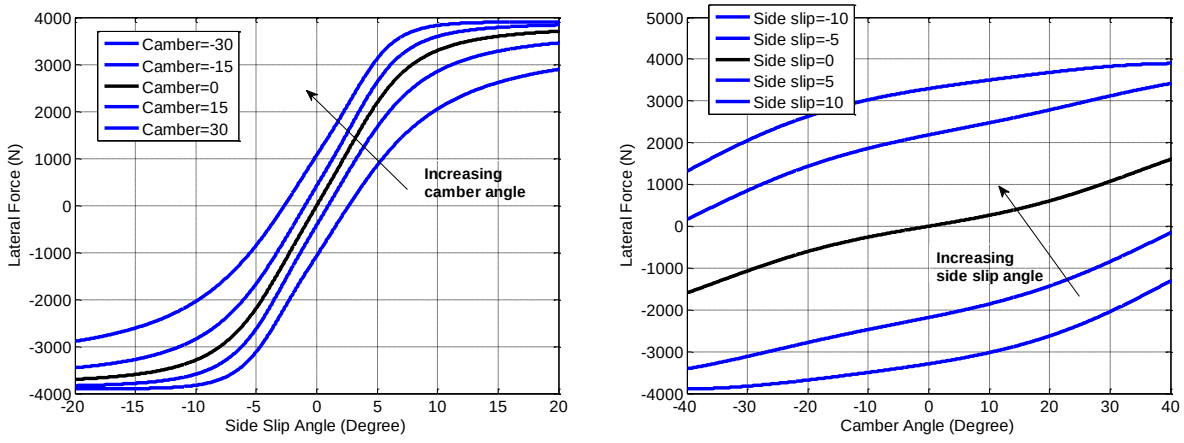

(a) (b)

Figure 5-3: Lateral tire force in cambering

Figure 5-3a shows lateral tire forces versus side slip angle for different camber angles and Figure 5-3b shows lateral tire forces versus camber angle for different side slip angles. Figure 5-3a shows that lateral tire forces increase by applying camber angle especially for side slip angles of less than 10 degrees. As can be seen from Figure 5-3b, for a zero side slip angle, the generated lateral force by camber remains almost linear for a wide range of camber change from -40 to 40 degrees. The linear behavior is also observed for side slip angle of 5 degrees. This linear behavior is useful for controller design. Another observation is that the cambering can increase the lateral forces even for large side slip angles (e.g. 10 degrees) as shown in Figure 5-3b.

5.1.3 Camber and vehicle geometry

Besides the increased lateral tire forces, there are some other effects of cambering on vehicle characteristics that can be useful, especially for narrow vehicles. The camber angle also changes CG height (H) and vehicle track (T). To see this, two different configurations for camber change are illustrated in Figure 5-4. The first configuration shows that the wheels' angles change in opposite directions (Figure 5-4a) while the second configuration shows that they change in parallel directions (Figure 5-4b).

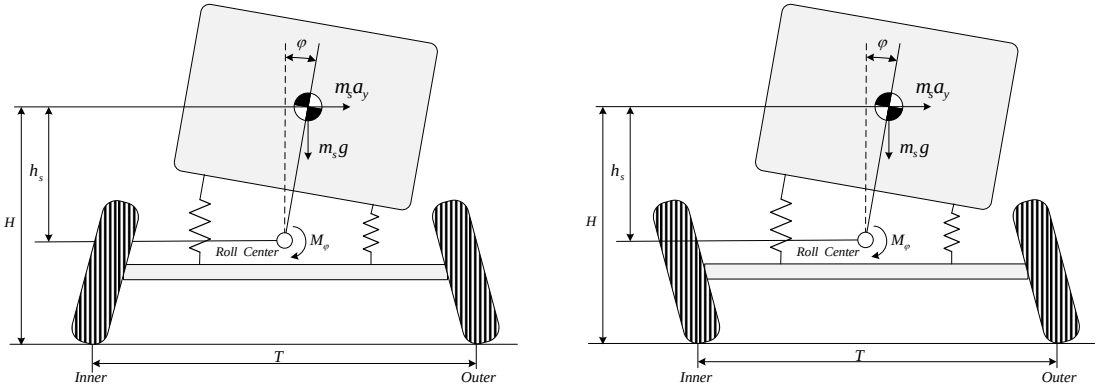

Figure 5-4: a) First configuration: Cambering in opposite direction, and b) Second configuration: Cambering in parallel direction

a) CG height

Considering wheel dimensions and angles, the new CG height can be represented as a function of camber angle for both configurations as

$$H(\gamma) = H_0 - R(1 - \cos(\gamma)) \tag{5-2}$$

where H_0 and R denote initial CG height and wheel radius, respectively.

b) Vehicle track

As shown in Figure 5-4a, the vehicle track (T) changes for the first configuration. In this case, the track changes due to the camber angle can be represented as

$$T(\gamma) = T_0 + 2R\sin(\gamma) \tag{5-3}$$

where T_0 represents initial vehicle track. For the second configuration, the effects of camber for two wheels cancel each other, so the vehicle track does not change. However, the horizontal distance of the CG to the contact point of the outer wheel changes by

$$R\sin(\gamma) \tag{5-4}$$

This change in the distance of CG location from outer wheel can be important in vehicle dynamics especially in rollover behavior and will be discussed in next sections.

5.2 Active camber for lateral stability

As discussed above, the camber angle affects tire lateral forces. To investigate this effect on vehicle dynamics of urban vehicles, a simplified 3-DOF linear model for a Tadpole configuration 3W vehicle is employed. The longitudinal velocity is assumed to be constant. Wheel dynamics are not included, and linear lateral tire forces are assumed as:

$$F_{yi} = c_{\alpha_i}\alpha_i + c_{\gamma_i}\gamma_i \quad for\ i = 1\ to\ 4 \tag{5-4}$$

Note that the positive and negative camber angles are defined differently from those in conventional suspension systems. Here, the camber angle is calculated about XYZ axis, and thus having similar values of camber angles means that the wheels are parallel. Then, the linear state-space vehicle model is obtained as:

$$\begin{gathered}\dot{X} = AX + B\delta + E\gamma \\ X = [v \quad r \quad \varphi \quad \dot{\varphi}]^T \\ \delta = [\delta_1 \quad \delta_2]^T \\ \gamma = [\gamma_1 \quad \gamma_2 \quad \gamma_3]^T\end{gathered} \tag{5-5}$$

where

$$B = \begin{bmatrix} \frac{c_{\alpha_1}}{m+n_I} & \frac{c_{\alpha_2}}{m+n_I} \\ \frac{ac_{\alpha_1}}{I_z} & \frac{ac_{\alpha_2}}{I_z} \\ 0 & 0 \\ \frac{-m_s h_s c_{\alpha_1}}{I_x(m+n_I)} & \frac{-m_s h_s c_{\alpha_2}}{I_x(m+n_I)} \end{bmatrix} \quad E = \begin{bmatrix} \frac{c_{\gamma_1}}{m+n_I} & \frac{c_{\gamma_2}}{m+n_I} & \frac{c_{\gamma_3}}{m+n_I} \\ \frac{ac_{\gamma_1}}{I_z} & \frac{ac_{\gamma_2}}{I_z} & \frac{-bc_{\gamma_3}}{I_z} \\ 0 & 0 & 0 \\ \frac{-m_s h_s c_{\gamma_1}}{I_x(m+n_I)} & \frac{-m_s h_s c_{\gamma_2}}{I_x(m+n_I)} & \frac{-m_s h_s c_{\gamma_3}}{I_x(m+n_I)} \end{bmatrix}$$

where $n_I = \frac{-{m_s}^2 {h_s}^2}{I_x}$. In this model the steer input for each wheel is separately modelled in order to be able to compare the effect of cambering of each wheel with the effect of steering of a single wheel, so $\delta_1 = \delta_2 = \delta_f$. Matrix A is shown in Appendix B. Using the state-space model, the characteristics of the lateral cambering force can be investigated and compared with lateral steering force.

5.2.1 Camber on Front wheels

What is interesting in the state-space form of vehicle model (Eq. (5-5)) is that the matrix A is independent from camber coefficients (while it is dependent to cornering coefficients). Thus the cambering lateral force acts just as an input for the system. In this section, the effects of front wheel camber is analyzed and compared with the effects of steering. The first columns of matrixes B and E represent the effects of first wheel steering and first wheel cambering, respectively. As can be seen, the relation between these two columns is

$$B(:,1) = \frac{c_{\alpha_1}}{c_{\gamma_1}} E(:,1) \tag{5-6}$$

Applying Laplace transform to the state space equation of the vehicle (Eq. (5-5)) results in:

$$sX = AX + B\delta + E\gamma \tag{5-7}$$

where s denotes the Laplace transform variable. Let $X_{\delta 1}$ and $X_{\gamma 1}$ represent vehicle responses to steering and cambering of the first wheel, respectively, then

$$sX_{\delta_1} = AX_{\delta_1} + B(:,1)\delta_1 \tag{5-8}$$

$$sX_{\gamma_1} = AX_{\gamma_1} + E(:,1)\gamma_1 \tag{5-9}$$

Rewriting the equations for $X_{\delta 1}$ and $X_{\gamma 1}$ yields

$$X_{\delta_1} = (sI - A)^{-1} B(:,1)\delta_1 \tag{5-10}$$

$$X_{\gamma_1} = (sI - A)^{-1} E(:,1)\gamma_1 \tag{5-11}$$

Substituting Eq. (5-6) in Eq. (5-11) yields

$$X_{\gamma_1} = (sI - A)^{-1} \frac{c_{\gamma_f}}{c_{\alpha_f}} B(:,1)\gamma_1 \tag{5-12}$$

Eq. (5-12) can be rewritten as

$$X_{\gamma_1} = \frac{c_{\gamma_f}}{c_{\alpha_f}} \frac{\gamma_1}{\delta_1} (sI - A)^{-1} B(:,1)\delta_1 \tag{5-13}$$

Combining Eq. (5-13) and Eq. (5-10), the ratio of cambering effects on vehicle response to the ones from steering is calculated as

$$X_{\gamma_1} = \frac{c_{\gamma_f}}{c_{\alpha_f}} \frac{\gamma_1}{\delta_1} X_{\delta_1} \tag{5-14}$$

The above equation shows that the proportion of cambering effects to steering effects is equal to the ratio of camber coefficient to cornering coefficient times the ratio of camber angle to steer angle. Figure 5-5 shows this relation graphically. It should be mentioned that the ratio of effects depends on the steer angle and not the tire side slip angle.

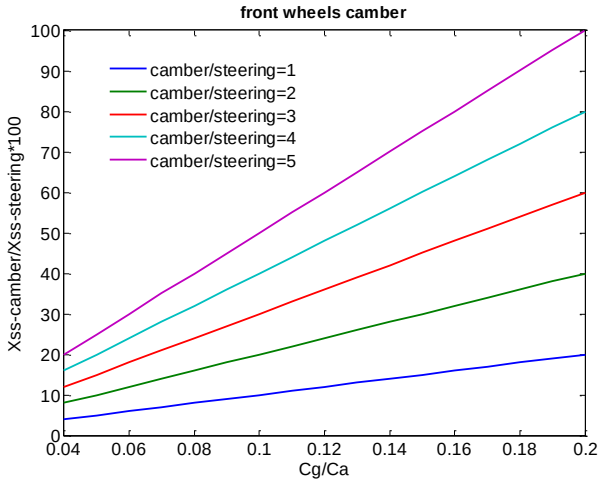

Figure 5-5: Ratio of vehicle response in steering and cambering

As a conclusion, front wheel cambering is able to provide a new steering option as its effects are similar to wheel steering. Therefore, the effects of front wheel camber are similar to steering effects

on all vehicle parameters such as yaw rate, vehicle side slip angle and roll response. In fact, the front wheel camber effect can be modelled as a second steering mechanism

$$\delta_t = \delta_\delta + \delta_\gamma \tag{5-15}$$

where δ_t represents the overall steering effects on the vehicle; also, δ_δ and δ_γ represent the steering effects from wheel steering and from cambering, respectively. However, as discussed, the important advantage of the camber is that it retrieves more friction capacity and provides more lateral forces. Furthermore, the lateral force provided by camber angle is almost linear even for large values of camber angles.

To have some idea on how the effect of cambering is compared to that of steering, let us assume that a regular tire has $\frac{c_{\gamma_f}}{c_{\alpha_f}} = 0.1$. Then, for 3 degrees of steering and 15 degrees of camber angle, the relation is

$$\frac{X_{\gamma_f}}{X_\delta} = \frac{c_{\gamma_f}}{c_{\alpha_f}} \times \frac{\gamma_f}{\delta} = 0.1 \times 5 = 0.5 = 50\% \tag{5-16}$$

Thus, the cambering effects will be half of the steering effects. For $\frac{c_{\gamma_f}}{c_{\alpha_f}} = 0.1$, every 10 degrees of cambering is equivalent to 1 degree of steering. In general, steering angle is small at high speeds and thus, even small change in steering angle can have considerable effects on vehicle responses. Moreover, special tires may be used for cambering that has greater camber cornering coefficient.

5.2.2 Camber on Rear Wheel

The relation for rear wheel camber and rear wheel steering can be achieved similarly. Thus, again the ratio is

$$X_{\gamma_r} = \frac{c_{\gamma_r}}{c_{\alpha_r}} \frac{\gamma_r}{\delta_r} X_r \tag{5-17}$$

However, the effects of rear camber on vehicle dynamic response are different from the effects of front camber. The third column (or fourth) of matrix E represents the effect of rear wheel camber on vehicle dynamic response, and the first (or second) column of that matrix shows the effect of front wheel camber. Comparing these two columns, similarities and differences can be seen. Their first elements are similar (assumed similar tire) that show the effects on lateral velocity (i.e. vehicle side

slip angle). These similar values show that for similar tire and similar camber angle the direct effects of both front and rear wheels on vehicle side slip angle are the same. On the other hand, comparing the second elements (second row) of these two columns, the proportion of them is $-\frac{b}{a}$. For the value of $\frac{b}{a} \approx 1$, the magnitude of effects are similar, but they are opposite to each other. It means that to have similar effects to the front wheel camber on yaw rate, rear wheel camber should be applied in opposite direction. The effects of front and rear camber angles on overall vehicle behavior are demonstrated in simulation part.

5.3 Active camber for rollover improvement

As discussed before, rollover is an important issue for narrow vehicles. In the following, the camber effects are taken into account for rollover analysis and stability. Maximum lateral acceleration and lateral load transfer are explored as important rollover criteria. Then, camber mechanism is compared with tilt mechanism which is a popular strategy for rollover prevention of narrow vehicles.

First, cambering effect is examined for four-wheeled vehicles, and then it is extended to three-wheeled vehicles. For modeling the vehicle, the roll axle is assumed to be parallel to the ground (roll center height is assumed to be equal for both front and rear axles). The suspension stiffness and damping are modelled as torsional spring and torsional damper that act on roll center. The effect of camber is investigated for both configurations as demonstrated in Figure 5-4. It is assumed that although cambering varies the CG height, the distance between roll center and CG does not change because the roll center height also changes similar to the CG height (shown in Figure 5-4). Therefore, based on this assumption, the h_s (h_{roll}) which is an effective factor in roll dynamics, will remain unchanged. It should also be mentioned that although cambering changes the vehicle track, it is assumed not to affect the effective track for suspension springs and dampers (l_s). Therefore, the torsional stiffness and the torsional damping coefficient also remain constant during vehicle cambering (these assumptions were also made in analyzing lateral stability in previous section).

5.3.1 Maximum lateral acceleration

The effect of cambering on maximum lateral acceleration (rollover threshold) is examined via two different approaches. For the first approach, the roll angle and camber angle are assumed to be small, so for them: $\sin(x) \cong x,\ \cos(x) \cong 1$. With this assumption, an explicit and general equation is derived which is applicable for different types of vehicles. Then, via second approach, a more

accurate model, that takes the exact values of $\sin(x)$ and $\cos(x)$ into account, is considered for a specific case. The first approach is called the general equation and the second is called the exact equation.

The rollover threshold occurs at the time that the inner wheel contact force is equal to zero, so the orientation of the inner wheel does not affect the rollover threshold. In fact, for calculation of the maximum lateral acceleration, only the situations of the outer wheels are important which are the same for both configurations. Thus, both configurations have similar effect in changing the maximum lateral acceleration and the following investigation would be valid for both of them.

Considering zero contact force for the inner wheel and taking moments about the outer wheel's contact point give (as shown in Figure 5-4):

$$\begin{aligned} m\big(H_0 - R(1-\cos(\gamma)) - h_s(1-\cos(\varphi))\big)a_{yc} \\ = (m-m_s)g\left(\frac{T_0}{2} + R\sin(\gamma)\right) + m_s g\left(\frac{T_0}{2} + R\sin(\gamma) - h_s\sin(\varphi)\right) \end{aligned} \tag{5-18}$$

Then, rewriting Eq. (5-18) yields:

$$m\big(H_0 - R(1-\cos(\gamma)) - h_s(1-\cos(\varphi))\big)a_{yc} = mg\left(\frac{T_0}{2} + R\sin(\gamma)\right) - m_s g h_s\sin(\varphi) \tag{5-19}$$

And the maximum lateral acceleration is

$$\frac{a_{yc}(\gamma)}{g} = \frac{\left(\frac{T_0}{2} + R\sin(\gamma)\right) - \frac{m_s}{m}h_s\sin(\varphi)}{H_0 - R(1-\cos(\gamma)) - h_s(1-\cos(\varphi))} \tag{5-20}$$

For a given suspension system in a vehicle, steady-state roll angle is a function of lateral acceleration as

$$\varphi = \frac{-m_s g h_s}{k_\varphi - m_s g h_s}\frac{a_{yc}}{g} \tag{5-21}$$

For each camber angle, solving Eq. (5-20) and Eq. (5-21) simultaneously, the maximum possible lateral acceleration can be found. It should be noted that it is not possible to find a simple explicit function for $a_{yc}(\gamma)$ in this model. However, assuming small angles for roll angle and camber angle the model can be considerably simplified. These assumptions are applied to find a simple and general equation which is valid for a wide range of vehicles.

5.3.1.1 General equation

Applying the small angle assumptions, i.e., $\sin(\varphi) = \varphi$, $\cos(\varphi) = 1$, $\sin(\gamma) = \gamma$,and $\cos(\gamma) = 1$, Eq. (5-20) is simplified to

$$\frac{a_{yc}(\gamma)}{g} = \frac{\left(\frac{T_0}{2} + R\gamma\right)}{H_0} - \frac{m_s}{m}\frac{1}{H_0}h_s\varphi = \frac{T_0 + 2R\gamma}{2H_0}\left(1 - 2\frac{m_s}{m}\frac{1}{T_0 + 2R\gamma}h_s\varphi\right) \tag{5-22}$$

Using roll gain (Eq. (5-21)) and substituting it in Eq. (5-22), yields

$$\frac{a_{yc}(\gamma)}{g} = \frac{T_0 + 2R\gamma}{2H_0}\left(1 - 2\frac{m_s}{m}\frac{1}{T_0 + 2R\sin\gamma}h_s\frac{-m_s h_s a_{yc}(\gamma)}{k_t - m_s g h_s}\right) \tag{5-23}$$

Rewriting the equation to have an explicit function for $a_{yc}(\gamma)$ gives:

$$\frac{a_{yc}(\gamma)}{g} = \frac{T_0 + 2R\gamma}{2H}\left(\frac{1}{1 - \frac{m_s}{m}\frac{h'}{H}\frac{1}{\left(\frac{k_t}{m_s g h'}\right) - 1}}\right). \tag{5-24}$$

This equation represents the critical lateral acceleration for a vehicle as a function of the camber angle. To eliminate most of vehicle parameters and obtain a general and simple equation, a ratio is considered by dividing the equation by the initial maximum lateral acceleration of the vehicle (without camber angle). Thus, most of the parameters are omitted and a simple equation is obtained as follows

$$\frac{a_{yc}(\gamma)}{a_{yc}} = \frac{T_0 + 2R\gamma}{T_0} = 1 + \frac{2R\gamma}{T_0} \tag{5-25}$$

Using the above equation, the percentage of change in the presence of a camber angle will be

$$\frac{a_{yc}(\gamma) - a_{yc}}{a_{yc}} = \frac{2R\gamma}{T_0} \times 100 \tag{5-26}$$

This equation is a function of initial vehicle track, camber angle, and radius of wheel. For a constant wheel radius of $R = 0.3$, the percentage of change in critical acceleration is plotted in Figure 5-6. Figure 5-6a shows the percentage of change in critical acceleration versus vehicle track for three different values of camber angles. Figure 5-6b shows this change versus camber angle for three different vehicle tracks.

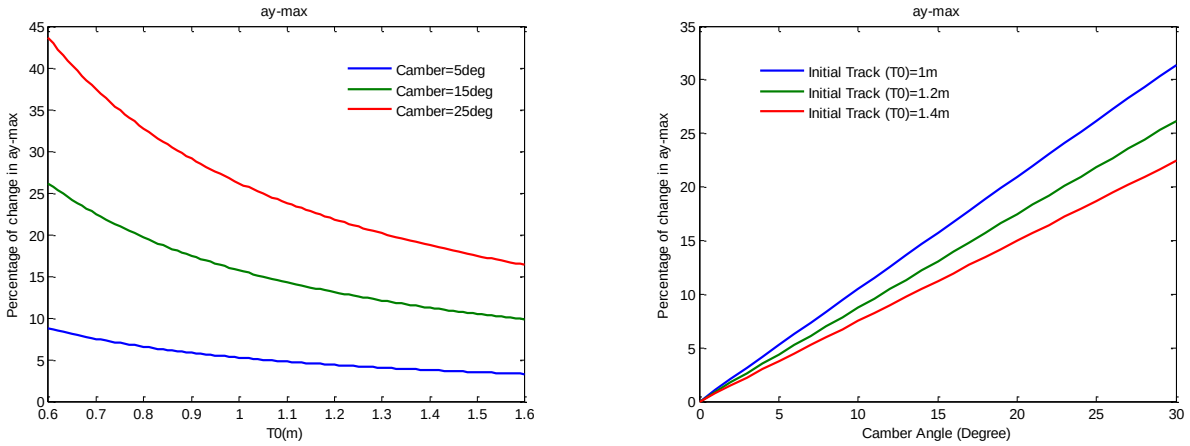

(a) (b)

Figure 5-6: The effect of cambering on critical acceleration (general equation)

As shown in Figure 5-6, the effect of camber angle on critical acceleration increases rapidly for narrow vehicles. For narrow vehicles with track of about or less than $1\,m$ the change in critical acceleration is considerable. For example, for a vehicle with a track of $1\,m$, 15 and 25 degrees of camber angle increase the maximum lateral acceleration by about 16 and 27 percent, respectively. It should also be mentioned that Eq. (5-26), and consequently, the graph is independent of CG height, so the percentage of change for a specific value of camber angle depends only on the vehicle track and is the same for all values of CG height.

5.3.1.2 Exact solution

The exact solution (without simplification of using small angles) can be solved numerically if the parameter values are known. Thus, a specific case is considered to solve the equations and then to compare the results with those from the general equation. A four-wheeled vehicle is used with vehicle parameters shown in table 2.

Figure 5-7a shows the change in maximum lateral acceleration for various camber angles. Figure 5-7b demonstrates the percentage of change in maximum lateral acceleration using the exact solution, and the result is compared with the result of the general equation.

Table 5-1: Four-wheeled vehicle's parameters

Parameters	*Values*	*Descriptions*
m	800 kg	Vehicle Mass
m_s	680 kg	Sprung Mass
H	0.5 m	CG Height
h_s	0.4 m	Distance of CG from roll center
T	1.2 m	Vehicle Track
k_φ	11760 N/rad	Torsional Stiffness

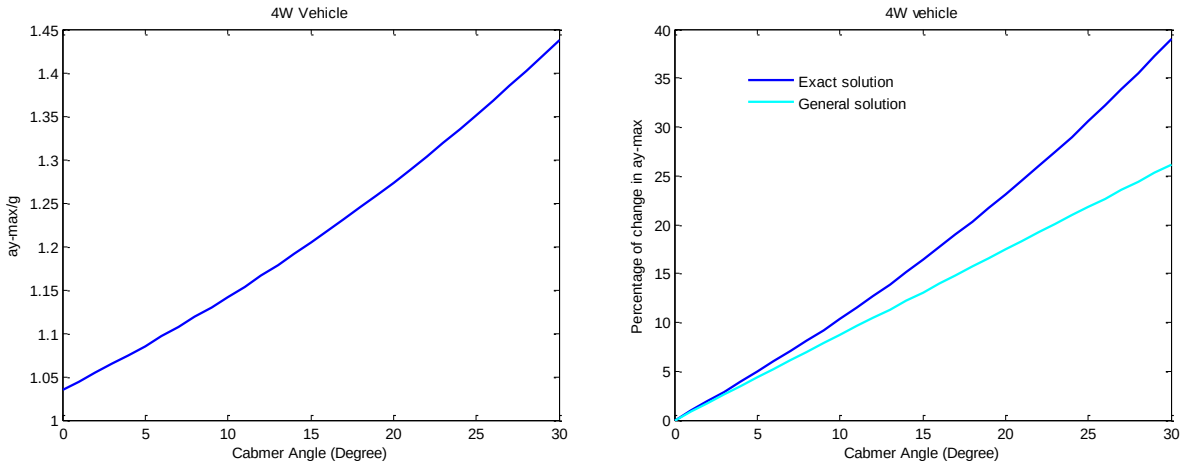

(a) (b)

Figure 5-7: The effect of cambering on critical acceleration (exact equation)

As can be seen in Figure 5-7a, for 15 degrees of camber angle, the critical acceleration increases from $1.035g$ to $1.204g$ and for 30 degrees of camber angle it increases from $1.035g$ to $1.438g$.

5.3.1.3 Three-wheeled vehicles

Three-wheeled vehicles are less tolerable to rollover compared to four-wheeled vehicles because they have tracks on only one side (front or rear). Therefore, a modification is applied in the equation to derive the equations of three-wheeled vehicles s discussed in previous chapter. In fact, the effect of each front or rear track is multiplied by the ratio of location of CG to the baseline of the vehicle. For a Tadpole three-wheeled vehicle (with one wheel in rear), taking moments about the outer wheel's contact point gives

$$m\big(H_0 - R(1-\cos(\gamma)) - h_s(1-\cos(\varphi))\big)a_{yc} = mg\frac{b}{l}\left(\frac{T_0}{2} + R_f\sin\big(\gamma_f\big)\right) + mg\frac{a}{l}(R_r\sin(\gamma_r)) - m_s g h_s\sin(\varphi) \tag{5-27}$$

Then, the maximum lateral acceleration is

$$\frac{a_{yc}(\gamma)}{g} = \frac{\frac{b}{l}\left(\frac{T_0}{2} + R_f\sin\big(\gamma_f\big)\right) + \frac{a}{l}\big(R_r\sin(\gamma_r)\big) - \frac{m_s}{m}h_s\sin(\varphi)}{H_0 - R(1-\cos(\gamma)) - h_s(1-\cos(\varphi))} \tag{5-28}$$

where a and b represent the distance of CG from front and rear wheels, respectively. R_f, R_r, γ_f, and γ_r denote front wheel radius, rear wheel radius, front camber, and rear camber, respectively. Again assuming small angles for roll and camber, and substitution of φ from Eq. (5-21) in Eq. (5-28) and rewriting for $a_{yc}(\gamma)$, give

$$\frac{a_{yc}(\gamma)}{g} = \frac{\frac{b}{l}\big(T_0 + 2R_f\gamma_f\big) + \frac{a}{l}(2R_r\gamma_r)}{2H_0}\left(\frac{1}{1 - \frac{m_s}{m}\frac{h_s}{H_0}\frac{1}{\left(\frac{k_t}{m_s g h_s}\right) - 1}}\right). \tag{5-29}$$

Using similar approach to the four-wheeled case, the general solution for a three-wheeled vehicle is obtained as

$$\frac{a_{yc}(\gamma)}{a_{yc}} = \frac{\frac{b}{l}\big(T_0 + 2R_f\gamma_f\big) + \frac{a}{l}(2R_r\gamma_r)}{\frac{b}{l}T_0} = 1 + \frac{\frac{b}{l}\big(2R_f\gamma_f\big) + \frac{a}{l}(2R_r\gamma_r)}{\frac{b}{l}T_0} = 1 + \frac{\big(2R_f\gamma_f\big) + \frac{a}{b}(2R_r\gamma_r)}{T_0} \tag{5-30}$$

and the percentage of change is calculated as

$$\frac{a_{yc}(\gamma) - a_{yc}}{a_{yc}} = \frac{\big(2R_f\gamma_f\big) + \frac{a}{b}(2R_r\gamma_r)}{T_0} \times 100 \tag{5-31}$$

Eq. (5-31) implies that a change in the camber angle introduces larger change in the maximum acceleration for a three-wheeled vehicle compared to a four-wheeled vehicle (Eq. (5-26)). If the front and rear wheel radius and camber angle are similar for front and rear wheels, then the equation can be simplified to

$$\frac{a_{yc}(\gamma) - a_{yc}}{a_{yc}} = \frac{l}{b}\frac{2R\gamma}{T_0} \times 100 \tag{5-32}$$

Thus, the percentage of change of maximum acceleration for a three-wheeled vehicle is $\frac{l}{b}$ times the percentage of change for a four-wheeled vehicle ($\frac{l}{b} > 1$). The plots for the general equation of Tadpole three-wheeled vehicles are shown in Figure 5-8.

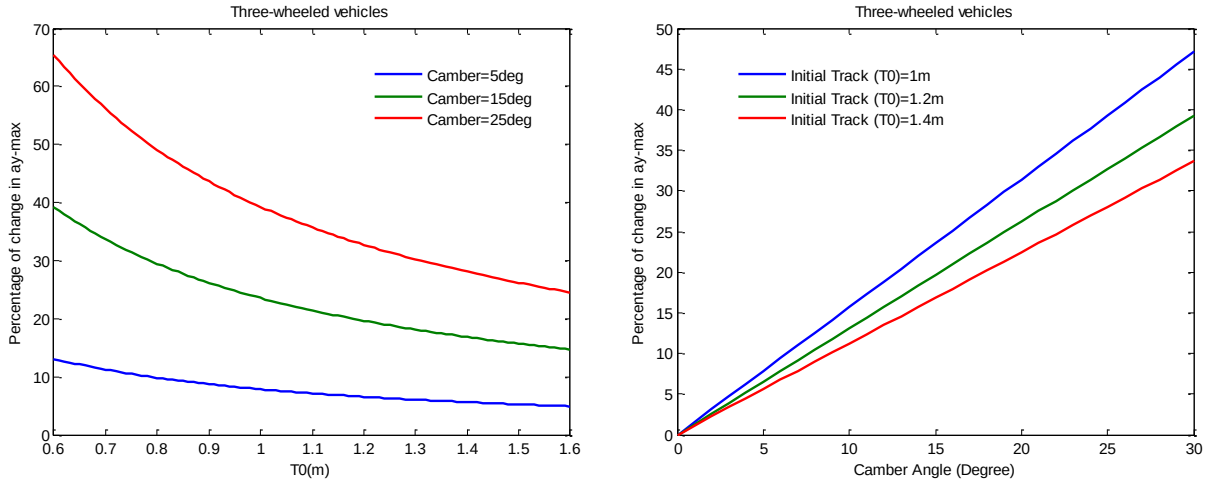

Figure 5-8: Cambering effects in three-wheeled vehicles (general equation)

Similar to four-wheeled vehicles, the maximum possible lateral acceleration for a three-wheeled vehicle can be found by solving two exact equations simultaneously for each camber angle (Eqs. (5-28) and (5-21)). A three-wheeled case with vehicle parameters shown in table 5-2 is used to plot the exact equation (Eq. (5-28)).

Table 5-2: Tadpole three-wheeled vehicle's parameters

Parameters	***Values***	***Descriptions***
m	800 kg	Vehicle Mass
m_s	680 kg	Sprung Mass
a	0.75 m	Distance of front wheels to CG
b	1.75 m	Distance of rear wheel to CG
H	0.4 m	CG Height
h_s	0.25 m	Distance of CG from roll center
T	1.4 m	Vehicle Track
k_φ	11760 N/rad	Torsional Stiffness

Figure 5-9 shows the results for this three-wheeled case.

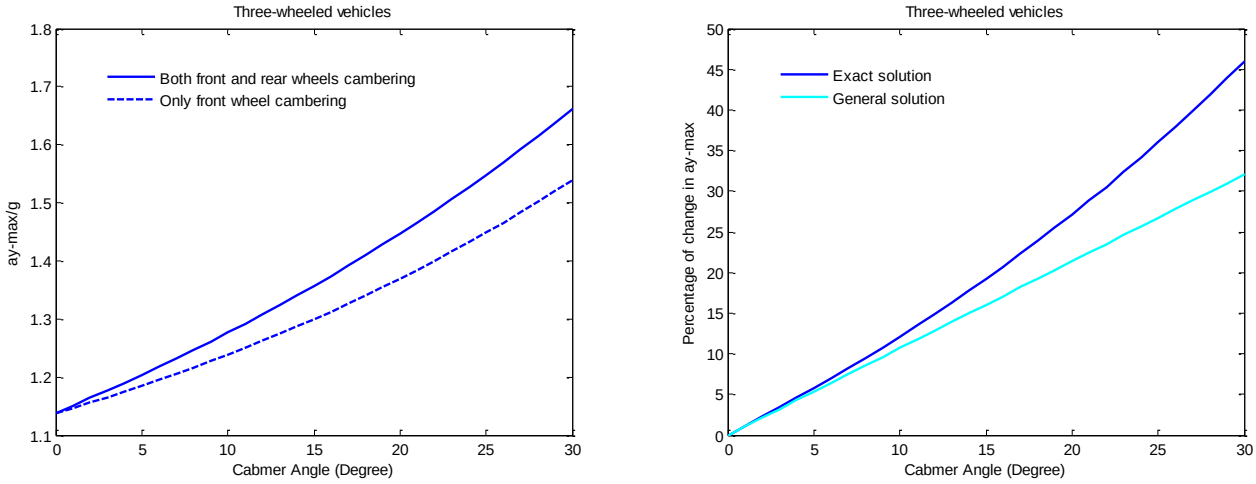

Figure 5-9: Cambering effects on the three-wheeled vehicles (exact equation)

5.3.2 Comparison with tilt mechanism

5.3.2.1 Four-wheeled vehicles

As mentioned, a well-known solution to rollover problem of narrow vehicles is a tilting mechanism. This section provides a comparison between a camber mechanism and a tilting mechanism in vehicle rollover. First, a simplified model is used to obtain a simple and general equation, and then the exact solution is employed for comparison between specific cases with the two mechanisms. To obtain the maximum possible lateral acceleration for a vehicle with a tilting mechanism, contact force for the inner wheel is considered to be zero and moments are taken about the outer wheel's contact point (as shown in Figure 5-10)

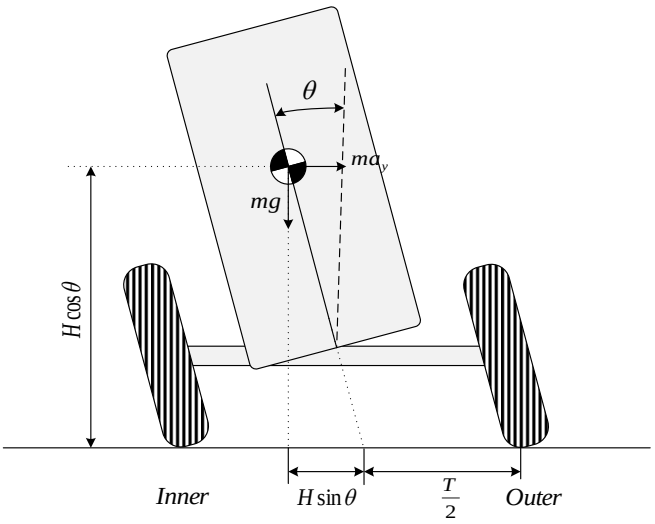

Figure 5-10: Tilt mechanism

$$mH\cos(\theta)a_{y\_\max\_tilt} = mg\left(\frac{T}{2} + H\sin(\theta)\right) \tag{5-33}$$

Thus, the maximum possible lateral acceleration is

$$\frac{a_{y\_\max\_tilt}}{g} = \frac{\frac{T}{2} + Hsin(\theta)}{Hcos(\theta)} \tag{5-34}$$

where θ represents tilting angle. For a small tilt angle

$$\frac{a_{y\_\max\_tilt}}{g} \approx \frac{\frac{T}{2} + H\theta}{H} = \frac{T}{2H} + \theta \tag{5-35}$$

where $\frac{T}{2H}$ is the value of maximum acceleration without tilting, and the increase in the maximum acceleration by using the tilting mechanism is equal to θ.

For simplicity, the suspension system is ignored for the vehicle with camber change (assuming rigid body), so the maximum lateral acceleration is

$$\frac{a_{y\_\max\_camber}}{g} = \frac{\frac{T}{2} + Rsin(\gamma)}{H - R(1 - \cos(\gamma))} \tag{5-36}$$

Assuming small angles yields

$$\frac{a_{y\_\max\_camber}}{g} = \frac{\frac{T}{2} + R\gamma}{H} = \frac{T}{2H} + \frac{R}{H}\gamma \tag{5-37}$$

Thus, for the camber mechanism, the maximum acceleration is increased by $\frac{R}{H}\gamma$. Comparing Eq. (5-35) and Eq. (5-37), it is concluded that the effect of the camber is $\frac{R}{H}$ times to the effect of the tilt mechanism (for similar camber and tilt angles). For example, for a vehicle with CG height of $H = 0.5$ and wheel radius of $H = 0.3$

$$\frac{R}{H} = \frac{0.3}{0.5} = 0.6 = 60\%$$

Thus, for this case the effect of the camber angle will be 60 percent of the effect of the tilt mechanism. In fact, the effective parameters in a tilting mechanism is the CG height (H), and for a camber mechanism is the wheel radius (R). The exact value of maximum lateral acceleration for the four-wheeled case is calculated and plotted for both cambering and tilting mechanisms as shown in Figure 5-11.

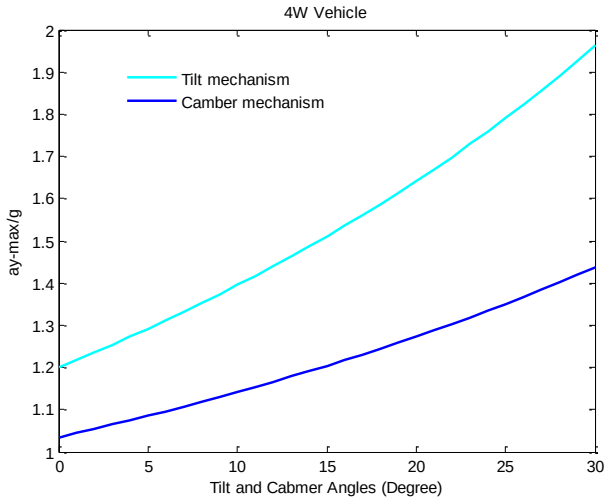

Figure 5-11: Camber mechanism and tilt mechanism for the four-wheeled case

5.3.2.2 Three-wheeled vehicles

For tilt mechanism of a three-wheeled vehicle, the maximum lateral acceleration is

$$\frac{a_{y\_\max\_tilt}}{g} = \frac{\frac{T}{2}\frac{b}{l} + Hsin(\theta)}{Hcos(\theta)} \tag{5-38}$$

For small tilt angle, it is

$$\frac{a_{y\_\max\_tilt}}{g} \approx \frac{\frac{T}{2}\frac{b}{l} + H\theta}{H} = \frac{T}{2H}\frac{b}{l} + \theta \tag{5-39}$$

and for a vehicle with camber change without suspension system (assuming rigid body)

$$\frac{a_{y\_\max\_camber}}{g} = \frac{\left(\frac{T}{2} + R\gamma\right)\frac{b}{l} + (R\gamma)\frac{a}{l}}{H} = \frac{\frac{T}{2}\frac{b}{l} + R\gamma}{H} = \frac{T}{2H}\frac{b}{l} + \frac{R}{H}\gamma \tag{5-40}$$

Again the effect of the camber is $\frac{R}{H}$ times the effect of the tilt mechanism similar to four-wheeled vehicles. The exact solution for both tilt and camber mechanisms of our three-wheeled case is also calculated and plotted as shown in Figure 5-12.

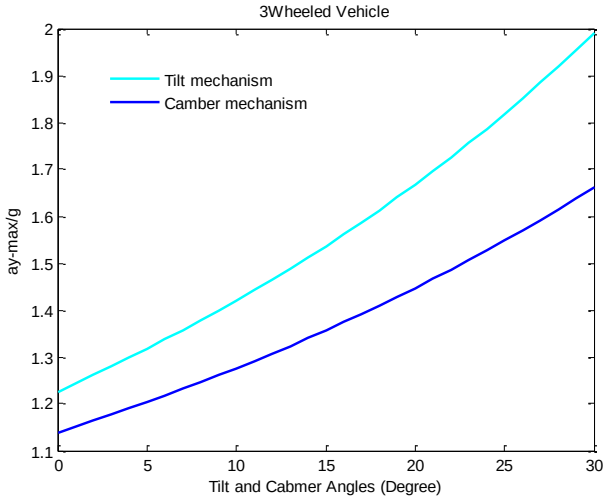

Figure 5-12: Camber mechanism and tilt mechanism for the three-wheeled case

5.3.3 Rollover Index including camber effects

This section explores the effects of camber on the lateral load transfer ratio (LTR) and explains the derivation of a dynamic rollover index including camber effects based on the LTR. Only effects of camber on un-tripped rollovers are considered in this section. Figure 5-13 shows a half car vehicle rollover model including wheels' camber angles.

The equation for the sprung mass around the roll center is again Eq. (4-8) in Chapter 4. The moment balance for the un-sprung mass around the contact point of the left wheel yields

$$F_{zr}(T - R\sin\gamma_r + R\sin\gamma_l) = mg\left(\frac{T}{2} + R\sin\gamma_l\right) + m_u a_y h_u + m_s a_y h_R + k_\varphi \varphi + c_\varphi \dot{\varphi} \tag{5-41}$$

The moment balance for the un-sprung mass around the contact point of the right wheel yields

$$F_{zl}(T - R\sin\gamma_r + R\sin\gamma_l) = mg\left(\frac{T}{2} - R\sin\gamma_r\right) - m_u a_y h_u - m_s a_y h_R - k_\varphi \varphi - c_\varphi \dot{\varphi} \qquad (5\text{-}42)$$

Subtracting Eq. (5-42) from Eq. (5-43) yields:

$$F_{zr} - F_{zl} = \frac{mg(R\sin\gamma_l + R\sin\gamma_r) + 2m_u a_y h_u + 2m_s a_y h_R + 2k_\varphi \varphi + 2c_\varphi \dot{\varphi}}{T - R\sin\gamma_r + R\sin\gamma_l} \qquad (5\text{-}43)$$

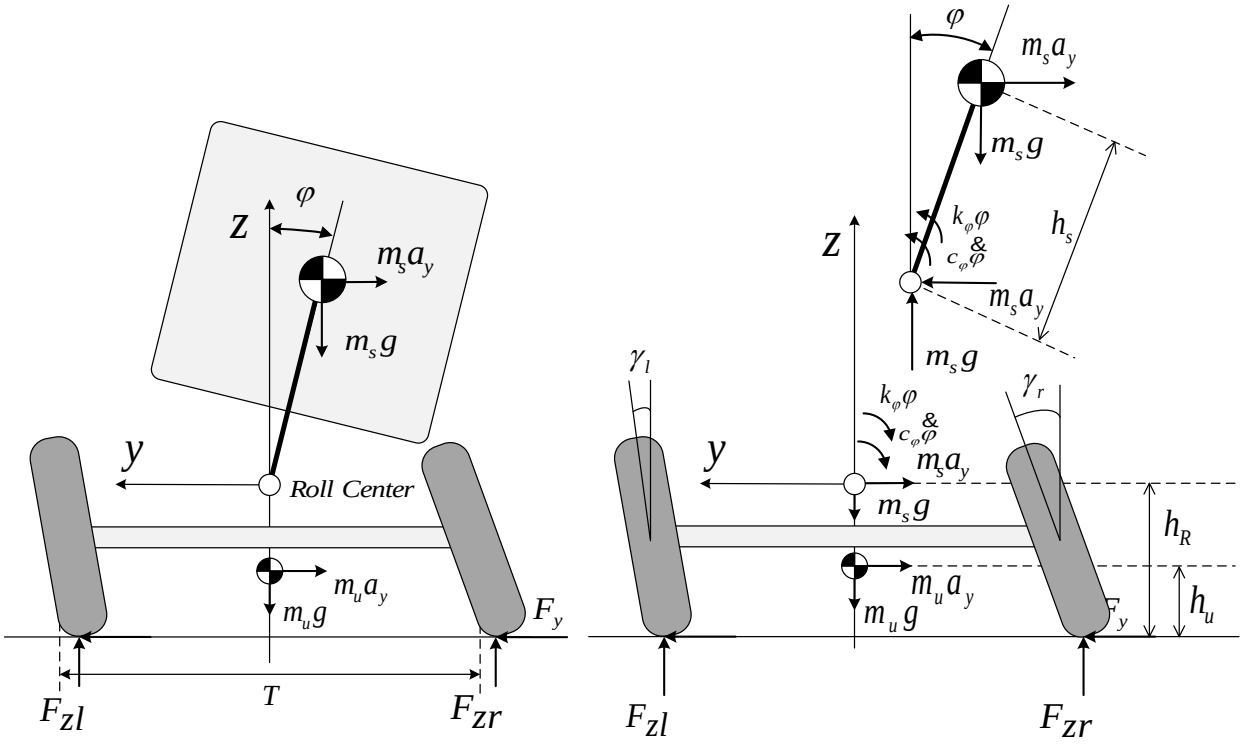

Figure 5-13: Vehicle rollover model including camber effects

Then, substituting Eq. (4-8) (for flat roads ($\varphi_r = 0$)) into Eq. (5-43) gives

$$F_{zr} - F_{zl} = \frac{mg(R\sin\gamma_l + R\sin\gamma_r) + 2m_u a_y h_u + 2m_s a_y h_R + 2m_s a_y h_s \cos\varphi + 2m_s g h_s \sin\varphi - 2(I_{xx} + m_s h_s^2)\ddot{\varphi}}{T - R\sin\gamma_r + R\sin\gamma_l} \qquad (5\text{-}44)$$

Assuming a small roll angle ($\cos\varphi \approx 1$, $\sin\varphi \approx \varphi$) and using $m_u h_u + m_s h_R + m_s h_s = mH$, Eq.(5-44) can be simplified as:

$$F_{zr} - F_{zl} = \frac{mg(R\sin\gamma_l + R\sin\gamma_r) + 2ma_yH + 2m_sgh_s\varphi - 2(I_{xx} + m_sh_s^2)\ddot{\varphi}}{T - R\sin\gamma_r + R\sin\gamma_l} \quad (5\text{-}45)$$

Finally, using $F_{zr} + F_{zl} = mg$ and substituting Eq. (5-45) into Eq. (4-1), a dynamic RI for 4W vehicles including camber effects is proposed as:

$$RI = \frac{1}{T - R\sin\gamma_r + R\sin\gamma_l}\left(\frac{mg(R\sin\gamma_l + R\sin\gamma_r) + 2ma_yH + 2m_sgh_s\varphi - 2(I_{xx} + m_sh_s^2)\ddot{\varphi}}{mg}\right) \quad (5\text{-}46)$$

This equation shows rollover risk when right and left wheels can have independent camber angles. Two specific configurations were discussed before when right and left camber angle were dependent with similar values in opposite direction (first configuration) and parallel direction (second configuration). For the first configuration, $\gamma = \gamma_l = -\gamma_r$ and rollover index is

$$RI = \frac{1}{T + 2R\sin\gamma_l}\left(\frac{2ma_yH + 2m_sgh_s\varphi - 2(I_{xx} + m_sh_s^2)\ddot{\varphi}}{mg}\right) \quad (5\text{-}47)$$

So the effect of camber angle for the first configuration is a change in vehicle track. For the second configuration, $\gamma_l = \gamma_r = \gamma$ and the RI is

$$RI = \frac{1}{T}\left(\frac{2ma_yH + 2m_sgh_s\varphi - 2(I_{xx} + m_sh_s^2)\ddot{\varphi} + mg(2R\sin\gamma)}{mg}\right) \quad (5\text{-}48)$$

As can be seen from the equation, the vehicle track remains unchanged, but camber angle is still effective on rollover as contributes to lateral load transfer.

It should be mentioned that depending on the suspension design, camber angle may change effective stiffness and damping coefficient and even tire stiffness. However, these changes will not affect RI equation since this equation is written based on vehicle states. In fact, although changes of effective stiffness and dapping are important in rollover, they do not appear directly in RI equation. In fact, these changes affect vehicle states, so their effects will be indirectly detected by the RI through vehicle states like lateral acceleration and roll angle.

5.3.3.1 Lateral Load Transfer

To evaluate the effects of camber on lateral load transfer, the small angle assumption is considered again in this subsection. The effect of the roll acceleration ($\ddot{\varphi}$) is ignored since it is small based on sensitive analysis in Chapter 4. Then, the LTR (or the RI) for the first configuration (Figure 5-4) is

$$LTR(\gamma) = \frac{2ma_yH + 2m_sgh_s\varphi}{mg(T_0 + 2R\gamma)} \tag{5-49}$$

Dividing $LTR(\gamma)$ by its initial value (LTR without camber angle), yields

$$\frac{LTR(\gamma)}{LTR} = \frac{T_0}{T_0 + 2R\gamma} = 1 - \frac{2R\gamma}{T_0 + 2R\gamma} \tag{5-50}$$

The change in lateral load transfer is then given as

$$\frac{LTR(\gamma) - LTR}{LTR} = -\frac{2R\gamma}{T_0 + 2R\gamma} \tag{5-51}$$

And the percentage of change is:

$$Percentage\ of\ change\ in\ LTR = \left|\frac{2R\gamma}{T_0 + 2R\gamma}\right| \times 100 \tag{5-52}$$

The resulting values of the percentage of change in LTR for a constant value of $R_w = 0.3$ are plotted in Figure 5-14. For example, for a vehicle with track of 1m, 15 degrees of camber angle results in about 15 percent of decrease in the lateral load transfer.

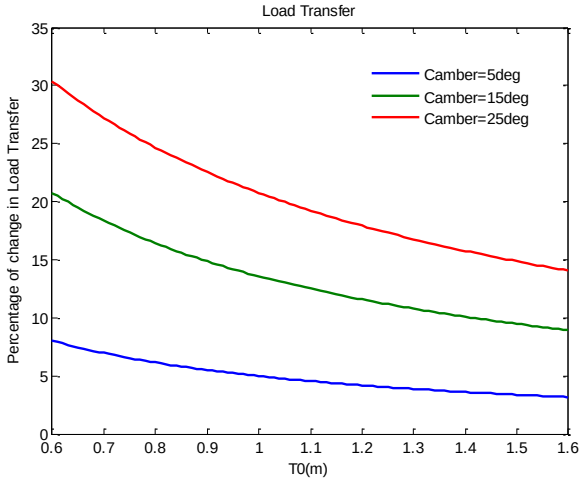

Figure 5-14: Cambering effect on lateral load transfer (first configuration)

In contrast to the result of the maximum lateral acceleration, the change of the lateral load transfer for the second configuration is different from that of the first configuration. The equation for lateral load transfer of the second configuration can be simplified as

$$LTR(\gamma) = \frac{2ma_yH + 2m_sgh_s\varphi + 2mgR\gamma}{mgT} \tag{5-53}$$

As can be seen, the equation for lateral load transfer of the second configuration is different from the equation for the first configuration. It is shown in Appendix C that the load transfer for the second configuration is always less than the first configuration. In fact, using the second configuration, the vehicle experiences less load transfer in turning. In fact, for $LTR < 1$

$$\frac{2ma_yH + 2m_sgh_s\varphi}{mg(T + 2R\gamma)} > \frac{2ma_yH + 2m_sgh_s\varphi + 2mgR\gamma}{mgT} \tag{5-54}$$

and for $LTR = 1$ (i.e. zero contact force of inner wheel) they are equal ($LTR_1 = LTR_2$). Figure 5-15 illustrates the load transfer effects for the four-wheeled case.

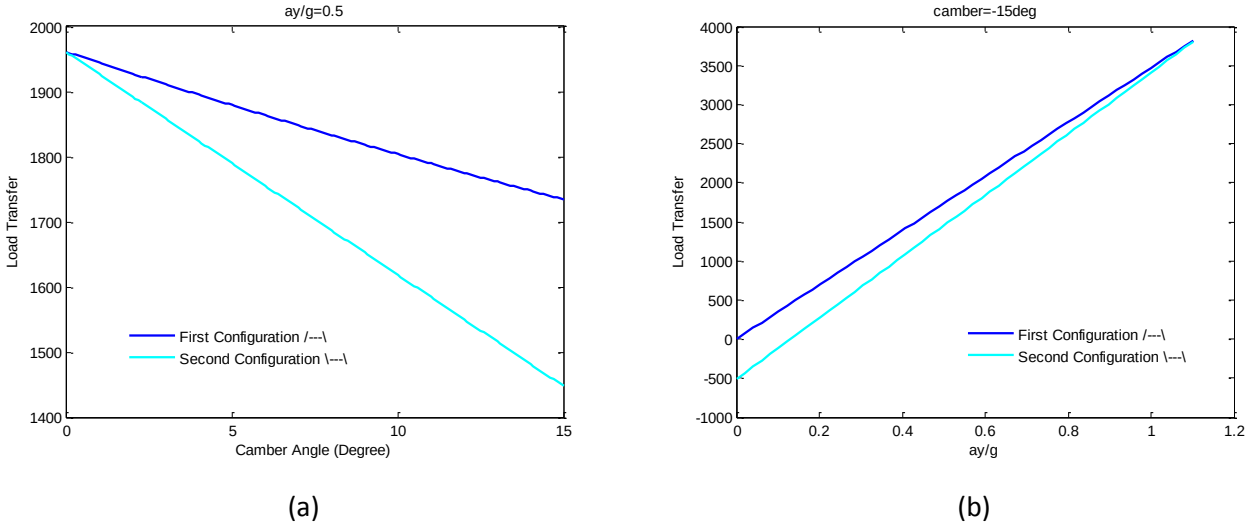

(a) (b)

Figure 5-15: Lateral load transfer for both configurations

Figure 5-15 shows the different behaviors of two configurations in load transferring. Figure 5-15a shows the value of load transfer versus camber angle for a constant lateral acceleration. It can be seen that the load transfer value for the second configuration is always less than that for the first configuration. Figure 5-15b shows the same trend. Another observation for the second configuration is that it is possible to make the lateral load transfer equal to zero for a range of lateral accelerations by applying camber angle. To achieve the relation, it is assumed that the lateral load transfer is equal to zero and the equation for camber angle is derived

$$
\begin{gathered}
LTR(\gamma) = 0 \;\Rightarrow \\
\frac{ma_y H + m_s g h_s \varphi - mgR\gamma}{T} = 0 \;\Rightarrow \\
\gamma = \frac{mH + m_s g h_s \dfrac{m_s h_s}{k_t - m_s g h_s}}{mgR} a_y \;\Rightarrow \gamma = K_\gamma a_y
\end{gathered}
\tag{5-55}
$$

Therefore, by choosing the camber angle as a multiplication of a constant value (K_γ) to the lateral acceleration, the lateral load transfer for the second configuration can be made zero. However, this equation can be used only for small values of lateral acceleration because of the limitation of maximum possible camber angle.

5.4 Simulation results

For further investigation, simulation results for specific cases are discussed in this section. Since the existing suspensions in CarSim do not provide commanded real-time camber change, the provided mathematics vehicle models in Chapter 3 (Eqs. (5-28)-(5-30)) along with the motorcycle tire model with camber (Eq. (5-1)) are used for vehicle's dynamics simulation for lateral stability study. The motorcycle tire is used that suitably matches the urban vehicles with lower weight than the conventional vehicles. However, for rollover study, vehicle models in CarSim are used while camber angle are statically changed and simulations are run with and without camber angles.

5.4.1 Camber effects on lateral dynamics

The vehicle parameters for simulations in this section are provided in Appendix D. Different scenarios of front and rear camber angles are explored to examine the effects of camber on vehicle lateral dynamics as shown in Figure 5-16. Three scenarios are: 1- Front camber 10 degrees and rear camber 0 degree, 2- Front camber 0 degree and rear camber 10 degrees, 3- Front camber 10 degrees and rear camber 10 degrees.

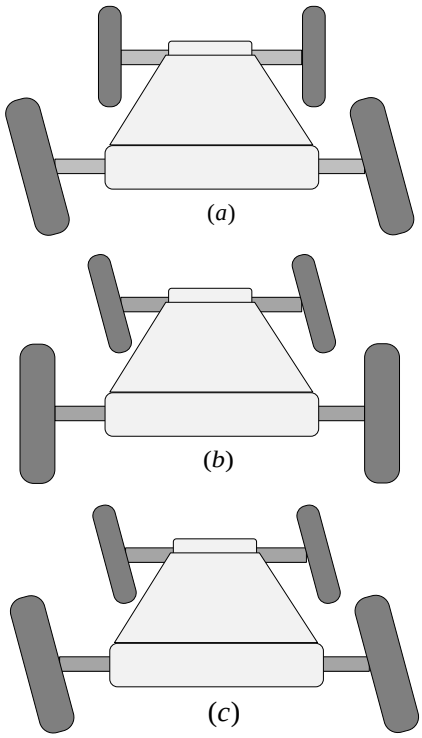

Figure 5-16: Three scenarios for cambering (front view): a) front wheel cambering, b) rear wheel cambering, c) front and rear cambering

Longitudinal velocity is $U_c = 20m/s$, and a constant 3 degree steering angle is applied. A low-pass filter is used to have a smooth steering change as shown in Figure 5-17.

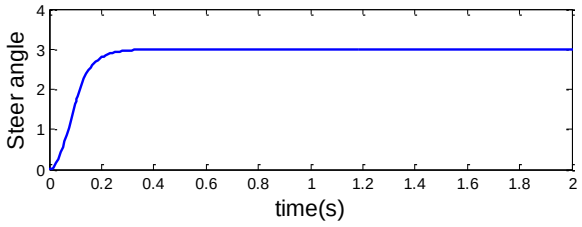

Figure 5-17: Steering input

Vehicle dynamic responses including yaw rate, vehicle's side slip angle, roll angle and vehicle's path are plotted for each scenario as shown in Figure 5-18. The results are compared with the case without cambering.

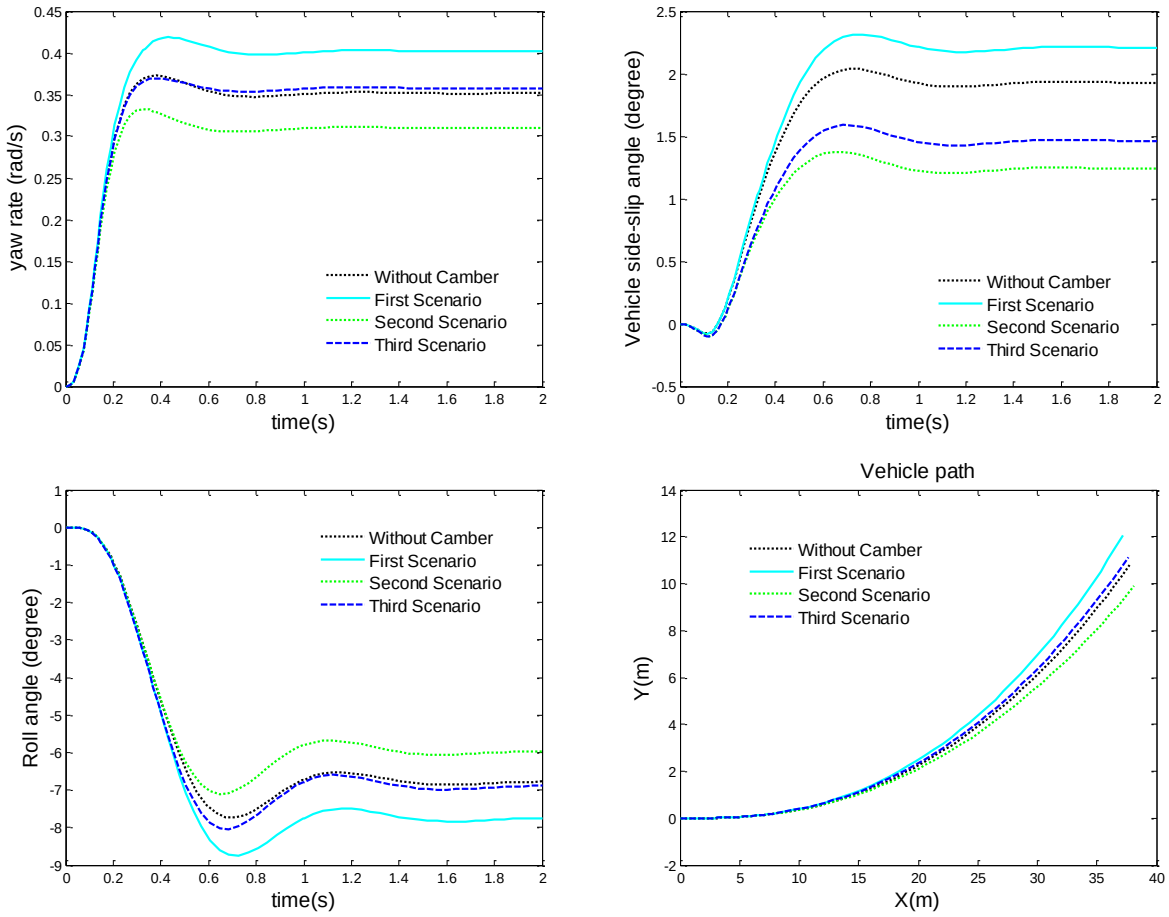

Figure 5-18: Vehicle response for the three scenarios

The first scenario represents the effects of front wheel cambering. As can be seen, the front wheel camber increases the yaw rate response. The sideslip angle also increases. The roll angle and vehicle path are mostly influenced by yaw rate and, as can be seen in this figure, the roll angle increases following the increase of the yaw rate. The second scenario represents the effects of rear wheel cambering. The rear wheel camber, in contrast to front wheel camber, decreases yaw rate response. The sideslip angle and the roll angle also decrease. For the third scenario, similar camber angles are applied to both front and rear wheels. As discussed, the effect of front camber and rear camber are in contrast. The results of this part show that they neutralize the effects of each other in yaw response when they are both applied to the vehicle. Therefore, for roll angle and vehicle path which mainly depend on the yaw rate, the effects are approximately neutralized similar to the yaw rate. On the other hand, the side slip angle considerably decreases. In fact, by applying similar camber angle to both

front and rear wheel, the effect is a pure change in side slip angle response (i.e. lateral velocity) of the vehicle without considerable change in other vehicle states. In other words, having camber angle for both front and rear wheels reduces vehicle slipping without considerable change on yaw rate. This fact could be very useful for decoupling control of yaw rate from control of side slip angle in the vehicles. Results of the second and third scenarios show that the rear camber angle can be very useful for control of vehicle side slip angle.

Figure 5-19 shows the dynamics responses for the first configuration when 10 degrees of camber angle is applied on the front wheels. The results are compared with the results of equivalent increase in steering angle as mentioned in previous part. It can be seen that, for the nonlinear case, the vehicle behavior for applying camber and for increasing steering are very close to each other. Thus, the simulation results also confirm that the front camber acts like steering.

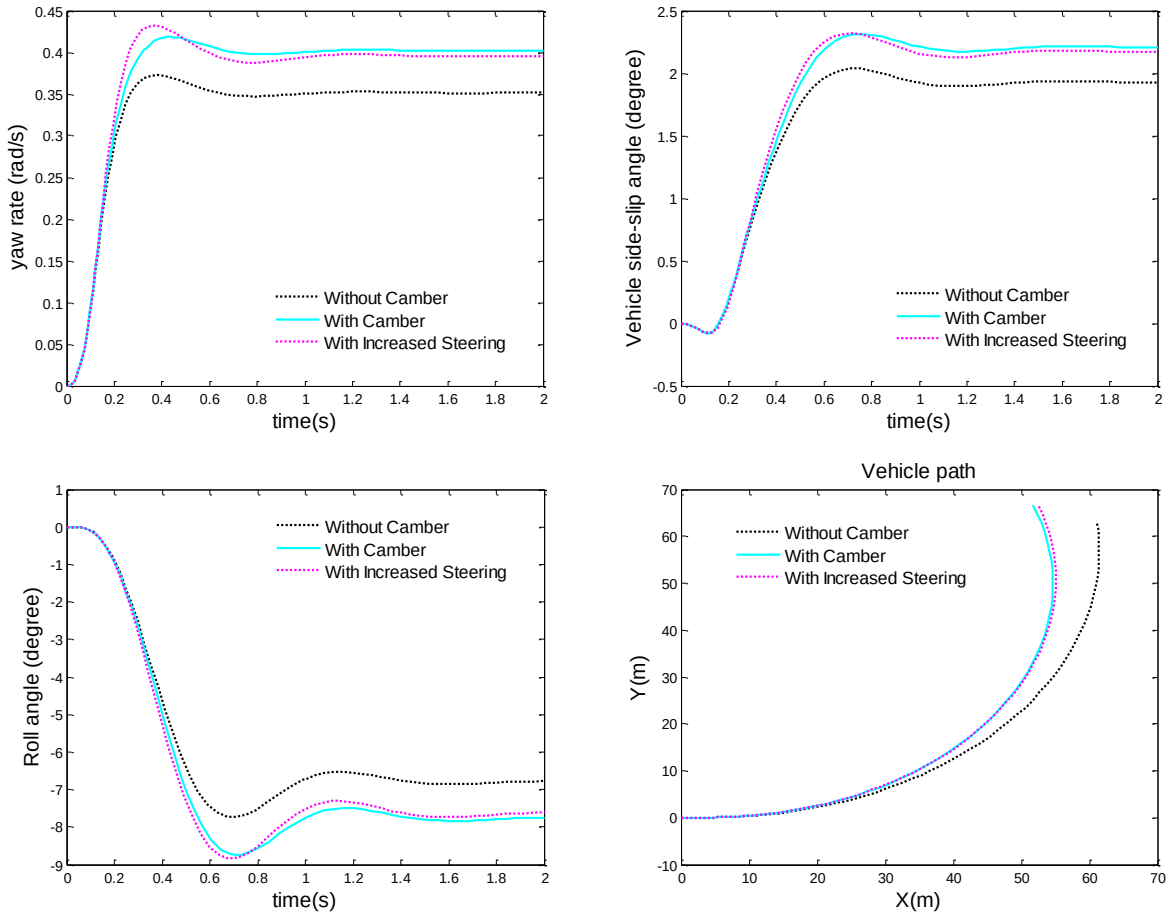

Figure 5-19 : Vehicle response: first scenario compared with increased steering

The load transfer difference between steering and cambering can be important for large camber angles. Figure 5-20 shows the differences in lateral load transfer for 20 degrees of cambering and the equivalent steering.

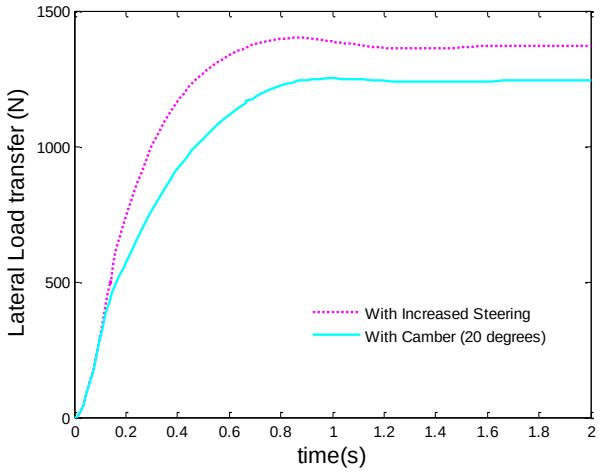

Figure 5-20: lateral load transfer for cambering and the equivalent steering

5.4.2 An active camber system for stability improvement

In this section, an active camber system is provided for lateral stability control of an urban vehicle. The linear vehicle model in Eq. (5-5) is employed and an LQR controller is developed assuming front and rear camber systems as the actuators. The performance index of the optimal controller is defined as

$$J = \frac{1}{2}\int_0^\infty [(X_d - X)^T Q(X_d - X) + U^T RU]dt \tag{5-56}$$

where X_d and U represent desired response and control input, respectively; Q and R are the weighting matrixes. The optimal control input to minimize this performance index is given by [134]

$$U = -R^{-1}B_g^T(PX + S) \tag{5-57}$$

where P and S are the controller parameters. For a constant steering input and infinite time, by ignoring the transient part of the solution, P and S will be obtained from the following algebraic equations [134]

$$A^T P + PA - PBR^{-1}B^T P + Q = 0 \tag{5-58}$$

$$(A^T - PBR^{-1}B^T)S - QX_d + PE\delta_d = 0 \tag{5-59}$$

The control law (Eq. (5-57)) has the state feedback term and the feed-forward term. The control input can be rewritten as

$$U = K_v v + K_r r + K_\varphi \varphi + K_{\dot{\varphi}} \dot{\varphi} + K_\delta \delta_d \tag{5-60}$$

where K_v, K_r, K_φ, $K_{\dot{\varphi}}$ and K_δ represent control gains for lateral velocity, yaw rate, roll angle, roll rate, and driver steering command, respectively, and can be achieved from Eqs. (5-28)-(5-59). The desired values for the states are $X_d = [0,\ r_d, 0, 0]^T$ where r_d is the desired yaw response obtained from the following equation:

$$\frac{r_d}{\delta_d} = \frac{u}{l + k_{us\_d} u^2} \tag{5-61}$$

l is wheelbase and k_{us_d} is the desired understeer coefficient for the vehicle. In general, the understeer coefficient is an important criterion for evaluation of the handling characteristics of vehicles and describes the sensitivity of vehicles to the steering input.

The performances of the front and the rear camber mechanisms are explored individually and together to see the behavior of each of them. The desired understeer coefficient for our case is intended to be $k_{us\_d} = 0.001$. For the weighting matrixes, Q is a diagonal matrix and selected as $Q = diag(0.001,1,0,0)$; with this matrix for weighting the states, the main objective is to control the yaw rate response. The weighting matrix for control inputs is selected as $R = diag(5e-3, 5e-3, 5e-3, 5e-3)$ which shows similar weights for all four camber inputs. The performance is again investigated for a constant 3 degree steering input. The vehicle is assumed to have a constant longitudinal velocity of 25 m/s.

Figure 5-21 demonstrates the vehicle responses for the active front camber, the active rear camber, and the active front and rear camber compared with the reference value and the non-controlled vehicle response. As it can be seen from the yaw rate responses, all of the three active camber systems follow the reference command accurately and quickly. These active systems have considerably improved the vehicle's behavior compared to the non-controlled case.

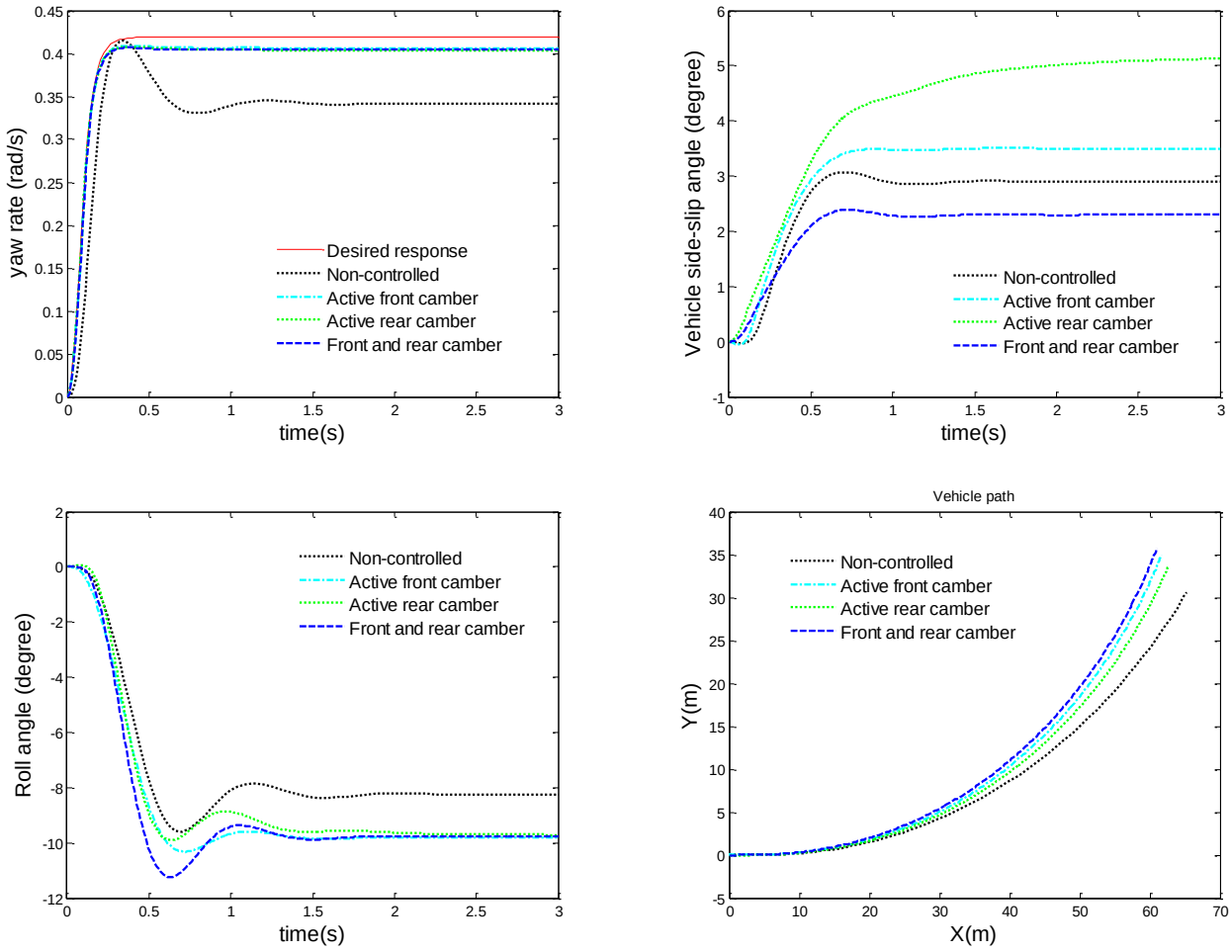

Figure 5-21: Vehicle's response for active camber system

Other important characteristics of the vehicle are also illustrated in Figure 5-21 including vehicle side slip angle, roll angle, and the vehicle's path. The effectiveness of the active systems for improvement of the vehicle performance is shown also in these plots. The active systems have similar behavior in all vehicle responses except the vehicle side slip angle and, consequently, the lateral velocity. As discussed in the previous section, the effect of rear camber angle on vehicle side slip angle is more than that of front camber angle for similar change on the yaw rate which is also confirmed in this figure. On the other hand, using both front and rear camber angle, it is possible to increase the vehicle's yaw rate while the side slip angle is decreased. Therefore, the combination of front and rear camber angle can control both yaw rate and side slip angle, simultaneously. This combined camber

system is capable of not only improving the yaw response and turning ability, but also decreasing the side slip angle (i.e. vehicle slip) of the vehicle.

The applied camber angle on the vehicle are shown in Figure 5-22 for both front and rear wheels when they are independent or integrated. As can be seen, to increase the vehicle yaw rate, the active front camber system applies positive camber angle while the active rear camber system applies negative camber angle which was expected based on the desscusion in previous section about the dynamic bahavior. For the case of integrated front and rear camber, both front and rear camber angles are positive while the value of the front camber angle is more than the value of rear camber angle. This combination of front and rear camber angles results in increasing the yaw rate while simultanously decreasing side slip angle.

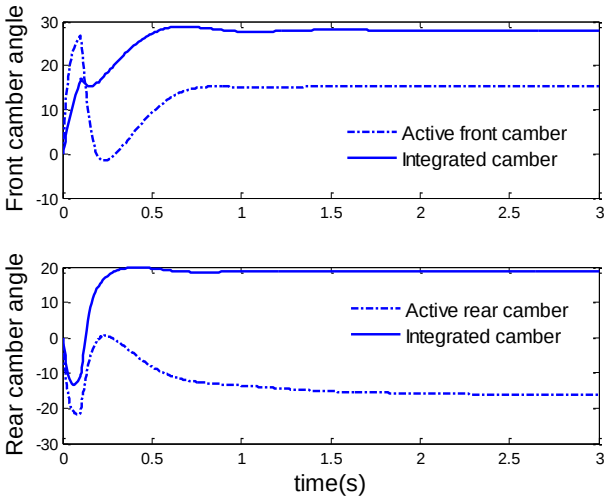

Figure 5-22: Camber angles in active camber system

5.4.3 Comparison of active camber and active steering

Active camber system is compared with active steering system in this part. Active front steering, as a well-known mechanism for lateral stability control, is largely investigated and discussed in the literature. As mentioned before, for the linear zone of tire lateral forces, active camber system works similar to active steering system. The purpose of this part is to compare the performances of these two mechanisms at the nonlinear zone. Therefore, a certain working condition is selected to deliberately push the vehicle to the nonlinear zone. In this regard, a constant speed of $u = 25\ m/s$ with road condition of $\mu = 0.8$ (friction coefficient) is assumed. Figure 5-23 indicates the vehicle performances for both controllers compared with the non-controlled vehicle. As can be seen, the active front camber

system can follow the desired yaw rate response better than the active front steering system for this working condition. Vehicle side slip angle, roll angle, and vehicle path are also shown in Figure 5-23. It is apparent that by increasing the yaw rate, the vehicle side slip, roll angle and lateral acceleration have also increased. The vehicle path shows that using active camber system the vehicle can have a faster turn in cornering. As a result, the vehicle performances indicate that the vehicle with active front camber is more maneuverable than the one with active front steering at the limits of handling.

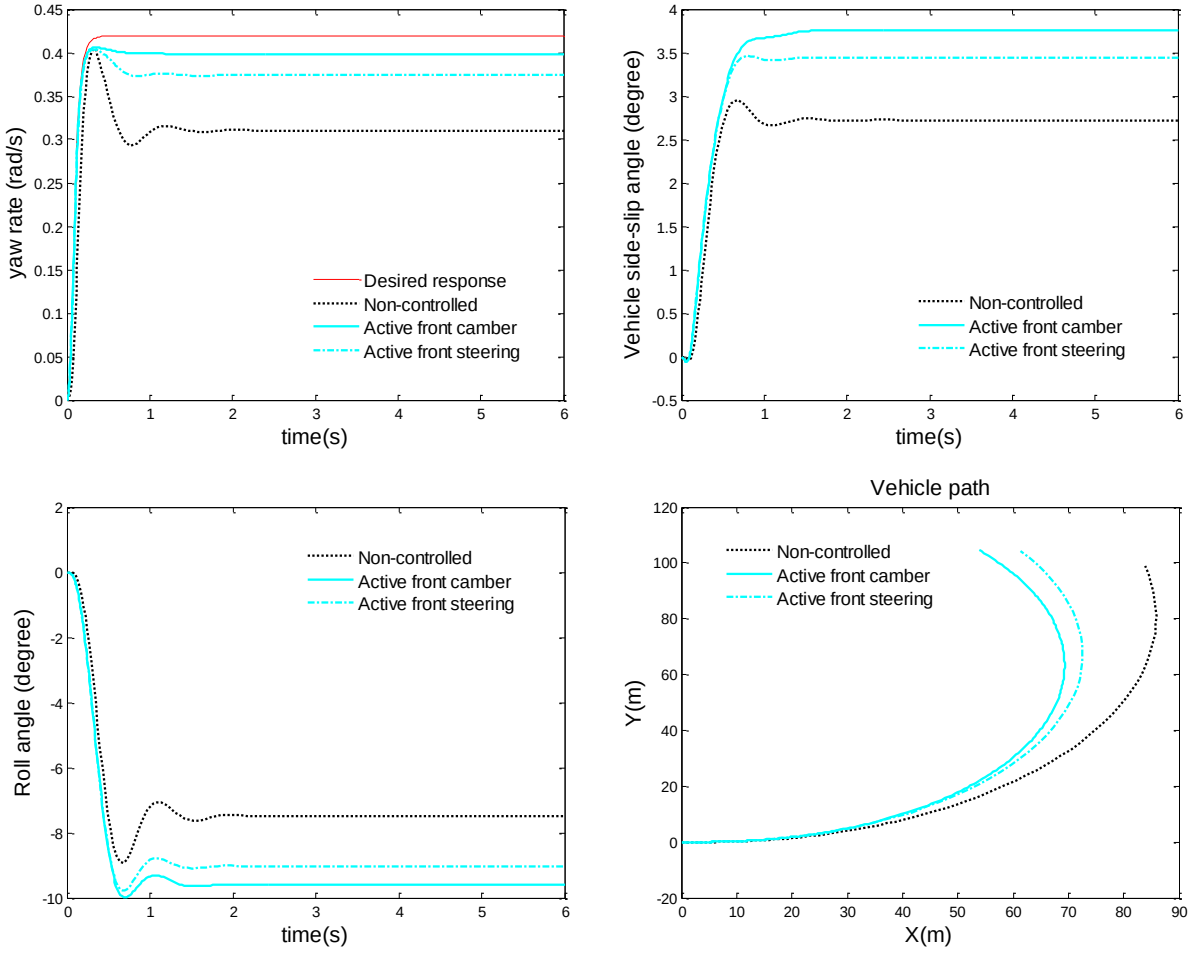

Figure 5-23: Vehicle performances for active front camber and active front steering

Figure 5-24 shows the value of camber angle and front steering angle (from the controller) for these two control systems. The relation that was discussed for linear zone is not applicable for this region (camber angle is 30 and steer angle is 4 degrees) which confirms that the vehicle has entered the nonlinear region of working conditions. Figure 5-25 shows front wheel side slip angles for these two

control systems. The active camber system not only works better than the active front steering, but also it has a considerably smaller front side slip angle that prevents the vehicle from entering the saturation zone. Moreover, Figure 5-26 indicates the working points of the vehicle without control and the working points of active camber and active steering systems. The capability of providing more tire lateral forces and the ability of the control strategy to properly employ this lateral forces can be seen from this figure.

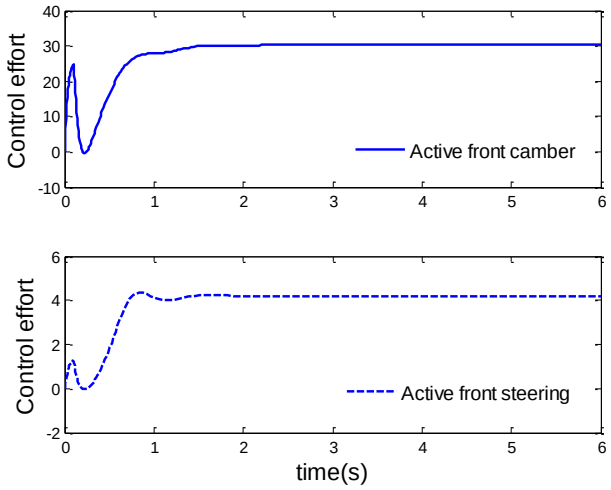

Figure 5-24: Control efforts for controllers

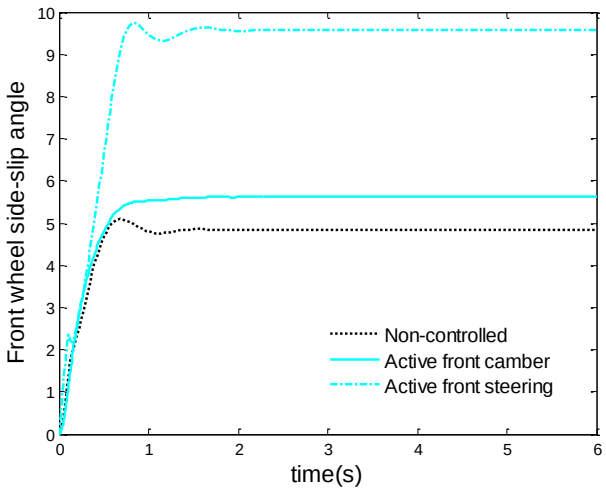

Figure 5-25: Front wheel side slip angles for both controllers

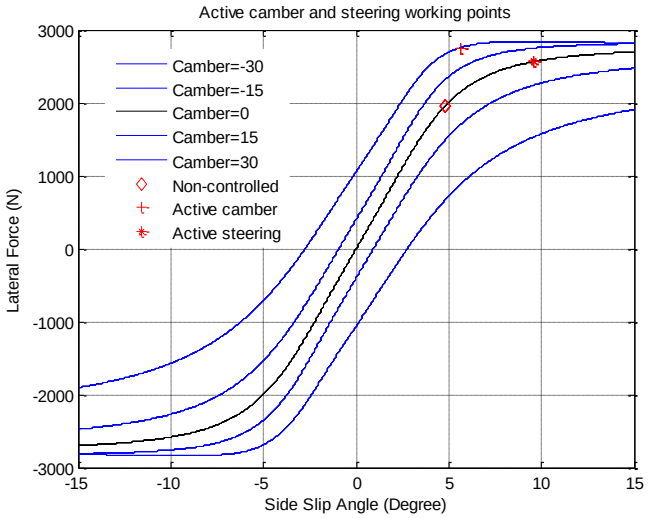

Figure 5-26: working points of active camber and active steering systems

5.4.4 Camber effects on rollover stability

Camber effects on rollover stability of different vehicles are investigated through simulations in this part. Camber angles for rollover prevention of three-wheeled vehicles in Delta and Tadpole configurations are considered as well as a 4W SUV. The simulations are conducted for first configuration of camber angles where the wheels on one track have similar camber angles in opposite direction (outward camber). CarSim vehicle model are considered for simulations in this section, and camber angle are applied statically before running the simulation and then compared with the simulations without camber.

5.4.4.1 Three-wheeled vehicle with Delta configuration

A fishhook maneuver is considered with maximum 100 degrees steer angle on driver's wheel with longitudinal speed of 35 km/h to evaluate the rollover index performance. The steering angle for the fishhook maneuver is shown in Figure 5-27. The proposed rollover index including camber angle is shown in Figure 5-28 which is compared with the measured LTR from CarSim with camber angle of 15 degrees. As can be seen, the proposed RI properly detects rollover danger when camber angle is also included.

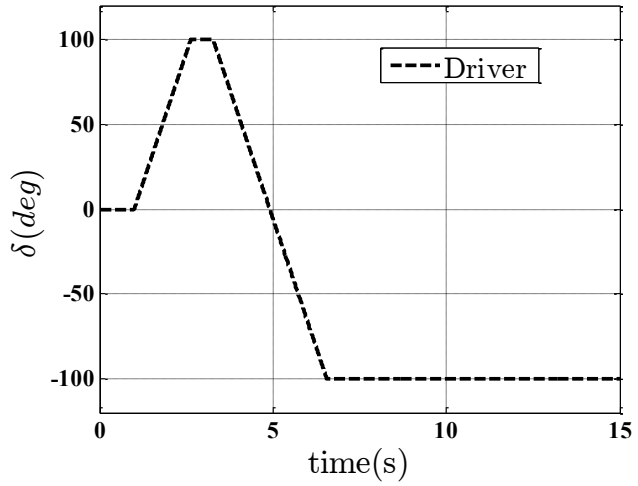

Figure 5-27: Steering angle for the fishhook maneuver

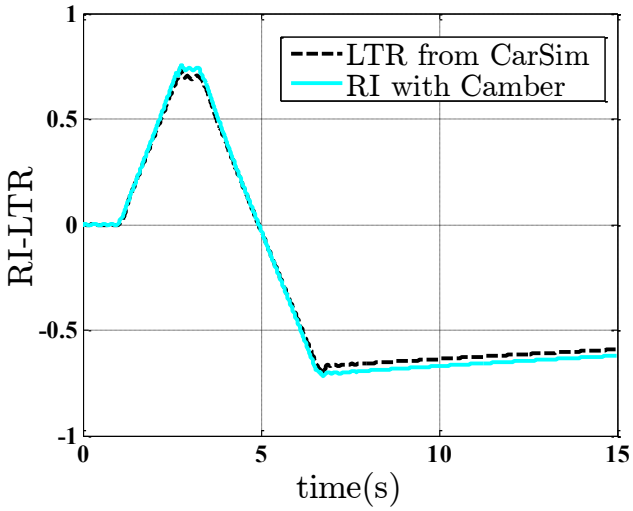

Figure 5-28: Comparison of the proposed RI with the LTR for a Delta 3W vehicle (15 degrees of camber)

Effect of camber angle to decrease rollover danger for this case is shown in Figure 5-29. LTR is shown for the vehicle in same fishhook maneuvers without camber angle and with two different values of 15 and 30 degrees of camber angles. As can be seen, the LTR as the more realistic rollover indication is considerably reduced when camber angles are applied to the vehicle.

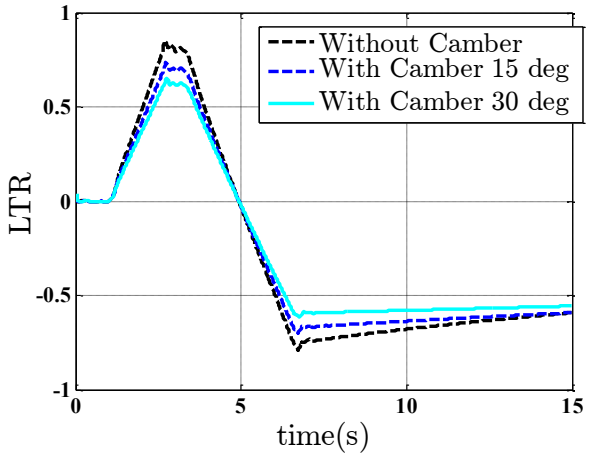

Figure 5-29: Effects of camber on rollover danger for a Delta 3W

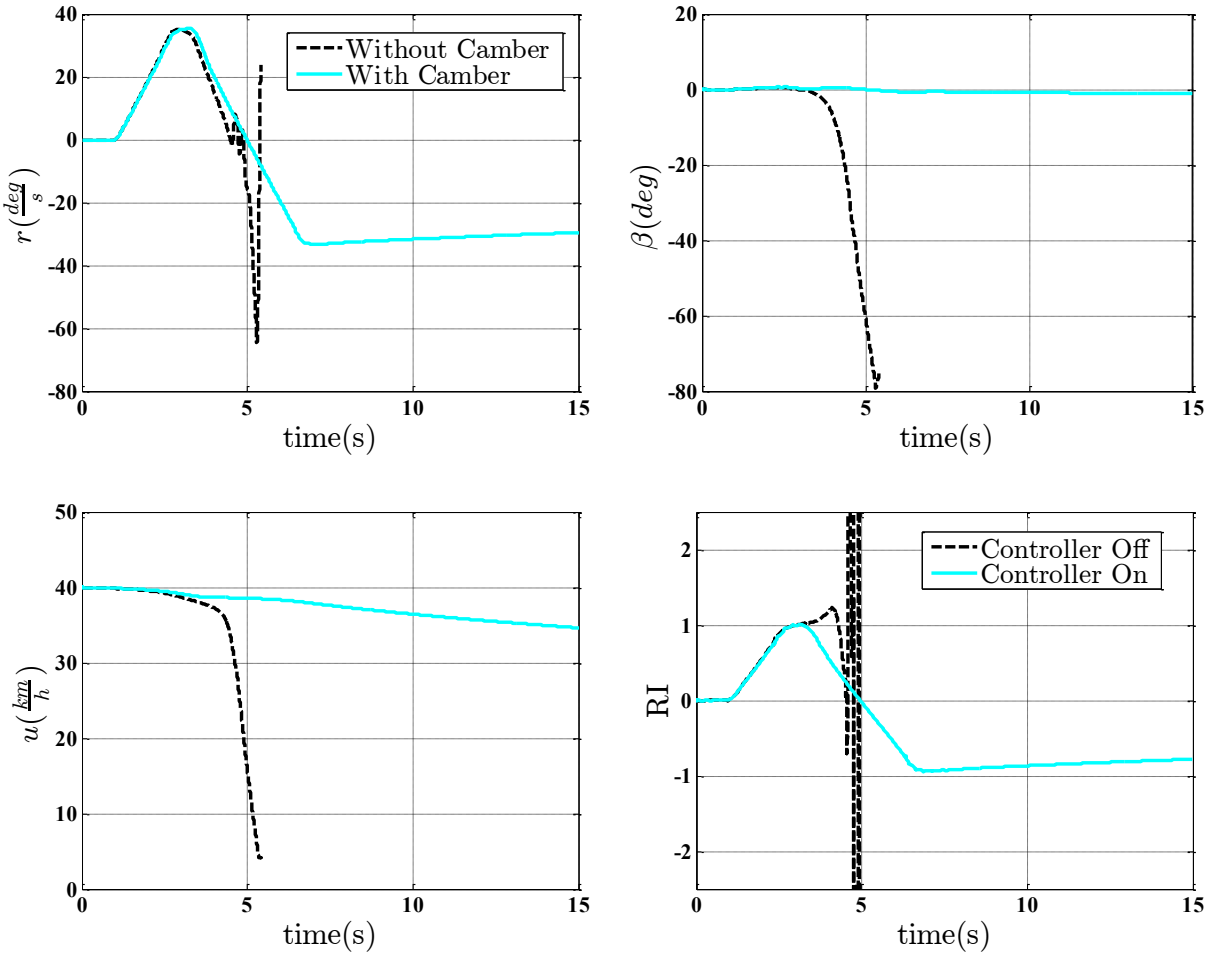

Figure 5-30: Effect of 15 degrees camber on rollover prevention of a Delta 3W

Figure 5-30 shows the mentioned fishhook maneuver when the vehicle speed is increased to 40 km/h. As can be seen, the vehicle has rollover when no camber angle is applied; however, after applying 15 degrees of camber angle it is prevented from rollover and the maneuver is safe.

5.4.4.2 Three-wheeled vehicle with Tadpole configuration

The fishhook maneuver explained in previous subsection is considered also for a Tadpole 3W vehicle with the vehicle speed of 45 km/h. Figure 5-31 shows the effect of camber angle in rollover prevention of this vehicle. The vehicle has rollover when no camber angle is applied; however, applying 15 degrees of camber angle prevents the vehicle from rollover.

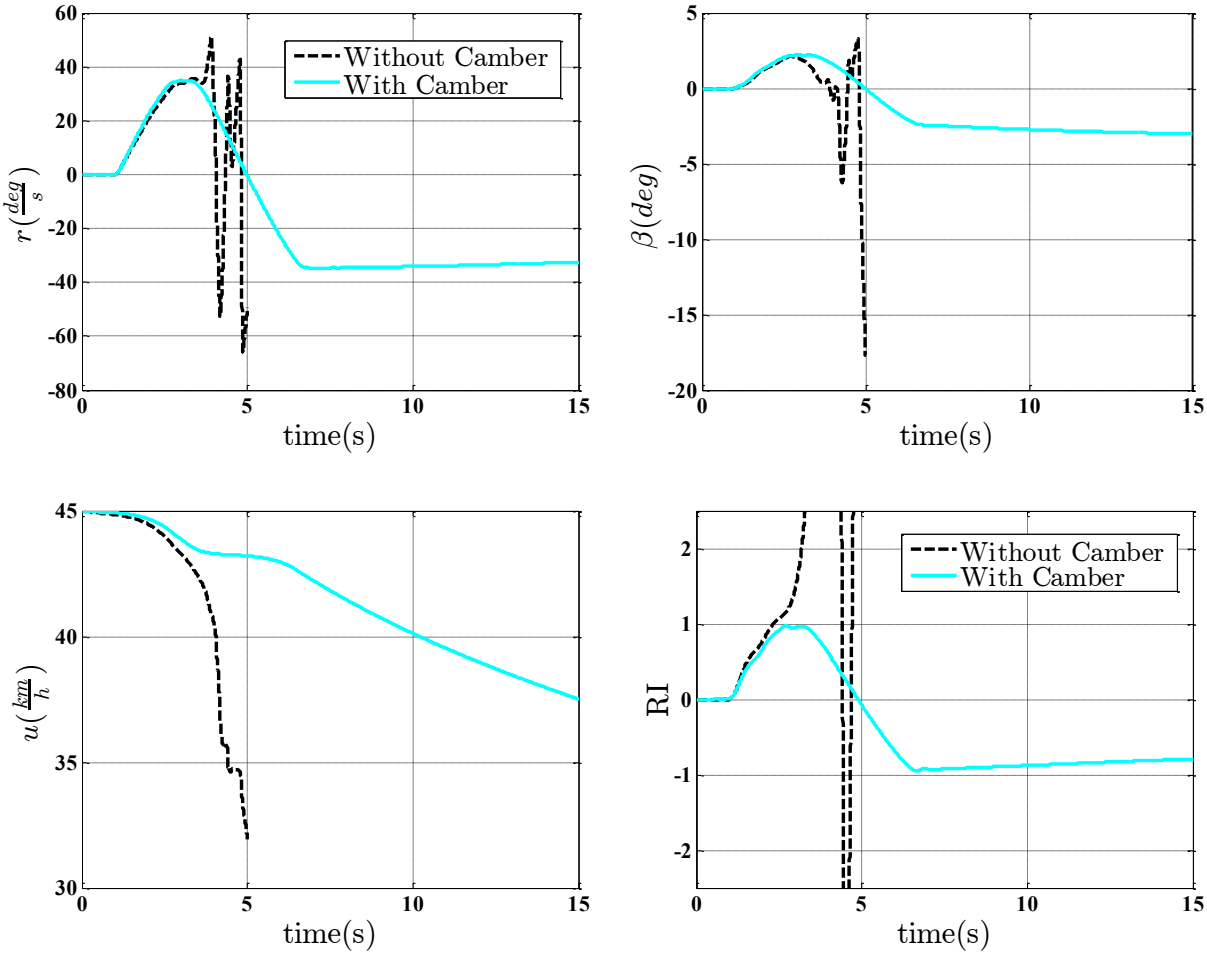

Figure 5-31: Effect of 15 degrees camber on rollover prevention of Tadpole 3W

5.4.4.3 Four-wheeled SUV vehicle

A fishhook maneuver is also considered for a SUV vehicle. The maximum steering angle is 294 degrees and the vehicle speed is 80 km/u. Figure 5-32 shows the proposed rollover index including camber angle which is compared with the measured LTR from CarSim with camber angle of 15 degrees on front and rear wheels. As can be seen, the proposed RI properly detects rollover danger when camber angle is also included.

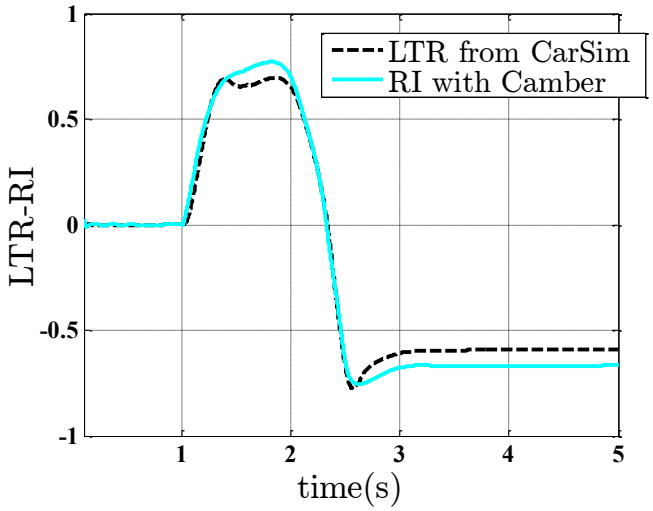

Figure 5-32: Comparison of the proposed RI with the LTR for a SUV (15 degrees of camber)

Effect of camber angle to decrease rollover risk for the SUV is shown in Figure 5-33. LTR is shown for the vehicle without camber angle and with two different values of 15 and 30 degrees of camber angles. As can be seen, the LTR is considerably reduced when camber angles are applied to the vehicle.

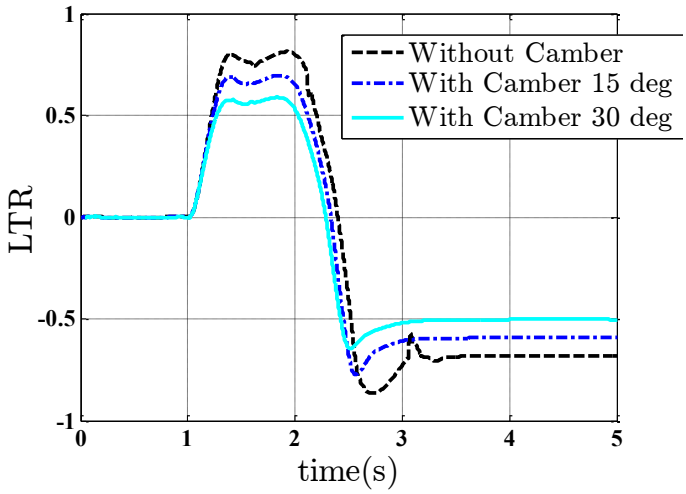

Figure 5-33: Effects of camber on rollover risk for a SUV

Figure 5-34 shows the effect of camber angle to prevent rollover for an unstable situation through the fishhook maneuver. A roof cargo box is added to the vehicle as a payload to increase rollover risk and make it unstable. The vehicle has rollover when no camber angle is applied; however, applying 15 degrees of camber angle prevents the vehicle from rollover.

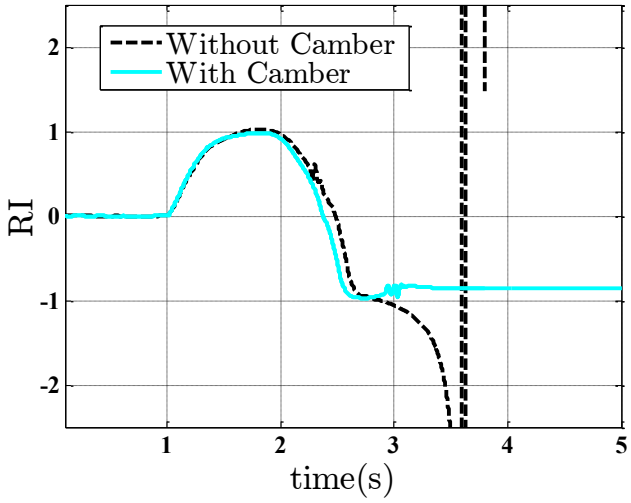

Figure 5-34: Effect of 15 degrees camber on rollover prevention of an SUV

5.5 Conclusions

In this chapter, camber mechanism is investigated as a potential means to improve lateral and rollover stability. Using a linear model, the effects of cambering lateral forces on overall vehicle behavior is analytically evaluated and compared with steering effects. It is shown that for the linear region of tire lateral force, the effects of cambering is similar to steering effects and camber mechanism works like a second steering mechanism. On the other hand, the cambering provides more lateral force and its behavior is linear for a wide range of camber angles. Then, an active camber system is developed for improvement of vehicle lateral stability of an urban vehicle. The camber effects are also examined for rollover analysis and stability. The maximum lateral acceleration and the lateral load transfer are explored as important rollover criteria. Camber mechanism is also compared with tilt mechanism which is a popular strategy for rollover prevention of narrow vehicles. Cambering effects are examined for four-wheeled and three-wheeled vehicles. The simulation results show the effectiveness of camber system for improvement of lateral stability of vehicles as well as rollover prevention.

Chapter 6: Integrated reconfigurable control design

This chapter provides a general integrated control structure which can handle different stability and safety objectives of urban vehicles and is also reconfigurable to be used for three- and four-wheeled vehicles with any types and combinations of control actuations. Handling improvement, lateral stability, slip control in traction and braking, rollover prevention, and longitudinal control are the control objectives that are considered for the design of the general integrated controller. The controller can also readily be adjusted for different configurations of three- and four-wheeled vehicles as well as different types of actuators including differential braking, torque vectoring, active front steering, active rear steering, and active camber system.

The reconfigurable state-space vehicle model which was developed in Chapter 1 is used in this chapter to design a model-based reconfigurable integrated controller [135][136]. In this study, a Model Predictive Control (MPC) approach is employed to stablish the controller. Figure 6-1 shows the general structure for the proposed controller.

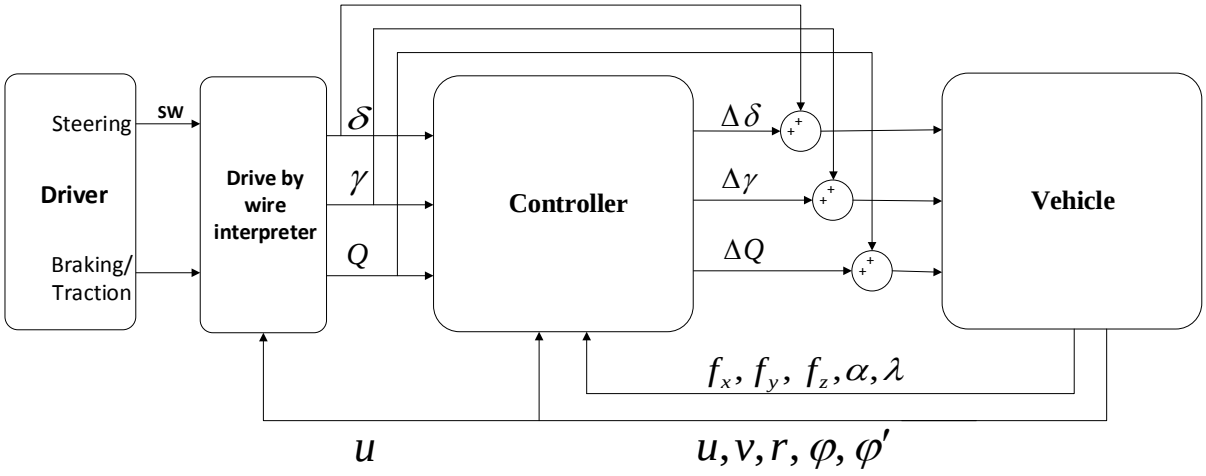

Figure 6-1: Control Structure

The driver applies steering and braking/traction on the vehicle. The drive-by-wire interpreter distributes the driver commands to the wheels as steer, camber, and torque on each wheel. The control block receives the state variables which are measured or estimated from the vehicle. Also, the controller block uses the driver commands on wheels. Employing the reconfigurable vehicle model, the measured/estimated state variables, and the driver commands, the integrated controller provides corrections on driver commands to stabilize the vehicle and improves the performance.

6.1 Control Objectives

The proposed controller is general and considers multiple control objectives as follows.

6.1.1 Handling improvement

Handling improvement can be achieved by tracking the desired yaw rate response based on the driver's intended command. A linear bicycle model is used to generate the reference yaw rate response. The desired yaw response from the bicycle model can be obtained as:

$$r_b = \frac{u}{l + k_{us\_d} u^2} \delta_d \tag{6-1}$$

where k_{us_d} is the desired understeer coefficient for the vehicle. The understeer coefficient is an important criterion for evaluation of the handling characteristics of vehicles and describes the sensitivity of vehicles to the steering input. The controller is supposed to improve handling performance of the vehicle to behave as closely as possible to a vehicle with understeer coefficient of k_{us_d}. However, the maximum friction capacity between tires and the road limits the maneuverability of the vehicle. Thus, the steady-state yaw rate associated with the maximum lateral tire forces are considered as the limit of the yaw rate [40]. Regarding the maximum lateral forces on each axle of the vehicle, the yaw rate is limited as [40]:

$$r_{max} = \begin{cases} \dfrac{f_{yr\_max}(1 + b/a)}{mu} & f_{yf\_max} \geq \dfrac{b}{a} f_{yr\_max} \\ \dfrac{f_{yf\_max}(1 + a/b)}{mu} & f_{yf\_max} < \dfrac{b}{a} f_{yr\_max} \end{cases} \tag{6-2}$$

Where f_{yf_max} and f_{yr_max} denote the maximum available lateral forces on front axle and rear axle, respectively. To simplify the equation, f_{yf_max} and f_{yr_max} are calculated using the normal force distribution in static situations as:

$$f_{yf\_max} = \frac{b}{a + b} mg\mu_y \tag{6-3}$$

$$f_{yr\_max} = \frac{a}{a + b} mg\mu_y \tag{6-4}$$

where μ_y is the lateral friction coefficient. Then $f_{yf\_max} = \frac{b}{a} f_{yr\_max}$, and Eq.(6-2) will be simplified as:

$$r_{max} = \frac{\mu_y g}{u} \tag{6-5}$$

It should be mentioned that these equation are derived using the bicycle model, and they are also valid for 3W vehicles without any change. Then, the desired yaw rate is defined as:

$$r_d = sign(\delta_d) \times \min(|r_b|, r_{max}) \tag{6-6}$$

which means the desired response of the bicycle model before reaching the saturation of lateral forces.

6.1.2 Lateral stability

To maintain the vehicle laterally stable, sideslip angle of the vehicle should be limited within a determined region. A constant threshold on the sideslip angle has been widely used for the vehicle sideslip angle. Recently, a new approach is suggested to define the limit considering also the vehicle longitudinal speed and the yaw rate [40]. Specifically, the sideslip angle of the rear tire is constrained which depends on the speed and the yaw rate of the vehicle. The rear tire's sideslip is:

$$\alpha_r = \delta_r - \frac{v - br}{u} \tag{6-7}$$

where δ_r is the steer angle of the rear tire. The sideslip angle of the vehicle is $\beta = -\frac{v}{u}$, and the limits for the sideslip angle are defined as $\left|\beta + \delta_r - \frac{b}{u} r\right| < \alpha_{r\_max}$; where α_{r_max} is the maximum allowable sideslip angle of the rear tire. It should be mentioned that the limits on yaw rate and rear sideslip angle (Eqs. (6-5) and (6-7)) results in envelope boundaries appearing as a parallelogram in yaw rate-sideslip plane [40].

6.1.3 Rollover Prevention

The rollover prevention system can also be applied by limiting the RI within the acceptable region. The RI can be defined as a linear combination of the roll angle and the roll rate which are the state variables in the vehicle model. The general rollover index which was introduced in previous section included a variety of rollover situations and road configurations. In this section, only control of un-tripped rollovers is considered so the terms related to the tripped rollover are removed and a simplified RI is used for vehicle rollover control. The RI for un-tripped rollover of vehicles with constant speed on flat roads can be written as:

$$RI = \frac{2}{T_{eff}} \cdot \frac{mHa_y + m_s g h_s \varphi - I_{xx}\ddot{\varphi}}{mg} \tag{6-8}$$

where T_{eff} denotes the effective vehicle track in rollover which is equal to $(T + 2R\gamma)\frac{a}{l}$, $(T + 2R\gamma)\frac{b}{l}$, and $(T + 2R\gamma)$ for Tadpole 3W, Delta 3W, and 4W vehicles, respectively. This representation of RI includes the roll angle (φ), the lateral acceleration (a_y), and the roll acceleration ($\ddot{\varphi}$). Due to the acceleration terms, the RI in Eq. (6-8) cannot be directly used for the model-based control. To get around this problem, using the roll motion dynamics of the vehicle, the RI is rewritten in terms of the roll angle and the roll rate of the vehicle instead of lateral and roll accelerations [48]. The derivation of the new RI is explained as follows.

Noting that only the sprung mass has roll motion, the effects of sprung and un-sprung masses can be separated. The term of mH in Eq.(6-8) is replaced by $(m_s h_s + m_s h_R + m_u h_u)$, and the RI is rewritten as:

$$RI = \frac{2}{mgT_{eff}}\left(m_s h_s a_y + m_s h_R a_y + m_u h_u a_y + m_s g h_s \varphi - I_{xx}\ddot{\varphi}\right) \tag{6-9}$$

The effects of the sprung mass on rollover can be substituted by using Eq. (4-8) for small roll angles and flat roads ($\varphi_r = 0$). Namely, combing Eqs. (4-8) and (6-9) yields

$$RI = \frac{2}{mgT_{eff}}\left(c_\varphi \dot{\varphi} + k_\varphi \varphi + m_s h_R a_y + m_u h_u a_y\right) \tag{6-10}$$

where the terms of $m_u h_u a_y$ are the effects of the un-sprung mass, and the terms of $m_s h_R a_y$ are the effects of overturning moments from the roll center to the ground. Previous studies have often ignored these terms to simplify the model [53][98][99][137]. In this study, these effects are included for a more accurate RI. The summation of these four terms can be rewritten as $a_y(m_s h_R + m_u h_u)$. Since the effect of the un-sprung mass on rollover is considerably less than the effect of the sprung mass, and also the effect of the roll acceleration is considerably less than the effects of the lateral acceleration, the term $I_{xx}\ddot{\varphi}$ is ignored when calculating the effects of the un-sprung mass on rollover. Thus, rewriting Eq. (4-8) for a_y results in

$$a_y(m_s h_R + m_u h_u) = \frac{m_s h_R + m_u h_u}{m_s h_s}\left(c_\varphi \dot{\varphi} + k_\varphi \varphi - m_s g h_s \varphi\right) \tag{6-11}$$

Consequently, the terms in the right-hand side of Eq. (6-11) are written in terms of the roll angle (φ) and the roll rate ($\dot{\varphi}$). Substituting Eq. (6-11) in Eq. (6-10), the RI can be simplified into terms of the roll angle and the roll rate as

$$RI = C_1\varphi + C_2\dot{\varphi} \tag{6-12}$$

where C_1 and C_2 depend on vehicle parameters and bank and grade angles of the road as:

$$C_1 = \frac{2}{mgT_{eff}}\left(k_\varphi\left(1 + \frac{m_s h_R + m_u h_u}{m_s h_s}\right) - (m_s h_R + m_u h_u)g\right) \tag{6-13}$$

$$C_2 = \frac{2c_\varphi}{mgT_{eff}}\left(1 + \frac{m_s h_R + m_u h_u}{m_s h_s}\right) \tag{6-14}$$

It should be mentioned that, in general, the damping coefficients in compression and extension are different. However, the effective torsional damping can be assumed to be constant because, during the roll motion, the dampers of one side are compressed while those on the other side are extended.

6.1.4 Longitudinal speed control

The longitudinal speed control can be used for different purposes such as cruise control, autonomous driving, and/or decreasing speed in harsh maneuvers to stabilize the vehicle. Thus, the desired longitudinal speed can be defined based on the mission that is defined for the controller. The longitudinal speed can be controlled by tracking the desired longitudinal speed or dropping speed under harsh conditions.

6.1.5 Slip control

Including wheel dynamics in the vehicle model, the slip control for braking and traction can be implemented through the proposed structure by limiting the slip ratio within the acceptable range. Assuming S_{i_max} as the maximum allowable slip ratio, the critical values for wheel speeds can be defined by rearranging Eq. (3-73) as:

$$\omega_{i\_c} = \frac{u}{R_w} \pm S_{i\_max}\max\left(\frac{u}{R_w}, \omega_i\right) \tag{6-15}$$

Since the wheel speeds are defined as state variables in the vehicle model, the slip ratios of the tires can be controlled through these state variables.

6.2 Actuator's constraints

The constraints are also applied to the actuators for the MPC control design. Two main types of constraints should be considered. The first is the limitation in the maximum capacity of the actuators such as the maximum possible torque, maximum steering angle, and maximum camber angle that the vehicle can provide. The other type of constraints comes from the maximum tire force capacity that depends on the friction between tires and the road. For the first constraints, the available capacity for the controller is equal to the total capacity of the actuators minus the employed portion by the driver or the feed-forward commands. As a common approach in the MPC structure, since the future driver and/or the feed-forward commands are unknown, they are assumed constant during the prediction horizon. Thus, the constraints of actuator capacities can be written as:

$$Q_i^{min} - Q_i(t) \leq \Delta Q_i(t) \leq Q_i^{max} - Q_i(t) \tag{6-16}$$

$$\delta_i^{min} - \delta_i(t) \leq \Delta \delta_i(t) \leq \delta_i^{max} - \delta_i(t) \tag{6-17}$$

$$\gamma_i^{min} - \gamma_i(t) \leq \Delta \gamma_i(t) \leq \gamma_i^{max} - \gamma_i(t) \tag{6-18}$$

where Q_i^{min} and Q_i^{max} are the minimum and maximum torque capacity, δ_f^{min} and δ_f^{max} are the minimum and maximum possible steering angles, and γ_i^{min} and γ_i^{max} are the minimum and maximum possible camber angles for i^{th} wheel. $Q_i(t)$, $\delta_i(t)$, and $\gamma_i(t)$ are the driver or/and feed-forward commands.

As mentioned, the next type of constraints comes from the tire force capacity. The maximum longitudinal tire force can be achieved as:

$$f_{xi\_max} = \mu_x f_{zi} \tag{6-19}$$

where μ_x is the longitudinal friction coefficient, and f_{zi} is the normal force for i^{th} tire. The maximum lateral tire force can similarly be achieved as:

$$f_{yi\_max} = \mu_y f_{zi} \tag{6-20}$$

where μ_y is the lateral friction coefficient. For the combined slip situations that lateral and longitudinal forces are applied simultaneously, a simple model called the *friction ellipse* [90] is suggested to reflect the effects of lateral-longitudinal force coupling. In fact, for combined slip cases, the longitudinal and lateral forces cannot reach the maximum values, and the friction ellipse defines the force boundaries. The friction ellipse for i^{th} tire is given as:

$$\left(\frac{f_{xi}}{f_{xi\_max}}\right)^2 + \left(\frac{f_{yi}}{f_{yi\_max}}\right)^2 = 1 \tag{6-21}$$

Due to the importance of the lateral force for vehicle stability, the longitudinal force is constrained as a function of lateral force in this study. Using the friction ellipse, the longitudinal force can be bounded as:

$$-f_{xi\_max}\sqrt{1-\left(\frac{f_{yi}}{f_{yi\_max}}\right)^2} \le f_{xi} \le f_{xi\_max}\sqrt{1-\left(\frac{f_{yi}}{f_{yi\_max}}\right)^2} \tag{6-22}$$

To simplify the notation, the maximum available longitudinal force is defined as:

$$f_{xi}^{p} = f_{xi\_max}\sqrt{1-\left(\frac{f_{yi}}{f_{yi\_max}}\right)^2} \tag{6-23}$$

Then, using $f_{xi} = \frac{1}{R_w}(Q_i + \Delta Q_i)$, the bounds for the control torque due to the friction capacity can be written as:

$$-f_{xi}^{p}R_w - Q_i \le \Delta Q_i \le f_{xi}^{p}R_w - Q_i \tag{6-24}$$

6.3 MPC controller development

In this study, a Model Predictive Control (MPC) approach is employed to stablish the reconfigurable control structure. The controller is designed to track the desired yaw rate. The lateral stability (side slip angle control), rollover prevention, and slip control are also treated as other objective functions in the MPC optimization problem. These control objectives involve the control of the state variables or linear combinations of them. Thus, the corresponding objective functions can be written in terms of state cost functions.

Discretization of Eq. (3-77) by using the zero-order-hold (ZOH) results in the discrete-time state-space form of the vehicle model as:

$$X^{k+1} = A_d X^k + B_d U^k + E_d W^k + D_d \tag{6-25}$$

where $A_d \in \mathbb{R}^{9\times9}$, $B_d \in \mathbb{R}^{9\times12}$, and $E_d \in \mathbb{R}^{9\times12}$ are system matrices and $D_d \in \mathbb{R}^{9\times1}$ is the constant input. The superscript k denotes the discrete time index associated with the sampling time T_s. As is customary in developing the MPC for vehicle stability control, it is assumed that the driver inputs

such as the steer angles and torques on wheels as well as the vehicle speed are constant during the prediction horizon. Then, the MPC problem considered in this thesis can be stated as:

$$\min_{\bar{U}} \ \frac{1}{2}\left\|X^N - X_d^N\right\|_{Q_X}^2 + \frac{1}{2}\sum_{k=0}^{N-1}\left(\left\|X^k - X_d^k\right\|_{Q_X}^2 + \left\|U^k\right\|_R^2\right) \tag{6-26a}$$

$$s.t: \ X^{k+1} = A_d X^k + B_d U^k + E_d W^0 + D_d \tag{6-26b}$$

$$k = 0,\ 1,\ 2,\ \ldots,\ N-1$$

$$X^0 = X(0), \tag{6-26c}$$

$$W^0 = W(0) \tag{6-26d}$$

where $\bar{U} = [(U^0)^T, (U^1)^T, \ldots, (U^{N-1})^T]^T \in \mathbb{R}^{mN}$. The objective function includes the costs for the state tracking and the input energy. The subscripts of the norms (i.e. Q_X and R) show the positive semi-definite weight matrices for the corresponding cost functions. The desired responses are defined as $X_d = [0 \quad r_d \quad 0 \quad 0 \quad \frac{u}{R_w} \quad \frac{u}{R_w} \quad \frac{u}{R_w} \quad \frac{u}{R_w}]^T$ where r_d is defined in Eq. (6-6). The desired states for the lateral velocity (v), roll angle (φ), and roll rate ($\dot{\varphi}$) are zero which represent the most stable situations for corresponding objectives (v for the lateral stability and φ and $\dot{\varphi}$ for the rollover stability). The desired wheel speed is selected as $\omega_{i\_d} = \frac{u}{R_w}$ $(i = 1\ to\ 4)$ which represents zero slip ratio.

Thus, the constraints of actuator capacities can be written as:

$$Q_i^{min} - Q_i(0) \le \Delta Q_i^k \le Q_i^{max} - Q_i(0) \tag{6-27}$$

$$\delta_i^{min} - \delta_i(0) \le \Delta \delta_i^k \le \delta_i^{max} - \delta_i(0) \tag{6-28}$$

$$\gamma_i^{min} - \gamma_i(0) \le \Delta \gamma_i^k \le \gamma_i^{max} - \gamma_i(0) \tag{6-29}$$

where Q_i^{min} and Q_i^{max} are the minimum and maximum torque capacity, δ_f^{min} and δ_f^{max} are the minimum and maximum possible steering angles, and γ_i^{min} and γ_i^{max} are the minimum and maximum possible camber angles for i^{th} wheel. $Q_i(0)$, $\delta_i(0)$, and $\gamma_i(0)$ are the driver or/and feed-forward commands at the beginning of the corresponding step time.

And for the MPC structure during each horizon, they can be written as:

$$f_{xi}^{p}(0) = \mu_x f_{zi}(0)\sqrt{1-\left(\frac{f_{yi}(0)}{\mu_y f_{zi}(0)}\right)^2} \tag{6-30}$$

$$-f_{xi}^{p}(0)R_w - Q_i(0) \le \Delta Q_i^k \le f_{xi}^{p}(0)R_w - Q_i(0) \tag{6-31}$$

where $f_{zi}(0)$ and $f_{yi}(0)$ are the vertical and lateral forces at the beginning of the step time.

6.3.1 Objectives' weights

An important part of the proposed control strategy is to provide an integrated control to handle all objectives simultaneously. This can be achieved by a proper selection of the weights on different objective functions. As mentioned, for the objectives of lateral stability (side slip angle control), rollover prevention (RI control), and slip control in traction/braking, the state variables need to be confined inside safe regions while they are free of control when they are within the acceptable values. Thus, the weights for these objectives have been chosen as barrier functions with respect to the corresponding objectives. These weights are close to zero for small values of the objectives and grow fast as the objectives approach the critical limits.

For Example, the weight for the RI has been chosen as a barrier function with respect to the RI as shown in Figure 6-2.

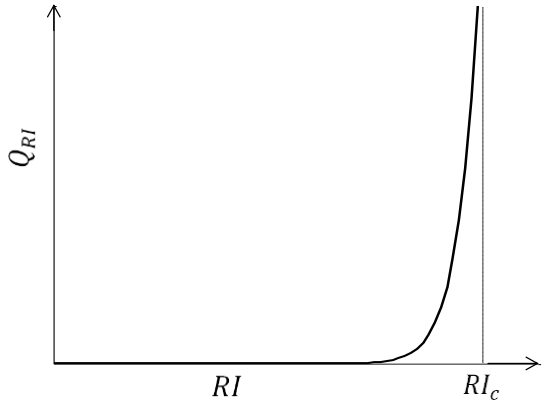

Figure 6-2: Rollover Index weight

This weight is close to zero for a small RI and grows fast as the RI approaches the critical limit. Such a weight can be achieved by defining it as a function of RI. Thus, the weight function is defined as

$$Q_{RI} = \gamma\left(|RI| + (1 - RI_c)\right)^n \tag{6-32}$$

where γ is a constant positive number, RI_c is the critical value for the RI, and n is a sufficiently large positive number.

6.3.2 Linear Quadratic Optimal Control

The Batch approach is used to find the optimal solution for the MPC controller. A specified approach for vehicle stability control application is developed including the driver commands and the desired tracking response. The objective function can be expressed as a function of the initial state $X(0)$, the driver input trajectory, the control input trajectory, and the constant input. The state trajectory X^1, X^2, …, X^N is:

$$\begin{bmatrix} X(0) \\ X^1 \\ \vdots \\ \vdots \\ X^N \end{bmatrix} = \begin{bmatrix} I \\ A \\ \vdots \\ \vdots \\ A^N \end{bmatrix} X(0) + \begin{bmatrix} 0 & \cdots & \cdots & 0 \\ B & 0 & \cdots & 0 \\ AB & \ddots & \ddots & \vdots \\ \vdots & \ddots & \ddots & \vdots \\ A^{N-1}B & \cdots & \cdots & B \end{bmatrix} \begin{bmatrix} U^0 \\ U^1 \\ \vdots \\ \vdots \\ U^{N-1} \end{bmatrix} + \begin{bmatrix} 0 & \cdots & \cdots & 0 \\ E & 0 & \cdots & 0 \\ AE & \ddots & \ddots & \vdots \\ \vdots & \ddots & \ddots & \vdots \\ A^{N-1}E & \cdots & \cdots & E \end{bmatrix} \begin{bmatrix} W^0 \\ W^0 \\ \vdots \\ \vdots \\ W^0 \end{bmatrix} + \begin{bmatrix} 0 \\ D \\ AD \\ \vdots \\ A^{N-1}D \end{bmatrix} \tag{6-33}$$

To simplify the notation, the following parameters are defined:

$$\bar{X} = \begin{bmatrix} X(0) \\ X^1 \\ \vdots \\ \vdots \\ X^N \end{bmatrix}, \bar{U} = \begin{bmatrix} U^0 \\ U^1 \\ \vdots \\ \vdots \\ U^{N-1} \end{bmatrix}, \bar{W} = \begin{bmatrix} W^0 \\ W^0 \\ \vdots \\ \vdots \\ W^0 \end{bmatrix}$$

$$S_x = \begin{bmatrix} I \\ A \\ \vdots \\ \vdots \\ A^N \end{bmatrix}, S_u = \begin{bmatrix} 0 & \cdots & \cdots & 0 \\ B & 0 & \cdots & 0 \\ AB & \ddots & \ddots & \vdots \\ \vdots & \ddots & \ddots & \vdots \\ A^{N-1}B & \cdots & \cdots & B \end{bmatrix}, S_w = \begin{bmatrix} 0 & \cdots & \cdots & 0 \\ E & 0 & \cdots & 0 \\ AE & \ddots & \ddots & \vdots \\ \vdots & \ddots & \ddots & \vdots \\ A^{N-1}E & \cdots & \cdots & E \end{bmatrix}, S_d = \begin{bmatrix} 0 \\ D \\ AD \\ \vdots \\ A^{N-1}D \end{bmatrix}$$

Then, the equation can be rewritten as:

$$\bar{X} = S_x X(0) + S_u \bar{U} + S_w \bar{W} + S_d \tag{6-34}$$

The objective function also can be rewritten as:

$$J = \frac{1}{2}(\bar{X} - \bar{X}_d)^T \bar{Q}\ (\bar{X} - \bar{X}_d) + \frac{1}{2}\bar{U}^T \bar{R}\ \bar{U} \tag{6-35}$$

where

$$\bar{X}_d = \begin{bmatrix} X_d^0 \\ X_d^1 \\ \vdots \\ \vdots \\ X_d^N \end{bmatrix} \tag{6-36}$$

and

$$\bar{Q} = \text{Blockdiag}\{Q, Q, \dots, Q\} \tag{6-37}$$

$$\bar{R} = \text{Blockdiag}\{R, R, \dots, R\} \tag{6-38}$$

Then, substituting Eq. (6-34) into Eq. (6-35), the objective function is obtained as:

$$J = \frac{1}{2}\bar{U}^T(S_u^T\bar{Q}S_u + \bar{R})\bar{U} + X(0)^T S_x^T\bar{Q}S_u\bar{U} + \bar{W}^T S_w^T\bar{Q}S_u\bar{U} + S_d^T\bar{Q}S_u\bar{U} - \bar{X}_d^T\bar{Q}S_u\bar{U} + Const. \tag{6-39}$$

Eq. (6-39) can be rewrite in standard form for quadratic programming as:

$$J = \frac{1}{2}\bar{U}^T H\bar{U} + \left(X(0)^T F_1 + \bar{W}^T F_2 + F_3 + \bar{X}_d^T F_4\right)\bar{U} + Const. \tag{6-40}$$

where

$$H = S_u^T\bar{Q}S_u + \bar{R} \tag{6-41}$$

$$F_1 = S_x^T\bar{Q}S_u \tag{6-42}$$

$$F_2 = S_w^T\bar{Q}S_u \tag{6-43}$$

$$F_3 = S_d^T\bar{Q}S_u \tag{6-44}$$

$$F_4 = -\bar{Q}S_u \tag{6-45}$$

Then, the standard quadratic optimization problem can be solved to obtain the optimal control commands. Constraints are also considered for solving this problem as mentioned in the previous subsection. The achieved control commands are for the entire horizon at each sampling time. According to the MPC approach, the first control action is applied to the vehicle for the entire horizon. At the next step, another constrained finite-time optimal control problem is solved over a shifted horizon, based on new state measurements. These steps are repeated in real-time.

The main advantage of the proposed control design procedure is the reconfigurability. In fact, using the reconfigurable structure, the control actuations that are not available for the vehicle will be completely removed from the optimization problem without any modification on the control design

procedure. Thus, the optimal solution can be achieved with respect to only the available control actuations. This is an important advantage of the introduced structure.

6.4 Simulation Results

Simulations are conducted to evaluate the performance of the reconfigurable controller for different configurations of urban vehicles as well as conventional 4W vehicles with different actuators. The reconfigurable controller can be simply used for a specific vehicle by including the corresponding vehicle parameters, adjusting the reconfiguration matrices, and tuning the objectives' weights. The proposed controller is used for three different vehicles in the simulation. The first case is a Delta-configuration of 3W vehicles with rear-wheel drive and front steering. A Tadpole-configuration of 3W vehicles with three-wheel drive and three-wheel steering is considered as the second case. As the third case, the proposed controller is used for a typical E-Class SUV vehicle with four-wheel drive and front steering. The performance of the proposed controller is examined through different maneuvers including different stability objectives and different actuators. Vehicle models in CarSim are employed and the MPC controller is developed in Simulink. The control parameters are shown in Table 6-1.

Table 6-1: MPC controller parameters

Parameters	***Definition***	***Delta-3W***	***Tadpole-3W***	***SUV***	***Unit***
N	MPC horizon	10	10	10	$-$
T_s	MPC time step	0.02	0.02	0.02	s
S_{i_max}	Slip ratio limit for tires	0.1	0.1	0.1	$-$
α_{r_max}	Sideslip angle limit for rear tires	6	6	6	deg
RI_c	Critical value for rollover index	0.7	0.7	0.7	$-$
Q_{max}	Maximum wheel's torque	800	800	1600	$N.m$
δ_{max}	Maximum steering	20	20	20	deg

6.4.1 Delta three-wheeled vehicle

As mentioned, the first case is a Delta-configuration of 3W vehicles with rear-wheel drive and front steering. Different maneuvers for different road conditions are considered to evaluate the performance

of the controller to manage different stability objectives. Torque vectoring on rear wheels and integrated torque vectoring and active front steering are assumed as the control actuations for the maneuvers.

6.4.1.1 Handling improvement and lateral stability control-torque vectoring

For the first maneuver, torque vectoring is used on rear wheels to improve handling and lateral stability of the vehicle. The actuator reconfiguration matrix for rear torque vectoring is:

$$T_w = diag(0,0,0,0,0,0,1,0,0,1,0,0)$$

The maneuver is considered on a slippery road with $\mu = 0.4$. The vehicle moves with a constant speed of $40km/h$. A $\frac{1}{8}$ Hz sinusoidal steering input with 100 degrees of magnitude is applied to the vehicle from $t = 4s$ to $t = 16s$. Figure 6-3 shows the applied steering on front wheels.

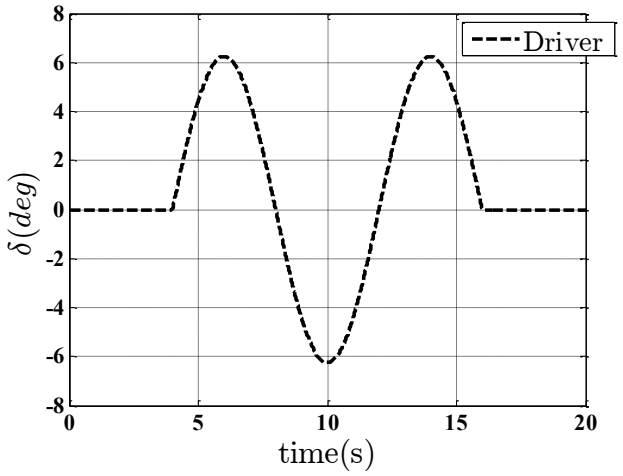

Figure 6-3: The applied steering and torques on Delta 3W vehicle

The state variables for the vehicle including the yaw rate, lateral velocity, longitudinal velocity, rollover index, and slip ratio for the controlled and uncontrolled vehicles are shown in Figure 6-4. The state variables represent different stability objectives. The plots for the yaw rate and the RI also show the limits. The applied torques by the controller on rear-left and rear-right wheels are also shown. The results show that the proposed controller properly stabilizes the vehicle as can be seen through the yaw rate and the sideslip angle responses for the vehicle with and without controller. The controlled vehicle properly tracks the desired yaw rate while the vehicle's response is kept within the limits.

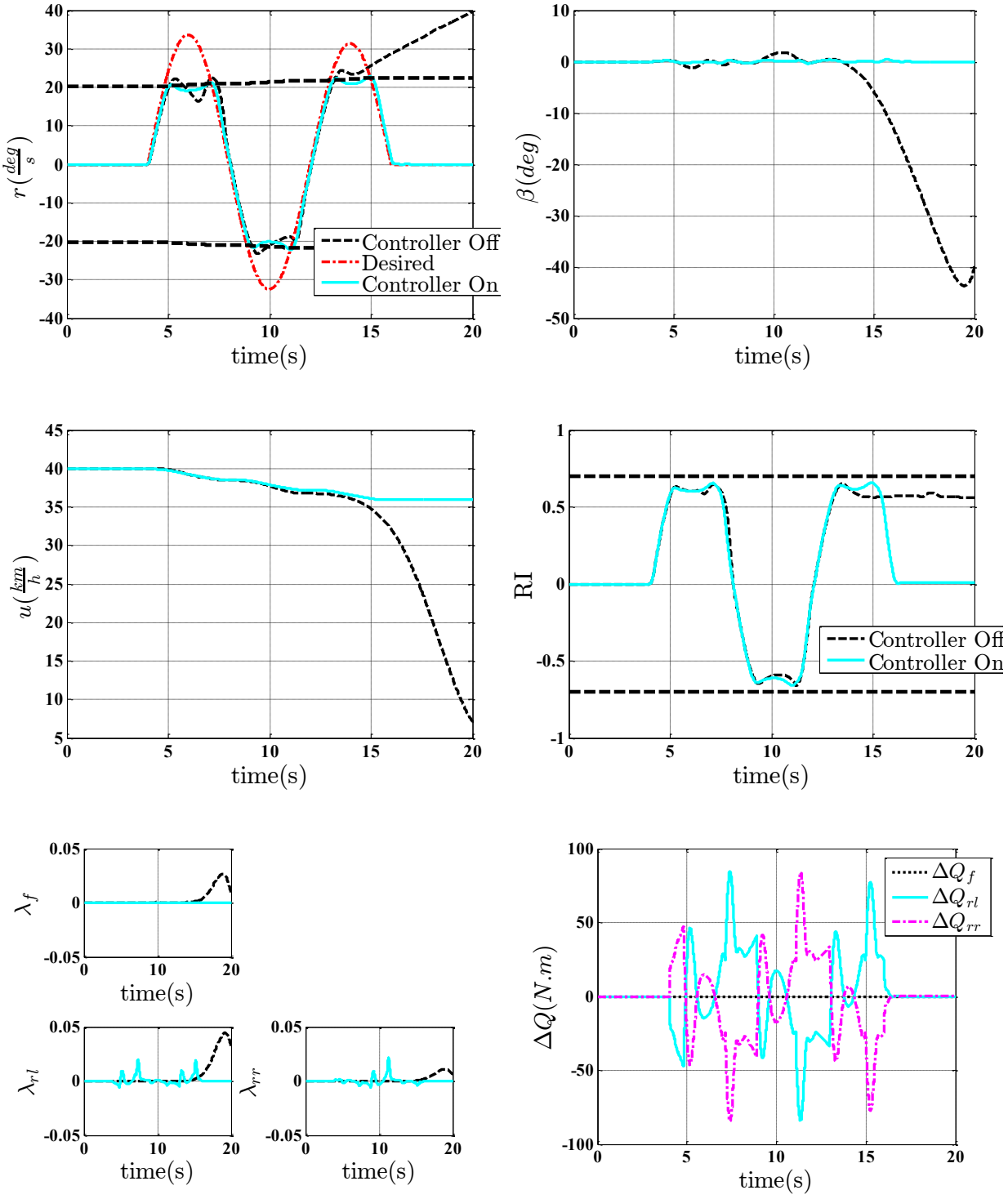

Figure 6-4: State variables for controlled and un-controlled Delta 3W vehicles through TV

6.4.1.2 Integrated handling, lateral stability, and traction control-torque vectoring

As the next maneuver, simultaneous steering and acceleration is considered on a slippery road with $\mu = 0.4$. The simulation starts with the vehicle moving at a constant speed of $20km/h$. Then, from $t = 0s$ to $t = 10s$, the vehicle is accelerated by constantly increasing throttle to 40%. A $\frac{1}{8}$ Hz sinusoidal steering input with 100 degrees of magnitude is applied to the vehicle from $t = 4s$ to $t = 16s$. The state variables and the applied torques by the controller are shown in Figure 6-5. As can be seen, for the un-controlled vehicle, the slip ratios for all the wheels increase when the vehicle starts to accelerate, and the vehicle loses its lateral stability. However, the proposed controller can properly control the yaw rate, sideslip angle, and slip ratio to stabilize the vehicle. During the acceleration, not only the handling is improved by applying yaw moment through torque vectoring but also the slip ratios of the wheels are maintained within the acceptable values. The applied torques by the controller are symmetric for some instances during the maneuver showing that the controller is applying pure moments. However, at some instances the torques are not symmetric showing that the slip control is involved. In fact, the controller is integrated and the applied torques simultaneously control the slip ratio and track the desired yaw rate by providing direct yaw moment on vehicle body.

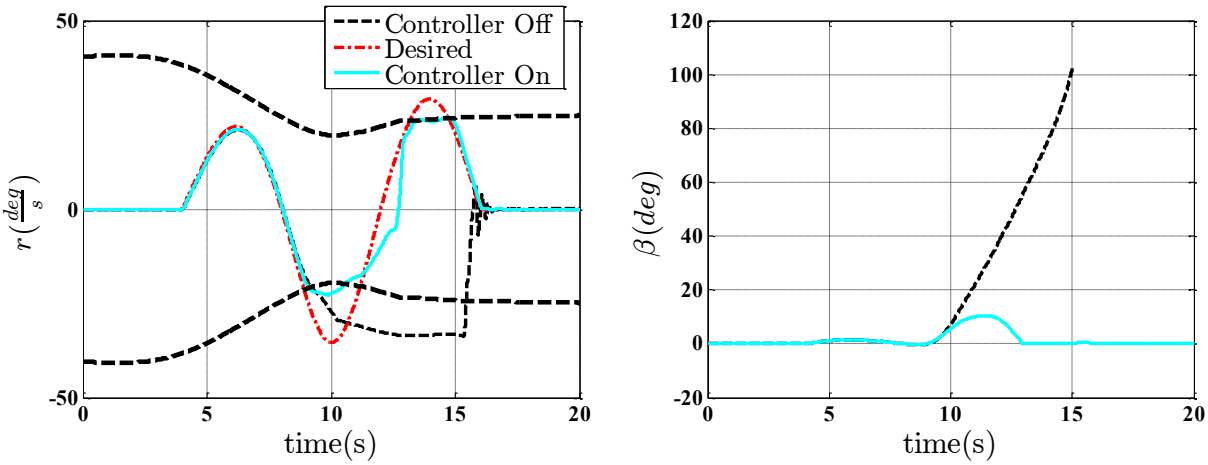

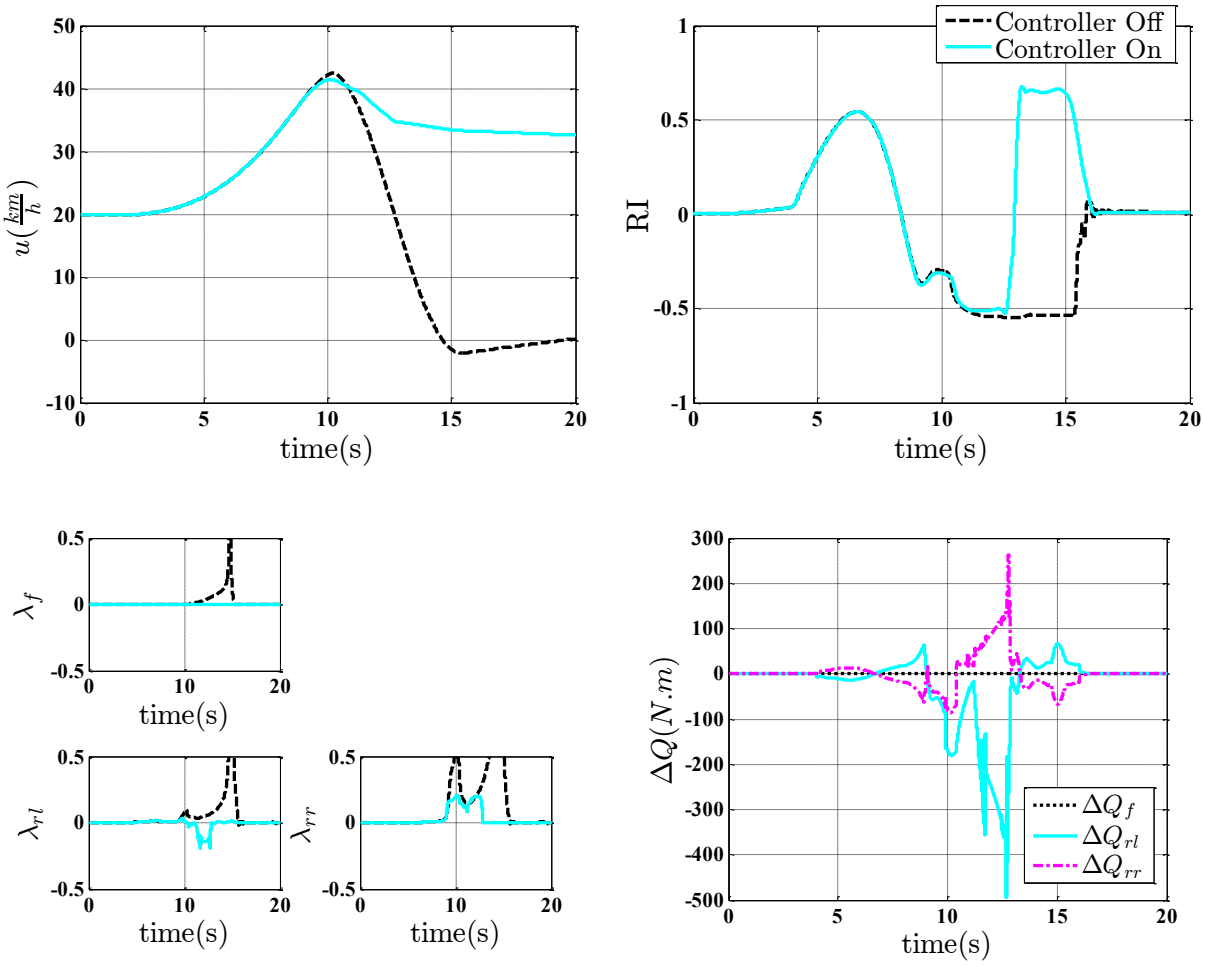

Figure 6-5: State variables for acceleration in turn of a Delta 3W vehicle through TV

6.4.1.3 Integrated handling, lateral stability, and braking control-torque vectoring

For the next maneuver, simultaneous steering and braking is considered on a slippery road with $\mu = 0.4$. The simulation starts with the vehicle moving at a constant speed of $60km/h$. Then, from $t = 11s$ to $t = 17s$, the vehicle is braking by constantly increasing pedal pressure to 1 MPa which is equal to 100 $N.m$ braking torque on each wheel. A sinusoidal steering input similar to the previous maneuvers is also applied to the vehicle. The state variables and the applied torques by the controller are shown in Figure 6-6. The results show that the proposed controller can properly control the yaw rate, sideslip angle, and slip ratio to stabilize the vehicle also for braking in turn.

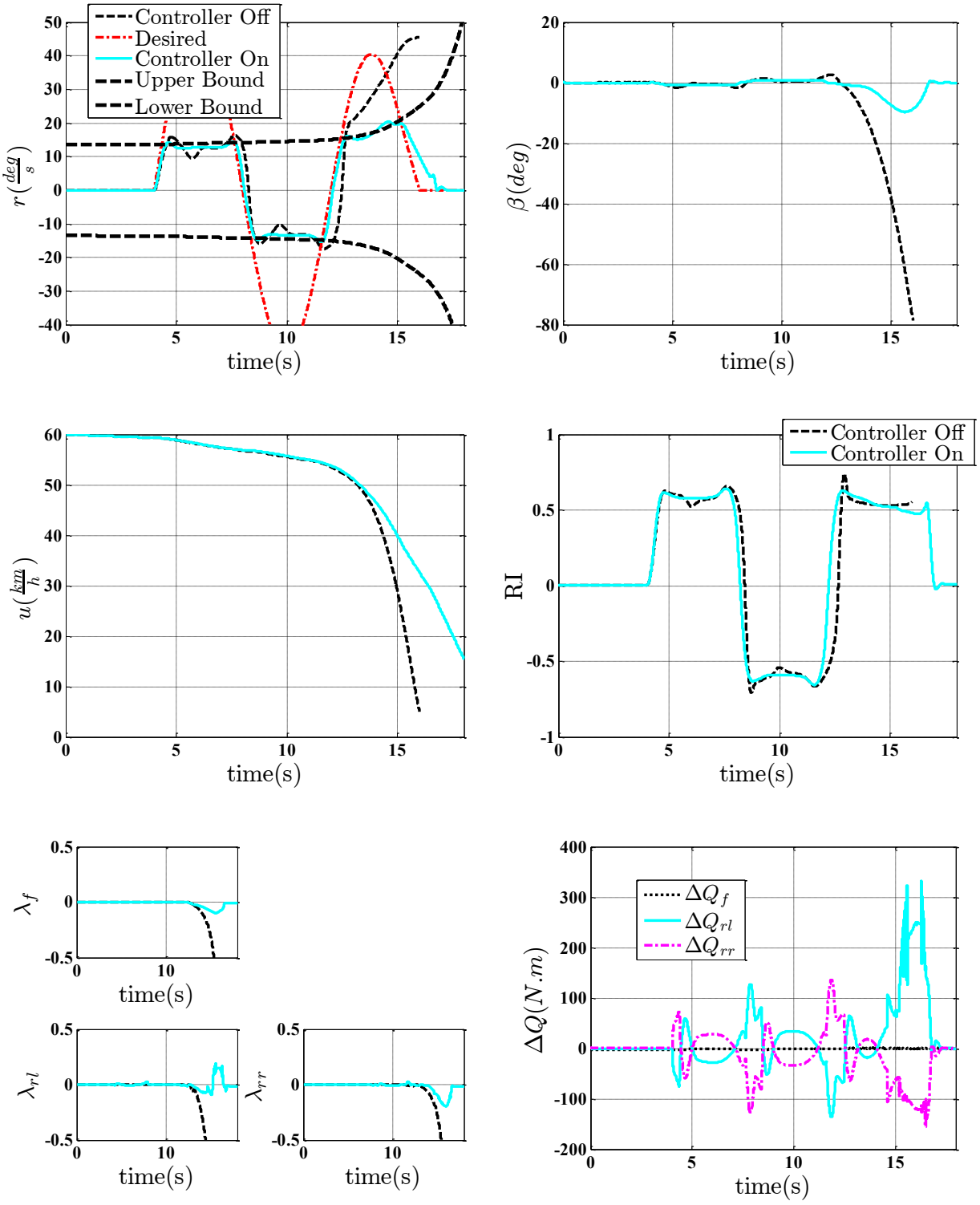

Figure 6-6: State variables for braking in turn of a Delta 3W vehicle through TV

6.4.1.4 Cruise control

Another capability of the integrated controller is that it can be used for cruise control. To evaluate this objective, the vehicle is assumed to move on an uphill graded road. The vehicle starts with a constant speed of $50km/h$. The controller is intended to keep this constant speed for the vehicle when moving on the graded road. The longitudinal speeds for the controlled and un-controlled cases are shown in Figure 6-7. As can be seen, the controller properly keeps the constant speed. The applied torques by the controller and the slip ratio are also shown in Figure 6-7.

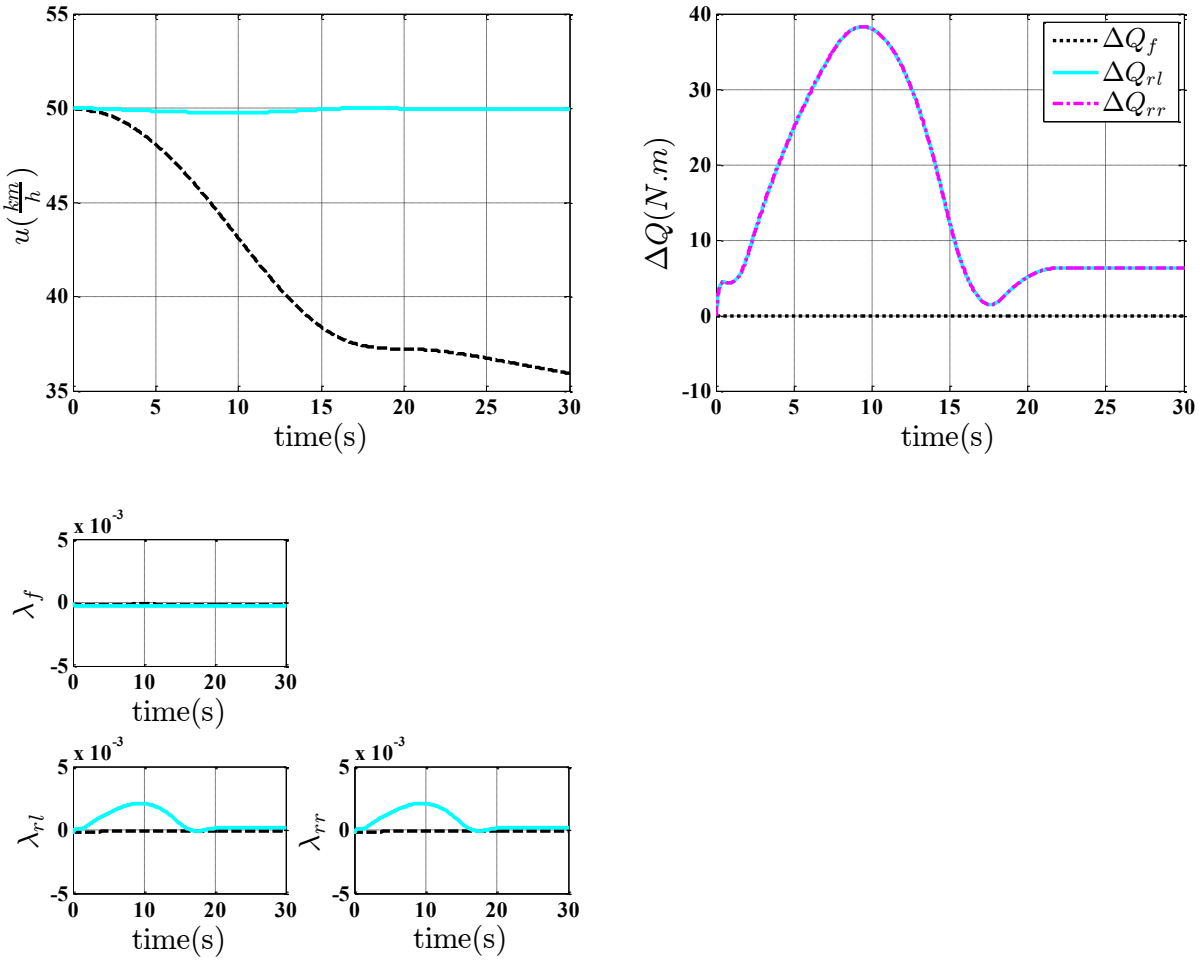

Figure 6-7: State variables for cruise control of a Delta 3W vehicle

6.4.1.5 Rollover prevention-torque vectoring

For the next maneuver, the controller is employed for rollover prevention of this 3W vehicle on a dry road with $\mu = 1$. The simulation starts with the vehicle moving at a constant speed of $50km/h$. A $\frac{1}{8}$ Hz sinusoidal steering input with 50 degrees of magnitude is also applied to the vehicle. The state variables and the applied torques by the controller are shown in Figure 6-8. As can be seen, for the uncontrolled case, RI is beyond the acceptable region while it is restricted within the safe region for the controlled case using the reconfigurable controller.

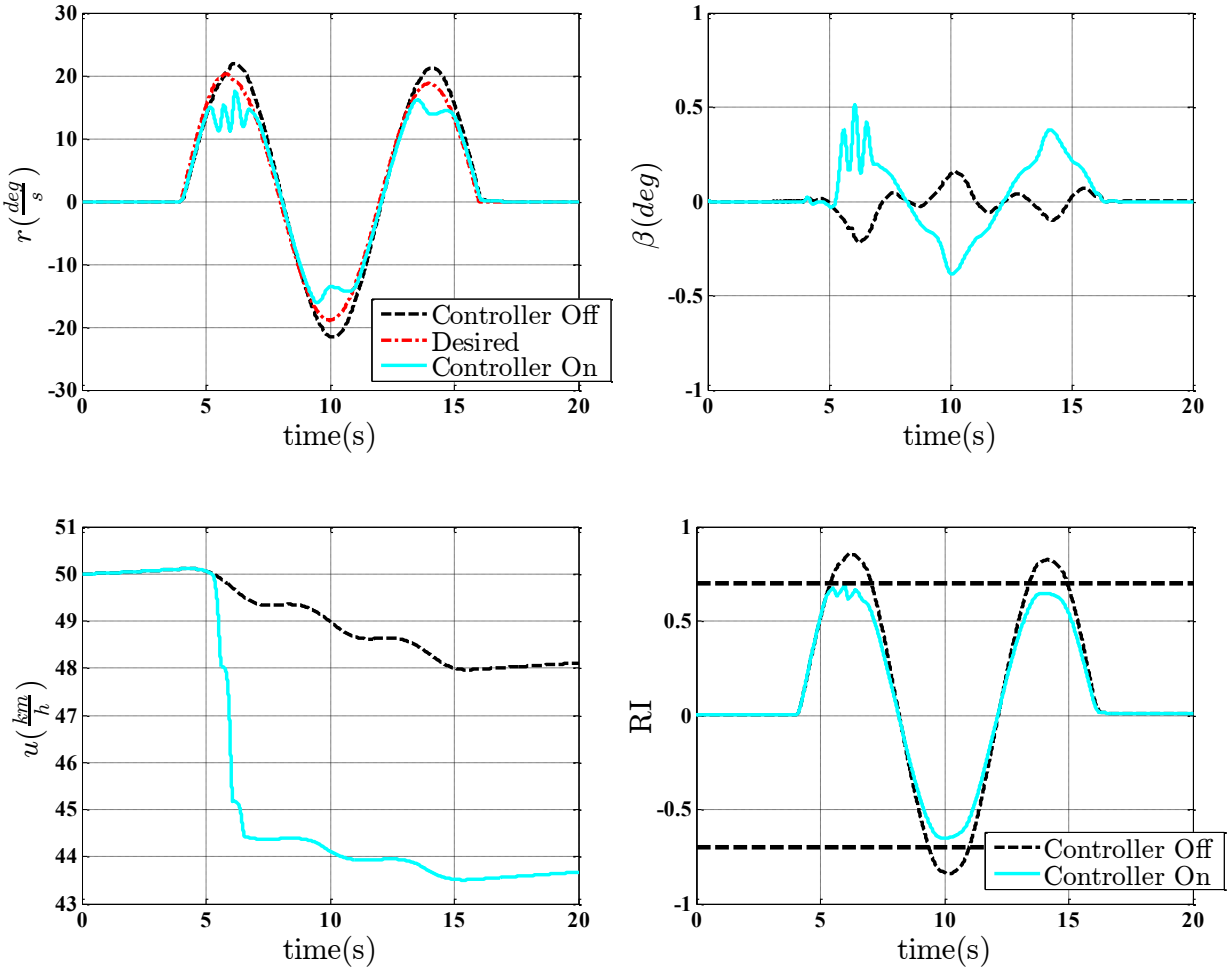

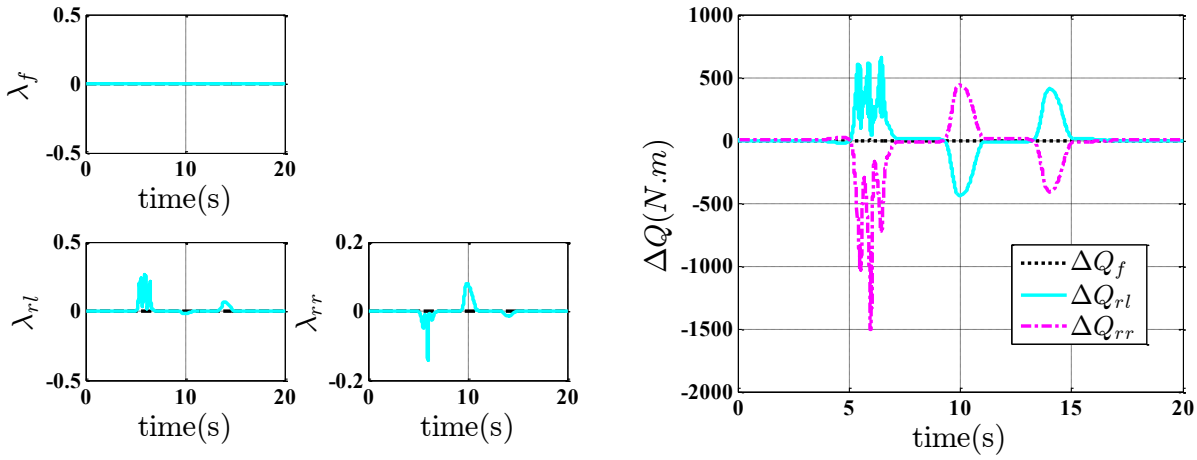

Figure 6-8: State variables for rollover prevention of a Delta 3W vehicle through TV

6.4.1.6 Integrated handling, lateral stability, and traction control – torque vectoring and active front steering

Integrated torque vectoring and active front steering is also examined to improve stability of the vehicle. The actuator reconfiguration matrix for rear torque vectoring and active front steering is:

$$T_w = diag(0,1,0,0,0,0,1,0,0,1,0,0)$$

This combination of torque vectoring and active front steering is used for integrated control of handling improvement, lateral stability, and traction control which was discussed before through only torque vectoring. The state variables and the applied control inputs are shown in Figure 6-9. As can be seen, the results are almost similar to the results for torque vectoring. In fact, again torque vectoring is mainly controlling the objectives, and active steering is not very effective for this slippery road.

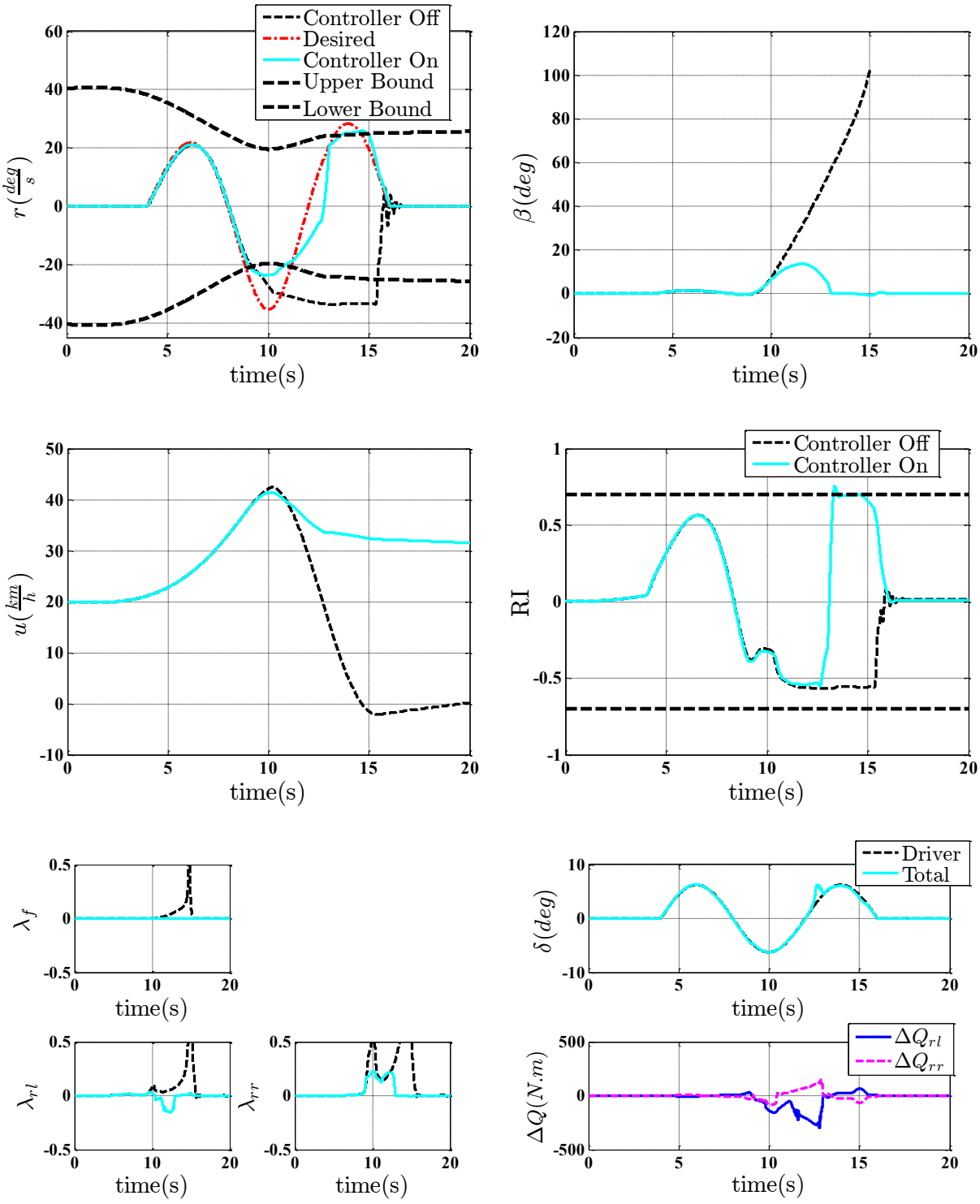

Figure 6-9: State variables for acceleration in turn through integrated TV and AS

6.4.1.7 Rollover prevention-integrated torque vectoring and active front steering

The integrated torque vectoring and active front steering is used for the previous rollover prevention maneuver (torque vectoring case). The state variables and the applied control inputs are shown in Figure 6-10. As can be seen, the RI is again restricted within the safe region. However, comparing Figure 6-10 and Figure 6-8, it can be concluded that the integration of torque vectoring and active steering results in a smoother maneuver and more effective rollover prevention results. The maneuver is also performed with less speed drop and smaller slip ratio that come from smaller demanded torque for rollover prevention. Thus, active steering is considerably effective in rollover prevention on a dry road while it was not very effective for lateral stability on slippery roads.

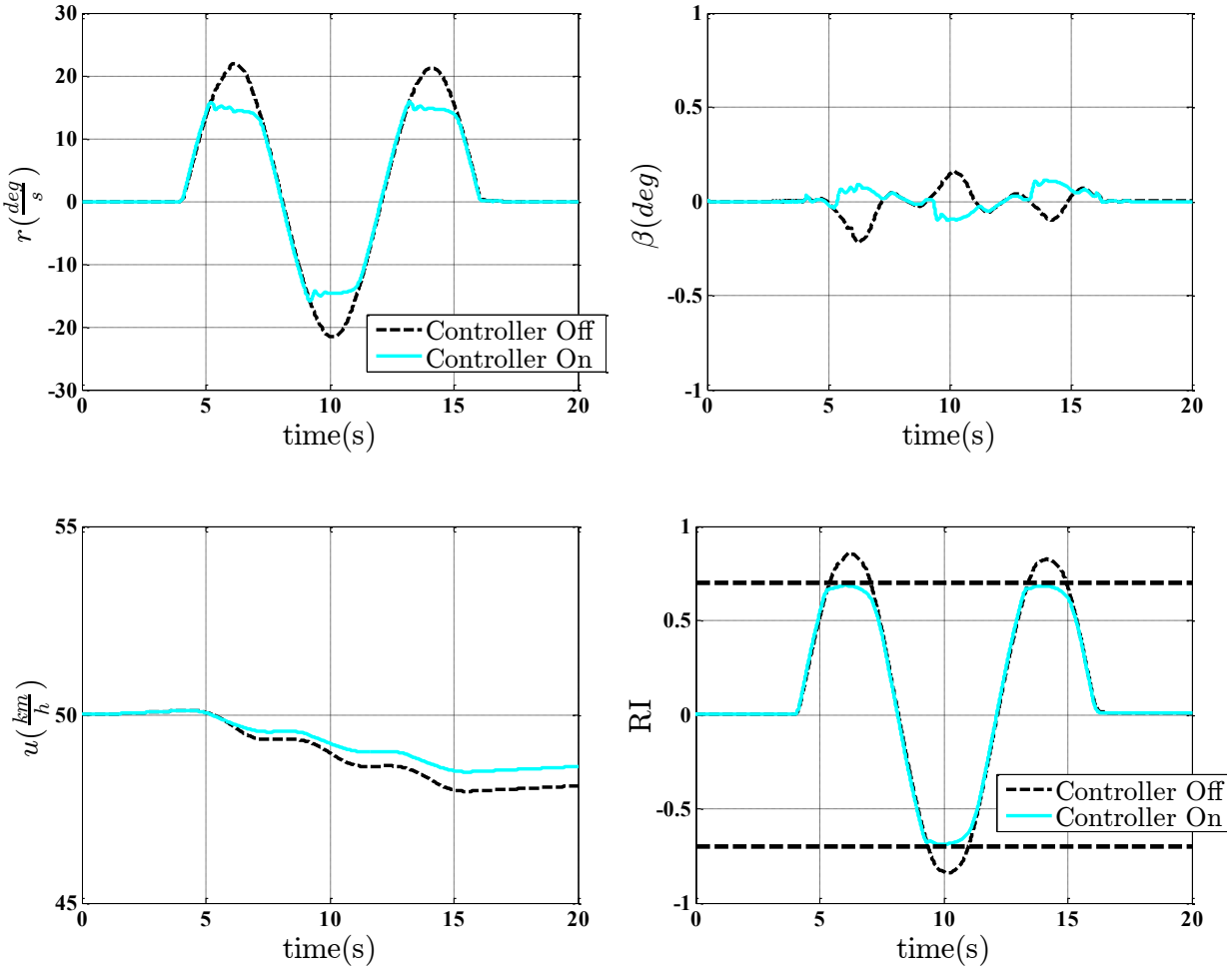

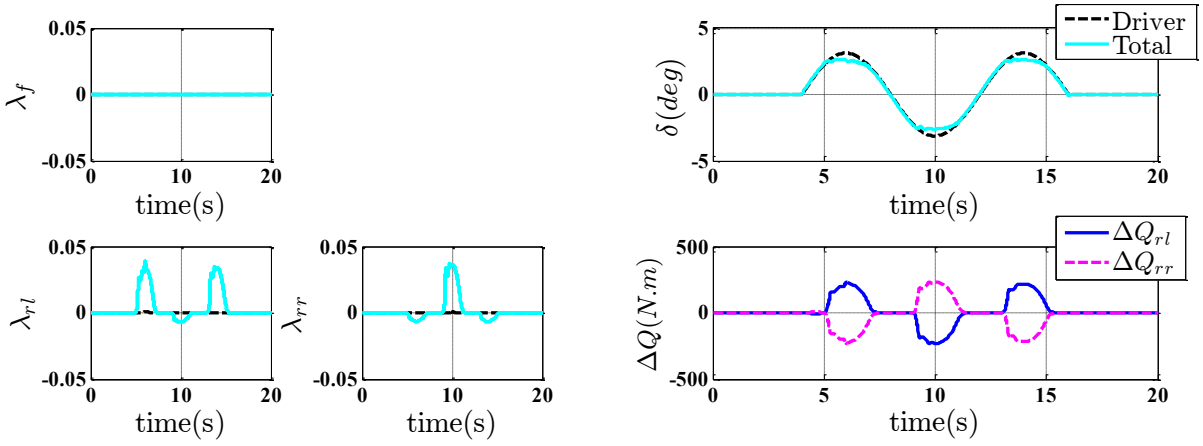

Figure 6-10: State variables for rollover prevention through integrated TV and AFS

6.4.2 Tadpole three-wheeled vehicle

The next vehicle for the simulations is a Tadpole-configuration of 3W vehicles with three-wheel drive and three-wheel steering. Torque vectoring on front wheels and active rear steering are assumed as the control actuations.

6.4.2.1 Integrated handling, lateral stability, and traction control-torque vectoring

For the first maneuver, torque vectoring is used on front wheels to improve stability of the vehicle. The actuator reconfiguration matrix for front torque vectoring is:

$$T_w = diag(1,0,0,1,0,0,0,0,0,0,0,0)$$

The maneuver is considered again on a slippery road with $\mu = 0.4$. The simulation starts with the vehicle moving at a constant speed of $20km/h$. Then, from $t = 0s$ to $t = 10s$, the vehicle is accelerated by constantly increasing throttle to 40%. A $\frac{1}{8}$ Hz sinusoidal steering input with 100 degrees of magnitude is applied to the vehicle from $t = 4s$ to $t = 16s$. The state variables and the applied torques by the controller are shown in Figure 6-11. As can be seen, the proposed controller can properly control the yaw rate, sideslip angle, and slip ratio to stabilize the Tadpole 3W vehicle. It should be mentioned that this vehicle is three-wheel drive while only the front wheels can be used for torque vectoring. However, the controller also provides traction control for the single rear wheels. Thus, as can be seen, controller applies torques for all wheels.

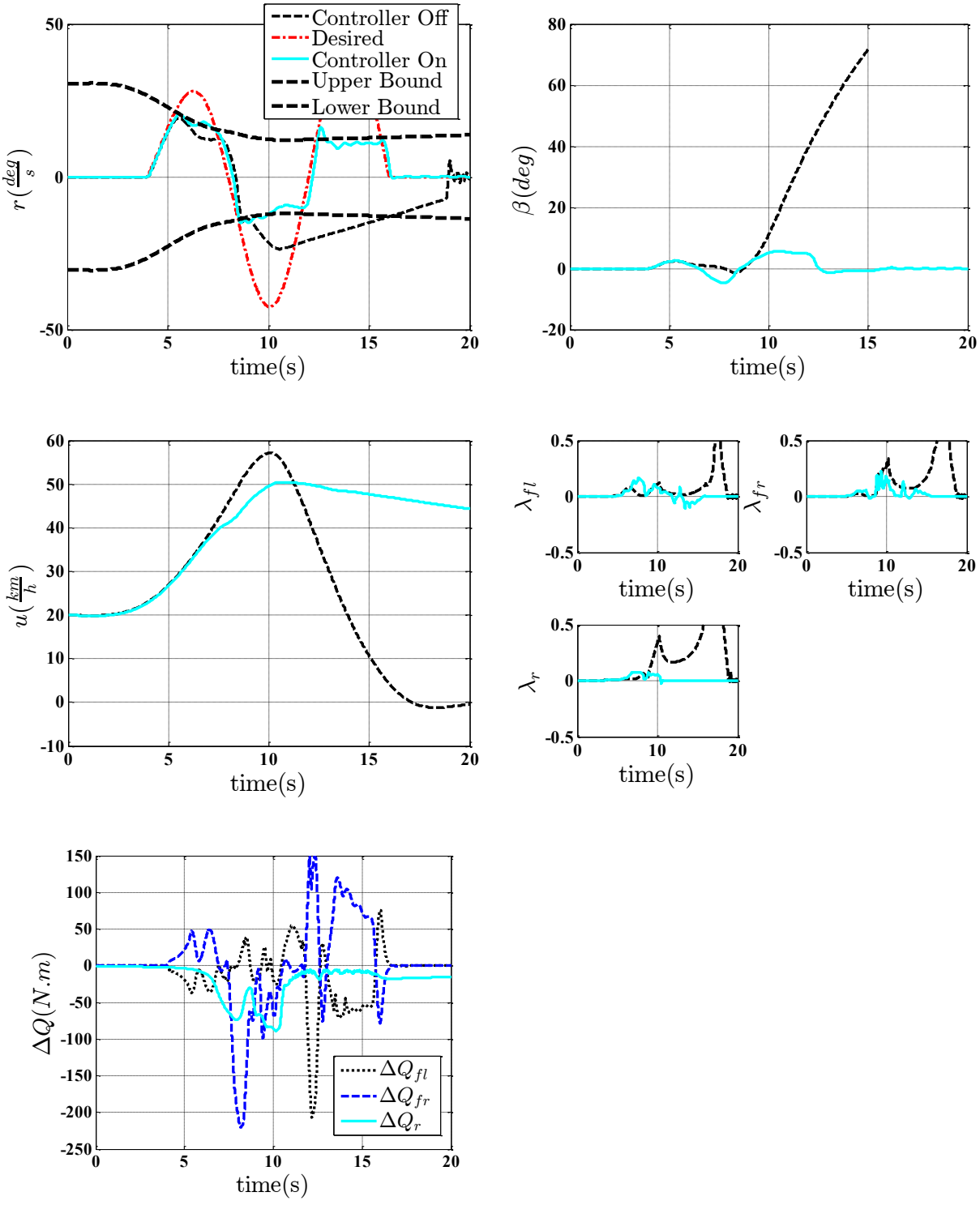

Figure 6-11: State variables for acceleration in turn of a Tadpole 3W vehicle through TV

6.4.2.2 Handling improvement - rear steering

Rear steering is examined for handling improvement of the Tadpole 3W vehicle as the next maneuver. The actuator reconfiguration matrix for rear steering of this vehicle is:

$$T_w = diag(0,0,0,0,0,0,0,1,0,0,0,0)$$

The previously mentioned sinusoidal steering input with constant speed of 50 km/h is applied to the vehicle. The state variables and the applied torques by the controller are shown in Figure 6-12. As can be seen, rear steering is applied and handling of the vehicle is improved by tracking the desired yaw rate response.

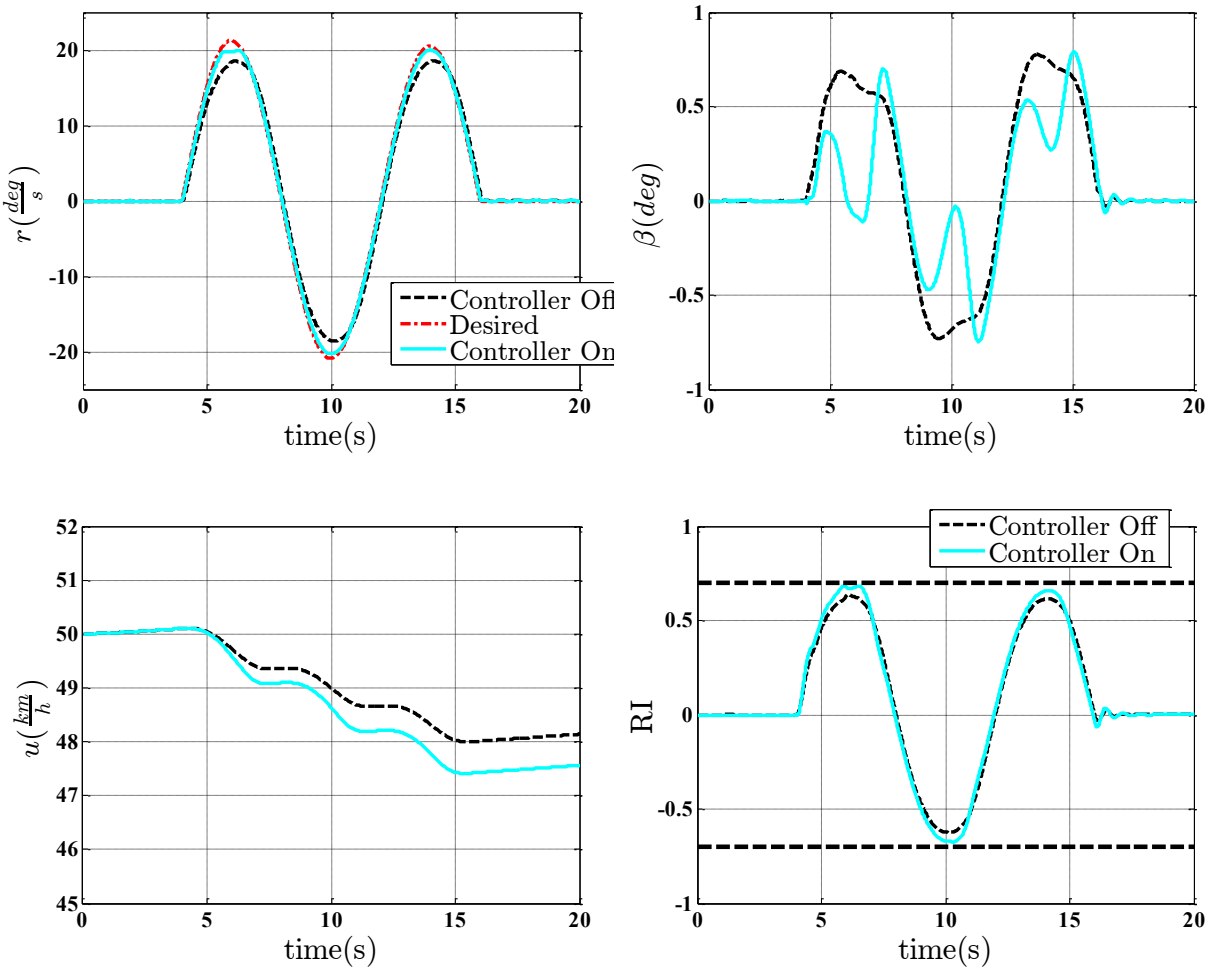

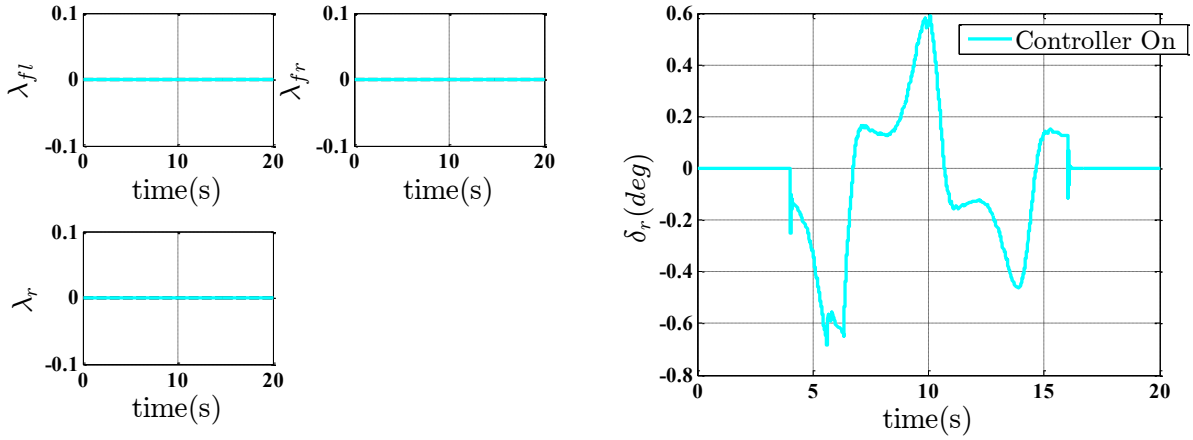

Figure 6-12: State variables handling improvement of a Tadpole 3W vehicle through ARS

6.4.3 Four-wheeled vehicle-SUV

An SUV vehicle wcich is four-wheel drive with front steering is used as the last case to evaluate the performance of the reconfigurable controller. Different maneuvers are considered purposefully to involve different stability objectives using various control actaution.

6.4.3.1 Traction and braking control

At first, the controller is examined for slip control on traction and braking in a straight line. The road is slippery with $\mu = 0.3$. The simulation starts with the vehicle moving at a constant speed of $50km/h$. Then, from $t = 0s$ to $t = 10s$, the vehicle is accelerated by constantly increasing throttle to 65%. From $t = 11s$ to $t = 17s$, the vehicle is braking by constantly increasing pedal pressure to $1\ MPa$ which is equal to $-350\ N.m$ braking torque on front wheels and $-150\ N.m$ braking torque on rear wheels. The vehicle's responses with and without controller are shown in Figure 6-13. As can be seen, the controller properly controls slip ratio for both traction and braking. Applied torques and longitudinal speeds are also shown.

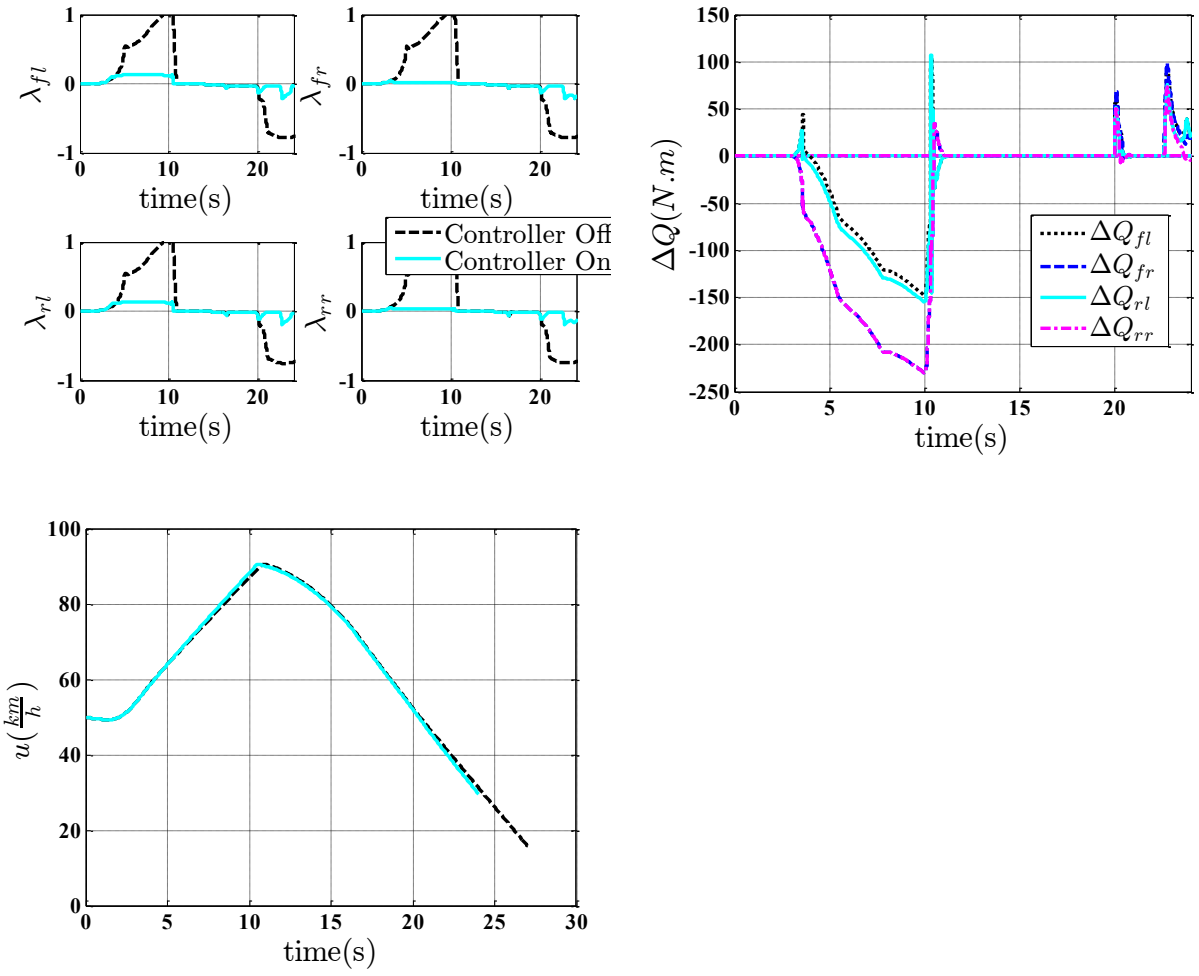

Figure 6-13: Slip control in traction and braking for a SUV on a slippery road

6.4.3.2 Rollover prevention- torque vectoring

The controller is also evaluated for rollover prevention of the SUV vehicle through torque vectoring. The actuator reconfiguration matrix for torque vectoring of the SUV vehicle is:

$$T_w = diag(1,0,0,1,0,0,1,0,0,1,0,0)$$

As a well-known rollover procedure, a fishhook maneuver is simulated for the SUV at speed of 80 km/h with the maximum steering wheel angle of about 294 $degrees$. Results for the vehicle with and without the controller are shown in Figure 6-14. As can be seen, RI is beyond the limits for the vehicle without control while the controller properly restricted the RI within the safe region. Also, it can be seen that applied torques are not symmetric showing that the controller not only provides

torque vectoring for rollover prevention, but also simultaneously considers slip control for the wheels to keep them within the acceptable region.

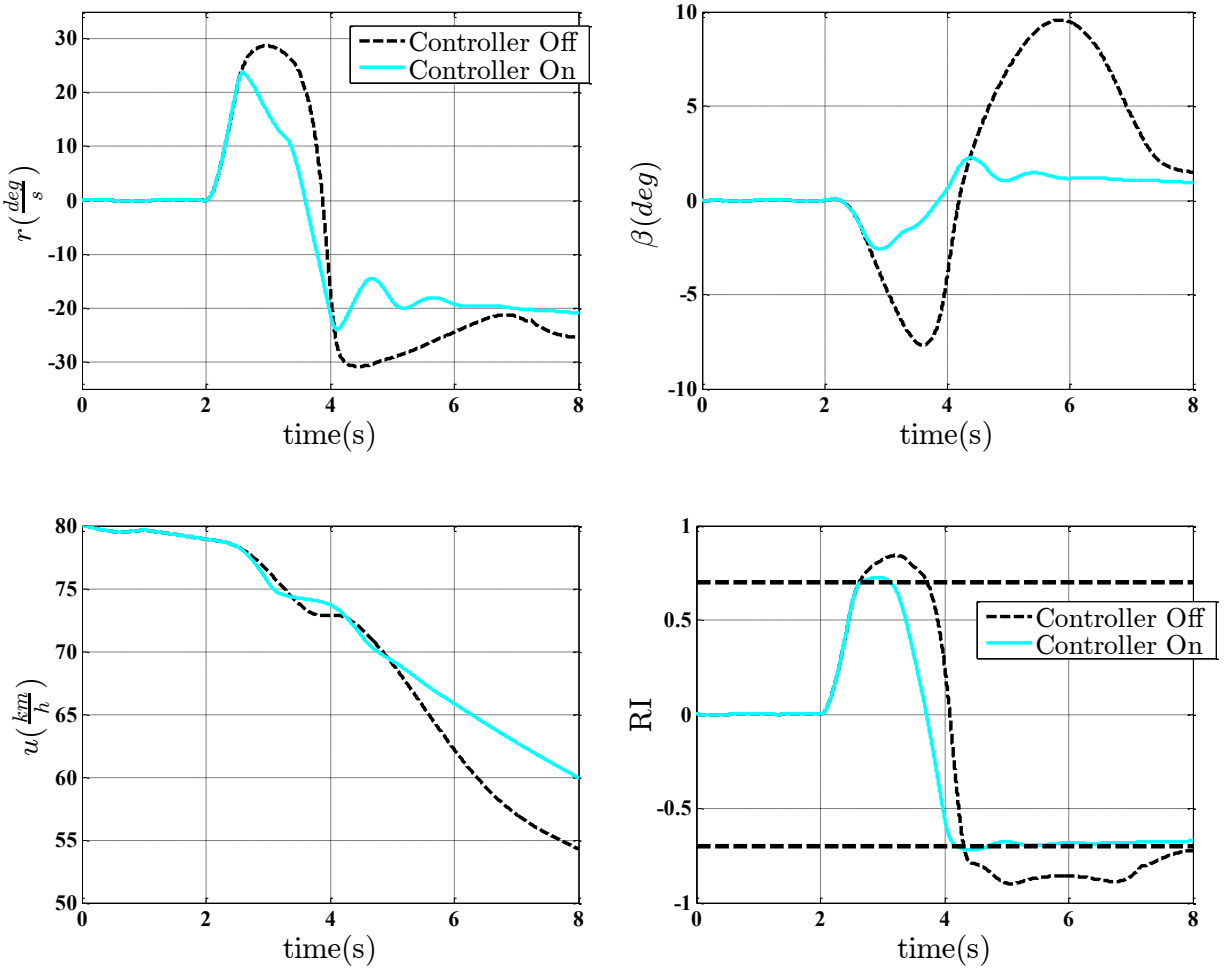

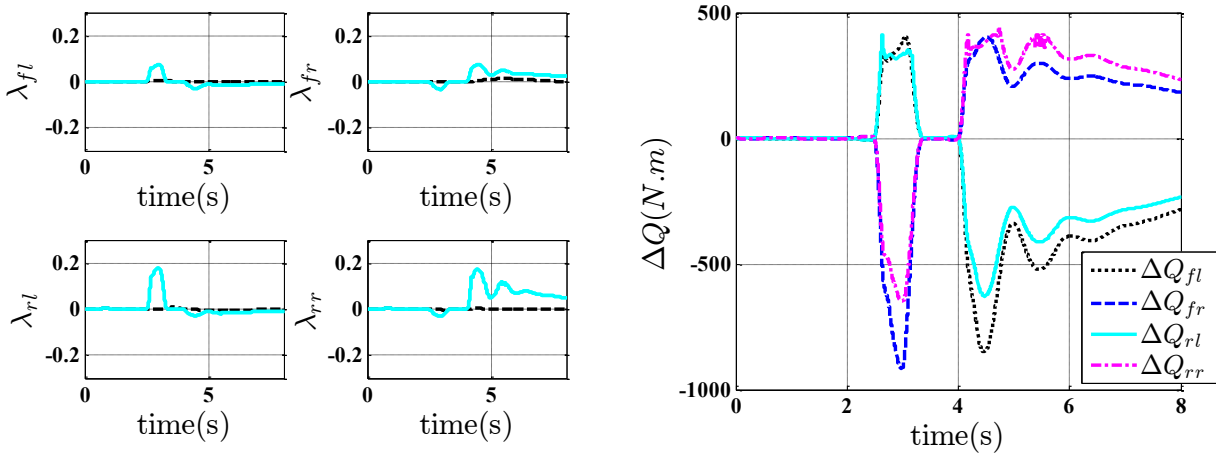

Figure 6-14: Rollover prevention for a SUV through torque vectoring

6.4.3.3 Integrated handling, lateral stability, traction and braking control-torque vectoring

The performance of the controller is evaluated for lateral stability in a slippery road. The maneuver includes simultaneous accelerating/braking and steering on a slippery road with $\mu = 0.3$ to examine the performance of the controller for integrated traction control, braking control, and lateral stability. The simulation starts with the vehicle moving at a constant speed of 60km/h. The vehicle is accelerated from $t = 0s$ to $t = 10s$ by constantly increasing throttle from 0 to 65%. Then, from $t = 11s$ to $t = 17s$, increasing braking pressure is applied from 0 to 1 MPa which applies $-350\ \text{N.m}$ of braking torque on the front wheels and $-150\ \text{N.m}$ torque on rear wheels. A $\frac{1}{4}$ Hz sinusoidal steering input with 50 degrees of magnitude is simultaneously applied to the vehicle starting from $t = 2s$. State variables for the vehicle with and without controller are shown in Figure 6-15, which include yaw rate, vehicle sideslip angle, longitudinal speed, and slip ratio. This figure shows that the proposed controller can properly control the objectives including traction control, braking control, and lateral stability to stabilize the vehicle. The applied torques on four wheels are shown in Figure 6-15. Note that, for some instances, the torques on left and right wheels have the same magnitude in opposite directions indicating pure torque vectoring. For other instances, the torques on front and rear wheels are not symmetric showing that either traction or braking control is involved , and the controller provides torques for integrated control of objectives.

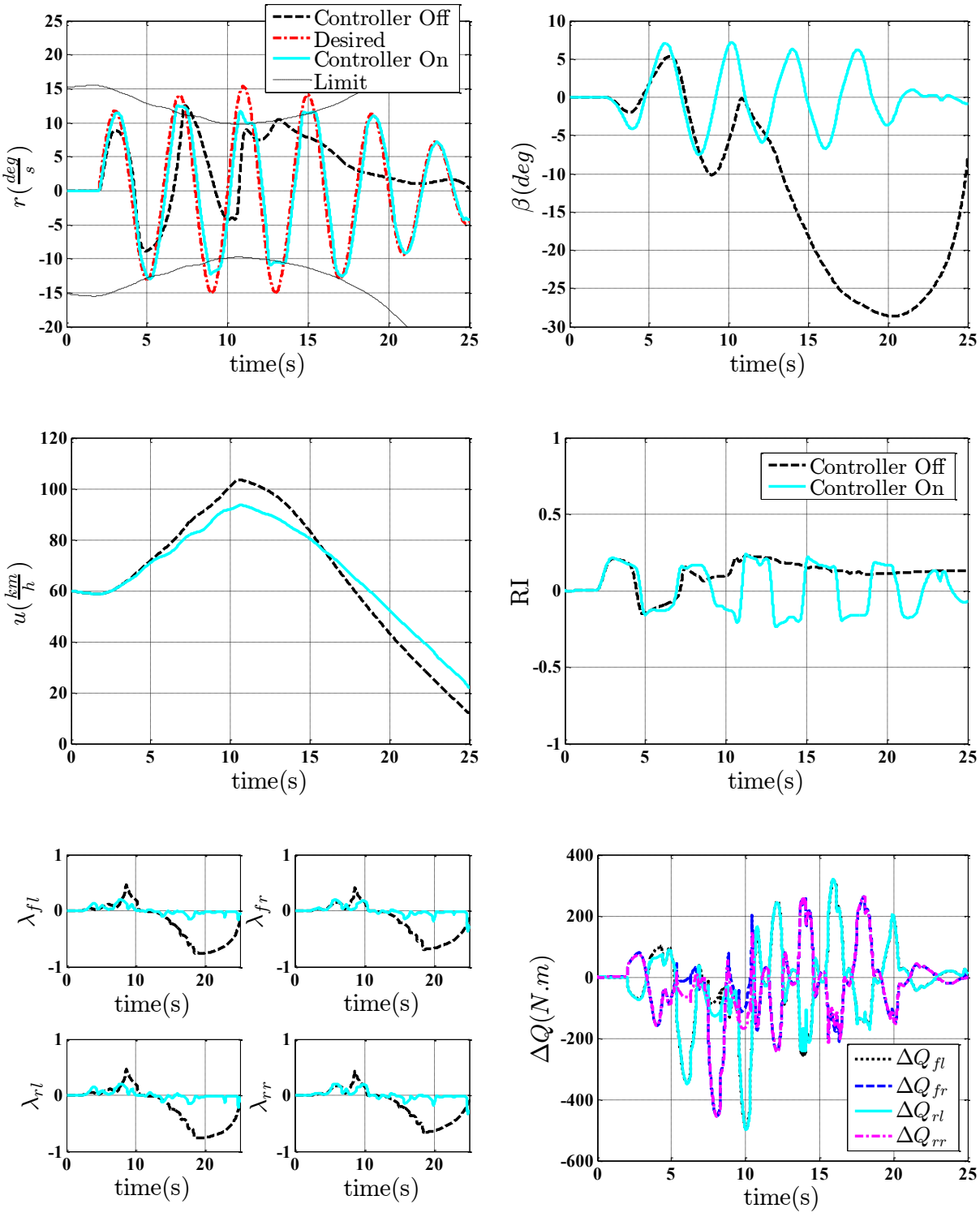

Figure 6-15: State variables for the SUV with and without controller through torque vectoring

6.4.3.4 Integrated handling and lateral stability- active front steering

The controller is also evaluated for the SUV with active front steering. The actuator reconfiguration matrix for active front steering of the SUV is:

$$T_w = diag(0,1,0,0,1,0,0,0,0,0,0,0)$$

First, active front steering is employed for handling improvement on a dry road with $\mu = 1$. Vehicle speed is $100km/h$. A $\frac{1}{8}$ Hz sinusoidal steering input with 50 degrees of magnitude is applied to the vehicle starting from $t = 2s$ to $t = 8s$. The vehicle's responses with and without controller are shown in Figure 6-16. As can be seen, the controlled vehicle properly tracks the desired response showing that the reconfigurable controller can be easily adjusted for active front steering.

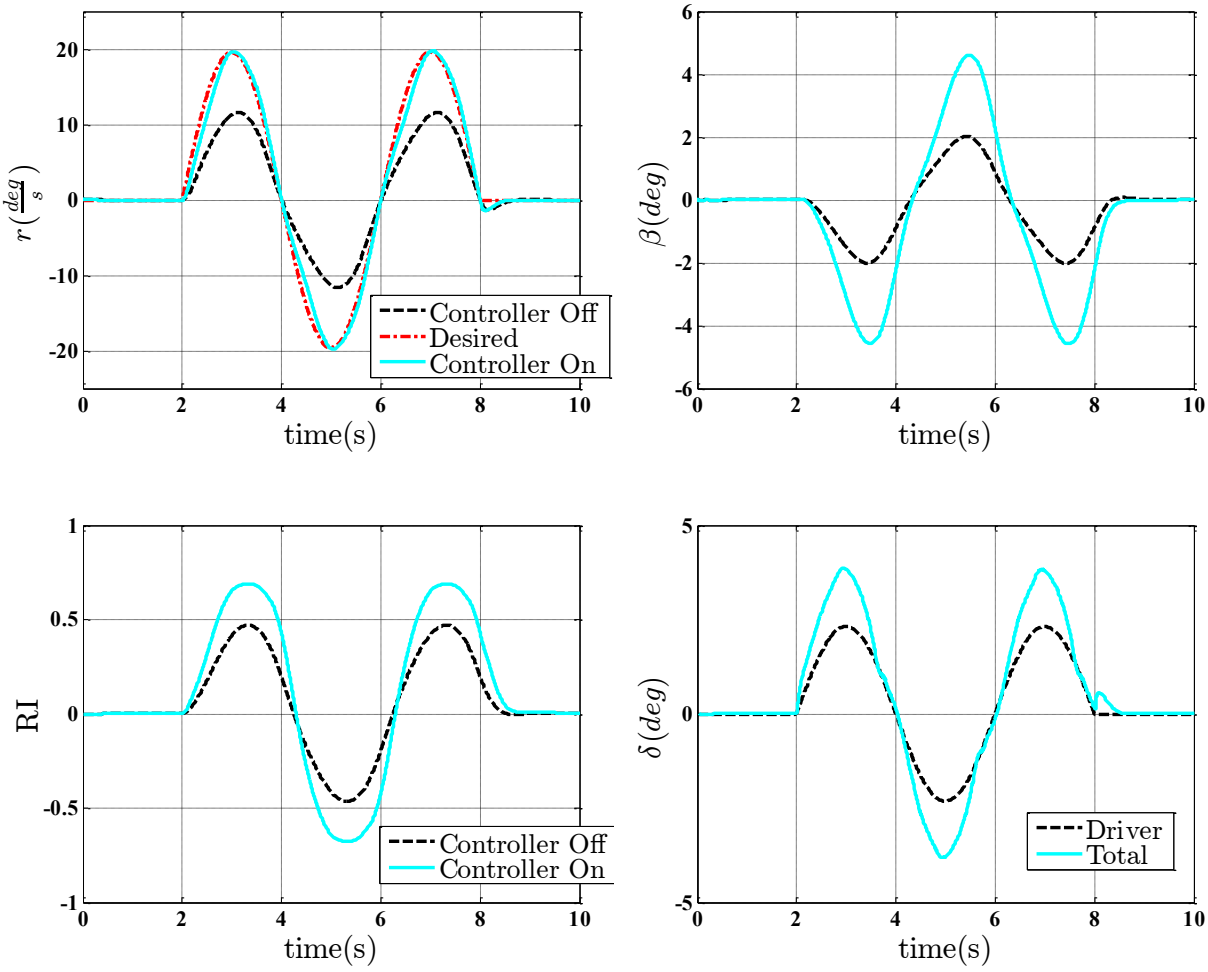

Figure 6-16: Handling improvement for the SUV through active front steering

6.4.3.5 Integrated handling, lateral stability, traction and braking control- active front steering

The performance of the controller is evaluated through the same maneuver that was explained in previous subsection for the integrated traction control, braking control, and lateral stability. State variables for controlled and un-controlled cases are shown in Figure 6-17. The results show that the proposed controller can be used for stability control with active front steering. The yaw rate, sideslip angle, and slip ratio are controlled to stabilize the vehicle for this maneuver. The applied steering by the driver and the total steering by the driver and the controller are also shown in this figure. Note that relatively large steering input needs to be applied to stabilize the vehicle through active steering. This is because of the low friction capacities for lateral forces in slippery roads near the saturation points. Although active steering is mainly used for stabilization of the vehicle in this case (no torque vectoring), the controller still provides traction and braking control. The applied torques for control of slip ratio in traction and braking are shown in Figure 6-17. As can be seen, torques exhibit small values and the slip ratio is properly controlled during traction and braking.

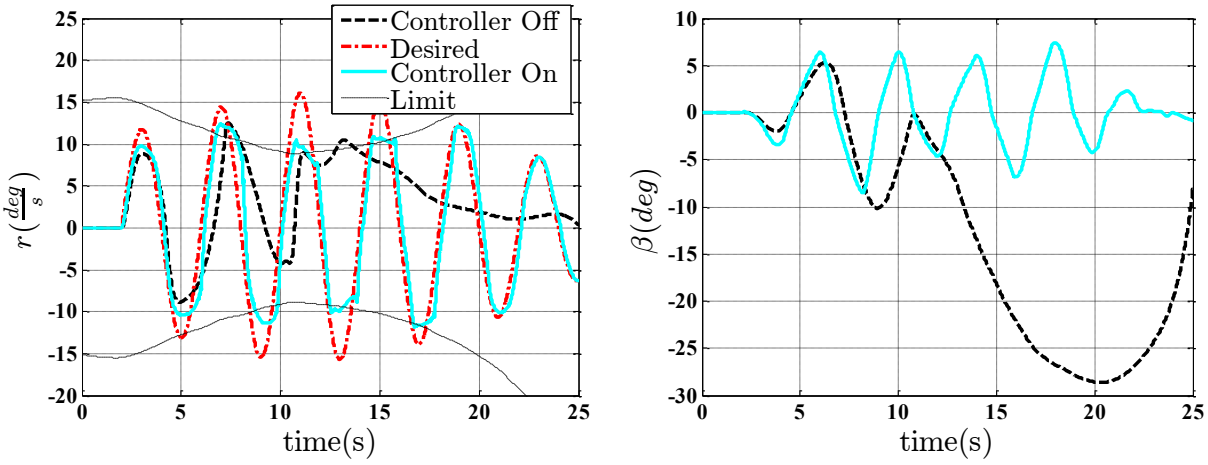

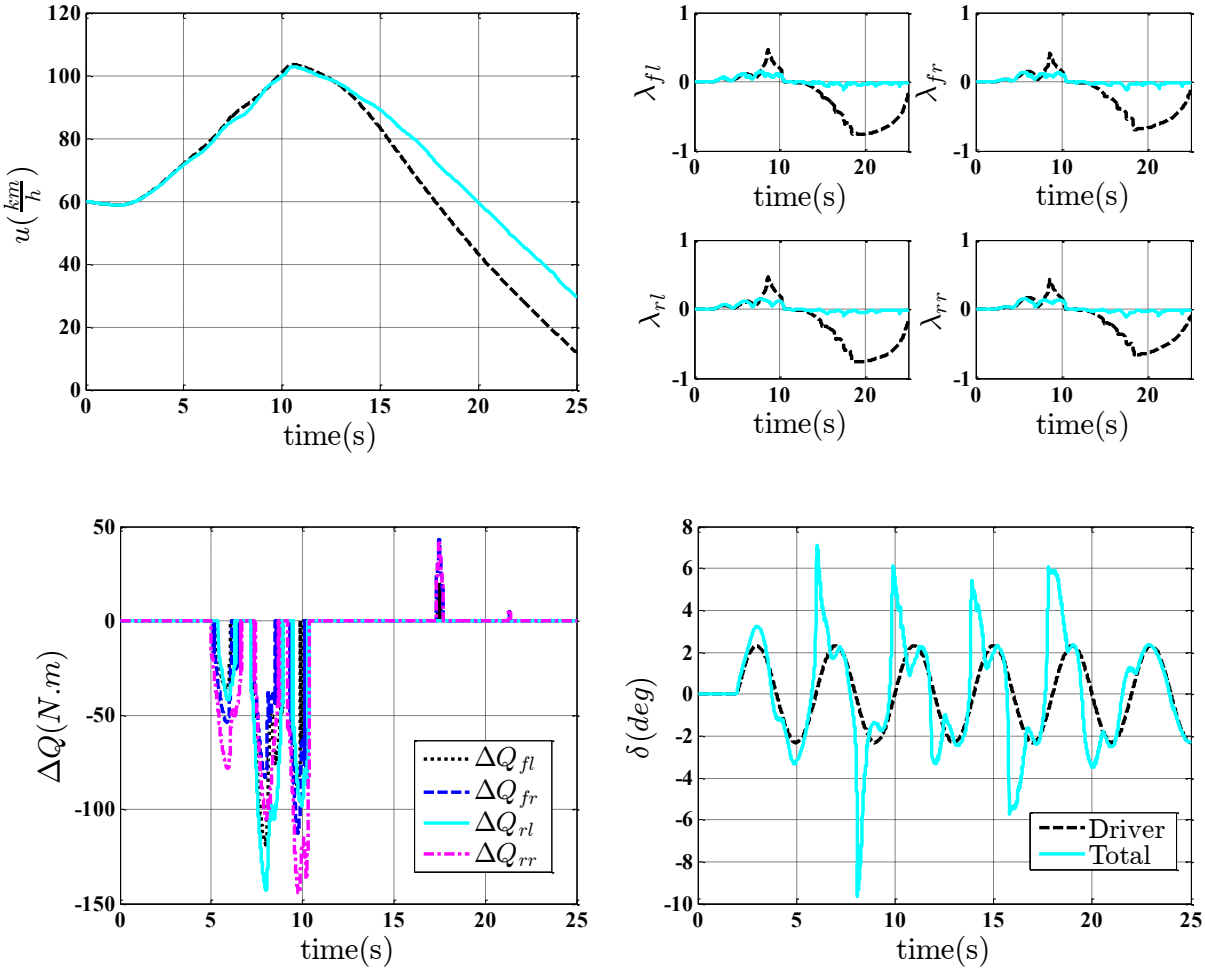

Figure 6-17: State variables for the SUV with and without controller through AFS

6.4.3.6 Handling improvement-differential braking

The controller is also evaluated for the SUV with differential braking. The actuator reconfiguration matrix for differential braking is similar to the one for torque vectoring. To apply the controller through differential braking, the upper bound, Q_i^{max}, is set to zero. In fact, for differential braking, only negative torques can be applied on wheels. Differential braking is first employed for handling improvement on a dry road with $\mu = 1$. Vehicle speed is $100km/h$. A $\frac{1}{8}$ Hz sinusoidal steering input with 50 degrees of magnitude is applied to the vehicle. The vehicle's responses with and without controller are shown in Figure 6-18. As can be seen, the controlled vehicle improves vehicle behavior

by tracking the desired response. Thus, the reconfigurable controller can also be easily used for differential braking.

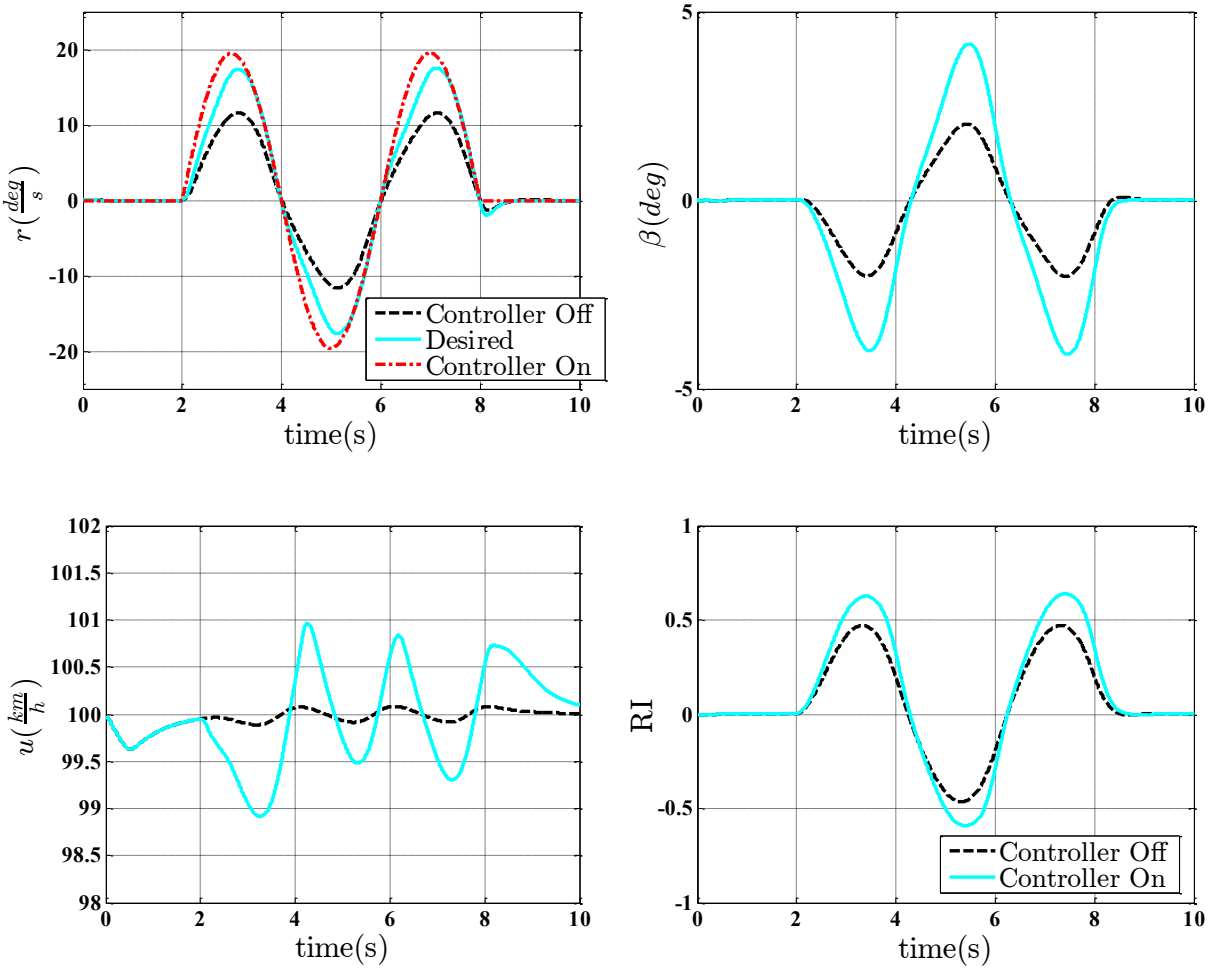

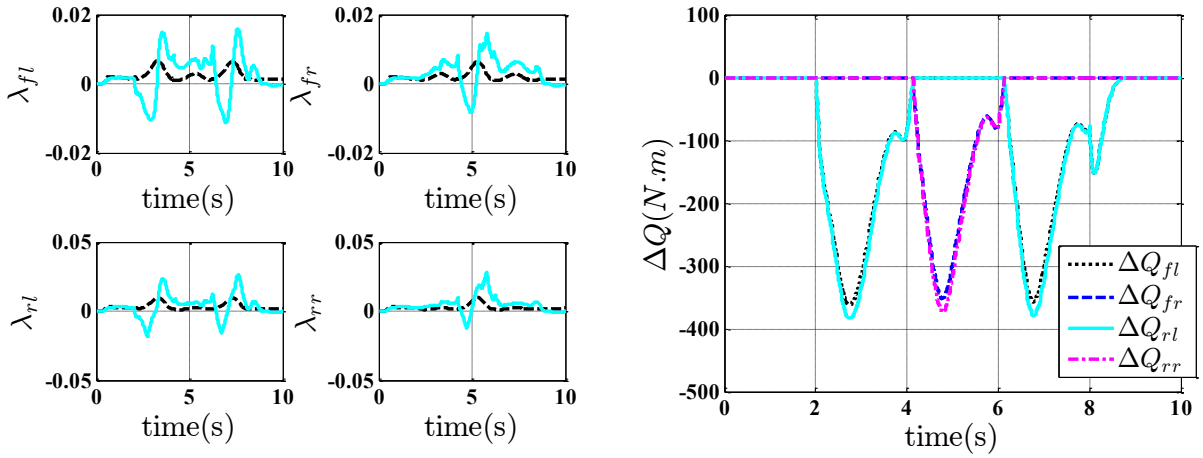

Figure 6-18: Handling improvement for the SUV through differential braking

6.4.3.7 Integrated handling, lateral stability, traction and braking control- differential braking

The same maneuver as the one in the previous subsections is again used including traction, braking, and steering on a slippery road. Simulation results for yaw rate, sideslip angle, longitudinal speed, and slip ratio for the controlled and un-controlled cases are shown in Figure 6-19. As can be seen, the controller considerably improves stability of the vehicle by tracking the desired yaw rate response, keeping small sideslip angle, and preventing large slip ratio in traction and braking. The braking torques on wheels are shown in Figure 6-19. The applied torques realize control of the slip ratio and provide lateral stability by applying moment for yaw control, simultaneously.

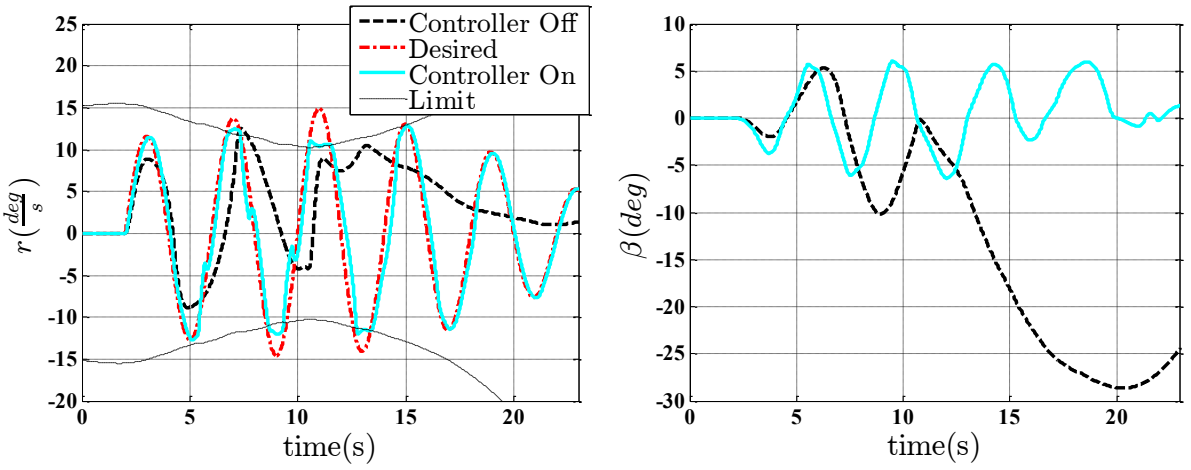

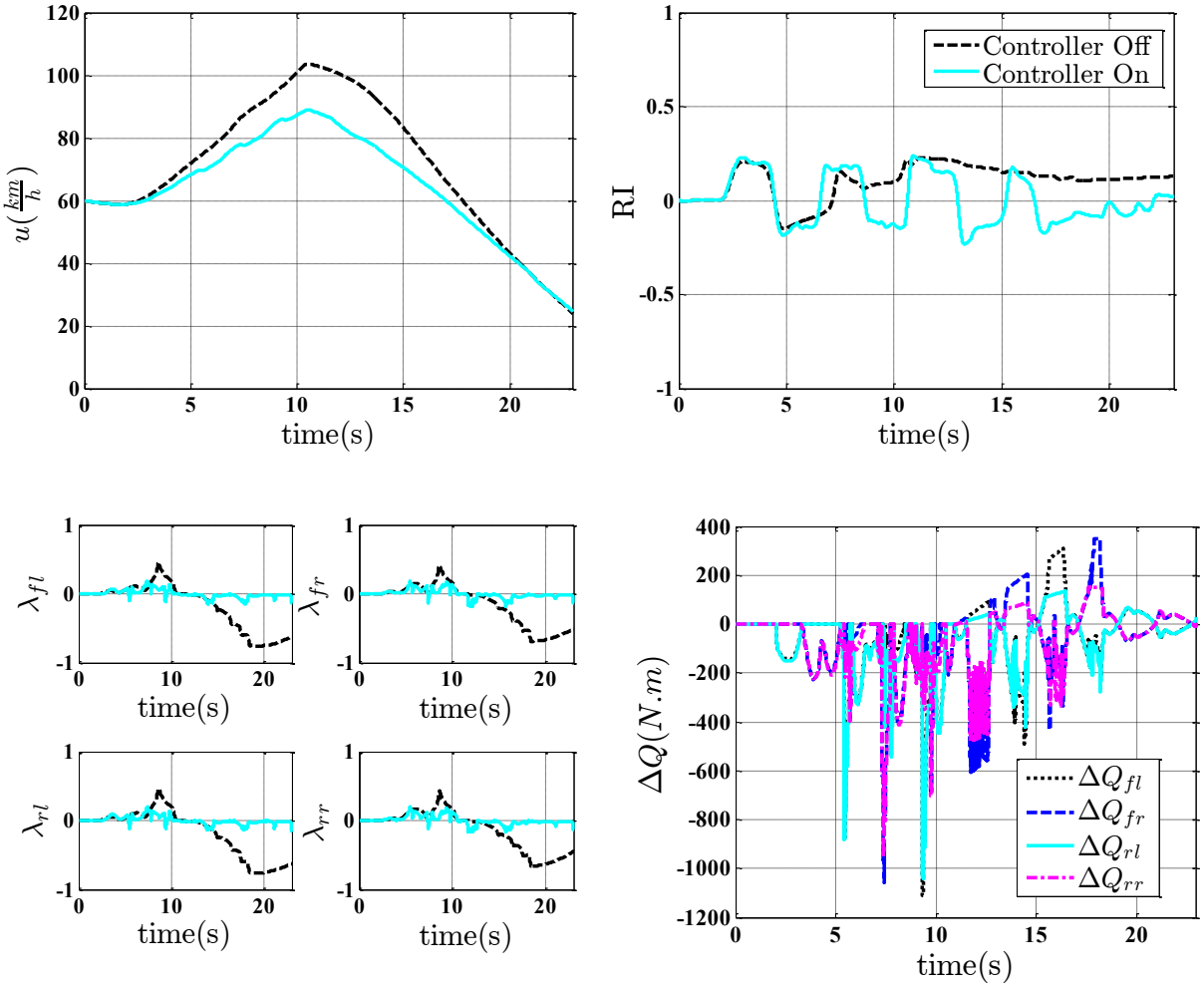

Figure 6-19: State variables for the SUV with and without controller through differential braking

6.5 Conclusion

A general reconfigurable control structure is introduced in this study which can be used for integrated stability control of a wide range of vehicles including three- and four-wheeled vehicles with any type and combinations of control actuations. The reconfigurable vehicle model which was introduced in Chapter 3 is employed in this chapter to develop the reconfigurable controller. The advantage of the proposed reconfigurable model for the MPC control design is demonstrated. The general integrated reconfigurable control structure can be used for control of different stability

objectives of vehicles including handling improvement, lateral stability, rollover prevention, cruise control, and slip control in traction and braking. The reconfigurability of the controller allows using differential braking, torque vectoring, active steering, and active camber on all or selected wheels to handle the stability objectives. Simulations are conducted for different three- and four-wheeled vehicles equipped with different actuators to evaluate the performance of the reconfigurable controller. Simulation results show that the general reconfigurable controller can be effectively used for different vehicles with different control actuation and can improve stability and safety of vehicles in harsh conditions.

Chapter 7: Conclusions and future work

7.1 Conclusions

This study investigated stability analysis of small narrow urban vehicles and proposed a general integrated reconfigurable controller to handle different stability objectives of such vehicles. The reconfigurable controller can be adjusted for a wide range of vehicles including 3W and 4W vehicles with different types and combinations of control actuations.

First, a general integrated reconfigurable vehicle model was developed that could be used for stability analysis and control design of 4W and 3W vehicles. The proposed reconfigurable vehicle model was then employed to develop a general integrated reconfigurable controller. The proposed controller considers different stability objectives including handling improvement, lateral stability, rollover prevention, and slip control in traction and braking. The reconfigurability of the controller allows using any type of control actuation such as active steering, differential braking, torque vectoring, and active camber on all or selected wheels to handle the stability objectives. Simulation results showed that the general reconfigurable controller could be effectively used for different vehicles with any control actuation to improve stability and safety of the vehicles.

The innovative reconfigurable integrated controller can be readily adapted to any urban vehicle configuration. Typically, vehicles are not equipped with all possible control actuations. Thus, the proposed controller can be used for various vehicles when actuator configuration changes. More specifically, the proposed controller can be reconfigured for torque vectoring or differential braking on rear, front or both axels, front, rear, or all wheel active steering, and also any of such control actuations combinations. The Model Predictive Control (MPC) strategy was used to develop the controller. The proposed model-based reconfigurable structure allows the control actuations that are not available to be completely removed from the optimization problem; thereby the optimal control solution can be achieved only with available control actuations. In summary, the proposed unified controller can considerably facilitate control design for a wide range of urban, conventional, and electric vehicles as it can be used for any vehicle without reformulating the problem.

This study also investigated the rollover stability of 3W vehicles and introduced a new rollover index to detect different rollover situations. The rollover stability of both Delta and Tadpole configurations of 3W vehicles were investigated and compared. The lateral load transfer ratio was used for rollover study as the most reliable definition of a rollover. Since the normal tire force is not

easy to directly measure, the proposed RI is in the terms of measurable parameters and state variables of the vehicle. This study considers not only the effects of lateral acceleration and roll angle, but also the effects of longitudinal acceleration and pitch angle on the un-tripped rollover of 3W vehicles. In addition, the effects of road angles were considered in the new RI development. Tripped rollovers were also considered including the effects of lateral and vertical road disturbances to represent bumps, curbs, and soft soil effects. In order to evaluate its performance, the proposed RI was compared to the LTR measured in CarSim. The simulation results show that the RI's indication is very close to that of the LTR. The proposed RI was also compared with two existing RIs to show its effectiveness in situations that the other RIs fail to detect rollover threat. The proposed RI is useful not only for the detection of real-time rollover threat but also can be used for the design of 3W vehicles and the design of rollover mitigation systems. In fact, it properly reflects the effects of different vehicle parameters and state variables on the rollover of 3W vehicles.

The capability of camber mechanism for improvement of vehicle's lateral and rollover stability was also investigated. Using a linear model, the cambering effect on overall vehicle behavior was analytically evaluated and compared with steering effect. It was shown that for the linear region of tire lateral force, the effects of cambering was similar to steering effects and camber mechanism worked like a second steering mechanism. On the other hand, the cambering provides more lateral force and its behavior is linear for a wide range of camber angle. Then, an active camber system was developed for improvement of vehicle lateral stability of an urban vehicle. Comparing to active steering, active camber provides more lateral stability which is due to two important advantages of increased lateral forces and its linear behavior. In addition, the capability of cambering to improve rollover stability of narrow vehicles was also investigated. The maximum lateral acceleration and the lateral load transfer were explored as important rollover criteria. The simulation results indicated that active camber systems could considerably improve rollover stability for 3W and 4W vehicles.

7.2 Future work

1- Adding vertical motion to the reconfigurable vehicle model

As mentioned, the proposed reconfigurable vehicle model considers four degrees of freedom for vehicle's body dynamics including longitudinal, lateral, yaw, and roll motions. It can be extended to include also vertical motion of vehicle's body to be useful for control of ride comfort and also for

tripped rollover control. Vertical actuators such as active or semi-active suspensions can be added to have more generalized reconfigurable vehicle model for different aspects of vehicle dynamics control.

2- Implementation of active camber system

A corner module with the capability of camber change is currently being designed and prototyped in the Mechatronic Vehicle Systems Laboratory and will be used as a platform for the validation of the results obtained in this work.

3- Integration of actuators

Control actuations are not independent form one another when they are simultaneously used in one wheel. In fact, the provided forces from the actuators are the tire forces while longitudinal and lateral forces are coupled based on the friction ellipse. Thus, for the future work, the combined slip tire models should be used to accurately model the tire forces and to develop an optimum strategy to distribute control actions between different actuators.

4- Real-time fault-tolerant controller

The reconfigurable controller is also applicable for the design and development of real-time fault-tolerant controllers in active vehicle stability systems. The proposed controller can be easily adjusted when there is a failure in any of the actuators, and the controller can be redesigned instantly by redistributing the control efforts to the remaining actuators. Thus, for the future work, fault-tolerant controllers can be developed using the proposed structure.

Bibliography

[1] R. Rajamani, J. Gohl, L. Alexander, and P. Starr, "Dynamics of Narrow Tilting Vehicles," Math. Comput. Model. Dyn. Syst., vol. 9, no. 2, pp. 209–231, Jun. 2003.

[2] J.-C. Chiou and C.-L. Chen, "Modeling and Verification of a Diamond-Shape Narrow-Tilting Vehicle," IEEE/ASME Trans. Mechatronics, vol. 13, no. 6, pp. 678–691, Dec. 2008.

[3] J. J. Michalek, P. Y. Papalambros, and S. J. Skerlos, "A Study of Fuel Efficiency and Emission Policy Impact on Optimal Vehicle Design Decisions," J. Mech. Des., vol. 126, no. 6, pp. 1062–1070, 2004.

[4] R. S. Vieira, L. C. Nicolazzi, and N. Roqueiro, "Modelling a tilting three-wheeled narrow vehicle with six degrees of freedom," in 20th International Congress of Mechanical Engineering, 2009.

[5] "http://www.traffictechnologytoday.com/news.php?NewsID=51978."

[6] R. Hibbard and D. Karnopp, "Twenty First Century Transportation System Solutions - a New Type of Small, Relatively Tall and Narrow Active Tilting Commuter Vehicle," Veh. Syst. Dyn., vol. 25, no. 5, pp. 321–347, May 1996.

[7] S. M. Savaresi, "Automatic-Control Challenges in Future Urban Vehicles: A Blend of Chassis, Energy and Networking Management," Oil Gas Sci. Technol. – Rev. d'IFP Energies Nouv., vol. 67, no. 4, pp. 633–645, Oct. 2012.

[8] L. Mourad, F. Claveau, and P. Chevrel, "A Lateral Control Strategy for Narrow Tilting Commuter Vehicle Based on the Perceived Lateral Acceleration .," in Proceedings of the IFAC World Congress, 2011.

[9] J. J. H. Berote, "Dynamics and Control of a Tilting Three Wheeled Vehicle," PhD Thesis, University of Bath, 2010.

[10] C. R. Van den Brink and H. M. Kroonen, "Dynamic Vehicle Control for Enclosed Narrow Vehicles," in 6th European Congress, 1997.

[11] B. Schofield, "Vehicle Dynamics Control for Rollover Prevention," Licentiate Thesis, Lund University, 2006.

[12] A. Sears, "Low Speed Motorcycle Stabilization Device," PhD Thesis, Worcester Polytechnic Institute, 2012.

[13] A. Goodarzi, A. Soltani, M. H. Shojaeefard, and A. Khajepour, "An integrated vehicle dynamic control strategy for three-wheeled vehicles," Proc. Inst. Mech. Eng. Part K J. Multi-body Dyn., vol. 229, no. 3, pp. 225–244, Nov. 2014.

[14] J. C. Huston, B. J. Graves, and D. B. Hohnson, "Three Wheeled Vehicle Dynamics," SAE Tech. Pap., vol. 820139, 1982.

[15] J. Berote, A. van Poelgeest, J. Darling, K. Edge, and A. Plummer, "The dynamics of a three-wheeled narrow-track tilting vehicle," in FISITA World Automotive Congress 2008, 2008.

[16] J. Gohl, R. Rajamani, P. Starr, and L. Alexander, "Development of a Novel Tilt-Controlled Narrow Commuter Vehicle," 2006.

[17] C. R. Van Den Brink and H. M. Kroonen, "DVC - The banking technology driving the CARVER vehicle class," in AVEC'04, 2004.

[18] J. C. Chiou, C. Lin, C. Chen, and C. Chien, “Tilting Motion Control in Narrow Tilting Vehicle Using Double-Loop PID Controller,” in Proceedings of the 7th Asian Control Conference, 2009.

[19] J. Gohl, R. Rajamani, L. Alexander, and P. Starr, “Active Roll Mode Control Implementation on a Narrow Tilting Vehicle,” Veh. Syst. Dyn., vol. 42, no. 5, pp. 347–372, Dec. 2004.

[20] D. Piyabongkarn, T. Keviczky, and R. Rajamani, “Active direct tilt control for stability enhancement of a narrow commuter vehicle,” Int. J. Automot. Technol., vol. 5, no. 2, pp. 77–88, 2004.

[21] S. Kidane, L. Alexander, R. Rajamani, P. Starr, and M. Donath, “A fundamental investigation of tilt control systems for narrow commuter vehicles,” Veh. Syst. Dyn., vol. 46, no. 4, pp. 295–322, Apr. 2008.

[22] S. Kidane, R. Rajamani, L. Alexander, P. J. Starr, and M. Donath, “Development and Experimental Evaluation of a Tilt Stability Control System for Narrow Commuter Vehicles,” IEEE Trans. Control Syatem Technol., vol. 18, no. 6, pp. 1266–1279, 2010.

[23] “http://www.carstyling.ru/en/cars.1961_Ford_Gyron.html.”

[24] “http://lefthandedcyclist.blogspot.ca/2012/02/drymer-and-varna-lean-forward.html.”

[25] “http://www.gizmag.com/go/3628/.”

[26] “http://www.conceptcarz.com/view/photo/135656,964/1997-Mercedes-Benz-F300-Life-Jet_photo.aspx.”

[27] T. Concept and T. Challenge, “Slender Comfort Vehicles : Offering the Best of Both Worlds,” AutoTechnology, vol. 4, no. 1, pp. 56–59, 2004.

[28] “Web site. [Online]. Available: http://www.pluginamerica.org/vehicles/lumeneo-smera.” .

[29] “http://www.motorauthority.com/news/1029074_driving-the-wacky-carver-one-three-wheeled-tilt-car.”

[30] “http://jalopnik.com/363973/lumeneo-smera-80-mph-ev-gets-geneva-started-down-path-of-weird.”

[31] “Web site. [Online]. Available: http://www.worldcarfans.com/109100722301/nissan-land-glider-concept-highlighted-for-tokyo-motor-show.”

[32] “http://www.autoblog.com/2009/10/07/tokyo-2009-preview-nissan-unveils-land-glider-concept-w-video/#image-6.”

[33] N. Owano, “Toyota’s i-Road to debut at the Geneva Motor Show,” http://phys.org/news/2013-03-toyota-i-road-debut-geneva-motor.html, 2013.

[34] “http://www.design42day.com/transportation/toyota-i-road/.”

[35] A. Khajepour, M. Fallah, and A. Goodarzi, Electric and Hybrid Vehicles: Technologies, Modeling and Control - A Mechatronic Approach. John Wiley & Sons, 2014.

[36] W. Chen, H. Xiao, L. Liu, J. Zu, and H. Zhou, “Integrated Control of Vehicle System Dynamics: Theory and Experiment,” Adv. Mechatronics, InTech, 2011.

[37] M. Ataei, E. Asadi, A. Goodarzi, A. Khajepour, and M. B. Khamesee, “Multi-objective optimization of a hybrid electromagnetic suspension system for ride comfort, road holding and regenerated power,” JVC/Journal Vib. Control, vol. 23, no. 5, 2017.

[38] R. Rajamani, Vehicle Dynamics and Control. Springer Science & Business Media, 2011.

[39] M. Doumiati, O. Sename, L. Dugard, J.-J. Martinez-Molina, P. Gaspar, and Z. Szabo, "Integrated vehicle dynamics control via coordination of active front steering and rear braking," Eur. J. Control, vol. 19, no. 2, pp. 121–143, Mar. 2013.

[40] C. E. Beal and J. C. Gerdes, "Model Predictive Control for Vehicle Stabilization at the Limits of Handling," IEEE Trans. Control Syst. Technol., vol. 21, no. 4, pp. 1258–1269, Jul. 2013.

[41] M. Tai and M. Tomizuka, "Robust longitudinal velocity tracking of vehicles using traction and brake control," in 6th International Workshop on Advanced Motion Control Proceedings, 2000, pp. 305–310.

[42] J. C. Gerdes and J. K. Hedrick, "Vehicle speed and spacing control via coordinated throttle and brake actuation," Control Eng. Pract., vol. 5, no. 11, pp. 1607–1614, 1997.

[43] Y. Chen and J. Wang, "Adaptive Vehicle Speed Control With Input Injections for Longitudinal Motion Independent Road Frictional Condition Estimation," IEEE Trans. Veh. Technol., vol. 60, no. 3, pp. 839–848, Mar. 2011.

[44] L. Nouvelière and S. Mammar, "Experimental vehicle longitudinal control using a second order sliding mode technique," Control Eng. Pract., vol. 15, no. 8, pp. 943–954, Aug. 2007.

[45] J. Yoon, W. Cho, J. Kang, B. Koo, and K. Yi, "Design and evaluation of a unified chassis control system for rollover prevention and vehicle stability improvement on a virtual test track," Control Eng. Pract., vol. 18, no. 6, pp. 585–597, Jun. 2010.

[46] B.-C. Chen and H. Peng, "Differential-Braking-Based Rollover Prevention for Sport Utility Vehicles with Human-in-the-loop Evaluations," Veh. Syst. Dyn., vol. 36, no. 4–5, pp. 359–389, Aug. 2010.

[47] M. Ataei, A. Khajepour, and S. Jeon, "A General Rollover Index for Tripped and Un-tripped Rollovers on Flat and Sloped Roads," Proc. Inst. Mech. Eng. Part D J. Automob. Eng., 2017.

[48] M. Ataei, A. Khajepour, and S. Jeon, "Model Predictive Rollover Prevention for Steer-by-wire Vehicles with a New Rollover Index," Submitted.

[49] P. Falcone, F. Borrelli, J. Asgari, H. E. Tseng, and D. Hrovat, "Predictive Active Steering Control for Autonomous Vehicle Systems," IEEE Trans. Control Syst. Technol., no. January, pp. 1–14, 2007.

[50] P. Falcone, H. Eric Tseng, F. Borrelli, J. Asgari, and D. Hrovat, "MPC-based yaw and lateral stabilisation via active front steering and braking," Veh. Syst. Dyn., vol. 46, no. sup1, pp. 611–628, Sep. 2008.

[51] M. Jalali, A. Khajepour, S. Chen, and B. Litkouhi, "Integrated stability and traction control for electric vehicles using model predictive control," Control Eng. Pract., vol. 54, pp. 256–266, Sep. 2016.

[52] C. E. Beal, "Applications of Model Predictive Control to Vehicle Dynamics for Active Satefy and Stability," PhD Thesis, Stanford University, 2011.

[53] S. Leel, F. Yakubl, and Y. Moril, "Rollover Prevention with Predictive Control of Differential Braking and Rear Wheel Steering," in Robotics, Automation and Mechatronics (RAM), 2013 6th IEEE Conference on. IEEE, 2013, vol. 2, no. 2.

[54] T. A. Johansen, I. Petersen, J. Kalkkuhl, and J. Lüdemann, "Gain-Scheduled Wheel Slip

Control in Automotive Brake Systems," IEEE Trans. Control Syst. Technol., vol. 11, no. 6, pp. 799–811, 2003.

[55] H. Mirzaeinejad and M. Mirzaei, "A novel method for non-linear control of wheel slip in anti-lock braking systems," Control Eng. Pract., vol. 18, no. 8, pp. 918–926, Aug. 2010.

[56] M. Wu and M. Shih, "Simulated and experimental study of hydraulic anti-lock braking system using sliding-mode PWM control," Mechatronics, vol. 13, no. 4, pp. 331–351, May 2003.

[57] S. Zheng, H. Tang, Z. Han, and Y. Zhang, "Controller design for vehicle stability enhancement," Control Eng. Pract., vol. 14, no. 12, pp. 1413–1421, Dec. 2006.

[58] S. Solyom, A. Rantzer, and J. LÜdemann, "Synthesis of a Model-Based Tire Slip Controller," Veh. Syst. Dyn., vol. 41, no. 6, pp. 475–499, Dec. 2004.

[59] K. Fujii and H. Fujimoto, "Traction Control based on Slip Ratio Estimation Without Detecting Vehicle Speed for Electric Vehicle," in 2007 Power Conversion Conference - Nagoya, 2007, pp. 688–693.

[60] K. R. Buckholtz, "Reference Input Wheel Slip Tracking Using Sliding Mode Control," SAE Tech. Pap., no. 2002-01–03, 2002.

[61] K. Yi, T. Chung, J. Kim, and S. Yi, "An investigation into differential braking strategies for vehicle stability control," Proc. Inst. Mech. Eng. Part D J. Automob. Eng., vol. 217, no. 12, pp. 1081–1093, 2003.

[62] T. Pilutti, G. Ulsoy, and D. Hrovat, "Vehicle steering intervention through differential braking," in Proceedings of 1995 American Control Conference - ACC'95, 1995, vol. 3, no. November 2016.

[63] J. He, D. A. Crolla, M. C. Levesley, and W. J. Manning, "Integrated Active Steering and Variable Torque Distribution Control for Improving Vehicle Handling and Stability," SAE Tech. Pap., no. 2004-01–1071, 2014.

[64] J. Tjønnås, T. A. Johansen, and S. Member, "Stabilization of Automotive Vehicles Using Active Steering and Adaptive Brake Control Allocation," IEEE Trans. Control Syst. Technol., vol. 18, no. 3, pp. 545–558, 2010.

[65] L. De Novellis, A. Sorniotti, P. Gruber, L. Shead, V. Ivanov, and K. Hoepping, "Torque Vectoring for Electric Vehicles with Individually Controlled Motors : State-of-the-Art and Future Developments," in 26th Electric Vehicle Symposium, 2012.

[66] W. Liang, H. Yu, R. McGee, M. Kuang, and J. Medanic, "Vehicle Pure Yaw Moment control using differential tire slip," in 2009 American Control Conference, 2009.

[67] K. Jalali, T. Uchida, S. Lambert, and J. Mcphee, "Development of an Advanced Torque Vectoring Control System for an Electric Vehicle with In-wheel Motors using Soft Computing Techniques," SAE Int. J. Altern. Powertrains 2, no. 2013-01–0698, pp. 261–278, 2013.

[68] Y. Chen and J. Wang, "Design and Evaluation on Electric Differentials for Overactuated Electric Ground Vehicles With Four Independent In-Wheel Motors," IEEE Trans. Veh. Technol., vol. 61, no. 4, pp. 1534–1542, May 2012.

[69] J. Ackermann and T. Bünte, "Yaw disturbance attenuation by robust decoupling of car steering," Control Eng. Pract., vol. 5, no. 8, pp. 1131–1136, 1997.

[70] P. Yih, J. Ryu, and J. C. Gerdes, "Modification of vehicle handling characteristics via steer-

by-wire," IEEE Trans. Control Syst. Technol., vol. 13, no. 6, pp. 965–976, 2005.

[71] P. Falcone, F. Borrelli, J. Asgari, H. E. Tseng, and D. Hrovat, "Predictive Active Steering Control for Autonomous Vehicle Systems," IEEE Trans. Control Syatem Technol., vol. 15, no. 3, pp. 566–580, 2007.

[72] B. Zheng and S. Anwar, "Yaw stability control of a steer-by-wire equipped vehicle via active front wheel steering," Mechatronics, vol. 19, no. 6, pp. 799–804, Sep. 2009.

[73] S. Mammar and D. Koenig, "Vehicle Handling Improvement by Active Steering," Veh. Syst. Dyn., vol. 38, no. 3, pp. 211–242, 2002.

[74] H. Fujimoto and K. Maeda, "Optimal yaw-rate control for electric vehicles with active front-rear steering and four-wheel driving-braking force distribution," IECON 2013 - 39th Annu. Conf. IEEE Ind. Electron. Soc., pp. 6514–6519, Nov. 2013.

[75] Y. Furukawa, N. Yuhara, S. Sano, H. Takeda, and Y. Matsushita, "A Review of Four-Wheel Steering Studies from the Viewpoint of Vehicle Dynamics and Control," Veh. Syst. Dyn., vol. 18, no. 1–3, pp. 151–186, Jul. 2007.

[76] J. Sridhar and H. Hatwal, "A Comparative Study of Four Wheel Steering Models Using the Inverse Solution," Veh. Syst. Dyn., vol. 21, no. 1, pp. 1–18, Jan. 1992.

[77] S. M. Laws, "An active camber concept for extreme maneuverability: mechatronic suspension design, tire modeling, and prototype development," PhD Thesis, Stanford University, 2010.

[78] B. Németh and P. Gáspár, "Challenges and Possibilities in Variable Geometry Suspension Systems," Period. Polytech. Transp. Eng., vol. 40, no. 2, p. 81, 2012.

[79] F. Yu and D. L. D. A. Crolla, "Integrated Vehicle Dynamics Control —state-of-the art review," 2008 IEEE Veh. Power Propuls. Conf., pp. 1–6, Sep. 2008.

[80] S. Di Cairano, H. E. Tseng, D. Bernardini, and A. Bemporad, "Vehicle Yaw Stability Control by Coordinated Active Front Steering and Differential Braking in the Tire Sideslip Angles Domain," IEEE Trans. Control Syst. Technol., vol. 21, no. 4, pp. 1236–1248, Jul. 2013.

[81] B. Lee and A. Khajepour, "Vehicle Stability through Integrated Active Steering and Differential Braking," vol. 2006, no. 724, 2015.

[82] A. Tavasoli, M. Naraghi, and H. Shakeri, "Optimized coordination of brakes and active steering for a 4WS passenger car.," ISA Trans., vol. 51, no. 5, pp. 573–83, Sep. 2012.

[83] D. Bianchi, A. Borri, M. D. Di Benedetto, S. Di Gennaro, and G. Burgio, "Adaptive integrated vehicle control using active front steering and rear torque vectoring," Int. J. Veh. Auton. Syst., vol. 8, no. 2/3/4, p. 85, 2010.

[84] J. Yoon and K. Yi, "A Rollover Mitigation Control Scheme Based on Rollover Index," in proceeding of the 2006 American Control Conference, 2006.

[85] S. Lapapong, "Vehicle rollover prevention for banked surfaces," PhD Thesis, The Pennsylvania State University, 2010.

[86] R. W. Goldman, "Development of a Rollover-Warning Device for Road Vehicles," PhD Thesis, The Pennsylvania State University, 2001.

[87] R. W. Goldman, M. El-Gindy, and B. T. Kulakowski, "Rollover Dynamics of Road Vehicles: Literature Survey," Int. J. Heavy Veh. Syst., vol. 8, no. 2, pp. 103–141, 2001.

[88] T. J. Wielenga, "A Method for Reducing On-Road Rollovers -- Anti-Rollover Braking," SAE

Tech. Pap., no. 1999-01–0123, 1999.

[89] T. J. Wielenga and M. A. Chace, “A Study in Rollover Prevention Using Anti-Rollover Braking,” SAE Tech. Pap., no. 2000-01–1642, 2000.

[90] B. Schofield and T. Hagglund, “Optimal control allocation in vehicle dynamics control for rollover mitigation,” in 2008 American Control Conference, 2008.

[91] B. Schofield, T. Hagglund, and A. Rantzer, “Vehicle Dynamics Control and Controller Allocation for Rollover Prevention,” in 2006 IEEE International Conference on Control Applications, 2006.

[92] C. R. Carlson and J. C. Gerdes, “Optimal rollover prevention with steer by wire and differential braking,” in ASME 2003 International Mechanical Engineering Congress and Exposition, 2003.

[93] C. E. Beal and J. C. Gerdes, “Predictive control of vehicle roll dynamics with rear wheel steering,” in Proceedings of the 2010 American Control Conference, 2010.

[94] R. Rajamani and D. N. Piyabongkarn, “New paradigms for the integration of yaw stability and rollover prevention functions in vehicle stability control,” IEEE Trans. Intell. Transp. Syst., vol. 14, no. 1, pp. 249–261, Mar. 2013.

[95] G. Phanomchoeng and R. Rajamani, “New Rollover Index for the Detection of Tripped and Untripped Rollovers,” IEEE Trans. Ind. Electron., vol. 60, no. 10, pp. 4726–4736, Oct. 2013.

[96] J. Ackermann and D. Odenthal, “Damping of vehicle roll dynamics by gain scheduled active steering,” in Proceedings of European Control Conference, 1999.

[97] R. Rajamani, D. Piyabongkam, V. Tsourapas, and I. Y. Lew, “Real-Time Estimation of Roll Angle and CG Height for Active Rollover Prevention Applications,” in American Control Conference, 2009, no. 2.

[98] S. Solmaz, M. Corless, and R. Shorten, “A methodology for the design of robust rollover prevention controllers for automotive vehicles: Part 2-Active steering,” in 2007 American Control Conference, 2007, no. 1.

[99] H. Dahmani, O. Pagès, A. El Hajjaji, and N. Daraoui, “Observer-Based Robust Control of Vehicle Dynamics for Rollover Mitigation in Critical Situations,” IEEE Trans. Intell. Transp. Syst., vol. 15, no. 1, pp. 274–284, 2014.

[100] P. Gaspar, I. Szaszi, and J. Bokor, “Reconfigurable control structure to prevent the rollover of heavy vehicles,” Control Eng. Pract., vol. 13, no. 6, pp. 699–711, Jun. 2005.

[101] M. J. L. Boada, B. L. Boada, A. Quesada, A. Gauchía, and V. Díaz, “Active roll control using reinforcement learning for a single unit heavy vehicle,” Int. J. Heavy Veh. Syst., vol. 16, no. 4, pp. 412–430, 2009.

[102] H. Yu, L. Güvenç, and Ü. Özgüner, “Heavy duty vehicle rollover detection and active roll control,” Veh. Syst. Dyn., vol. 46, no. 6, pp. 451–470, Jun. 2008.

[103] S. Yim, Y. Park, and K. Yi, “Design of active suspension and electronic stability program for rollover prevention,” Int. J. Automot. Technol., vol. 11, no. 2, pp. 147–153, Apr. 2010.

[104] Y. I. Ryu, D. O. Kang, S. J. Heo, and J. H. In, “Rollover mitigation for a heavy commercial vehicle,” Int. J. Automot. Technol., vol. 11, no. 2, pp. 283–287, Apr. 2010.

[105] T. J. Wielenga and M. A. Chace, “A Study in Rollover Prevention Using Anti-Rollover

Braking," in Proceedings of the Automotive Dynamics & Stability Conference, 2000, no. 724.

[106] B. Schofield and T. Hagglund, "Optimal control allocation in vehicle dynamics control for rollover mitigation," 2008 Am. Control Conf., pp. 3231–3236, Jun. 2008.

[107] J.-S. Jo, S.-H. You, J. Y. Joeng, K. I. Lee, and K. Yi, "Vehicle stability control system for enhancing steerabilty, lateral stability, and roll stability," Int. J. Automot. Technol., vol. 9, no. 5, pp. 571–576, Oct. 2008.

[108] C. Larish, D. Piyabongkarn, V. Tsourapas, and R. Rajamani, "A New Predictive Lateral Load Transfer Ratio for Rollover Prevention Systems," IEEE Trans. Veh. Technol., vol. 62, no. 7, pp. 2928–2936, Sep. 2013.

[109] S. Lapapong and S. N. Brennan, "Terrain-aware rollover prediction for ground vehicles using the zero-moment point method," in 2010 American Control Conference, 2010.

[110] N. Bouton, R. Lenain, B. Thuilot, and J. Fauroux, "A rollover indicator based on the prediction of the load transfer in presence of sliding : application to an All Terrain Vehicle," in 2007 IEEE International Conference on Robotics and Automation, 2007, no. April.

[111] H. Dahmani, M. Chadli, A. Rabhi, and A. El Hajjaji, "Fuzzy observer for detection of impending vehicle rollover with road bank angle considerations," in 18th Mediterranean Conference on Control and Automation, MED'10, 2010.

[112] P. J. Liu, S. Rakheja, and A. K. W. Ahmed, "Dynamic rollover thresshold of articulated freight vehicles," Int. J. Heavy Veh. Syst., vol. 5, no. 3–4, pp. 300–322, 1998.

[113] M. Ataei, A. Khajepour, and S. Jeon, "Rollover stability of three-wheeled vehicles including road configuration effects," Proc. Inst. Mech. Eng. Part D J. Automob. Eng., 2017.

[114] A. Zandieh, "Dynamics of a Three-Wheel Vehicle with Tadpole Design," M.S. Thesis, University of Waterloo, 2014.

[115] A. Soltani, A. Goodarzi, and A. Khajepour, "An Investigation on Dynamic Behavior of Different Three-Wheeled Vehicle Configurations," in 12th international symposium on advanced vehicle control, AVEC'14., 2014.

[116] A. Soltani and A. Goodarzi, "An Investigation on Dynamic Behavior of Different Three-Wheeled Vehicle Configurations," pp. 791–798, 2014.

[117] R. G. Longoria, "Coordinated and Reconfigurable Vehicle Dynamics Control," IEEE Trans. Control Syst. Technol., vol. 17, no. 3, pp. 723–732, May 2009.

[118] Z. X. -, T. Y. -, and W. Y. -, "Model Predictive Control Allocation Based Coordinated Vehicle Dynamics Control with In-Wheel Motors," Int. J. Adv. Comput. Technol., vol. 4, no. 3, pp. 75–83, Feb. 2012.

[119] "Unified Control of Brake- and Steer-by-Wire Systems Using Optimal Control David Doman and Michael Oppenheimer," vol. 2006, no. 724, 2014.

[120] M. M. Kale and a. J. Chipperfield, "Stabilized MPC formulations for robust reconfigurable flight control," Control Eng. Pract., vol. 13, no. 6, pp. 771–788, Jun. 2005.

[121] T. D. Gillespie, Fundamentals of vehicle dynamics. 1992.

[122] B. Nemeth and P. Gaspar, "Integration of control design and variable geometry suspension construction for vehicle stability enhancement," IEEE Conf. Decis. Control Eur. Control Conf., pp. 7452–7457, Dec. 2011.

[123] S.-J. Park and J.-H. Sohn, “Effects of camber angle control of front suspension on vehicle dynamic behaviors,” J. Mech. Sci. Technol., vol. 26, no. 2, pp. 307–313, Apr. 2012.

[124] M. Hotiguchi, A. Mizuno, M. Jones, and K. Futamura, “Active Camber Control,” in Proceedings of the FISITA 2012 World Automotive Congress, 2012.

[125] D. Ammon, “Vehicle dynamics analysis tasks and related tyre simulation challenges,” Veh. Syst. Dyn., vol. 43, no. sup1, pp. 30–47, Jan. 2005.

[126] H. Pacejka, Tire and vehicle dynamics. Elsevier, 2005.

[127] “https://carsim.com/products/carsim/index.php.”

[128] J.-I. Park, J.-Y. Yoon, D.-S. Kim, and K.-S. Yi, “Roll state estimator for rollover mitigation control,” Proc. Inst. Mech. Eng. Part D J. Automob. Eng., vol. 222, no. 8, pp. 1289–1312, Aug. 2008.

[129] J. C. Gerdes and J. Ryu, “Estimation of Vehicle Roll and Road Bank Angle,” in American Control Conference, 2004.

[130] H. Jansson, E. Kozica, P. Sahlholm, and K. H. Johansson, “Improved road grade estimation using sensor fusion Improved road grade estimation using sensor fusion,” in Proceedings of the 12th Reglermöte in Stockholm, 2006, no. August.

[131] H. E. Tseng, “Dynamic Estimation of Road Bank Angle,” Veh. Syst. Dyn., vol. 36, no. 4–5, pp. 307–328, Aug. 2010.

[132] D. M. Hamby, “A review of techniques for parameter sensitivity analysis of environmental models.,” Environ. Monit. Assess., vol. 32, no. 2, pp. 135–54, Sep. 1994.

[133] S. Evangelou, “Control and Stability Analysis of Two-wheeled Road Vehicles,” PhD Thesis, University of London, 2003.

[134] E. Esmailzadeh, a. Goodarzi, and G. R. Vossoughi, “Optimal yaw moment control law for improved vehicle handling,” Mechatronics, vol. 13, no. 7, pp. 659–675, Sep. 2003.

[135] M. Ataei, A. Khajepour, and S. Jeon, “A Novel Reconfigurable Integrated Vehicle Stability Control with Omni Actuation Systems,” IEEE Trans. Veh. Technol., 2017.

[136] M. Ataei, A. Khajepour, and S. Jeon, “Reconfigurable Integrated Stability Control for Four- and Three-wheeled Urban Vehicles with Flexible Combinations of Actuation Systems,” Submitted.

[137] M. Akar and A. Dinçer Dere, “A Switching Rollover Controller Coupled With Closed-Loop Adaptive Vehicle Parameter Identification,” IEEE Trans. Intell. Transp. Syst., vol. 15, no. 4, pp. 1579–1585, 2014.

Appendix A:
Tire model

Pajeca tire model for lateral forces in pure side-slip and camber is [133]

$$F_{yo} = D_y \sin[C_y \arctan\{B_y\alpha - E_y(B_y\alpha - \arctan(B_y\alpha))\} + C_\gamma \arctan\{B_\gamma\gamma - E_\gamma(B_\gamma\gamma - \arctan(B_\gamma\gamma))\}]$$

$D_y = \mu_y F_z$	$K_{y\alpha o} = p_{Ky1} F_{zo} \sin[p_{Ky2} \arctan\{F_z/((p_{Ky3} + p_{Ky4}\gamma^2)F_{zo})\}]$
$C_y = p_{Cy1}$	$C_\gamma = p_{Cy2}$
$\mu_y = p_{Dy1} \exp(p_{Dy2} df_z) /(1 + p_{Dy3}\gamma^2)$	$E_\gamma = p_{Ey5}$
$E_y = p_{Ey1} + p_{Ey2}\gamma^2 + p_{Ey4}\gamma sgn(\alpha)$	$B_\gamma = K_{y\gamma}/(C_\gamma D_\gamma)$
$B_y = K_{y\alpha}/(C_y D_y)$	$K_{y\gamma} = (p_{Ky6} + p_{Ky7} df_z)F_z$
$K_{y\alpha} = K_{y\alpha o}/(1 + p_{Ky5}\gamma^2)$	

where α and γ represent side-slip and camber angles. F_z and F_{zo} represent normal load and nominal normal load, respectively; we also have $df_z = \frac{F_z - F_{zo}}{F_{zo}}$. The parameters for a 160/70 ZR17 tire is as following:

$$F_{zo} = 1600\ N$$

$p_{Cy1} = 0.93921$	$p_{Ey4} = -1.6416$	$p_{Cy2} = 0.50732$
$p_{Dy1} = 1.1524$	$p_{Ky1} = 26.601$	$p_{Ky6} = 0.7667$
$p_{Dy2} = -0.01794$	$p_{Ky2} = 1.0167$	$p_{Ky7} = 0$
$p_{Dy3} = -0.065314$	$p_{Ky3} = 1.4989$	$p_{Ey5} = -4.7481$
$p_{Ey1} = -0.94635$	$p_{Ky4} = 0.52567$	
$p_{Ey2} = -0.098448$	$p_{Ky5} = -0.24064$	

Appendix B

Matrix A is

$$A = \begin{bmatrix} a_{11} & a_{12} & a_{13} & a_{14} \\ a_{21} & a_{22} & a_{23} & a_{24} \\ a_{31} & a_{32} & a_{33} & a_{34} \\ a_{41} & a_{42} & a_{43} & a_{44} \end{bmatrix}$$

where

$a_{11} = \frac{-(2c_{\alpha f} + c_{\alpha r})}{(m + \frac{-{m_s}^2{h_s}^2}{I_x})u}$	$a_{12} = \frac{-(\frac{-{m_s}^2{h_s}^2u^2}{I_x} + mu^2 + 2ac_{\alpha f} - bc_{\alpha r})}{(m + \frac{-{m_s}^2{h_s}^2}{I_x})u}$	$a_{13} = \frac{\frac{-{m_s}^2{h_s}^2g}{I_x} + \frac{k_\varphi m_s h_s}{I_x}}{(m + \frac{-{m_s}^2{h_s}^2}{I_x})}$	$a_{14} = \frac{\frac{c_\varphi m_s h_s}{I_x}}{(m + \frac{-{m_s}^2{h_s}^2}{I_x})}$
$a_{21} = \frac{-(2ac_{\alpha f} - bc_{\alpha r})}{uI_z}$	$a_{22} = \frac{-(2a^2c_{\alpha f} + b^2c_{\alpha r})}{uI_z}$	$a_{23} = 0$	$a_{24} = 0$
$a_{31} = 0$	$a_{32} = 0$	$a_{33} = 0$	, $a_{34} = 1$
$a_{41} = \frac{\frac{2c_{\alpha f}m_s h_s + c_{\alpha r}m_s h_s}{I_x}}{(m + \frac{-{m_s}^2{h_s}^2}{I_x})u}$	$a_{42} = \frac{\frac{2ac_{\alpha f}m_s h_s - bc_{\alpha r}m_s h_s}{I_x}}{(m + \frac{-{m_s}^2{h_s}^2}{I_x})u}$	$a_{43} = \frac{-\frac{mk_\varphi - mgm_s h_s}{I_x}}{(m + \frac{-{m_s}^2{h_s}^2}{I_x})}$	$a_{44} = \frac{-\frac{mc_\varphi}{I_x}}{(m + \frac{-{m_s}^2{h_s}^2}{I_x})}$

Appendix C

It is proved that the value of load transfer for second configuration is always less than the value of the first configuration.

$$\Delta F_{z1} = \frac{Ma_yH + m_sghSin(\varphi)}{T + 2\Delta T}$$

$$\Delta F_{z2} = \frac{Ma_yH + m_sghSin(\varphi) - 2F_{z0}\Delta T}{T}$$

For $F_{z0} > \Delta F_z$, we have

$$F_{z0} > \Delta F_z \quad \Rightarrow$$

$$F_{z0} > \Delta F_z = \frac{Ma_yH + m_sghSin(\varphi)}{T + 2\Delta T} \quad \Rightarrow$$

$$F_{z0}(T + 2\Delta T) > Ma_yH + m_sghSin(\varphi) \quad \Rightarrow$$

$$F_{z0}T + 2F_{z0}\Delta T > Ma_yH + m_sghSin(\varphi)$$

$$both\ sides \times 2\Delta T \quad \Rightarrow$$

$$2F_{z0}T\Delta T + 4F_{z0}(\Delta T)^2 > 2\Delta T\left(Ma_yH + m_sghSin(\varphi)\right)$$

$$both\ sides + T(Ma_yH + m_sghSin(\varphi) \Rightarrow$$

$$T\left(Ma_yH + m_sghSin(\varphi)\right) > T\left(Ma_yH + m_sghSin(\varphi)\right) + 2\Delta T\left(Ma_yH + m_sghSin(\varphi)\right) - 2F_{z0}T\Delta T - 4F_{z0}(\Delta T)^2 \quad \Rightarrow$$

$$T\left(Ma_yH + m_sghSin(\varphi)\right) > T\left(Ma_yH + m_sghSin(\varphi) - 2F_{z0}\Delta T\right) + 2\Delta T\left(Ma_yH + m_sghSin(\varphi) - 2F_{z0}\Delta T\right) \quad \Rightarrow$$

$$T\left(Ma_yH + m_sghSin(\varphi)\right) > (T + 2\Delta T)\left(Ma_yH + m_sghSin(\varphi) - 2F_{z0}\Delta T\right) \Rightarrow$$

$$\frac{Ma_yH + m_sghSin(\varphi)}{T + 2\Delta T} > \frac{Ma_yH + m_sghSin(\varphi) - 2F_{z0}\Delta T}{T}$$

$$\Delta F_{z1} > \Delta F_{z2}$$

And for

$$F_{z0} = \Delta F_z$$

$$\Delta F_{z2} = \frac{Ma_yH + m_sghSin(\varphi) - 2F_{z0}\Delta T}{T} \quad \Rightarrow$$

$$\Delta F_{z2} = \frac{Ma_yH + m_sghSin(\varphi) - 2\Delta F_{z2}\Delta T}{T} \quad \Rightarrow$$

$$T\Delta F_{z2} = Ma_yH + m_sghSin(\varphi) - 2\Delta F_{z2}\Delta T$$

$$T\Delta F_{z2} + 2\Delta F_{z2}\Delta T = Ma_yH + m_sghSin(\varphi)$$

$$\Delta F_{z2}(T + 2\Delta T) = Ma_yH + m_sghSin(\varphi)$$

$$\Delta F_{z2} = \frac{Ma_yH + m_sghSin(\varphi)}{T + 2\Delta T}$$

$$\Delta F_{z2} = \Delta F_{z1}$$

Appendix D

Parameter values for a three-wheeled vehicle are listed in table D.

Table D: Three-wheeled vehicle's parameters

Parameters	***Values***	***Descriptions***
m	800 kg	Vehicle Mass
m_s	680 kg	Sprung Mass
a	0.75 m	Distance of front wheels to CG
b	1.75 m	Distance of rear wheel to CG
I_x	210 kgm^2	Roll Inertia
I_z	480 kgm^2	Yaw Inertia
H	0.4 m	CG Height
h_s	0.25 m	Distance of CG from roll center
T	1.4 m	Vehicle Track
k_φ	11760 N/rad	Torsional Stiffness
c_φ	784 Ns/rad	Torsional Damping
C_{α_f}	24803 N/rad	Front wheel cornering coefficient
C_{γ_f}	1453.5 N/rad	Front wheel camber coefficient
C_{α_r}	23310 N/rad	Rear wheel cornering coefficient
C_{γ_r}	1234.9 N/rad	Rear wheel camber coefficient